

UNIVERSITÉ DU QUÉBEC À MONTRÉAL

RESIDENCE TIME DISTRIBUTION OF GROUNDWATER SUSTAINING RIVERS AS A
NEW TOOL FOR CATCHMENTS VULNERABILITY ASSESSMENTS (SAINT-
CHARLES RIVER, QUÉBEC, CANADA)

THESIS

PRESENTED

AS A PARTIAL REQUIREMENT

TO DOCTORATE IN EARTH AND ATMOSPHERIC SCIENCES

BY

ANTOINE PICARD

MAY 2025

UNIVERSITÉ DU QUÉBEC À MONTRÉAL

UN NOUVEL OUTIL DE DESCRIPTION DE LA VULNÉRABILITÉ DES BASSINS-
VERSANTS TENANT COMPTE DE LA DISTRIBUTION D'ÂGE DES APPORTS D'EAU
SOUTERRAINE AUX RIVIÈRES (RIVIÈRE SAINT-CHARLES (QUÉBEC, CANADA))

THÈSE

PRÉSENTÉE

COMME EXIGENCE PARTIELLE

AU DOCTORAT EN SCIENCES DE LA TERRE ET DE L'ATMOSPHÈRE

PAR

ANTOINE PICARD

MAI 2025

UNIVERSITÉ DU QUÉBEC À MONTRÉAL
Service des bibliothèques

Avertissement

La diffusion de cette thèse se fait dans le respect des droits de son auteur, qui a signé le formulaire *Autorisation de reproduire et de diffuser un travail de recherche de cycles supérieurs* (SDU-522 – Rév.12-2023). Cette autorisation stipule que «conformément à l'article 11 du Règlement no 8 des études de cycles supérieurs, [l'auteur] concède à l'Université du Québec à Montréal une licence non exclusive d'utilisation et de publication de la totalité ou d'une partie importante de [son] travail de recherche pour des fins pédagogiques et non commerciales. Plus précisément, [l'auteur] autorise l'Université du Québec à Montréal à reproduire, diffuser, prêter, distribuer ou vendre des copies de [son] travail de recherche à des fins non commerciales sur quelque support que ce soit, y compris l'Internet. Cette licence et cette autorisation n'entraînent pas une renonciation de [la] part [de l'auteur] à [ses] droits moraux ni à [ses] droits de propriété intellectuelle. Sauf entente contraire, [l'auteur] conserve la liberté de diffuser et de commercialiser ou non ce travail dont [il] possède un exemplaire.»

REMERCIEMENTS

Avant toute chose, je souhaiterais vivement remercier Florent Barbecot, directeur de cette thèse pour son encadrement tout au long de ce travail, sa motivation contagieuse et ses idées scientifiques originales. Un grand merci également pour les nombreuses opportunités auxquelles j'ai eu la chance d'avoir accès durant ces (presque) quatre ans, au Canada, aux États-Unis, en Suisse, en Autriche et au... Vanuatu bien sûr ! Je remercie également chaleureusement José Corcho-Alvarado, co-directeur, depuis la Suisse, qui a toujours été une source d'aide et d'apaisement lors de mes demandes de conseils et relectures, à distance comme en présentiel. Un grand merci à Karine Lefebvre et Janie Masse-Dufresne pour toute l'aide apportée, les bons conseils en matière de travail de terrain, de mesure de radon, et de recherche. Mais aussi pour l'écoute. Particulièrement, merci à Karine pour les moments café à l'UQAM (et aujourd'hui pour les sorties dans Montréal), et Janie pour ton accueil à Val-David et les activités extérieures.

Merci également à deux « mentors » qui étaient là au commencement et sans qui je n'aurais pas fait le choix d'amorcer une thèse. J'ai nommé Masaki Hayashi, pour la découverte de l'hydrogéologie alpine en Alberta en 2018, et Pierre Belle pour sa confiance, ses enseignements et sa gentillesse lors de mon passage à la S.A.E.M.E. entre 2019 et 2020.

Mes remerciements vont également aux membres de l'équipe du projet « Ville de Québec », avec qui j'ai pu travailler tout au long de la thèse. De l'Université Laval, je remercie Yohann Tremblay, Laura Gâtel, Benjamin Frot, René Therrien, Kevin Montoya et Jean-Michel Lemieux. Mes remerciements vont également à Baudelaire N'Da et Vincent Cloutier de l'UQAT. Merci à vous toutes et tous pour votre implication dans ce beau projet, depuis l'aide sur le terrain, aux aspects plus administratifs en passant par les journées partagées de restitution de connaissances scientifiques. Mention spéciale à toi, Benjamin, pour ton accueil toujours aussi légendaire à Québec et ta résilience face aux travaux de terrains en conditions « extrêmes ».

A la Ville de Québec, je souhaite d'abord adresser mes remerciements à François Proulx et Christine Beaulieu pour leur aide très précieuse concernant la récupération des données de suivi de qualité à la prise d'eau ainsi que la mise en place du suivi isotopes et silice. A ce propos, je souhaiterais également fortement remercier et souligner l'implication de Lucie-Anne Gagnon pour avoir réalisé la tournée d'échantillonnage des isotopes et de la silice dissoute à la prise d'eau en 2022 et 2023. Je souhaite également remercier Anne-Marie Cantin et Luc Audet pour leur confiance au cours du projet.

Merci également à Jean-François Hélie et André Poirier, pour votre accessibilité, votre disponibilité et tous les moments partagés, que ce soit au labo, ou autour d'un lunch au 7^{ème} étage, comme à l'autre bout du monde, là où les tabous permettent d'échantillonner l'eau en toute sécurité. Un grand merci à Agnieszka Adamowicz, dont il faut souligner le goût cinématographique, pour l'aide au laboratoire et lors du congrès ASITA en 2022. Merci à Daniele Pinti pour les discussions autour des gaz rares, et des spécialités italiennes.

Un vrai travail de thèse ne serait rien sans les échanges avec les camarades de labo et l'énergie qu'ils apportent avec eux... Alors un très, très, très grand merci à Cécile (mais aussi pour la découverte du chouchen et de nombreux bars dans Montréal !), Donovan (le plus breton des Rennais), Jorge, Amadou, Ahmed et Serena pour les moments passés ensemble ces dernières années, que ce soit dans les murs de l'UQAM, sur le terrain, ou autour d'un bon verre. Merci également à Benjamin, de l'ETS, pour ta grande motivation et ton aide lors de la campagne de terrain de février 2024. Merci aux stagiaires qui ont animé nos étés de doctorants : Matéo Lacheux pour qui je suis heureux de son choix de thèse, Pierre Cany pour les séances de course, Frédérick pour tes ondes positives et ton grand sérieux sur le terrain, ainsi que Tugdual Bobin et Océane Tardivel pour le terrain hivernal.

J'adresse également de chaleureux remerciements à toutes les personnes de sciences et collaboratrices et collaborateurs scientifiques que j'ai eu la chance de côtoyer : Roland Purtschert, Douglas Kip Solomon, Gérard Bardoux, Marina Gillon, Patrick Lachassagne, Vincent Schneider, Oliver Warr, Stéphanie Musy, Astrid Harjung, Matthias Brennwald et Pierre Agrinier.

Un grand merci à toute l'équipe étudiante d'Urgence Eau, pour l'organisation de ce projet qui s'est concrétisé en 2023. Cette formidable opportunité n'aurait pu se produire sans l'aide du Department of Water Resources du Vanuatu que je souhaiterais remercier pour l'accueil, l'aide et l'écoute. En particulier merci à Jonah Taviti, qui s'est plié en quatre pour nous, et une pensée à toi et ta famille quelques jours après le séisme qui a frappé Port-Vila. Le mont Yasur, les courants du Pacifique, les oiseaux exotiques, les baleines à bosse, les communautés d'Ambae et Tanna et le taro sont ancrés dans ma mémoire. *Tankiu tumas.*

Il faut également reconnaître l'impact des relations personnelles sur la réussite de ce travail. Il est évident que Benjamin et François ont été une grande source familiale de réconfort durant toute la thèse. Alors, un grand merci pour tout et pour avoir partagé le même toit pendant plus de trois ans. Merci également à Nath, depuis Géol jusqu'au Plateau, on peut réellement se dire que le monde est petit ! Merci à Marguerite et JB pour les sorties ornitho, en particulier les blongios de Montréal et les pygargues du lac du Der. Merci à Mathieu pour ton soutien à distance, je me rappellerai longtemps ce tour sportif en Chartreuse. Une pensée également pour Paco, Nico, Simon, Maxime et Clément pour le soutien moral. J'ai hâte de vous revoir à l'occasion d'un « weekend BDF ». Un merci très spécial à Marie-Ève, Richat, Hubert pour m'avoir accueilli dans une nouvelle maison et un quotidien aux nouvelles saveurs. Un grand merci aussi à Marie-Claude et toute la famille Cardinal pour leur accueil très chaleureux.

Une grosse pensée pour ma grand-mère, mes parents et mes sœurs, pour leur amour et leur écoute. Une pensée toute singulière pour mes grands-parents de Toulouse, à qui j'aurais aimé montrer ce travail.

~~

TABLE OF CONTENTS

LIST OF FIGURES	ix
LIST OF TABLES	xvii
RÉSUMÉ	xviii
ABSTRACT.....	xxi
INTRODUCTION.....	1
CHAPTER 1 Current state of the art: the links between catchment vulnerability, groundwater inflows to streams and water residence times	7
1.1 Résumé du Chapitre 1 en français	7
1.2 The groundwater – surface waters continuum.....	9
1.2.1 Global importance and roles of groundwater inflows to streams	9
1.2.2 Determination of the spatial distribution of groundwater inflows to streams	17
1.2.3 Determination of the temporal dynamics of groundwater inflows to streams.....	21
1.3 Water residence times in catchments	24
1.3.1 Concepts and definitions	24
1.3.2 Environmental tracers as groundwater dating tools	26
1.3.3 Determination of water residence times.....	30
1.3.4 Catchment scale transit time distribution determination	40
1.4 Conclusion and PhD objectives.....	43
1.4.1 Conclusions of the introduction.....	43
1.4.2 PhD objectives	44
CHAPTER 2 Innovative techniques to assess water resources vulnerability to anthropic forcings in vulnerable catchments	46
2.1 Résumé du Chapitre 2 en français	46
2.1.1 Introduction du Chapitre 2.....	46
2.1.2 Résumé en français de l'Article 1.....	47
2.1.3 Résumé en français de l'Article 2.....	48
2.2 Introduction to Chapter 2.....	49
2.3 The potential of isotopic tracers for precise and environmentally clean stream discharge measurements (<i>Article 1</i>)	51
2.3.1 Introduction	52
2.3.2 Materials and Methods.....	55

2.3.3	Results and discussion	62
2.3.4	Conclusions.....	72
2.3.5	Appendices	73
2.4	Simultaneous determination of major (N ₂ , O ₂), noble (Ar, He, Kr) and anthropic trace gases (CFC-12, CFC-11, SF ₆) contents from passive discrete samples (<i>Article 2</i>).....	78
2.4.1	Introduction	79
2.4.2	Materials and methods.....	81
2.4.3	Results.....	86
2.4.4	Conclusions.....	91
2.5	Conclusion of Chapter 2.....	93
CHAPTER 3 The true dependency of a surface water intake to groundwater inflows in a meso-scale, partially urbanised and snowmelt influenced catchment		
95		
3.1	Résumé du Chapitre 3 en français	95
3.1.1	Introduction du Chapitre 3.....	95
3.1.2	Résumé en français de l' <i>Article 3</i>	96
3.2	Introduction to Chapter 3.....	97
3.2.1	Stable isotopes of the water molecule	97
3.2.2	Conclusion of the introduction	102
3.3	The challenges of hydrograph separation and catchment mean transit time estimation in a mesoscale, urbanised, snowmelt-influenced catchment (<i>Article 3</i>).....	103
3.3.1	Introduction	104
3.3.2	Presentation of the study area.....	107
3.3.3	Materials and methods.....	109
3.3.4	Results.....	119
3.3.5	Discussion	127
3.3.6	Conclusions.....	135
3.4	Conclusion of Chapter 3.....	136
CHAPTER 4 Catchment water transit time distribution: the contribution of environmental and artificial tracing experiments in a partially frozen river		
139		
4.1	Résumé du Chapitre 4 en français	139
4.1.1	Introduction du Chapitre 4.....	139
4.1.2	Résumé en français de l' <i>Article 4</i>	141
4.2	Introduction to Chapter 4.....	141
4.3	Deciphering river baseflow age distribution through environmental and artificial tracing experiments in a partially ice-covered river (<i>Article 4</i>)	143
4.3.1	Introduction	144
4.3.2	Study site.....	145

4.3.3	Materials and methods.....	148
4.3.4	Results and discussion	160
4.3.5	Conclusions.....	168
4.3.6	Appendices	169
4.4	Conclusion of Chapter 4.....	174
CHAPTER 5	Conclusions.....	176
5.1	Conclusions en français.....	176
5.1.1	Principales contributions	177
5.1.2	Perspectives de recherche	184
5.2	Conclusions in English	186
5.2.1	Contributions of the research	186
5.2.2	Research and application perspectives	193
APPENDIX A	Development of the headspace method for simultaneous analysis of SF ₆ , CFC-12, CFC-11 and CFC-113 in environmental and tracing experiments samples	195
APPENDIX B	Description of the Saint-Charles River catchment.....	201
APPENDIX C	Monitoring of isotopes and geochemical parameters.....	210
BIBLIOGRAPHY	215

LIST OF FIGURES

Figure 1: Global map of modelled BFI values. (Beck et al., 2013).....	10
Figure 2: Scales of application for different methods of groundwater – surface water interactions characterization and quantification. Modified from Kalbus et al. (2006).	17
Figure 3: Discretization scheme of a river reach used for an inert volatile tracer mass-balance. .	19
Figure 4: a) Numerical simulations (the continuous line considers hyporheic exchanges while the dashed line does not) of tracer concentrations and river flow in a tropical river (modified from Cook et al. (2003)). b) Transversal cross section of depth and tracers indicating groundwater discharge near the right bank where the electrical conductivity (EC) is low and the radon activity is higher (Cook, 2013).....	20
Figure 5: Mixing diagram of chloride and $\delta^{18}\text{O}$ showing that stream samples variability is explained when considering three end-members: event water, groundwater and soil water (Bazemore et al., 1994).....	23
Figure 6: (a) Historical reconstruction of nitrogen input and nitrate concentration in groundwater plotted against time and CFC-12 model recharge dates for groundwater (Böhlke & Denver, 1995). (b) Reversal trend of nitrates concentration highlighted in Netherlands – the recharge year was determined using ^3H - ^3He (Visser et al., 2007).....	26
Figure 7: Spatial and temporal scales for use of different hydrological tracers including groundwater dating tracers (Sprenger et al., 2019).....	27
Figure 8: Transient tracers atmospheric input function used for dating of “young” groundwaters. Anthropogenic gases data was taken from the NOAA (https://gml.noaa.gov/dv/data/), radiokrypton data was retrieved from Kersting et al. (2021) and Ottawa tritium data was retrieved from the I.A.E.A Wiser (GNIP) portal (https://nucleus.iaea.org/wiser/).	29
Figure 9: Results from multi-tracing experiments in the Fontainebleau sands aquifer which is a complex mixture of recent and old groundwaters (Corcho Alvarado et al., 2007).....	30
Figure 10: Methodological steps to determine MTT and TTD from environmental tracers using the lumped parameter model approach (Suckow, 2014).....	32
Figure 11: TTD shapes of commonly used transfer functions ($\tau = 25$ years with a dispersion parameter of 0.7 for the dispersion model).....	35
Figure 12: TTD shapes for Gamma functions with different shape factors ($0.2 < \alpha < 7$; $\tau = 25$ years).	36

Figure 13: Noble gases components in a typical shallow groundwater sample normalized to their respective atmospheric equilibrium (Kipfer et al., 2002). Note that the noble gases are affected differently by excess air which helps to determine it (especially Ne and Xe, since they only have atmospheric sources).	38
Figure 14: On the left: monitoring of ^{85}Kr specific activities in stations across the globe (Kersting, Schlosser, Schmid, et al., 2020). The visible peaks for European stations (Freiburg, Schauinsland, Jungfrauoch) are due to the proximity to nuclear fuel reprocessing plants. On the right: spatial distribution of atmospheric SF_6 concentration in the eastern United States (Santella et al., 2008).	39
Figure 15: Cumulative daily CTTD of stream discharge during a 2 weeks wet and a 2 weeks dry periods. The TTD are also reported in the inserts. (Benettin et al., 2015).	41
Figure 16: Artificially released dissolved Kr and Xe concentration as a function of the distance to the injection site in a stream. The parameter “K” is the gas transfer velocity and represents the atmosphere/river gas exchange rate. Graphs taken from Solomon et al. (2015).	42
Figure 17: Map of Canada (on the left) and of the Ruisseau Rousse watershed (on the right). The red dots in both maps symbolise where the field work occurred.	55
Figure 18: On the left: picture of the stream at the injection site (under a small culvert). We ensured tracer homogeneity by manually fanning the water under the culvert. On the right: picture of the restitution site with the equipment used to monitor solute concentration.....	56
Figure 19: River working section (looking upstream) with equipment location.	57
Figure 20: Distribution of interpolated river water velocity ($n = 342$). A value of zero was forced at the streambed and above the water surface for the spatial interpolation. Velocities are expressed in m.s^{-1}	63
Figure 21: Upper graph: the seven salts concentration restitution functions and the composite restitution function. Lower graph: zoom-in around the peak time showing slight differences in peak heights. Background initial concentrations were removed, which explains the zero concentration at the beginning of the experiment.	64
Figure 22: ^2H , ^{37}Cl , Cl^- , Br^- and fluorescent tracers (uranine, tinopal) restitutions obtained at the centre of the stream.	67
Figure 23: Discharge measure uncertainty as a function of mass of injected tracer (^2H , ^{37}Cl) for the studied river (the blue dots represent this experiment). It is important to note that the x-axis refers to the actual isotopic tracer’s mass alone and not ^{37}Cl -enriched salt or deuterated water. Details on these calculations can be found in Appendix A.	68
Figure 24: Normalized tracer restitution showing different tracer behaviours at times $>1500 \text{ s}$. ..	70

Figure 25: Tracers' concentrations modelled using a binary mixing 1D dispersion model.	72
Figure 26: (a) Three examples of expected deuterium restitution curves with different tracer input masses. Note that $M^2_H = 403.1$ g is the mass of 2H that was injected in the stream. (b) The relationship between the measured mass of deuterium and its uncertainty (the black dots are from the field samples). (c) Graph showing the evolution of discharge uncertainties as a function of the mass of injected 2H (the experiment described in this paper is represented by the blue dot).....	76
Figure 27 : Scheme of the passive samplers. “T” stands for the stainless-steel tube (length: 30 cm), V1 and V2 are the two Swagelok valves, and M1 and M2 are the two gas-permeable silicone membranes (length: 10 cm each). A cross-section of the membranes is also shown.	81
Figure 28: On the left: scheme of the setup used in analysis mode. On the right: scheme of the equilibration experiments. Passive samplers are immersed vertically in the 100 L bucket with the two ball valves open. A diffuser continuously injects air as bubble from the bottom of the bucket.	83
Figure 29: Results from the direct measurement of dissolved gases with the GE-MIMS module of the miniRUEDI.....	87
Figure 30: Results of the equilibration experiments. The dashed line represents the partial pressures expected when the gas in the passive sampler is in equilibrium with the gases in water. The “errors bars” are the standard deviations calculated from the 25 measurements for each gas for each analysis of passive sampler.	88
Figure 31: Variation of the accuracy (standard deviation) in gas partial pressures as a function of the number of analyses of one passive sampler conducted with the miniRUEDI.	90
Figure 32: Comparison of the major, noble and anthropic trace gases measurements in the atmosphere and in equilibrium with the water in the bucket for the GE-MIMS and a fully equilibrated passive sampler.	91
Figure 33 : Biplot of isotopic signatures in precipitation, the LMWL for rainfall is also indicated as well as average and standard deviation for rainfall and snowpack values ($n_{rainfall} = 264$; $n_{snowpack} = 52$).....	98
Figure 34 : Temporal patterns of (i) monthly total precipitation, (ii) snow cover, (iii) daily minimal and maximal temperatures and (iv) isotopic signatures of rainfall and snowpack for the years 2021 – 2022. The climatic data is from the Jean Lesage airport station in Québec, operated by the Government of Canada (Station ID: 71212).....	99
Figure 35 : Relationship between the slope of the monthly rainfall LMWL and the d-excess values.	100

Figure 36 : Relationship between weighted average annual rainfall isotopic signatures and the elevation for the 15 stations.....	101
Figure 37 : (a) Biplot of isotopes in precipitation, rivers and groundwater ($n_{\text{river}} = 144$; $n_{\text{groundwater}} = 53$). The averages values are also given. (b) Box plots showing the variability of the four water masses: rainfall, snowpack, groundwater and rivers.....	102
Figure 38: Conceptual scheme of the time spent by water within the different hydrogeological compartments of a watershed.....	105
Figure 39: From left to right: map of Canada with red arrow indicating the study site location in the Province of Québec, watershed physiography, topography, hydrography and land use. The surface water intake of the Saint-Charles River is located at the outlet of the watershed (pink diamond).	107
Figure 40: Climate normals (1981-2010) from Jean Lesage airport station (OMM station 71708) and mean average monthly discharge at the outlet of the catchment between 2012 to 2023 (MELCCFP station 050904 corrected from abstracted water at the pumping station).	108
Figure 41: Three end-members put into evidence by PCA in the plane defined by the axes of dimension 1 and 2. The white dots represent the data from July 2012 to August 2023 (223 samples with $ IB \leq 15\%$).	112
Figure 42: Evolution of discharge, baseflow and dissolved silica from November 2022 to April 2023.	116
Figure 43: Relationship between the increasing stream Si concentration and the increasing “minimum mean transit time” (τ_m) for the three approaches. The range of thresholds for each model is indicated above the graph. The continuous red line represents the Si plateau concentration with $\pm 5\%$ values represented by dashed red lines.	118
Figure 44: Box plots of total river discharge, major ions and electrical conductivity in the Saint-Charles River for each month (period 2013-2023). The numbers in red represent extreme values for chloride, sodium and electrical conductivity values.....	120
Figure 45: Multi-annual trends in electrical conductivity, alkalinity, chloride and calcium concentrations (period 2003 – 2023).	121
Figure 46: Seasonality in the discharge – chloride relationship, indicating different controls of the chloride concentration according to the season (see black arrows in the graph).	122
Figure 47: Discharge and stable isotopes signatures of snowpack, groundwater, rainfall and stream over time.	123
Figure 48: Average of flow components for each month of the July 2012 – August 2023 period, according to the chemical hydrograph separation: (a) fixed groundwater end-member; (b)	

time-variant groundwater end-member. The red bar is the 50 % bar, helping to determine which end-member controls the stream water availability.	124
Figure 49: Continuous baseflow separation and results from the tracer-based baseflow separation from 2013 to 2023 (only the results from the time-variant groundwater end-member approach are presented).	125
Figure 50: Relationship between the groundwater fraction (f_{gw}) and major ions concentrations (alkalinity, Ca^{2+} , Mg^{2+} , K^+ , Na^+ and Cl^-), trace metals (Ni, Al, Fe, Zn and Pb) and pH. The points influenced by urban snowmelt contribution are highlighted in the pink circles for major ions.	128
Figure 51: a) Evolution of total discharge, baseflow, normalised alkalinity and dissolved silica concentrations during the years: 2022 – 2023. b) Zoom on the period Feb. 2023 to Sept. 2023. The contents were normalised to the maximum value measured during the 2022 – 2023 period.	130
Figure 52: a) Evolution of “minimum mean transit time (i.e. τ_m)”, discharge and baseflow during 2022 and 2023 for the three approaches; b) Age-discharge relationship determined using the exponential model approach; c) Groundwater Si concentration-age relationship determined with the exponential model approach.	134
Figure 53: Cumulative age distribution representative of different catchment wetness conditions (different τ_m): $\alpha = 1$ for grey lines (exponential), and $\alpha = 0.5$ for black lines.	135
Figure 54: Above: map of Canada with the red arrow indicating the location of the study site. Below: maps of the Nelson River watershed with the 6 sampling points (SW1 to SW6): topography and granular aquifer thickness on the left, and soil occupation on the right..	147
Figure 55: (a) Evolution of the Nelson River daily discharge from April 2023 to July 2024, and (b) zoom-in the 2023 – 2024 winter period, with sampling day highlighted (27/02/2024).	148
Figure 56: Apparatus used for in-situ sampling of ^{85}Kr (left) and river aspect during fieldwork showing the partial ice cover close to SW4 (right).	150
Figure 57: Scheme of the apparatus used to inject gas tracers in the stream. The immersed part was installed perpendicular to the direction of the streamflow.	152
Figure 58: Scheme of a river cell with water and solutes fluxes.	154
Figure 59: Tracer gas concentration plotted as a function of the distance from the injection point. The red and green points are the He and SF_6 concentrations, respectively. The dotted lines represent the equilibrium concentration relative to the atmosphere. The measurement uncertainties are smaller than the size of the points.	161

- Figure 60: Biplot of chloride and ^3H contents in river water samples. The average winter ^3H activity in precipitation was obtained from the Ottawa GNIP station (2005 – 2020) (blue dashed line). The chloride concentration in groundwater (red dashed line) was estimated from measurements in wells in the catchments. 162
- Figure 61: Spatial variation of stream discharge, groundwater inflows, urban snowmelt inflows and measured and modelled age-dating tracers (^3H , SF_6 , CFC-12 and ^{85}Kr). The solubility equilibrium for gases is also represented as dark violet dashed lines. 163
- Figure 62: a) Binary plot of ^3H and ^{85}Kr activities for two different models outputs (exponential and dispersion models) and modelled groundwater inflows, b) transit time distribution, and c) cumulative transit time distribution for the two model outputs. 165
- Figure 63: Grid for assessing the resilience and vulnerability of rivers as functions of baseflow mean residence time and river baseflow index respectively. The grey dot represents the long-term BFI value (0.77) with the baseflow mean residence time (10 years). 168
- Figure 64: a) Monthly variations of total discharge, baseflow from Picard, Barbecot, Proulx, et al. (2024) and ^3H activities in precipitation (GNIP station from Ottawa) between 2012 and 2019 and b) average values for each month for recharge (estimated from baseflow values) and precipitation ^3H activities. 170
- Figure 65: Comparison of the corrected (taking into account the recharge pattern) and measured annual average ^3H activities in precipitation at Ottawa. 173
- Figure 66: (a) Determination of the recession parameter of the Nelson River. (b) Baseflow separation of the Nelson River (BFI = 0.77). 174
- Figure 67: Modèle conceptuel de l'évolution de la signature géochimique de certains traceurs – silice dissoute, chlorures et alcalinité – en fonction du temps de résidence de l'eau, depuis les précipitations ①, passage dans la zone non saturée (ZNS), la zone saturée (ZS) jusqu'à la décharge dans les rivières du bassin-versant (③, ④, ⑤, ⑥). Le temps passé par l'eau souterraine dans l'aquifère avant d'alimenter les rivières varie en fonction des conditions météorologiques (hautes eaux/basses eaux) comme l'indique l'hydrographe à gauche et la position des points ③, ④, ⑤, ⑥ sur l'axe des abscisses. 180
- Figure 68: Alimentation des cours d'eau par différents compartiments aquifères pour les quatre saisons avec hydrogramme type (rivière Saint-Charles, année 2019). Dans ce modèle en colonne, le temps de résidence de l'eau souterraine dans l'aquifère augmente avec la profondeur. La taille des flèches représente les flux relatifs au cours d'eau. Une couleur bleu ciel pâle est utilisée pour l'eau souterraine aux temps de transit les plus courts en été et automne, associée aux épisodes de recharge ponctuels (orages, pluies). Les flux les plus faibles sont attribués au compartiment aquifère insensible à la saisonnalité naturelle dans les patterns de recharge (figure inspirée de Harman (2015)). 181

- Figure 69: Diagramme de la résilience des rivières face aux changements de qualité/quantité dans les eaux souterraines (décrite par le temps de résidence du débit de base) et de la vulnérabilité des rivières face aux contaminations de surface (décrite par l'indice de débit de base)..... 183
- Figure 70: Conceptual model of the evolution of the geochemical signature (dissolved Si, Cl^- and alkalinity) as a function of water residence time from precipitation ①, within the unsaturated zone (USZ), the saturated zone (SZ) to the discharge in the streams of the catchment (③, ④, ⑤, ⑥). The time spent by groundwater in the aquifer before discharging to streams varies accordingly to catchment wetness conditions (high flows/low flows) as indicated by the hydrograph on the left (see the position of the numbers ③, ④, ⑤, ⑥)... 189
- Figure 71: Differences in groundwater compartments sustaining the rivers of the catchment during the four seasons. In this “column” type model, the residence time of the groundwater increases with depth. The size of the arrows depict the relative fluxes to the stream. A light blue colour is used for groundwater in Summer and Autumn to represent the contribution of very young water to the streams during and shortly after storm events. The smallest fluxes are attributed to the aquifer compartment that is insensitive to natural seasonality in groundwater recharge patterns (inspired by Harman (2015))..... 190
- Figure 72: Plot of the resilience of rivers to groundwater changes in quality and quantity (controlled by the baseflow residence time) and the vulnerability of rivers to surface contamination (controlled by the baseflow index). 192
- Figure 73: The ratio between the gas in the headspace and the maximum gas quantity in the headspace ($n_{\text{headspace}}/n_{\text{max}}$) as a function of V_w/V_h for CFCs and SF_6 at $T = 22^\circ\text{C}$ (average laboratory temperature). The optimum V_w/V_h is found when $n_{\text{headspace}}/n_{\text{max}}$ is equal to 1 (here, the optimum V_w/V_h ratio is ≈ 14 for SF_6 at 22°C). The grey area is the typical range of V_w/V_h values obtained with our headspace preparation protocol. Note that CFC-12 and CFC-11 curves are very close since their respective solubility coefficients are similar at temperatures close to 20°C 196
- Figure 74: Results of the equilibrium experiments (March – April 2024). The analyses results have been transformed to atmospheric concentrations, assuming air saturated water. The dashed lines represent the measured concentration in the laboratory. A standard deviation of 10 % was adopted based on reproducibility results of samples and standards. 199
- Figure 75: From left to right: map of Canada with the red arrow indicating the location of the studied watershed, topography map and land-use map of the Saint-Charles river water intake catchment. 201
- Figure 76: Geological map of the study area (data source: SIGEOM). The geological formations listed in legend are only the ones found inside the catchment. 204

Figure 77: Average climatic data (climate normals: 1981 – 2010) for (a) Jean Lesage airport station (ID station: 71708) and (b) Forêt Montmorency station (ID station: 71212). The data was retrieved from https://climate.weather.gc.ca/climate_normals/	207
Figure 78: Hydrographs of the main rivers of the catchment (period: 2006 – 2024). The data were obtained from the governmental stations n° 050915, 050916 and 050904 and can be retrieved at the following address: https://www.cehq.gouv.qc.ca/hydrometrie/	208
Figure 79: The outlet of the catchment: the water intake of Saint-Charles river. The pumping system is immersed on the bottom right part of the picture.....	209
Figure 80 : On the left, Palmex® collector used at the lake Saint-Charles station. On the right, homemade rainfall collector installed in the catchment.	212

LIST OF TABLES

Table 1: Common groundwater dating models with the mathematical expression of their TTD and characteristics. From Jurgens et al. (Jurgens et al., 2012).	34
Table 2: Discharge values measured and associated uncertainties. Note that anion (Cl^- , Br^-) uncertainties were not available.	62
Table 3: Best-fit set of parameters for the modelling of solute transport affected by diffusive transfer in the hyporheic zone.	71
Table 4: Methods of measure of water quality parameters.	109
Table 5: Sensitivity analysis results. “HS” stands for “hydrograph separation”.	126
Table 6: Discharge measurements and concentrations of groundwater age dating tracers in the stream and in the local atmosphere. Uncertainties are of 1 % for He and Ne, 3 % for heavier noble gases and 10 % for the four anthropogenic trace gases.	157
Table 7: Modelling results of groundwater dating tracers. Monte-Carlo simulations were not performed for CFCs and SF_6 results since these tracers were not used to determine baseflow age information.	164
Table 8: Equilibration time necessary for SF_6 and CFCs. The headspace was constantly shaken under a lab temperature of 21 – 22 °C.	200
Table 9: Surface deposits found across the study site (from oldest to most recent).	204
Table 10: Number of samples analysed for water stable isotopes during the PhD.	212

RÉSUMÉ

A échelle globale comme au Québec, les grandes métropoles dépendent principalement des rivières pour leur alimentation en eau potable. La question de la vulnérabilité et de la résilience de ces systèmes de surface face aux pressions croissantes liées à l'urbanisation et aux effets du changement climatique doit être abordée afin d'assurer la disponibilité et la bonne qualité de l'eau utilisée pour la production d'eau potable. Toutefois, les analyses de vulnérabilité des hydrosystèmes, et en particulier des rivières, ne tiennent généralement pas compte des apports souterrains. Cela se traduit notamment dans la législation québécoise qui n'inclue actuellement pas le volet « eaux souterraines » dans les analyses de vulnérabilité des prises d'eau potable de surface. La littérature permet de mettre en évidence que les analyses de vulnérabilité des eaux de surface devraient considérer (i) les apports souterrains ainsi que (ii) leurs caractéristiques intrinsèques comme le temps de séjour dans l'aquifère avant qu'ils n'alimentent les rivières. La première composante du manuscrit rapporte les développements méthodologiques qu'il a été nécessaire de réaliser pour répondre aux deux principaux objectifs de recherche. Pouvoir réaliser des mesures du débit des cours d'eau quelles que soient les conditions climatiques via l'utilisation de traceurs isotopiques (^2H , ^{37}Cl) est un atout majeur dans les bassins versants vulnérables où le maintien de la qualité de l'eau est un enjeu important. La validation d'une méthode combinant l'échantillonnage passif des gaz dissous, et notamment des gaz rares, et leur analyse par combinaison de spectrométrie de masse et de chromatographie gazeuse est également un résultat important. Il est maintenant plus facile d'utiliser les traceurs gazeux pour la datation des eaux récentes (gaz rares, CFCs, SF_6) contribuant au débit des rivières mais aussi pour tracer artificiellement les relations nappe/rivière. La seconde partie du manuscrit concerne la quantification des apports d'eaux souterraines à la prise d'eau potable de surface de la rivière Saint-Charles. La base de données de la qualité (ions majeurs, métaux traces) à la prise d'eau a été utilisée dans le but d'identifier les pôles contrôlant la qualité de l'eau de surface entre 2013 et 2023. Couplé aux données hydrodynamiques et à un modèle mathématique de séparation d'hydrogramme, ce suivi a permis de quantifier la part d'eau souterraine alimentant la rivière sur la période. Il a été possible de démontrer que la disponibilité et la qualité de l'eau dans la rivière

Saint-Charles sont largement dominées par les apports d'eaux souterraines, en particulier en hiver. En incluant la période printanière influencée par la fonte du manteau neigeux, 55 % du débit moyen annuel de la rivière est constituée d'apports souterrains. Ces apports représentent plus de la moitié du débit de la rivière pour plus de 75 % des jours de l'année. Cela signifie que les rivières du bassin versant sont relativement bien protégées des contaminations à la surface, et donc peu vulnérables. Plus largement, ce travail révèle que les gestionnaires de l'eau au Québec bénéficieraient grandement du suivi de traceurs environnementaux en rivière. En particulier, l'alcalinité se révèle être un excellent traceur de la part d'eau souterraine en rivière puisqu'elle est directement héritée du passage de l'eau dans la zone non saturée. Le couplage avec la silice dissoute, dont la concentration est directement fonction du temps d'interaction eau/roche dans l'aquifère, met en évidence les différents processus contrôlant la disponibilité de l'eau en rivière avec (i) la vidange préférentielle en rivière de l'eau récemment rechargée à la fonte des neiges au printemps et en été, (ii) l'augmentation progressive du temps de séjour des eaux souterraines se déchargeant en rivière en hiver et (iii) la décharge d'eaux relativement vieilles au début de la fonte des neiges. La troisième partie du manuscrit propose une investigation du temps de séjour du débit de base en rivière par bilan massique des traceurs de temps de séjour des eaux récentes (CFCs, SF₆, ³H, ⁸⁵Kr) en rivière, pour la première fois au Canada. Cette approche permet de révéler les informations d'âge du débit de base à l'échelle du bassin versant. La période hivernale a été choisie pour mener à bien ce projet car les conditions particulières (couche de glace partielle sur la rivière, conditions d'étiage prononcé) facilitent l'utilisation de telles méthodes. Bien que les CFCs et le SF₆ se soient révélés inutilisables à des fins de datation à cause d'une pollution locale de l'aquifère, le ³H et le ⁸⁵Kr ont permis de déterminer un temps de séjour moyen de 10 ans. Cela démontre que les éventuelles contaminations de la partie de l'aquifère alimentant la rivière peuvent se déverser en rivière pendant des décennies, ce qui fait le lien avec la relative faible résilience de la partie de l'aquifère qui soutient la rivière. Cette recherche démontre le rôle clé des eaux souterraines dans le cycle des eaux de surface au Québec, et l'intérêt de coupler leur quantification et leur datation pour une meilleure gestion.

Mots clés : vulnérabilité des bassins versants, traceurs environnementaux, relations nappe/rivière, datation de l'eau souterraine, eau potable, traçages artificiels.

ABSTRACT

On a global scale, but also in Québec, major cities depend mainly on rivers for their drinking water supply. The vulnerability and resilience of these surface systems to the growing pressures of urbanisation and the effects of climate change must be addressed to ensure the availability and the quality of the water for drinking water production. Generally, vulnerability assessments of hydrosystems, and particularly of rivers, do not consider groundwater inflows. This is for example the case in the current Québec's legislation. The scientific literature shows that surface water vulnerability assessments should consider (i) groundwater inputs and (ii) their intrinsic characteristics, such as their residence time in the aquifer before they feed rivers. The first component of the manuscript reports on the methodological developments required to meet the two main research objectives. The possibility to measure river discharge under any climatic conditions using isotopic tracers (^2H , ^{37}Cl) is a major advantage in vulnerable catchments where maintaining water quality is an important issue. The validation of a method for measuring dissolved gases by combining both mass spectrometry and gas chromatography is also an important result. It enables an easier access to the use of gaseous tracers for young groundwater dating with noble gases, CFCs and SF_6 , to map groundwater/surface water interactions, but also to conduct artificial tracing experiments. The second part of the manuscript concerns the quantification of groundwater inputs to the Saint-Charles River surface drinking water intake. The water intake quality database helped to identify the chemical end-members controlling surface water quality between 2013 and 2023. This monitoring (major ions, trace metals) was combined to hydrodynamic data and a mathematical hydrograph separation model to quantify the proportion of groundwater feeding the river over the period. It is shown that the water availability and quality in the Saint-Charles River are largely dominated by groundwater inputs, particularly in winter. Year-round, 55 % of the river flow is constituted by groundwater (including the spring period), and groundwater accounts for more than half of the river flow on more than 75 % of the days of the year. This suggests that the rivers of the catchment are relatively well protected from surface contamination. More largely, this work shows that water managers in Québec would benefit greatly from monitoring environmental tracers in rivers. In particular,

alkalinity is an excellent indicator of the proportion of groundwater in the river, since it is directly inherited from the transport of water through the unsaturated zone. The coupling with dissolved silica, which concentration is a direct function of the water/rock interaction time in the aquifer, highlights the various processes controlling the availability of water in the river, with (i) the preferential discharge into the river of recently recharged water during snowmelt in spring and summer, (ii) the gradual increase of the residence time of groundwater discharging to the river in winter and (iii) the discharge of relatively old water at the start of snowmelt. The third component involves the investigation of the residence time of river baseflow by the application of the mass balance of young groundwater dating tracers (freons, SF₆, ³H, ⁸⁵Kr), for the first time in Canada. This approach makes it possible to integrate baseflow age information at the catchment scale. The winter period was chosen to carry out this project because of the field conditions (partial ice cover on the river, high low-water conditions) that facilitate the use of such methods. Although freons and SF₆ proved unusable for dating purposes due to local pollution of the aquifer, ³H and ⁸⁵Kr were used to determine a mean residence time of around 10 years. This shows that any groundwater contamination can flow into the rivers for decades, demonstrating the relatively low resilience of the aquifer sustaining the river. This research highlights the critical role of groundwater in sustaining surface water systems in Quebec, and particularly the benefits of coupling the groundwater inflows quantification and their dating for a better management.

Keywords: catchment vulnerability, environmental tracers, groundwater/surface waters interactions, groundwater dating, drinking water, artificial tracing.

INTRODUCTION

The preservation of the good quantitative and qualitative states of water resources is one of the biggest challenges currently faced by humanity as illustrated by the 6th United Nations Global Sustainable Development Goal (SDG) which aims to promote availability and sustainable management of water and sanitation for all. Currently, half of the world's population rely on surface waters (lakes, rivers) for their daily consumption (Barnett et al., 2005) and Québec's province is not much different from this global number as the biggest cities (e.g. Montréal, Québec, Trois-Rivières) rely on river systems for the production of drinking water. In a context of global urbanisation and climate change, the question of the perennity of the availability and the quality of water resources is crucial. In 2018, a new legal framework was adopted in Québec for the vulnerability assessment of surface water intakes. These new vulnerability assessments are based on three steps: (i) the description of the catchment, (ii) the inventory of the factors likely to affect the exploited waters availability and quality, and (iii) the threats posed by human activities within the catchment. The monitoring of certain water quality parameters (ex: microbiology) is also mandated.

While being a significant advance for the preservation and the protection of exploited surface waters in Québec, this legal framework does not consider the roles played by groundwater to surface waters and the impact of these inflows to the resilience of surface waters. However, groundwater inflows to streams are expected to exert a huge role over the surface waters availability and quality in this area of the world (Beck et al., 2013). Conversely, the time spent by groundwater in the catchment (from recharge from precipitation to discharge to streams) is an important metric for the description of the vulnerability and resilience of natural water resources (Benettin et al., 2022). While the comprehension of the natural groundwater quality evolution gives a picture of the natural processes influencing the groundwater quality (Purtschert, 2008), it only describes qualitatively how groundwater might be affected by surface contamination. The determination of the groundwater residence time gives a quantitative answer to this issue by telling us how groundwater is naturally protected by the hydrogeological properties of the aquifer

and how fast contamination might be evacuated from the system (Klaus & McDonnell, 2013). In this context, this PhD work focused on the investigation of the temporal dynamics of the groundwater fraction (“hydrograph separation”) of a river supporting Quebec city water supply, and the evaluation of the residence times of the groundwater inflows as complementary tools to describe the vulnerability of the catchment.

This PhD project was carried out within the Hydro-Sciences UQAM-ETS research team, thanks to the supports of the City of Québec and the Natural Sciences and Engineering Research Council of Canada (NSERC), in close collaboration with the Université Laval and the Université du Québec en Abitibi-Témiscamingue (UQAT).

~~

Groundwater is a much more important and active compartment of the global water cycle than what was previously thought. It has been proven that it is the main contributor to surface waters at the global scale (Winter et al., 1998; Xie et al., 2024), providing a perennial baseflow necessary for ecosystems and life at the surface (Hayashi & Rosenberry, 2002). However, groundwater inflows to stream revealed to be difficult to characterize and measure because they vary much in time and space (Brunner et al., 2017). Physically-based methods may lack precision and representativity while they are easier to implement, although tracer-based methods (naturally present and deliberately injected) are very advantageous for studying these interactions at the catchment scale. The natural and/or artificial tracers signal varies both in space and time and pictures the catchment heterogeneities and physical processes, allowing for the study of groundwater circulation, groundwater replenishment times or groundwater/surface water interactions. River discharge measurements using tracers have often been performed using either fluorescent dyes or salts while the potential of cleaner, more precise tracers such as isotopic tracers and gases has been poorly to never tested. Their use in environmentally clean artificial tracing experiments could be very beneficial to vulnerable catchments, for example those used for drinking water production.

~~

Most rivers flowing under wet and temperate climates are largely sustained by groundwater outflowing from nearby shallow aquifers (Beck et al., 2013; Xie et al., 2024). In Eastern Canada (ex: Québec), groundwater contribution is obvious in winter when rivers continue to flow under the ice sheet and a snowpack starts building due to freezing conditions. The groundwater fraction is less influenced by rapid surface changes and controls the rivers vulnerability to surface contamination. The true quantification of the groundwater contribution to surface waters over time is thus a crucial information in catchments used to produce drinking water, such as the Saint-Charles River, close to the City of Québec. This catchment constitutes the study area of most field experiments conducted in the frame of this PhD work. This catchment is meso-scale (344 km²), partially urbanised (suburbs of the City of Québec and other municipalities) and influenced by snowmelt in spring. The urbanisation is already responsible for a degradation of the water quality, particularly because of the application of de-icing salts on roads in winter (Sérodès et al., 2021). Concerns about the preservation of the water availability and quality in the future, and especially the groundwater contribution to the rivers of the catchment, emerged recently. However, only a few examples of catchment scale determination of groundwater fluxes to streams are reported in the literature. Most of these studies rely on the use of mathematical filters, which can provide estimates of groundwater inflows but are severely lacking in physical meaning (Eckhardt, 2008). On the other hand, monitoring of environmental tracers in rivers, such as water stable isotopes or electrical conductivity, revealed to be the best tools to quantify groundwater inflows. Traditionally, the tracer approach is used in small, forested, undisturbed catchments (Klaus & McDonnell, 2013). Their use in larger and partially urbanised catchments has still to be developed, since there are few works reported in the literature in these settings (Saraiva Okello et al., 2018; Uhlenbrook et al., 2002). The hydrograph separation using environmental tracers in a catchment similar to the Saint-Charles River water intake still remains an open question.

~~

Additionally, groundwater timescales proved to be a fundamental metric to understand groundwater quality evolution from the recharge zones to the discharge zones in conjunction with soil occupation (Purtschert, 2008). Baseflow-dominated streams can be seen as natural, weighted integrator of catchment water transit times since they intersect groundwater flowpaths from upstream to downstream (Solomon et al., 2015). The knowledge of the groundwater inflows residence times is thus a relevant metric to analyse the resilience of baseflow-dominated rivers to changes in groundwater quantity and quality. Yet, only a few studies reported the use of environmental tracers to determine baseflow residence times (Humphrey et al., 2024; Jensen et al., 2022; Sanford et al., 2015; Solomon et al., 2015; Stolp et al., 2010). The application of tracers is generally complicated by the fact that most of them are in gaseous form and readily interact with the atmosphere that is in contact with the streams surface. To our knowledge, tracer methods were never used under “freezing” conditions, *i.e.* in ice-covered rivers. The study of residence times of winter baseflow takes its whole relevance at the study site, since (i) the streams are expected to be baseflow dominated, and (ii) the cold temperatures and the presence of an ice cover limit river – atmosphere exchanges, which preserves the groundwater signal in the rivers.

To summarize, three main goals are identified and addressed in this PhD thesis:

- (i) the development of new and innovative artificial tracers-based methods for the characterization of groundwater – surface waters interactions in vulnerable catchments.
- (ii) the quantification of groundwater inflows to streams in a meso-scale, partially urbanised, snowmelt influenced catchment used for the production of drinking water.
- (iii) the description of the catchment water residence times inferred from measurements in river baseflow.

~~

The thesis is organized as follows:

- Chapter 1 provides a detailed review of the methods for the quantification of groundwater – surface water interactions as well as the concepts and methods of characterization of water residence times in catchments. This introductory chapter ends with a presentation of the research problematic, and the detail of the research objectives addressed during this PhD work.
- Chapter 2 presents the methods developed for improving the characterization of groundwater – surface water interaction. This work is presented through two research papers, *Article 1* and *Article 2*. The potential of isotopic tracers, ^2H and ^{37}Cl , for the precise, discrete determination of stream discharge in vulnerable catchments is discussed in the first article. *Article 2* describes a new method for the sampling of dissolved gases using stainless steel, reusable samplers and the combination of mass spectrometry (miniRUEDI) and gas chromatography to determine the contents of major, noble and anthropogenic trace gases from a single sample. This work has serious implications regarding the use of inert gaseous tracers (ex: He , SF_6) in artificial tracing experiments in groundwaters and surface waters.
- Chapter 3 focuses on the catchment of the Saint-Charles River surface water intake. It first includes the presentation and interpretation of water stable isotopes results obtained during the PhD. These data are used to show that groundwater and surface water interact closely within the studied catchment. A detailed comprehension of the spatio-temporal controls on isotope signatures in precipitation is also provided (ex: first altitudinal gradient in Québec). This chapter also provides *Article 3*, which discusses the use of an exceptional decade-long monitoring series of major ions and trace metals at the outlet catchment. These data allow to perform a robust hydrograph separation and to quantify groundwater contribution to the river between 2013 and 2023. In addition, the dissolved silica contents, measured during the year 2023, are used to describe the transient nature of the catchment water residence times.

- Chapter 4 describes how winter baseflow mean residence time can be determined using a suite of groundwater residence time tracers. The winter baseflow of the Nelson River, one of the main tributary of the Saint-Charles river, was studied under the light of a unique combination of environmental tracers (^3H , noble gases, CFCs, SF_6 and ^{85}Kr), and deliberately injected tracers (He and SF_6). This study is the object of *Article 4*. One of the main particularities of this work is the fact that it was performed in winter, when the river was partially ice-covered. These field conditions have serious implications regarding the likelihood of success of application of such method and the method is very promising for most streams in Canada, especially under freezing conditions.
- The last part of the manuscript is the conclusion, presenting the general outcomes and contributions of this PhD work. The limitations and research perspectives are also discussed at the end of this chapter.

In addition, other works carried out during the PhD are presented in the annexes. Appendices A illustrates the progression of the already well-known headspace method (Busenberg & Plummer, 2010; Sliwka et al., 2004) for the analysis of SF_6 (and CFCs) in both environmental samples and spiked samples (artificial tracing experiments), carried out at the Hydro-Sciences UQAM ETS laboratory. This method was particularly useful to measure the dissolved SF_6 (and CFCs) in samples presented in *Article 4*. Appendix B and Appendix C include the description of the study site, the Saint-Charles River water uptake catchment, and the presentation of the monitoring program of stable isotopes and geochemical parameters that took place during the PhD.

~~

CHAPTER 1 Current state of the art: the links between catchment vulnerability, groundwater inflows to streams and water residence times

1.1 Résumé du Chapitre 1 en français

Ce premier chapitre comporte une revue de littérature permettant d'inscrire le projet de doctorat dans son contexte global et local ainsi que sa pertinence. Il s'organise autour de deux thématiques principales : la reconnaissance et la caractérisation des relations nappe/rivière et le temps de résidence de l'eau dans les bassins versants.

A échelle globale, les eaux de surface sont dominées par les apports d'eaux souterraines. Ceci est particulièrement vrai sous climat tempéré et humide où les rivières sont pérennes. Ces apports rendent de nombreux services écosystémiques en soutenant le débit de base, qui constitue une ressource cruciale tout au long de l'année en soutenant la qualité des eaux de surface. Toutefois, les changements climatiques globaux et l'urbanisation continue menacent la disponibilité et la qualité des ressources en eau souterraine, ce qui, à terme, constitue un enjeu pour les eaux de surface. Au Québec, la récente législation sur les analyses de vulnérabilité des prises d'eau potable de surface ne considère pas encore ces apports, bien qu'il soit attendu que ces derniers dominent l'écoulement de surface d'après la littérature scientifique. De nombreuses méthodes existent pour quantifier ces apports, par nature diffus : les méthodes à base physique (ex : application de la loi de Darcy, intégration de la vitesse de l'eau sur la surface de l'écoulement), et les méthodes par traçage (ex : suivi du panache de traceur en rivière pour mesure du débit). Ces dernières sont particulièrement pertinentes puisqu'elles tiennent directement compte des hétérogénéités naturelles des hydrosystèmes.

Conceptuellement, l'eau dans la rivière a traditionnellement été considérée comme un mélange d'eau de ruissellement– écoulement rapide – et d'eau souterraine – écoulement lent – dont les proportions varient dans le temps et l'espace. Ce modèle conceptuel a cependant ses limites, étant donné que chaque molécule d'eau participant à l'écoulement de surface est potentiellement arrivée dans le bassin versant à un instant différent. Cela conduit inmanquablement à un

« spectre d'âge » de l'eau alimentant la rivière, et non pas une simple dualité. Le temps de résidence de l'eau dans un bassin versant est défini comme étant le temps écoulé entre l'arrivée de l'eau sous forme de précipitations et sa sortie via l'exutoire du bassin, *i.e.* la rivière. C'est une métrique fondamentale puisqu'il décrit comment le bassin versant stocke et libère l'eau et les solutés, ce qui en retour contrôle les cycles biogéochimiques, la persistance des contaminants et la résilience des ressources en eau face aux forçages anthropiques. Il est donc particulièrement pertinent de déterminer le temps de résidence des apports d'eaux souterraines aux rivières, en particulier lorsque ces dernières sont dominées par ces apports comme c'est le cas dans l'Est du Canada (Beck et al., 2013). Les traceurs d'âge des eaux souterraines récentes (quelques décennies) sont principalement sous forme gazeuse, ce qui limite leur application en rivière. La méthodologie par bilan massique des gaz dissous se révèle alors la plus pertinente pour caractériser le signal des eaux souterraines alimentant la rivière en traceur et leur temps de séjour, à l'échelle du bassin versant complet.

Le Chapitre 1 comporte également la présentation des trois grands objectifs de ce travail de doctorat qui découlent de cette revue de littérature :

- (i) Le développement de méthodes pour faciliter la mesure et la caractérisation des relations nappe/rivière, en particulier dans les bassins versants vulnérables. Les méthodes décrites ici se basent sur l'utilisation de traceurs, isotopiques et gazeux. Ces travaux sont rapportés dans deux articles scientifiques (*Article 1* et *Article 2*).
- (ii) La quantification des apports d'eau souterraine en rivière au cours du temps dans un bassin versant utilisé pour l'eau potable. Une approche se basant sur l'utilisation de nombreux traceurs a été adoptée pour répondre à cet objectif (isotopes stables de la molécule d'eau, ions majeurs, métaux traces et silice dissoute). Ce travail fait l'objet d'un article scientifique (*Article 3*).
- (iii) Enfin, la détermination des temps de séjour du débit de base soutenant les rivières du bassin versant. Il s'agit de la première fois que la méthode de bilan massique de

traceurs gazeux de datation en rivière est utilisée au Canada. Cette expérience de terrain est rapportée dans un article scientifique (*Article 4*).

1.2 The groundwater – surface waters continuum

Groundwater is an essential resource, playing a major role in both hydrological and human systems (Giordano, 2009). It represents more than 99% of the global liquid freshwater. Currently, half of the world's population is directly sustained by groundwater (UNESCO, 2022). The resource is also essential for global food security as it is used for irrigation in most countries of the world (Aeschbach-Hertig & Gleeson, 2012; de Graaf et al., 2019). Often, extraction rates of groundwater are superior to the replenishment rate leading to a worldwide aquifer depletion trend (Aeschbach-Hertig & Gleeson, 2012; Barlow & Leake, 2012; Konikow & Kendy, 2005; Scanlon et al., 2012). This global situation have adverse impacts such as water access issues in a lot of developed and less-developed countries, global decrease of surface waters discharge, decrease of well yields, rise of pumping costs, decrease of water quality and perennial ecological damages (de Graaf et al., 2019; Konikow & Kendy, 2005).

1.2.1 Global importance and roles of groundwater inflows to streams

1.2.1.1 Global fluxes of groundwater to streams

Historically, surface waters and groundwater have been considered as separate hydrological compartments (Kalbus et al., 2006). However, groundwater and surface waters exchange intimately, as water fluxes can occur in two possible ways depending on the hydraulic gradient: either groundwater can seep from the streambed to the river, or stream water can infiltrate through the streambed and rejoin groundwater. Only a few studies have mapped the global distribution of baseflow importance to total streamflow (BFI: baseflow index) (Beck et al., 2013; Xie et al., 2024). These studies used hydrograph separation to determine the BFI in observation basins (see section 1.2.3). Beck et al. (2013) compiled data from more than 3 300 discharge stations over the world and applied neural network analysis to estimate the global distribution of the baseflow fraction. Xie et al. (2024) compiled discharge data from more than 15 000 discharge

stations in relatively small basins with the use of Earth system models. They found that the global river flow is dominated by groundwater inflows, with BFI values of 0.71 and 0.59 ± 0.07 .

These results highlight the global active role played by groundwater in the surface water cycle. In addition, the BFI is as a crucial metric in hydrology, reflecting the role of climate, geology, and anthropogenic factors in controlling streamflow availability and quality. A global understanding of the factors influencing BFI is essential for effective water resource management, particularly in the context of climate change and increasing water demand.

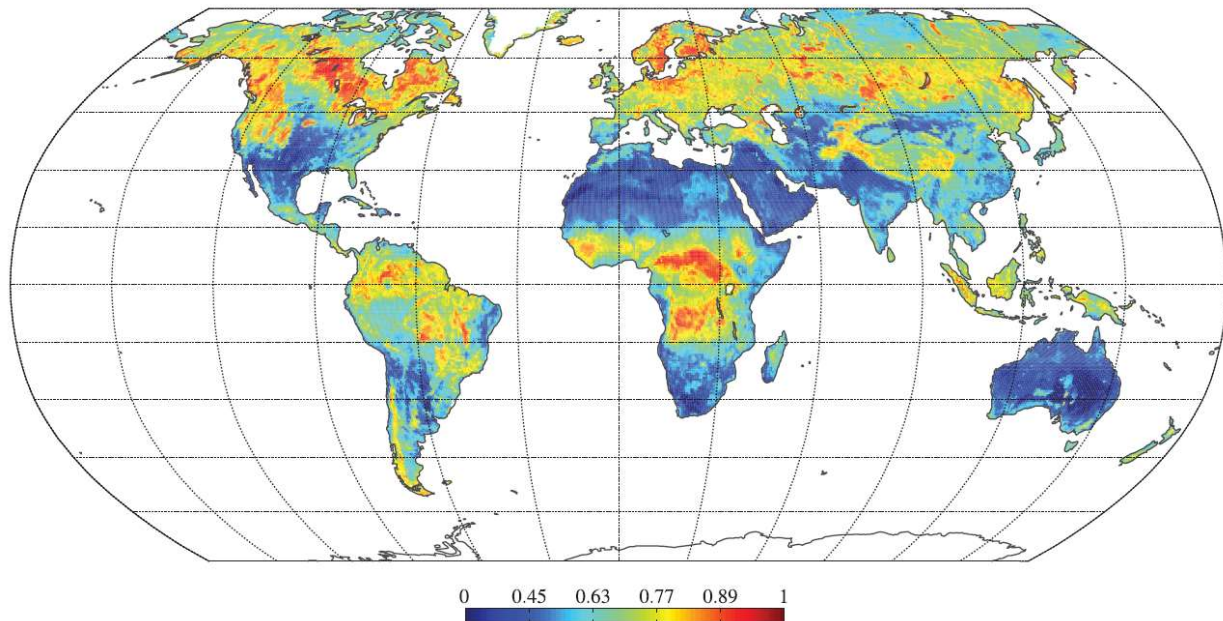


Figure 1: Global map of modelled BFI values. (Beck et al., 2013).

1.2.1.2 Primary factors affecting the baseflow index

The global variability in the BFI is a result of the complex interaction of climatic, geological, and anthropogenic factors. A nuanced understanding of these controls is essential for predicting how baseflow contributions may evolve under changing environmental conditions. This knowledge is particularly important for managing water resources in regions facing hydrological stress and ensuring sustainable ecosystem functioning:

- Climatic variables, particularly precipitation and evapotranspiration, significantly influence the BFI. Regions with consistent and moderate precipitation patterns tend to exhibit higher BFIs because the steady groundwater recharge conditions are responsible for shallow groundwater levels that enhance the groundwater contributions to stream. Conversely, arid and semi-arid regions, characterized by intermittent and intense rainfall, and a thick unsaturated zone, often have lower BFIs due to limited infiltration and rapid surface runoff (Beck et al., 2013; Xie et al., 2024). Temperature also plays an indirect role through its effect on evapotranspiration rates. High temperatures increase evapotranspiration, reducing soil moisture availability and consequently limiting groundwater recharge (Constantz, 1998). In colder environments, seasonal snowmelt can temporarily elevate baseflow contributions, though these contributions are highly variable and depend on the timing and magnitude of meltwater input (Barnett et al., 2005).
- Soil occupation characteristics, such as land cover, vegetation and soil and geological characteristics, play a significant role in controlling groundwater – surface water interactions and the BFI:
 - o Vegetation cover influences the BFI by modulating infiltration and evapotranspiration processes. Dense forests typically enhance infiltration due to the relatively high soil permeability and reduced surface runoff (Brujinzeel et al., 2002). However, forests also increase evapotranspiration, which has an adverse impact over groundwater recharge (Calder, 2005).
 - o Soil texture plays an important role in controlling BFI values. sandy soils with high permeability allow greater groundwater recharge compared to clayey soils, which are more prone to surface runoff (Rawls et al., 1982). Permeable geological formations, such as sandstone and limestone, facilitate higher infiltration and groundwater storage, leading to elevated BFIs. Conversely, low permeability geological formations, such as igneous rocks or shales restrict infiltration, resulting

in lower BFIs (Collischonn & Fan, 2013; Eckhardt, 2005; Fan et al., 2013; Freeze & Cherry, 1979; Taylor et al., 2012).

- The slope and relief of a watershed influences the partitioning of precipitation between surface runoff and groundwater recharge. Flat or terrains with low slopes facilitate infiltration which can enhance BFI, while steeper terrains increase surface runoff, which reduces the opportunity for groundwater recharge and leads to lower BFIs (Gonzales et al., 2009; Montgomery et al., 2002).

1.2.1.3 Ecological roles played by groundwater inflows

Groundwater inflows to rivers play an essential ecological role, as it shapes the physical, chemical, and biological characteristics of freshwater ecosystems (Boulton et al., 1998; Boulton & Hancock, 2006; Gleeson & Richter, 2017; Hancock et al., 2005; Hayashi & Rosenberry, 2002; Winter et al., 1998). The baseflow contributes to streamflow all the year and especially during dry periods, ensuring the persistence of aquatic habitats and the organisms that depend on them (Boulton et al., 1998; Boulton & Hancock, 2006; Hayashi & Rosenberry, 2002). By providing a consistent source of water, groundwater inputs help stabilize thermal regimes, which is particularly beneficial in maintaining suitable conditions for fish species sensitive to temperature and dissolved oxygen concentration (Constantz, 1998). Groundwater inflows create transitional zones where distinct ecological communities interact. These zones are often associated with a high biodiversity due to the mix of surface water and groundwater conditions, providing shelter for specialized organisms (Hancock et al., 2005). Additionally, hyporheic zones, formed by the mixing of groundwater and surface water, play a crucial role in nutrient cycling and organic matter decomposition (Boulton et al., 1998). Groundwater inflows can also buffer rivers from anthropogenic and climatic stressors. During periods of drought or reduced surface runoff, groundwater is a critical resource, sustaining ecosystem functions and mitigating the impacts of hydrological variability (Sophocleous, 2002). This buffering capacity is increasingly important in the context of global climate change, where altered precipitation patterns and increased water abstraction pose significant threats to freshwater ecosystems (Tockner et al., 2009).

Groundwater inflows are crucial to the health and functioning of riverine ecosystems, as they influence not only the availability of surface waters but also their quality and biodiversity. Both the spatial and temporal quantification, distribution and geochemical characterization of the groundwater inflows and the management of their quality is essential for sustaining the ecological roles and the ecological integrity of surface waters, particularly in a changing environmental context.

1.2.1.4 Effects of anthropogenic forcings on groundwater and baseflow availability and quality

Anthropogenic forcings, such as global climate change and urbanisation, pose a significant threat to the availability and quality conservation of water bodies by affecting the natural hydrological cycle. Since a few decades, the scientific community has demonstrated a lot of interest into assessing the effects of these disturbances to surface waters (Gleick, 1989; Green et al., 2011; Taylor et al., 2012).

1.2.1.4.1 Global population growth and increase of urbanisation effects

Global population growth, coupled with increasing urbanisation pose a significant threat to natural dynamics, resource availability and environmental quality (McGrane, 2016) and impacts every component of the water cycle at every scale. Water balance is heavily modified by the introduction of impervious surfaces, the removal of deep-rooted vegetation and the alteration of the subsurface drainage network in the urban landscape (Antrop, 2004; Haase, 2009). A lot of authors tried to assess the watershed scale response to urban development, particularly by quantifying the modification in runoff (Rose & Peters, 2001), but also the change in evapotranspiration, the change in aquifer recharge (Lerner, 2002; Paul & Meyer, 2001; Rose & Peters, 2001; Schoonover et al., 2006) or the groundwater flow dynamics due to pumping (Konikow & Kendy, 2005). The quantitative changes in the water cycle have also large consequences on the qualitative state of water (Burri et al., 2019; Gasperi et al., 2014; MacDonald et al., 2003; Muller et al., 2020) with new controls on water quality induced by human presence.

Urbanisation is inherently associated with a major change in land use. Accordingly, natural pathways of water are modified by the presence of impervious landscapes and the expansion and/or alterations of artificial drainage networks (Haase, 2009; McGrane, 2016). Hence, direct infiltration is considered to decrease. Nevertheless, the impact of urbanisation on subsurface flow dynamics, that are recharge and groundwater – surface water interactions, is still subject to debate (Bhaskar et al., 2016).

Baseflow reduction related to increase in total impervious areas is reported in the literature (Hardison et al., 2009; McGrane, 2016; O'Driscoll et al., 2005). Induced changes in groundwater recharge rates are found to have follow-on effects on baseflow in urban rivers (Paul & Meyer, 2001; Rose & Peters, 2001; Schoonover et al., 2006). Rose & Peters observed a decrease in the urban groundwater level relative to non-urban wells at the decade scale. It is attributed to a long-term decrease in groundwater recharge due to urbanisation. A decrease in baseflow recession constant of more than 35% in urban watersheds is also reported. This parameter, used to characterize the declining rate of baseflow during low flow periods, indicates that a lower quantity of groundwater discharges from surrounding aquifers to the urban rivers (Rose & Peters, 2001) meaning that recharge decreased. Other studies emphasize a recharge increase in urban areas due to (i) decrease in evapotranspiration (Klöcking & Haberlandt, 2002) and (ii) the leakage from worn urban water infrastructure (Barron et al., 2013; Lerner, 2002). Two factors seem to control direct contributions to subsurface flows: (i) the spatial expanse of the urban infrastructure network and (ii) the age and integrity of the sewage infrastructure (McGrane, 2016). Lerner (2002) suggests that the importation of water in cities represents a large supplementary amount of water, which is an opportunity for more recharge. Leakage from worn pipes is identified as the main process of artificial urban recharge, with leak rates commonly comprised between 20-25% and occasionally up to 50% (Lerner, 1986, 2002).

Groundwater quality can be affected by urbanisation and global population growth. Three processes may pollute groundwater, associated with different types of pollutants (Burri et al., 2019; Khatri & Tyagi, 2014): (i) direct addition of polluted wastewater from worn infrastructures,

(ii) infiltrations of polluted water from surrounding surface waters, downstream of wastewater treatment plants for example and (iii) recharge of aquifer by low quality water (e.g.: infiltration of polluted runoff, leaching from solid and liquid waste). Runoff, particularly during snowmelt in snow-dominated regions, is well known for conveying pollutants in urban areas (Muller et al., 2020). Vehicular transportation associated with release of hydrocarbons and heavy metals, road maintenance (de-icing salt road, littering (microplastics, trace metals, pollutant of emerging concern) and industrial activities are the main sources of stormwater pollution (Burri et al., 2019; Gasperi et al., 2014; Hahladakis et al., 2018; Muller et al., 2020; Sérodes et al., 2021; Tremblay et al., 2024). Nitrates, hydrocarbons, pesticides and pharmaceutical contaminations are among the most common types of groundwater pollution in both agricultural and urban areas.

Care must be taken to understand river and groundwater interactions when planning urban water management strategies in urban areas. Effects of urbanisation on groundwater and their interactions with surface waters are generally still not well understood (Barron et al., 2013), particularly because of the complexity of the urban environment and use of old and new urban drainage systems (McDonald et al., 2011; Soulsby et al., 2014), but also by the spatial and temporal complexity of groundwater – surface water interactions (Brunner et al., 2017).

1.2.1.4.2 Global climate change effects

Global climate change, the alteration of long-term climate patterns, caused by increasing atmospheric concentrations of greenhouse gases, has already an impact on ecosystems, economies, and communities. Hydrological cycle in particular is severely affected, with changes in quantity and quality of water resources (Gleick, 1989; Kundzewicz, 2008). Even though, impacts of climate change on surface water bodies have been extensively studied (Scanlon et al., 2012), its impacts on recharge mechanisms and groundwater quantity and quality are still poorly understood (Green et al., 2011). This is partly because groundwater systems reactions to seasonal and multi annual changes in climate are less visible than in surface waters.

Many studies emphasize the importance of actual recharge rates and mechanisms knowledge to assess the impact of climate change on groundwater resources (Amanambu et al., 2020; Arnoux, Barbecot, Gibert-Brunet, Gibson, & Noret, 2017). Indeed, climate is the first control on spatio-temporal recharge variability. In temperate and cold climates, recharge response to climate change will be linked to changes in evapotranspiration associated with global warming and increased runoff due to earlier snowmelt in cold climates (Okkonen & Kløve, 2012). The latter undoubtedly results in a decrease in recharge, while effects of temperature rising on evapotranspiration may be attenuated by higher humidity. Meixner et al. (2016) emphasized that climate change effect on recharge depends on recharge mechanisms: as examples, in the United States, diffuse recharge is expected to decrease due to temperature and evapotranspiration increase, but focused recharge is expected to increase due to increase in rainfall intensity.

These recharge regime changes, coupled with increasing human groundwater withdrawal, are expected to have a strong effect on the water table (Barlow & Leake, 2012). Many studies conclude that it has an indirect strong effect on groundwater and surface water interactions (Amanambu et al., 2020; Dragoni & Sukhija, 2008). Globally, these interactions are influenced by climate, and are modified by topography, geology and human withdrawal (Amanambu et al., 2020). In a groundwater depletion context, its discharge to surface bodies is expected to decrease, leading to a baseflow reduction threatening life in surface ecosystems during low-flow periods. The future trends in precipitation and temperature will have an influence on baseflow generation and the magnitude and timing of groundwater discharge to surface waters (Solder et al., 2016). For example, earlier snowmelt in winter, leading to an increase of runoff can be the cause of late summer baseflow reduction (Ahiablame et al., 2017; Tremblay et al., 2024). However, if higher recharge rates occur and compensate possible higher abstraction rates, groundwater fluxes to surface waters may increase as it was highlighted in New Brunswick, Canada (Kurylyk et al., 2014).

Two types of climate change impact on groundwater quality were highlighted in the literature (Amanambu et al., 2020): change in solute flushing to groundwater and over-exploitation of

coastal aquifers. In a context of increase in rainfall intensity, surface contaminants may be flushed to groundwater in higher quantities. In snow dominated climates, the higher snowmelt due to winter temperature increase may be a source of contaminants in the soil, to the saturated zone (Bloomfield et al., 2006). The increase of groundwater temperature is a direct consequence of global warmer climate. In river baseflow dominated regions, the temperature increase of baseflow may also threaten the life of species relying on colder groundwater influxes (Menberg et al., 2014; Riedel, 2019).

1.2.2 Determination of the spatial distribution of groundwater inflows to streams

Even though groundwater – surface water interactions are important in a diversity of climates as discussed in section 1.2.1.4.2, they can display a strong temporal and spatial variability in the same riverine system. Groundwater – surface water interactions are difficult to quantify and model, and a need for better comprehension is pointed out in the literature (Brunner et al., 2017). The methods for the quantification are already thoroughly reviewed by several authors, for example in Brunner et al. (2017) and in Kalbus et al. (2006). They are usually separated into two categories: the physical methods and the tracer-based methods (Figure 2).

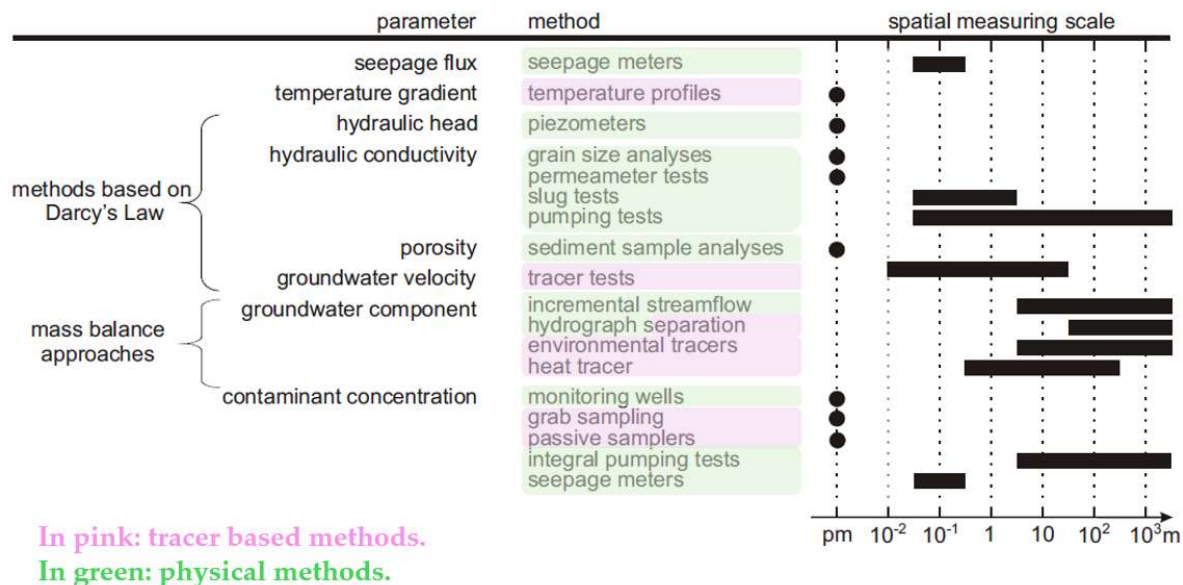


Figure 2: Scales of application for different methods of groundwater – surface water interactions characterization and quantification. Modified from Kalbus et al. (2006).

Physical methods rely (i) on the application of Darcy's law via the measurements of surface waters and adjacent groundwater levels, to quantify the water exchange flux and its direction (*i.e.* gaining reach or losing reach), and (ii) on the use of seepage meters placed on the streambed to quantify the seepage fluxes (Brunner et al., 2017; Kalbus et al., 2006). Punctual measurements of river discharge at various locations can also help to estimate the exchanging fluxes in small catchments, however this method may have large uncertainties and may not be adequate for regional scale catchments applications. As pointed out by Cook (2013), many of the physical methods are difficult to upscale, to the reach or catchment scales, because of the high spatial heterogeneity of catchments, streambed properties and aquifer properties (*e.g.* hydraulic conductivity). However, these limitations can be largely overcome by using environmental tracers (Cook, 2013; Cook & Herczeg, 2000; Gonzales et al., 2009; Kipfer et al., 2002; Klaus & McDonnell, 2013; Leibundgut et al., 2009; McGuire & McDonnell, 2006; Saraiva Okello et al., 2018; Uhlenbrook et al., 2002; Zhang et al., 2013).

Environmental tracers are substances that are naturally present, often globally, in the environment in trace amounts (*e.g.* ions, isotopes or gases). Some of them are particularly useful to trace the global and local water cycles, water fluxes and interactions between different hydrological compartments or the hydrobiogeosphere continuum (Clark & Fritz, 1997; Cook & Herczeg, 2000; Jasechko, 2019; Sprenger et al., 2019). Their contents in streams can be modified by a variety of processes such as: dilution or concentration due to groundwater or tributaries inflows, hyporheic exchanges, evaporation, production within the streambed, radioactive decay for radioactive tracers, bacterial consumption, air/water exchanges, etc. (Cook et al., 2003). In other words, physical heterogeneities and chemical processes are encapsulated in the streams tracers contents spatial and temporal variations, making them valuable for reach scale or catchment scale determination of groundwater inflows (Solomon et al., 2015). They are thus very useful to trace back all these processes while considering the natural and ubiquitous heterogeneities of catchments.

The *mass-balance approach* has been widely applied to determine the spatial (here, longitudinal and/or transversal) distribution of groundwater inflows to streams. The equation governing such mass balance is typically under the following form (Cook, 2013):

$$Q \frac{\partial c}{\partial x} = q_{gw}(c_{gw} - c) + wEc - kw(c - c_a) - dw\lambda c \quad \text{Eq. 1-1}$$

where c is the tracer concentration in the stream [ML^{-3}], c_{gw} is the tracer groundwater concentration [ML^{-3}], c_a is the tracer solubility equilibrium concentration with the atmosphere [ML^{-3}], Q the total river discharge [L^3T^{-1}], q_{gw} the groundwater inflows per unit of river length [L^2T^{-1}], E the evaporation rate [LT^{-1}], w the river width [L], d the river depth [L], λ the radioactive decay constant in case of a radioactive tracer [T^{-1}]. Terms accounting for the exchange with the hyporheic zone as well as the direct contribution of tributaries can also be added if needed (Cook, 2013; Lefebvre et al., 2015). The Eq. 1-1 is discretized (Figure 3) for the whole river length and the groundwater inflows are determined by fitting modelled tracer concentrations to field measurements.

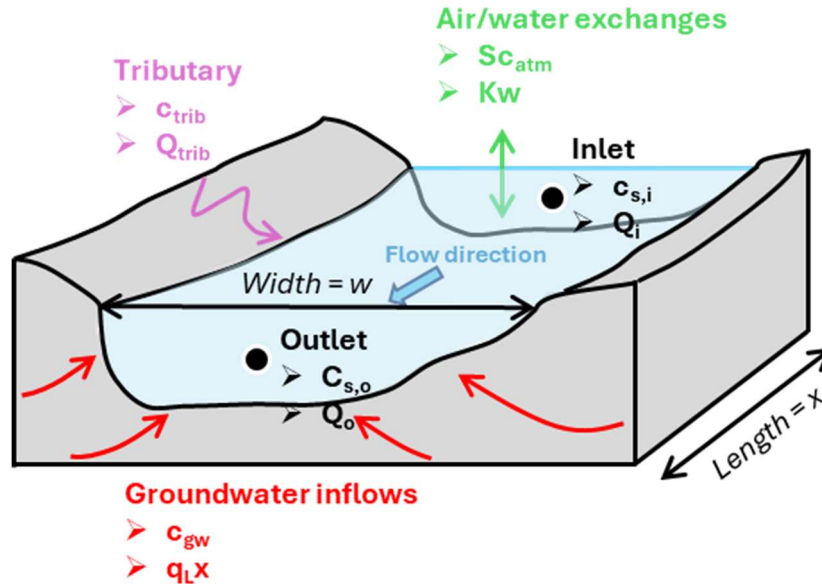


Figure 3: Discretization scheme of a river reach used for an inert volatile tracer mass-balance.

The radioactive short-lived ($t_{1/2} = 3.8$ days) noble (inert) gas radon-222 (^{222}Rn) has been extensively used for tracing and quantifying the spatial distribution of groundwater inflows to streams (Cook, 2013; Cook et al., 2003; Cook et al., 2006; Cranswick et al., 2014; Lamontagne et al., 2015; Lefebvre et al., 2015). Other tracers such as electrical conductivity and major ions can also be used in conjunction with radon (see Figure 4) (Cook, 2013; Cook et al., 2003).

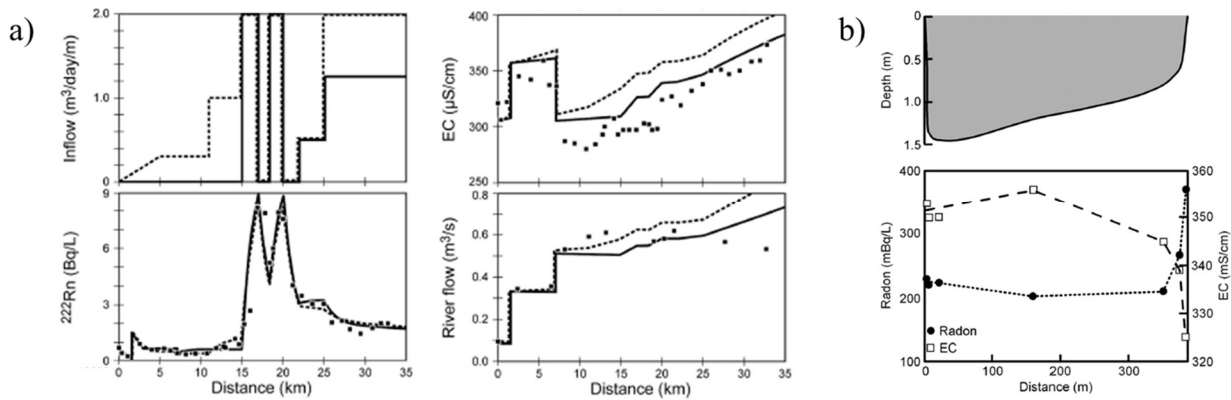


Figure 4: a) Numerical simulations (the continuous line considers hyporheic exchanges while the dashed line does not) of tracer concentrations and river flow in a tropical river (modified from Cook et al. (2003)). b) Transversal cross section of depth and tracers indicating groundwater discharge near the right bank where the electrical conductivity (EC) is low and the radon activity is higher (Cook, 2013).

The application of tracer-based methods main drawbacks include:

- The difficulty to accurately estimate the groundwater inflow concentration and its changes in space and time
- The possibility to observe a too small difference between the tracer concentration in groundwater and in the streams (Cook, 2013; Klaus & McDonnell, 2013).
- The spatial resolution of such methods can also decrease when the variations in river water concentration are either low by themselves or caused by other processes that compete with the effect of groundwater inflows. Such difficulties arise for example with the use of dissolved gaseous tracers that exchange with the atmosphere.

- Some tracers that are deliberately injected may have an adverse effect on the stream ecological functioning and the water quality (Hudson & Fraser, 2005). This is the case for example for salts and fluorescent dyes.
- The water sampling typically occurs once, in one point (in the middle of the stream for example). Issues of lateral representativity can be problematic where the mixing is not sufficient.
- The collection, duplication and storage of samples can become very costly.

Some of these drawbacks can be advantageously addressed with the recent development of field equipment, for example the portable mass spectrometer miniRUEDI dedicated to the measure of dissolved (noble) gases in the environment (Brennwald et al., 2016; Brennwald et al., 2020), facilitating the determination of tracers concentration in the environment, and enabling unprecedented time resolution. Mass spectrometry based on spectroscopy can also be used for *in situ* measurements of water stable isotopes (Klaus & McDonnell, 2013).

1.2.3 Determination of the temporal dynamics of groundwater inflows to streams

1.2.3.1 Hydrograph separation using mathematical filters

Hydrologists have been interested in partitioning event and pre-event (soil water, groundwater) waters from storm hydrographs for decades (Hubert et al., 1969). Mathematical models can be used to identify the baseflow contribution. They consist of simple analytical solutions that work as low-pass filters (Chapman, 1999; Duncan, 2019; Eckhardt, 2005; Lyne & Hollick, 1979). Their main advantage is that they “only” require river discharge data and can provide quick baseflow estimates at the same time resolution that the discharge data (ex: daily). For example, Chapman’s filter is under the following form:

$$b(t) = \frac{\alpha}{2 - \alpha} b(t - 1) + \frac{1 - \alpha}{2 - \alpha} q(t) \quad \text{Eq. 1-2}$$

Where α is the recession constant, b is baseflow, q is total flow. b and q are a function of time t . In the Eq.1-2, the value of baseflow at time t is linked to its value at the previous time step ($t-1$), the total streamflow at time t and the recession parameter. Rimmer and Hartmann (2014) provide three methods to determine the recession constant. This simple one-parameter mathematical filter assumes that there is a linear relationship between the groundwater storage and the streamflow, leading to exponential decay of streamflow during recession. This hypothesis is shown to be a very good approximation for typical recession periods up to the order of 10 days (Chapman, 1999). Later, Eckhardt (2005) showed that Chapman's filter is a particular case of a two parameters mathematical filter that has the following form:

$$b(t) = \frac{(1 - BFI_{max})\alpha}{1 - \alpha BFI_{max}} b(t - 1) + \frac{(1 - \alpha)BFI_{max}}{1 - \alpha BFI_{max}} q(t) \quad \text{Eq. 1-3}$$

The Eq. 1-3 follows the same hypotheses and has a second parameter, BFI_{max} which represents the maximum value of the baseflow. This parameter cannot be calculated and can only be calibrated against environmental tracer data (Eckhardt, 2005). For example, Saraiva Okello et al. (2018) used a temporal monitoring of punctual electrical conductivity measurements to calibrate an Eckhardt filter, allowing for a continuous baseflow separation.

1.2.3.2 Tracer-based hydrograph separations

The different water masses involved in streamflow generation may have very different tracer concentrations (ex: the chloride content in precipitation is much lower than the chloride content in groundwater, and the chloride content in the stream water would be a function of the mixing ratio of these two components – see Figure 5). If these concentration differences are accounted for and their temporal variation known, they can be used to partition the hydrograph into several components.

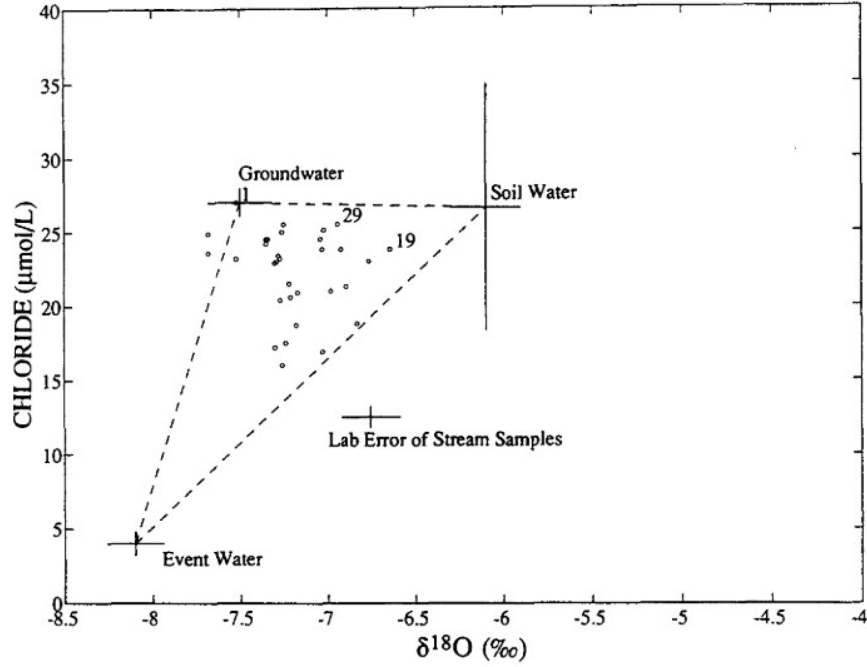


Figure 5: Mixing diagram of chloride and $\delta^{18}\text{O}$ showing that stream samples variability is explained when considering three end-members: event water, groundwater and soil water (Bazemore et al., 1994).

Water stable isotopes $\delta^2\text{H}$ and $\delta^{18}\text{O}$ have been extensively used to perform such hydrograph separation under the following assumptions: (i) event and pre-event waters have a significantly different isotopic signal, (ii) spatial and temporal variations in event and pre-event isotopic signal can be accounted for, (iii) vadose zone contribution is negligible or with the same isotopic signature than groundwater, and (iv) surface storage is minimal compared to the streamflow (Klaus & McDonnell, 2013). Other “inert” tracers can be used such as chloride, cations, electrical conductivity and dissolved silica depending on catchment configuration (Klaus & McDonnell, 2013). The decomposition of the hydrograph into two, three or more components (e.g. direct runoff, groundwater and soil water) is performed using the following mass-balance equations:

$$\begin{cases} Q(t) = \sum_{i=1}^n Q_i(t) \\ C(t)Q(t) = \sum_{i=1}^n C_i(t)Q_i(t) \end{cases} \quad \text{Eq. 1-4}$$

where $Q(t)$ and $C(t)$ are the total discharge and stream tracer concentration at time t and $Q_1, Q_2, \dots Q_n$ and $C_1, C_2, \dots C_n$ are the discharge and tracer concentration of the n different end-members respectively.

One of the most striking and important conclusion of tracer-based hydrograph separation is that they show that pre-event water, previously stored in the catchment, is usually the main contributor to streams even during storms (Gonzales et al., 2009; Klaus & McDonnell, 2013; Ladouche et al., 2000). This means that the water feeding rivers during and after storm events is mostly water that has already spent time within the catchment, days to months for soil water, and up to decades for groundwater (Jasechko et al., 2016). This also puts into perspective the substantial and active role played by groundwater in surface hydrology.

In addition, the tracer-based hydrograph separation can be very useful for the calibration of mathematical baseflow separation models (Chapman, 1999; Duncan, 2019; Eckhardt, 2005, 2008; Saraiva Okello et al., 2018; Zhang et al., 2013). However, the choice of the different end-members is the critical point of any tracer-based hydrograph separation and its application can be challenging when the end-members vary in time and space (Uhlenbrook et al., 2002). This explains why the method has been traditionally used in small, usually forested, catchments ($<1 - 10 \text{ km}^2$), and why the examples for meso-scales catchments are scarce.

1.3 Water residence times in catchments

1.3.1 Concepts and definitions

Water timescales within catchments are described through many definitions and concepts. The first is the concept of *water residence time*, defined as the time elapsed since it entered the catchment within a flow system. The *water transit time* is defined as the time between the entrance of the water parcel and its exit of a flow system (McGuire & McDonnell, 2006). Since any water sample is a combination of water molecules that potentially all entered the catchment at a different time, the concept of the *mean transit time* (MTT) or, better, the *transit time distribution* (TTD) are particularly relevant (Suckow, 2014). Conceptually, the TTD corresponds to the restitution

function of an instantaneous conservative tracer input over the entire catchment area assuming no background concentration and represents the cumulative fraction of the sample as a function of transit time. Alternatively, the catchment transit time distribution (CTTD) is the age distribution of all water outflowing from a catchment. The TTD (and the CTTD) is a fundamental and critical metric because it describes how catchments retain and release water and solutes which, in turn, control biogeochemical cycles (*i.e.* water quality – see section 1.2.1.3), contamination persistence but also water resources resilience to anthropic forcings (McGuire & McDonnell, 2006; Purtschert, 2008).

Groundwater dating is particularly relevant for water resources management as there are strong links between groundwater timescales and its vulnerability. As pointed out by Wachniew et al. (2016), the relevance of vulnerability assessments rely on their efficiency to describe time lags associated with contaminant transport. If the residence time of water is of the order of centuries or thousands of years, then the groundwater vulnerability to surface changes induced by human activities is low because the contaminants signal is delayed, diluted and attenuated. On the contrary, if the residence time of water is very low, the groundwater vulnerability is generally high. Young groundwaters (< 60 years) are traditionally considered as vulnerable because of their proximity in time to surface contamination. MTT can be considered as pragmatic indicators of intrinsic groundwater vulnerability reflecting the turnover time of groundwater bodies. In addition, groundwater TTD is a very powerful tool to assess groundwater vulnerability because it gives the time of first arrival of tracers/contaminants, the relative contributions of particular flow components and persistence of tracers/contaminants in the system (Wachniew, 2015). Indeed, a large number of studies highlighted links between the groundwater residence time and pollutant concentration. A good example is given in Böhlke and Denver (1995) where the authors link contaminant concentrations (here nitrate, chloride and magnesium derived from fertilizer application) and the year of recharge (Figure 6 (a)). Waters recharged prior to 1965 generally contain low nitrate concentrations, while the relationship between recharge date and nitrate concentration matches the historical fertilizer input with a delay of a few years. However, faster renewal times also mean that groundwater quality rehabilitation can be more quickly achieved.

Groundwater residence times can help to show trends in groundwater quality as highlighted by Visser et al. (2007) who demonstrate a reversal in nitrate concentration with time in the Netherlands (Figure 6 (b)).

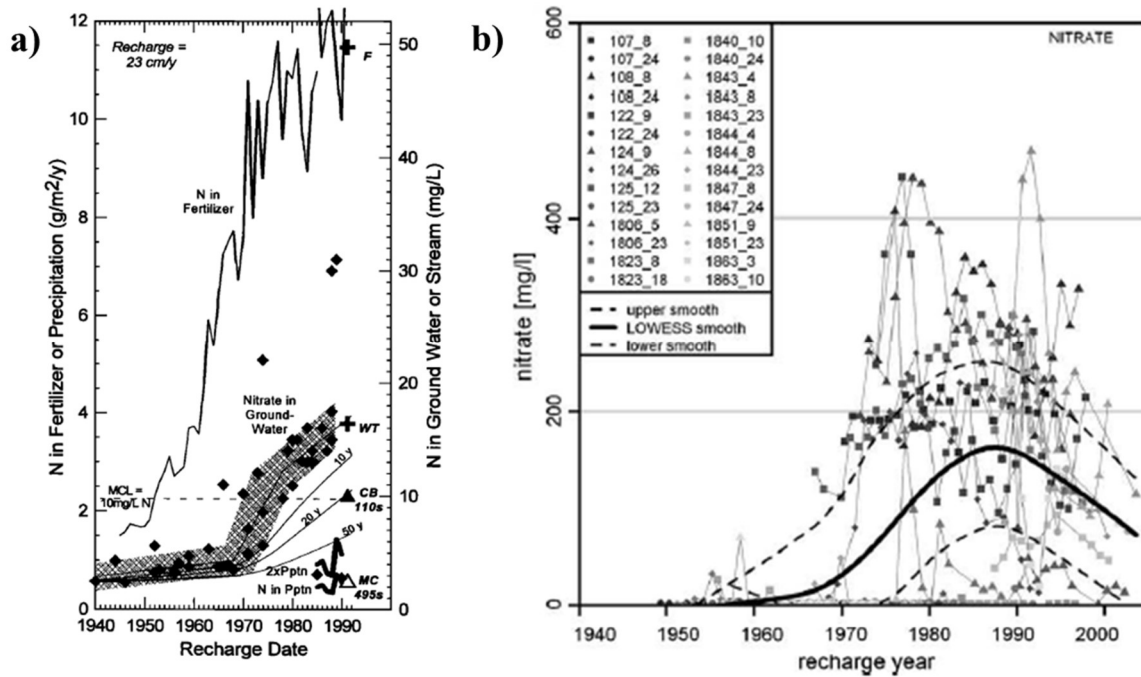


Figure 6: (a) Historical reconstruction of nitrogen input and nitrate concentration in groundwater plotted against time and CFC-12 model recharge dates for groundwater (Böhlke & Denver, 1995). (b) Reversal trend of nitrates concentration highlighted in Netherlands – the recharge year was determined using ^3H - ^3He (Visser et al., 2007).

1.3.2 Environmental tracers as groundwater dating tools

1.3.2.1 (Ground)water age-dating tracers

Environmental tracers (see section 1.2.1.4.2) are particularly useful to trace the global and local water cycles and the interactions between the different hydrological compartments or the hydrobiogeosphere continuum (Clark & Fritz, 1997; Jasechko, 2019; Sprenger et al., 2019). Three types of dating tracers exist: (i) radioactive tracers that undergo natural radioactive decay and are useful if the initial input concentration is either constant or well known, (ii) accumulating tracers, which are stable nuclides produced in the subsurface and accumulate at a steady state in

groundwater, and (iii) event markers that have a transient but well-known atmospheric function. Each tracer has a specific time window of application (Figure 7), which is defined by its intrinsic characteristics such as its half-life in case of a radioactive tracer (*e.g.* ^{81}Kr) and/or its transient input history in the environment (typically, ^3H , SF_6 , ^{85}Kr).

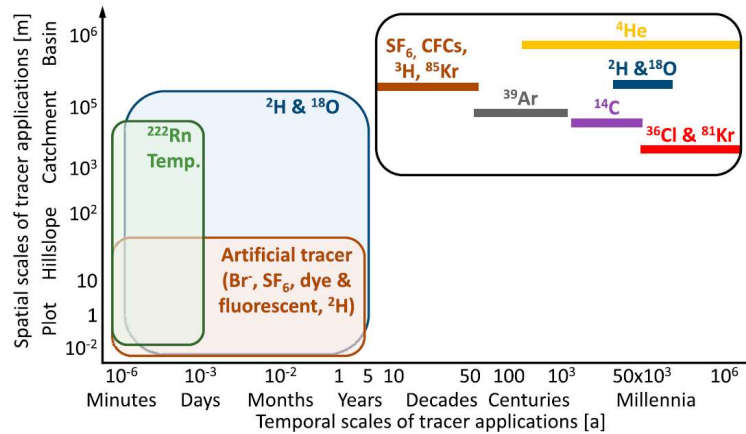


Figure 7: Spatial and temporal scales for use of different hydrological tracers including groundwater dating tracers (Sprenger et al., 2019).

The concept of (ground)water residence times was first introduced by Libby (1953) and further discussed, a bit later, in Begemann and Libby (1957) and in Eriksson (1958). In these pioneering works, the authors explored the potential of atmospheric tritium as a tracer for the investigation of groundwater and spring waters “storage times”. Since then, numerous tracer-based techniques have emerged for groundwater dating. Among them we find:

- For “very young” waters (less than 5 years old):
 - water stable isotopes ($\delta^2\text{H}$, $\delta^{18}\text{O}$) (Benettin, Soulsby, et al., 2017)
 - radon (^{222}Rn) (Popp et al., 2021)
- For “young” waters (up to 60 years):
 - the couple ^3H - ^3He (Aeschbach-Hertig et al., 1998; Mamyurin & Tolstikhin, 1984)
 - manmade greenhouse gases (chlorofluorocarbons – freons, CFCs – and sulphur hexafluoride – SF_6) (Busenberg & Plummer, 2000; Darling et al., 2012)

- bomb-derived radiocarbon (^{14}C) and radiochlorine (^{36}Cl) (Baudron et al., 2016; Corcho Alvarado et al., 2005)
- radiokrypton (^{85}Kr , with a half-life of 10.8 years) (Corcho Alvarado et al., 2007; Corcho Alvarado et al., 2005; Ekwurzel et al., 1994; Meyzonnat et al., 2023; Visser et al., 2013)
- For “old” waters (up to a few hundreds of years):
 - radioargon (^{39}Ar – half-life of 269 years) (Corcho Alvarado et al., 2007; Visser et al., 2013)
- For “very old” waters and fossil waters (more than a few thousands of years):
 - radiocarbon (^{14}C – half-life of 5 730 years) (Fontes, 1976)
 - radiochlorine (^{36}Cl – half-life of 301 000 years) (Purtschert et al., 2023)
 - radiokrypton (^{81}Kr – half-life of 229 000 years) (Kamdee et al., 2023; Purtschert et al., 2023)
 - ^4He (Bethke & Johnson, 2007)

Examples of atmospheric concentrations and activities of several tracers commonly used for the dating of “young” groundwaters are shown in Figure 8.

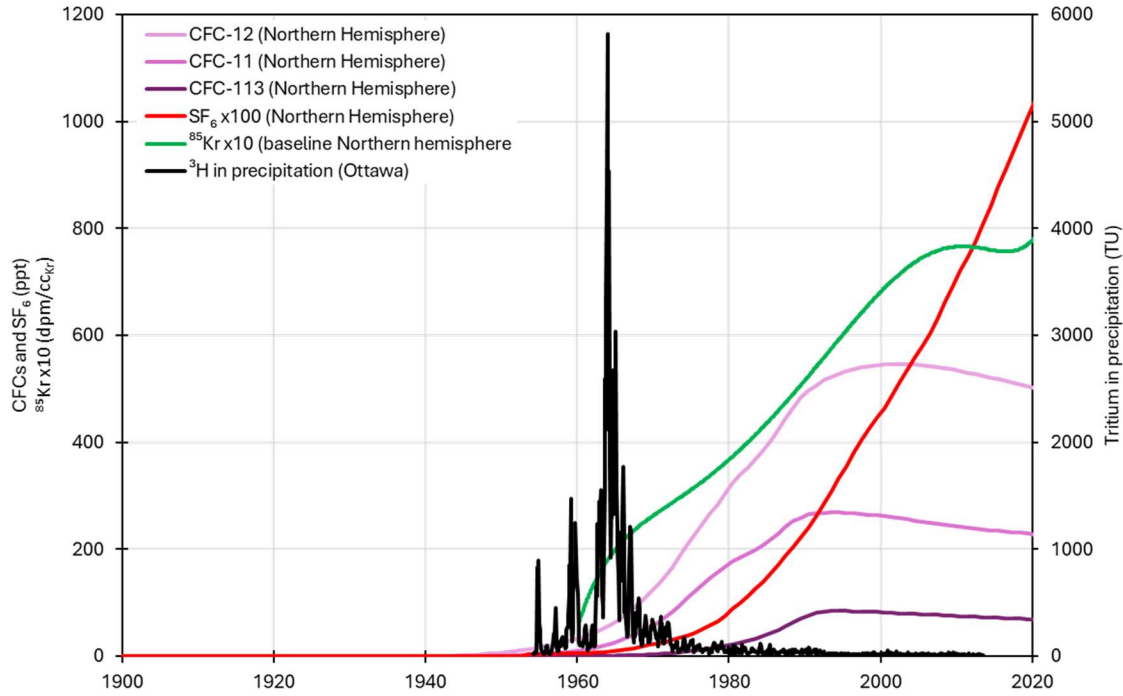


Figure 8: Transient tracers atmospheric input function used for dating of “young” groundwaters. Anthropogenic gases data was taken from the NOAA (<https://gml.noaa.gov/dv/data/>), radiokrypton data was retrieved from Kersting et al. (2021) and Ottawa tritium data was retrieved from the I.A.E.A Wiser (GNIP) portal (<https://nucleus.iaea.org/wiser/>).

1.3.2.2 Simultaneous use of different age dating tracers: multi-tracing

Since each environmental tracer has a working “time-window” and the TTD can have a very wide range of ages, it can be useful to simultaneously use multiple tracers to better constrain the TTD of a groundwater sample. This is especially the case in complex hydrogeological settings where groundwaters can be a mixture of young and older waters (Meyzonnat et al., 2023). For example, Corcho Alvarado et al. (2007) used a combination of ^3H - ^3He , ^{85}Kr , ^{39}Ar and ^{14}C to better constrain the modern, sub-modern and older fractions (> 100 years old to a few thousand years old) of groundwater in the semi-confined Fontainebleau sands aquifer, in France.

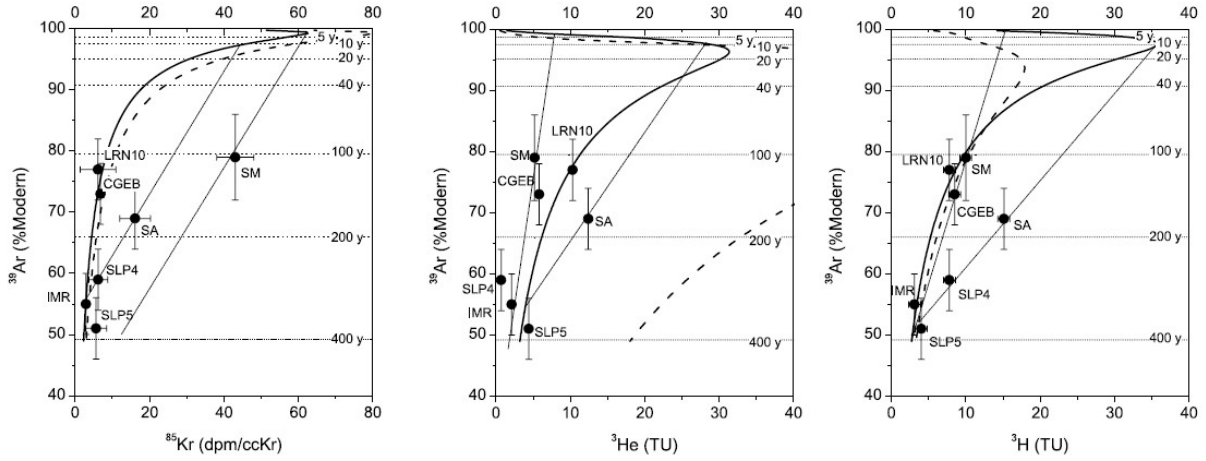


Figure 9: Results from multi-tracing experiments in the Fontainebleau sands aquifer which is a complex mixture of recent and old groundwaters (Corcho Alvarado et al., 2007).

1.3.3 Determination of water residence times

1.3.3.1 Theoretical equations in idealized conditions

Vogel (1967) was the first to derive theoretical equations of groundwater hydraulic age in simple idealized aquifer configurations. In the case of an unconfined, homogeneous aquifer of constant thickness receiving a uniform recharge, the age of a water parcel is given by the following equation:

$$t(z) = \frac{L\varepsilon}{R} \ln\left(\frac{L}{L-z}\right) \quad \text{Eq. 1-5}$$

where ε is the aquifer porosity, L is the aquifer thickness, R is the recharge and z is the depth of the water parcel ($0 < z < L$). The mean age of the water column, τ , is:

$$\tau = \frac{L\varepsilon}{R} \quad \text{Eq. 1-6}$$

In this very simple approach, the water age is a function of depth, recharge rate and aquifer porosity. However, TTD and CTTD revealed extremely difficult to anticipate (McDonnell et al.,

2010; McGuire & McDonnell, 2006). In natural systems, different controls at different spatial scales were identified. At regional scale, climatic and geological settings exert a control over the TTD, because these parameters will, in turn, control most of the recharge rates (O'Driscoll et al., 2005). The topography is the main catchment scale control as it controls gradients and mean flow path distance (McGuire et al., 2005). However, there is no correlation between catchment scale and MTT (Hrachowitz et al., 2010), although MTT variability tends to decrease when catchment scale increases (Tetzlaff et al., 2009).

Soulsby et al. (2014) showed that urbanisation increases the runoff component in urban surface waters which lowers the water MTT at the catchment scale. Indeed, stream MTT was divided by 2 when the urban cover exceeded 20 % of the total catchment area in Soulsby et al. (2014). However, the role of urbanisation on the longer transit times (*i.e.* the tailing part of the TTD) is not clearly identified since the TTD response to urbanisation may be much dampened and because urbanisation is often associated with higher recharge rate from leaking pipes (Lerner, 1986) which brings a high degree of heterogeneity to subsurface flows.

1.3.3.2 Lumped parameter model approach: theory and assumptions

The lumped parameter model is the most common approach to determine the TTD of a water sample. Any conservative tracer concentration measured in a water sample is the sum of all volume-weighted input concentration that occurred between the oldest input event (precipitation or recharge) and the sample date (Jurgens et al., 2012; Suckow, 2014):

$$C_{out}(t) = \int_{-\infty}^t C_{in}(T) g_{\tau}(t - T) e^{-\lambda(t-T)} dT \quad \text{Eq. 1-7}$$

where t is sampling date and T the date at which a water parcel entered the system ($t - T$ is the age of the water parcel), $C_{out}(t)$ is the measured tracer concentration at sampling date t , $C_{in}(t)$ is the tracer concentration at input time T and λ is the decay constant in case of a radioactive tracer. The function g_{τ} is the TTD and is usually chosen *a priori*, depending on the knowledge of the study site. When the TTD shape cannot be assumed to follow any particular mathematical model (ex: in

a context of groundwater pumping), some authors used a shape-free TTD approach (Cirpka et al., 2007; Visser et al., 2013). The TTD depends also on the parameter τ , which is the MTT. In the case of mixing of different water masses having different TTD shapes and MTT, it is possible to sum the relative contribution of each convolution integral given in Eq. 1-7 (binary mixing model in the case of two components).

The general methodology used with the lumped parameter model approach is shown in Figure 10. First, the relevant (see section 1.3.3.4.3 for comments and details) tracer input function is implemented in the model ($C_{in}(t)$). Then, a TTD shape is chosen according to the knowledge of the studied aquifer: $g_{\tau}(t-t')$ (three TTD models are shown here, piston flow in black, exponential in red and dispersion in blue). The output of the model is then fitted to the measured data by varying the MTT (τ) and other parameters if applicable (e.g. dispersion parameter, relative fractions of each model in binary mixing models) (Jurgens et al., 2012; Suckow, 2014)..

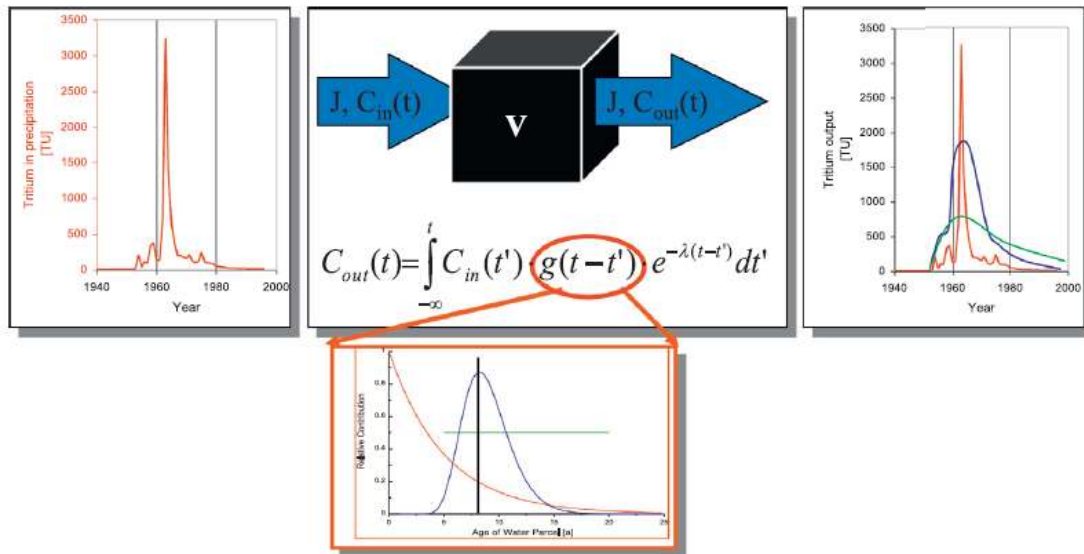


Figure 10: Methodological steps to determine MTT and TTD from environmental tracers using the lumped parameter model approach (Suckow, 2014).

One of the advantages of this approach is that it does not require a detailed knowledge of the studied site. However, one must be aware that this approach is highly idealized. Indeed, key

assumptions of application of stationarity and ideal aquifer geomorphology are usually not found in nature (McGuire et al., 2005)

It is noteworthy that Eq. 1-7 can be numerically integrated using the following simple integration scheme:

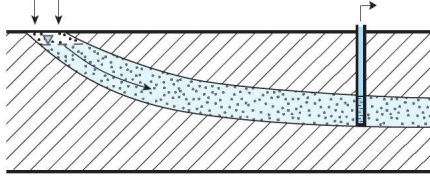
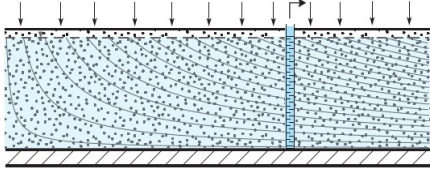
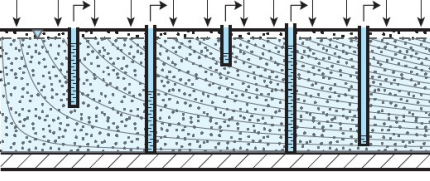
$$C_{out}(t) = \frac{1}{2} \sum_{i=-\infty}^t (T_{i+1} - T_i) [C_{in}(T_{i+1})g_{\tau}(t - T_{i+1}) + C_{in}(T_i)g_{\tau}(t - T_i)] \quad Eq. 1-8$$

This expression can then easily be implemented in Excel for example (see for example in Picard, Barbecot, Bardoux, et al. (2024) in section 2.3). Jurgens et al. (2012) also developed a robust and user-friendly software, TracerLPM, for groundwater dating applications using the lumped parameter model approach.

1.3.3.3 Shapes of transit time distribution

Most common TTD shapes are (i) the piston flow, (ii) the exponential model, and (iii) the dispersion model (Jurgens et al., 2012). The mathematical expression of their TTD as well as their applicability is summarized in the Table 1. The shape of their TTD is given in Figure 11 as an example, for a water sample having a mean age of 25 years.

Table 1: Common groundwater dating models with the mathematical expression of their TTD and characteristics. From Jurgens et al. (Jurgens et al., 2012).

Model name	TTD mathematical expression	Schematic diagram	Assumptions and use
Piston flow	$g_{\tau}(t - T) = \begin{cases} 1 & \text{for } T = \tau \\ 0 & \text{else} \end{cases}$		No hydrodynamic dispersion nor mixing (one single flowline is sampled). Piston flow can be assumed where linear velocity is high with short flowpaths.
Exponential	$g_{\tau}(t - T) = \frac{1}{\tau} e^{-\frac{t-T}{\tau}}$		Homogeneous, unconfined aquifer of constant thickness receiving a globally evenly distributed recharge. Assumes completely mixed reservoirs. Applicable for fully penetrating wells or aquifers that discharge to springs/streams.
Dispersion	$g_{\tau}(t - T) = \frac{1}{\tau} \frac{1}{\sqrt{4\pi D \frac{t-T}{\tau}}} e^{-\frac{\left(1 - \frac{t-T}{\tau}\right)^2}{4D \frac{(t-T)}{\tau}}}$		Based on a solution to a 1D advection dispersion equation. Versatile model applicable to various aquifer configurations. It considers hydrodynamic dispersion thanks to its dispersion parameter: D.

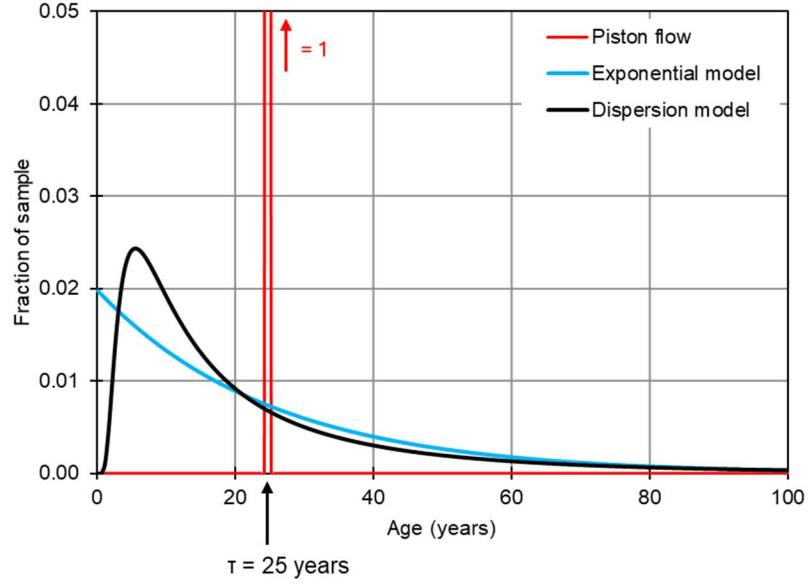


Figure 11: TTD shapes of commonly used transfer functions ($\tau = 25$ years with a dispersion parameter of 0.7 for the dispersion model).

As reviewed by Godsey et al. (2010), the majority of studies focusing on CTTD determination used exponential TTD shapes. However, this model is in fact a particular case of the Gamma-type TTD functions whose general mathematical expression is the following (Godsey et al., 2010; Kirchner et al., 2000):

$$g_{\tau}(t) = \frac{\tau^{\alpha-1}}{\left(\frac{\tau}{\alpha}\right)^{\alpha} \Gamma(\alpha)} e^{-\frac{\alpha t}{\tau}} \quad \text{Eq. 1-9}$$

where Γ is the gamma function, α is the so-called shape factor and τ is the MTT. The exponential model, assuming perfect mixing, is found with $\alpha = 1$. The value of the shape factor exerts a strong role on the shape of these functions: with $\alpha < 1$, distributions are strongly peaked at the shortest times with a long tailing effect, while $\alpha > 1$ will give distributions that rise and decline (Figure 11). An infinite value for α would yield a TTD similar to the one of a piston flow model (*i.e.* Dirac function). The cases $\alpha = 0.2$ or 0.5 in Figure 12 show how water is preferentially flushed out at very short times and is slowly released even at very long times. These TTD are relevant for contaminant transport as low α values predict large releases of water and solutes at short times and a

pronounced retention time because of the large tailing effect and high α values indicate a narrow range of ages (Godsey et al., 2010; Humphrey et al., 2024).

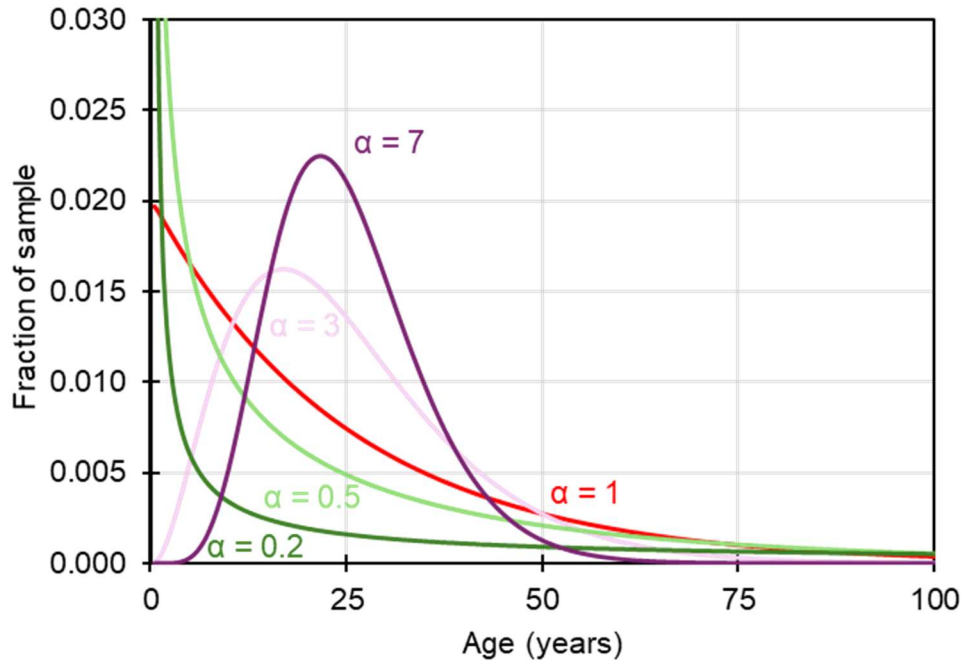


Figure 12: TTD shapes for Gamma functions with different shape factors ($0.2 < \alpha < 7$; $\tau = 25$ years).

1.3.3.4 Processes influencing age-dating environmental tracers

1.3.3.4.1 Transport in the unsaturated zone

Most gaseous tracers used for residence time investigation of young groundwaters have a transient input function (e.g. CFCs, SF_6 , ^{85}Kr). However, if the transport in the unsaturated zone is long, the soil gas composition in equilibrium with the water table might not be the same as the ambient atmosphere. This can play a significant role for transient gaseous tracers such as CFCs, SF_6 and ^{85}Kr . Usually, such dephasing is important for unsaturated zones thicker than 10 metres. This is the case in most arid regions but generally not under wet, temperate climates such as in Québec.

Tritium, being part of the water molecule, is very advantageous as it is one of the few groundwater dating tools that will record the time spent by water in the unsaturated zone (Clark, 2015; Clark & Fritz, 1997).

1.3.3.4.2 Excess air and degassing

The use of dissolved gases concentration for groundwater dating is complicated by the ubiquitous presence of “excess air” (Heaton & Vogel, 1981). Excess air occurs during recharge when the groundwater level rises and gas from the unsaturated zone is entrained with the water influx and dissolve in the groundwater (Aeschbach-Hertig et al., 2008). Degassing can also occur underground, for example, if biogenic (methane, carbon dioxide) gases exsolve or if total pressure decreases (Aeschbach-Hertig et al., 2008). Concentrations of gaseous tracers such as CFCs, SF₆ and ³He, must be corrected from excess air/degassing. However, no excess air/degassing correction is needed for ⁸⁵Kr, as it is the ratio of ⁸⁵Kr to total krypton that is measured and the fractionation between ⁸⁵Kr and stable krypton (e.g. ⁸⁴Kr) is negligible (Cook & Solomon, 1997; Kazemi et al., 2006; Musy et al., 2021).

The quantification of excess air or degassing is usually performed using gases with a known and stable concentration such as atmospheric noble gases (typically, Ne, Xe) or N₂. The expected solubility of these gases is computed and compared to what is measured to account for the amount of excess air or degassing. The software Panga was recently developed to determine excess air and degassing from noble gases samples (Jung & Aeschbach-Hertig, 2018). Different models, involving complete gas bubbles dissolution to partial reequilibration, can be used to interpret dissolved gases data in terms of excess air.

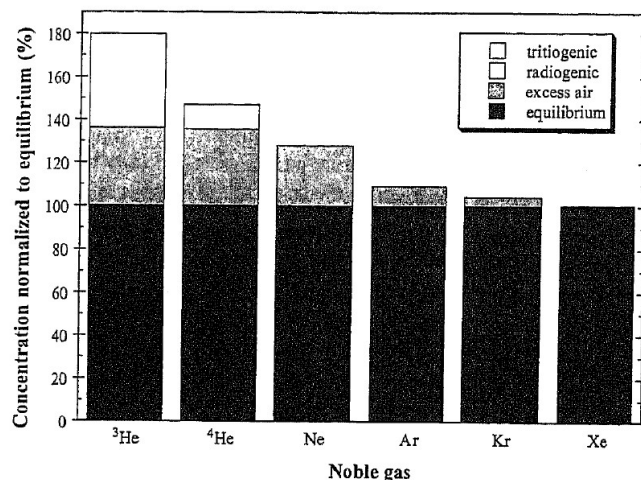


Figure 13: Noble gases components in a typical shallow groundwater sample normalized to their respective atmospheric equilibrium (Kipfer et al., 2002). Note that the noble gases are affected differently by excess air which helps to determine it (especially Ne and Xe, since they only have atmospheric sources).

1.3.3.4.3 Spatial heterogeneity of tracers input function

Local atmospheric and underground pollutions of environmental tracers might exist, especially near anthropic activities and facilities. It is critical to obtain a reliable input function, especially for transient tracers from anthropic origin.

This has been well known and documented for bomb-derived tritium, for which “local” input functions exist owing to the Global Network for Isotopes in Precipitation from the I.A.E.A. Most nuclear tests took place in the Northern Hemisphere (Clark, 2015), resulting in a dramatic increase of tritium activities (> 5 000 TU in 1963 in Ottawa, Canada). Since then, tritium activities in precipitation reached their pre-bomb era order of magnitude (1-2 TU near the equator and up to 20-30 TU in higher latitudes areas). However, there are still local punctual releases of anthropic tritium near nuclear plants. This has been documented in the Great Lakes area near Ottawa for which the implications on local groundwater dating have been discussed by Priebe et al. (2023).

Because of their extremely low atmospheric concentration (1 – 10² ppt), contamination of CFCs and SF₆ can be problematic regarding groundwater dating studies. As reviewed by Darling et al.

(2012), local CFCs contaminations are frequent, both in the local atmosphere and in the underground (*e.g.* buried refrigerators) especially in urban and peri-urban areas with fractured aquifers. Santella et al. (2008) showed that urban centres in the eastern United States have elevated atmospheric concentrations of SF₆ (sometimes, twice the global average value). However, SF₆ contamination are less frequent than CFCs contamination and mostly originate from high-voltage electricity supply equipment and landfills (Darling et al., 2012). Exceptionally, natural production of SF₆ might be significant in specific geological settings where fluorite (CaF₂) is present. Such case was reported in the island of Jeju, South Korea, with SF₆ excess up to 4 pptv (Koh et al., 2007).

⁸⁵Kr is mostly produced by the reprocessing of spent nuclear fuel (Kazemi et al., 2006). Therefore, areas near reprocessing plants (*e.g.* La Hague, France and Sellafield, U.K.) show elevated concentrations. This is especially the case in Western Europe (Figure 14). However, only the baseline curve is relevant for groundwater dating applications, such as the one shown in Figure 8 (Musy, 2018; Musy et al., 2021).

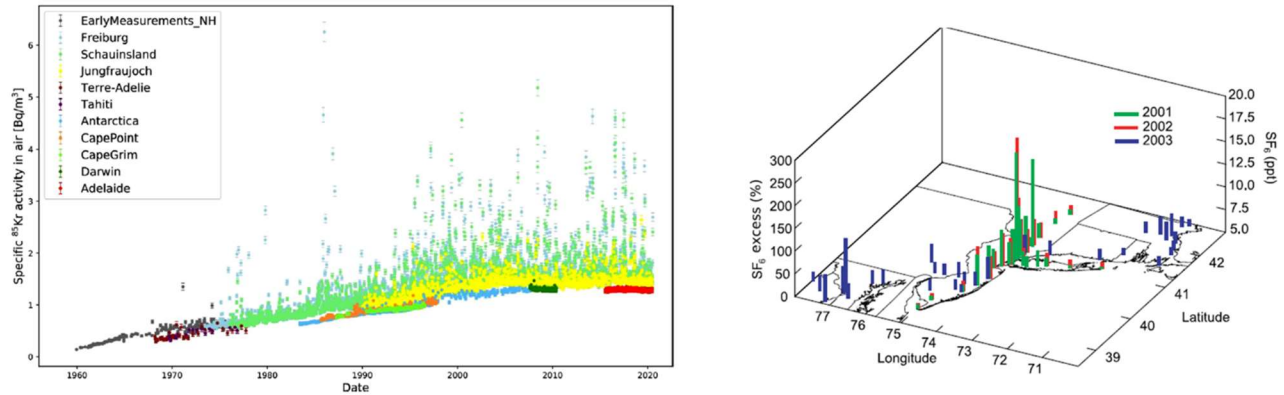


Figure 14: On the left: monitoring of ⁸⁵Kr specific activities in stations across the globe (Kersting, Schlosser, Schmid, et al., 2020). The visible peaks for European stations (Freiburg, Schauinsland, Jungfrauoch) are due to the proximity to nuclear fuel reprocessing plants. On the right: spatial distribution of atmospheric SF₆ concentration in the eastern United States (Santella et al., 2008).

1.3.4 Catchment scale transit time distribution determination

1.3.4.1 Investigation of CTTD using temporal monitoring of environmental tracers

The study of catchment scale TTD truly began in the early 1980s with the pioneering work of Maloszewski et al. (1983). The authors used a combination of tritium and deuterium measurements in stream to estimate the MTT of a small alpine catchment, starting in 1971 to 1979. The conversion and dampening of the input tracer signal to the stream is used to determine the CTTD as streams are seen as natural, weighted integrator of catchment transit times (Solomon et al., 2015). This approach was further developed with the studies of Welsh catchments in the early 2000's. Passive tracers, such as chloride and water stable isotopes, have been monitored both in precipitation and in the stream at a short time step for more than 3 decades (Kirchner et al., 2000; Kirchner & Neal, 2013).

The catchments-scale studies of Kirchner et al. (2000) and Godsey et al. (2010) revealed that CTTD were better explained by the use of Gamma-type models with $\alpha < 1$ rather than with the traditional exponential model approach (see section 1.3.3.3). This allowed to partially explain the fundamental paradox highlighted by Kirchner: *"how do [these] catchments store water for weeks or months, but then release it in minutes or hours in response to rainfall inputs?"* (Kirchner, 2003). In other words, CTTD shape and catchment MTT are transient: during wet periods (e.g. during or shortly after a storm event, during or after the spring snowmelt period in cold climates), α values are low as water moves quicker than during dry periods (e.g. winter low flow period in cold climates, or dry summer periods) when water is retained in the soil matrix (Benettin et al., 2022). The recent development of StorAge Selections (SAS) methods enabled the use of such transient TTD (Benettin & Bertuzzo, 2018; Benettin, Soulsby, et al., 2017; Harman, 2015; Harman et al., 2016; Kim et al., 2016; Rinaldo et al., 2015; Wang et al., 2023). SAS methods can provide invaluable information such as the daily CTTD if all the required inputs are available, usually soil moisture, stream discharge, precipitation inputs, evapotranspiration, tracer measurements in precipitation and stream (Figure 15) (Benettin et al., 2022; Harman, 2015).

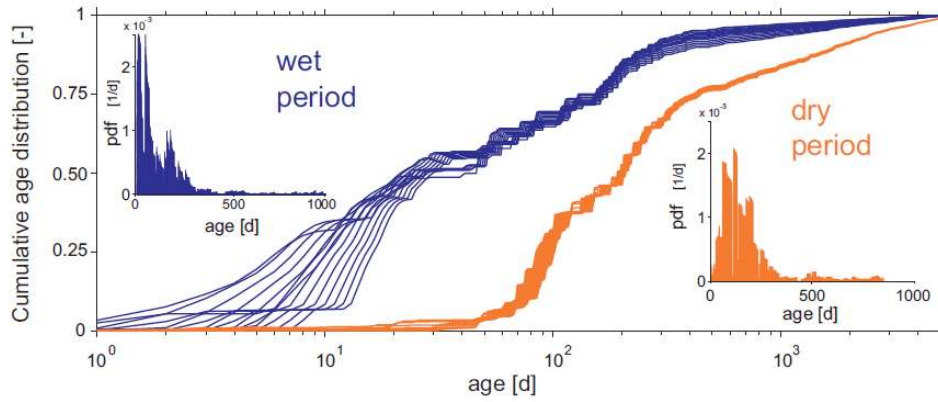


Figure 15: Cumulative daily CTTD of stream discharge during a 2 weeks wet and a 2 weeks dry periods. The TTD are also reported in the inserts. (Benettin et al., 2015).

However, these methods were developed in catchments where tracer data is available at very fine timesteps (daily to weekly) both in precipitation and stream discharge, for extended periods (> 4 years usually) which can hinder their development in ungauged basins or areas where data is scarce (Benettin et al., 2022). In addition, since these methods often rely on observations of stable isotopes data and because of the seasonality and natural dampening of the tracer signal, they hardly give information about longer water transit times (*e.g.* > 5 years).

1.3.4.2 Investigation of CTTD using punctual tracers observations

The investigation of river baseflow MTT and TTD by means of punctual field sampling using conservative and volatile tracers has been studied by a few authors (Cook et al., 2003; Gilmore et al., 2016; Humphrey et al., 2024; Jensen et al., 2022; Sanford et al., 2015; Solomon et al., 2015; Stolp et al., 2010).

1.3.4.2.1 Reach-scale mass balance of age-dating tracers

Reach scale mass balance (see 1.2.1.4.2) are used to evaluate the MTT of the discharging aquifer (Jensen et al., 2022; Solomon et al., 2015; Stolp et al., 2010). Such mass balance implies to estimate the inflowing (*e.g.* groundwater contribution, tributaries inflows, atmospheric exchange) and outflowing fluxes (*e.g.* evaporation, atmospheric exchange – especially for gaseous tracers,

radioactive decay) of tracers, often gases since most tracers used for young groundwater dating are under gaseous form (see Figure 3). The groundwater concentration of age dating tracers is then determined by solving the mass-balance equation after discretization.

The atmospheric exchange term is critical for gaseous tracers and is usually the main source of uncertainty. It is commonly estimated by artificial release of inert gases (*e.g.* SF₆, He, Kr, Xe, C₃H₈) (see Figure 16) (Clark et al., 1996; Jensen et al., 2022; Solomon et al., 2015; Stolp et al., 2010; Wanninkhof et al., 1990).

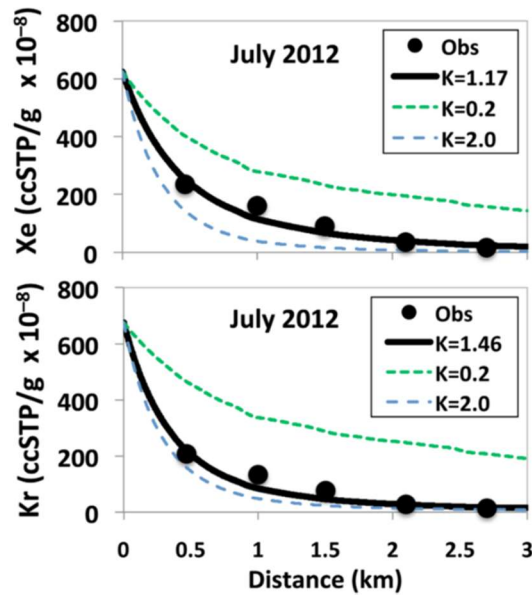


Figure 16: Artificially released dissolved Kr and Xe concentration as a function of the distance to the injection site in a stream. The parameter “K” is the gas transfer velocity and represents the atmosphere/river gas exchange rate. Graphs taken from Solomon et al. (2015).

One of the biggest advantages of these tracer-based methods is that they allow to identify the water parcels having the longer transit times (*i.e.* the tailing part of the TTD) because any (gaseous) groundwater age dating tracer can be sampled in theory (ex: from ³H to ¹⁴C). However, the success of these methods strongly depends on the persistence of the groundwater signal in the stream and is linked to the ratio between the atmosphere exchange rate and the groundwater inflows (Solomon et al., 2015). High ratio of groundwater recharge rate to stream density are also thought

to increase the likelihood of success (Jensen et al., 2022). It also often requires very specialised field (ex: sampling for noble gases, CFCs or SF₆) or lab equipment (ex: analysis of age dating tracers and/or noble gases) compared to the SAS approaches.

1.4 Conclusion and PhD objectives

1.4.1 Conclusions of the introduction

The following important conclusions can be drawn from what has been previously written:

- 1- River baseflow, *i.e.* groundwater inflows, is usually the main component of perennial streams under temperate and wet climates, because recharge is relatively high in those areas and the groundwater table is close to the surface. It describes well the vulnerability of rivers to surface contamination
- 2- Global urbanisation, population growth and climate change can have adverse, long-term effects over groundwater quality and quantity which can be conveyed to rivers via the baseflow.
- 3- The water mean transit time (and transit time distribution) of groundwater inflows are very useful metrics as they exert a strong control over (i) the natural groundwater quality and (ii) the rivers resilience to anthropic forcings (urbanisation, climate change) by telling us for how long groundwater contamination can last
- 4- Environmental tracers are the best tools to describe the groundwater inflows to river, both in the time domain and the spatial domain.
- 5- Environmental tracers are also the best tools to determine groundwater and/or catchment MTT and TTD.
- 6- Streams naturally integrate water flowpaths at the catchment scale, from the fast runoff contributions to the oldest groundwater parcels. They constitute the ideal hydrogeological object for the determination of the catchment water age structure.

In temperate, wet climatic contexts, the surface waters vulnerability to surface contamination and resilience to anthropic forcings are driven by two parameters: (i) the long-term groundwater fraction (baseflow index) and (ii) the age structure of these groundwater inflows.

Understanding the baseflow vulnerability to climate and land-use changes is relevant for sustainable water management and ensure better land use practices at the whole catchment scale. The relevance of this PhD work is also obvious considering that, in Québec, high river baseflow indexes values are expected and vulnerability assessments of surface water intakes for drinking water do not yet consider the groundwater fraction to stream. In this regard, this work is also the first of its kind for the management of Québec surface water resources.

1.4.2 PhD objectives

The computation of groundwater inflows to streams is one of the most important subjects of this PhD thesis. One of the easiest ways to determine these inflows is by accounting for the difference in river discharge between two points. However, one of the flaws of this technique is that the uncertainties can be quite high, and using tracers might have adverse effects on stream quality (ex: chloride) or might be very visible (ex: fluorescent dyes). Isotopic tracers, such as ^2H and ^{37}Cl can be injected in small quantities since they can be measured very precisely. In addition, tracers are very helpful to study exchanges between the streams and the transient storage zones (ex: surface transient storage or hyporheic zone). The 1st objective of this PhD work aims to test the potential of stable isotopes as quantitative tools for the precise determination of stream discharge in vulnerable catchments. To do so, a small stream was studied in Oka, Québec, in August 2022 via the instantaneous injection of a “cocktail” of tracers (salts, ^{37}Cl , ^2H , bromide, fluorescent dyes and isotopic tracers). The study shows how isotopic tracers can be used as reliable quantitative tools for precise and environmentally clean determination of streams discharge.

In addition, most tracer-based baseflow separation works were done under “unpractical” conditions regarding water resources management (*i.e.* very small to small, forested watersheds with no urbanisation). Only a few studies used these techniques in larger or urbanised catchments.

As far as we know, there is no example of tracer-based hydrograph separation in meso-scale, partially urbanised and snowmelt influenced catchment in the literature. However, such catchments are representative of most of Canadian and high-latitudes watersheds and are found in areas where high baseflow index values are expected. Thus, it is relevant to assess the potential of tracers for tracing the temporal variability of groundwater in these configurations. This constitutes the 2nd objective of the PhD and the methodology is used on the Saint-Charles River watershed, which has been the main study site during the PhD. Results of this work show that the surface water availability and quality are dominated by groundwater inflows at most temporal scales.

The third objective aims to determine the MTT and the TTD of the rivers baseflow. This is especially relevant in Québec as we show that rivers are baseflow dominated. In addition, as there is no liquid precipitation in winter, the streamflow during this period is expected to be exclusively constituted of groundwater as long as air temperature are sufficiently low to avoid snowpack to melt. This makes winter a favourable period to study groundwater in Québec's rivers. Since young (< 60 years old) waters are expected to feed the studied rivers, tracers of young groundwater (^3H , CFCs, SF_6 , ^{85}Kr) as well as quality parameters have been sampled in the Nelson River in March 2024, one of the main tributaries of the Saint-Charles River, in various locations, from upstream to downstream. The methodology helps to describe the (sub-)catchment vulnerability to anthropic forcings which can then be extremely useful for land use planning.

CHAPTER 2 Innovative techniques to assess water resources vulnerability to anthropic forcings in vulnerable catchments

2.1 Résumé du Chapitre 2 en français

2.1.1 Introduction du Chapitre 2

La première partie de ce second chapitre porte sur l'utilisation de traceurs artificiels, « exotiques », dans les eaux de surface comme traceurs quantitatifs précis avec un impact limité sur la qualité des cours d'eau. En particulier, c'est la mesure précise du débit dans les bassins versants vulnérables (ex : réserve écologique, bassins versants utilisés pour la production d'eau potable) qui est recherchée. Les traceurs fluorescents sont communément utilisés en faible quantité, mais sont malheureusement très voyants ce qui limite leur pertinence dans ces contextes, en particulier dans les bassins versants utilisés pour la production d'eau potable. Les traceurs salins sont également communément utilisés mais il est nécessaire d'injecter des quantités importantes de sel pour effectuer des mesures précises, ce qui a un impact ponctuel non négligeable sur la qualité des cours d'eau et la vie aquatique. L'utilisation de traceurs isotopiques, ^2H and ^{37}Cl ici, à ces fins n'est pas reportée dans la littérature malgré leur énorme potentiel pour des mesures à la fois précises et avec un impact très limité (voire nul) sur l'environnement. Ces traceurs ont été utilisés dans un petit cours d'eau de plaine, le Ruisseau Rousse, à Oka, au Québec au mois d'août 2022. Il est important de noter que ce travail est rendu possible grâce à une collaboration internationale entre le Geotop pour la préparation des standards (très) enrichis et la mesure du $\delta^2\text{H}$ et l'Institut de Physique du Globe de Paris (IPGP) pour les mesures de $\delta^{37}\text{Cl}$. Cette expérience de terrain fait l'objet d'une publication scientifique dans la revue internationale à comité de relecture *Hydrology* (section 2.3) dont le résumé en français est donné ci-dessous.

La deuxième partie de ce chapitre (section 2.4) contient le développement d'une méthode d'échantillonnage des gaz dissous par l'utilisation d'échantillonneurs passifs (tubes en acier munis de vannes étanches aux gaz Swagelok®). L'analyse du contenu de ces tubes est ensuite réalisée au laboratoire, d'abord à l'aide d'un spectromètre de masse (miniRUEDI) pour la détermination des teneurs en gaz majeurs et gaz rares (N_2 , O_2 , Ar, He, Kr), puis avec un

chromatographe en phase gazeuse muni d'un détecteur à capture d'électrons (GC-ECD) pour l'analyse des gaz anthropiques traces (SF_6 , CFCs) couramment utilisés pour la datation des eaux souterraines récentes. L'originalité de ce travail réside notamment dans la méthode d'échantillonnage, dite « passive ». En effet, des membranes en silicone, perméables aux gaz, sont installées à chaque bout du tube en acier. Lorsque ce dernier est plongé dans l'eau, les gaz dissous dans l'eau et ceux présents initialement à l'intérieur du tube vont échanger jusqu'à atteindre un équilibre régi par la loi de Henry. Ce type d'échantillonnage est intéressant lorsqu'il est appliqué aux eaux souterraines puisqu'aucun pompage n'est nécessaire, ce qui ne perturbe pas les lignes d'écoulement naturelles et donc la stratification naturelle des teneurs en gaz dissous dans l'aquifère améliorant ainsi grandement la représentativité des échantillons prélevés. Par ailleurs, dans le cas d'expériences de traçage souterrain aux gaz, il est possible de suivre l'évolution de la concentration des gaz en différents points (e.g. différents puits), ce qui aide grandement à la cartographie du panache de traceur. La combinaison des méthodes d'analyse, miniRUEDI d'une part et GC-ECD d'une autre part, permet d'avoir accès à tous les gaz communs, rares et anthropiques traces à partir d'un unique échantillon, ce qui est extrêmement utile pour la datation des eaux souterraines récentes. L'Article 2, en cours de soumission (revue visée : *Rapid Communications in Mass Spectrometry*), rapporte les développements méthodologiques de laboratoire ayant permis d'aboutir à cette technique, via notamment des expériences d'équilibration contrôlées et des comparaisons avec des méthodes « traditionnelles » (ex : module GE-MIMS du miniRUEDI).

2.1.2 Résumé en français de l'Article 1

La mesure précise du débit est indispensable à toute étude hydro(géo)logique. Alors que la méthode par l'utilisation de vélocimètres est adaptée aux écoulements laminaires, la méthode dite par « dilution » (injection de traceurs artificiels) est plus appropriée pour les cours d'eau turbulents. A échelle globale, la plupart des cours d'eau à faible pente ne sont ni totalement laminaires ni totalement turbulents et un gap méthodologique apparaît. Dans cette étude, nous démontrons que l'application de la méthode par « dilution » dans un petit cours d'eau à faible gradient produit des résultats très satisfaisants, tout en renseignant sur les processus d'échange entre la surface et la subsurface. Des traceurs chimiques et isotopiques ont été injectés de manière ponctuelle et simultanée dans le cours d'eau (anions, traceurs fluorescents,

et isotopes stables du chlore et de l'hydrogène). Nous rapportons la première utilisation du $\delta^{37}\text{Cl}$ pour la mesure du débit des cours d'eau et montrons que le $\delta^{37}\text{Cl}$ et le $\delta^2\text{H}$ peuvent être utilisés de manière fiable comme traceurs quantitatifs. Les calculs d'incertitude sur la mesure du débit montrent que le deutérium est la méthode de traçage utilisée la plus précise. Les différences des allures des courbes de restitution (« queue de traçage ») sont également comparées afin d'étudier le rôle des zones de stockage transitoire de surface et de la zone hyporhéique dans le transport des solutés, à l'aide d'une approche simple de modélisation du transport en rivière. Cette étude permet de conclure que les traceurs isotopiques peuvent être utilisés comme traceurs « respectueux de l'environnement » pour les mesures discrètes du débit des cours d'eau et que l'application du multi-traçage dans les cours d'eau ouvre la voie à une meilleure compréhension des processus d'interaction entre la surface et la subsurface.

2.1.3 Résumé en français de l'Article 2

Le développement récent de la spectrométrie de masse de terrain (par exemple, miniRUEDI) a permis un accès relativement facile et bon marché à la mesure des gaz avec une résolution temporelle sans précédent, directement sur le terrain, à partir de réservoirs qui sont constamment renouvelés (ex : air ambiant, masses d'eau). Cependant, il n'est pas adapté à l'analyse d'échantillons d'eau discrets de petits volumes (quelques cc). Nous abordons ce problème avec la présentation de « petits » (≈ 25 cc) échantillonneurs passifs pour l'échantillonnage des gaz dissous dans l'eau et un système simple et efficace construit pour connecter les échantillonneurs au miniRUEDI pour l'analyse des gaz. Les échantillonneurs sont laissés à équilibrer sous l'eau pendant quelques jours, puis récupérés et verrouillés lorsque l'équilibre entre l'intérieur de l'échantillonneur et l'eau est atteint, avant d'être analysés en combinant les techniques du miniRUEDI et de la chromatographie en phase gazeuse avec détecteur à capture d'électrons (GC-ECD) de retour au laboratoire. Cette nouvelle méthode permet de déterminer rapidement et avec précision les concentrations en gaz majeurs (N_2 , O_2), rares (ici, He, Ar et Kr) et transitoires utilisés pour la datation des eaux (SF_6 , CFC-12, CFC-113, etc.) à partir d'un seul échantillon. Cette approche peut être utilisée pour faciliter l'utilisation de traceurs gazeux anthropiques transitoires pour la détermination d'informations sur l'âge des eaux souterraines jeunes (< 70 ans). En outre, l'analyse de plusieurs gaz dans un seul échantillonneur ainsi que l'installation facile de plusieurs

échantillonneurs dans les eaux souterraines et les eaux de surface permettent de cartographier de manière avantageuse les panaches de traceurs gazeux pendant les expériences de traçages artificiels.

2.2 Introduction to Chapter 2

This chapter includes first the description, results and interpretation of artificial releases of “exotic” tracers for the quantification of stream discharge (*Article 1*). This work focuses on their potential as artificial tracers in vulnerable catchments where maintaining good water quality is crucial, for various reasons: ecological reserves or catchments used for the production of drinking water. Fluorescent dyes can be injected in small quantities and are often used for tracing experiments in streams, but they are very visible, which can hinder their use in these particular contexts. On the other hand, salt tracers, while being invisible have a strong, punctual effect over water quality when they are released in important quantities in streams.

A “cocktail” made of numerous tracers has been used for the experiment. One of the aims of the experiment was to compare isotopic tracers with conventional ones. Thus, the tracers injected are:

- Fluorescent dyes: uranine and tinopal
- Salts: NaBr and $\text{MnCl}_2 (4\text{H}_2\text{O})$
- Isotopic tracers: ^2H as $^2\text{H}_2\text{O}$, and ^{37}Cl in $\text{MnCl}_2 (4\text{H}_2\text{O})$ ($\delta^{37}\text{Cl} = 2.18 \pm 0.03 \text{ ‰}$ vs SMOC)

The use of ^{37}Cl is made possible here thanks to analytical developments made at the Institut de Physique du Globe de Paris (IPGP). Measurement uncertainties of the order of 0.01 – 0.03 ‰ are possible, which is less than the average uncertainties reported in the literature (0.1 ‰) (Godon et al., 2004). In addition, ^2H is particularly relevant as it is part of the water molecule, has basically no side effect regarding water quality and can now be precisely measured in a large number of facilities around the world. The main difficulties in using ^2H is the preparation, and measure of enriched standards for which the isotopic content should be calibrated against IAEA standards.

We report the first use of isotopic tracers, ^2H and ^{37}Cl , and test their robustness and reliability as quantitative tracers for discharge measurements in the Ruisseau Rousse, a small stream located in Oka, Québec, that discharges into a national park. It is also noteworthy that this work was made possible thanks to the international collaboration between Geotop and the IPGP for the ^{37}Cl preparation and analyses. A scientific paper, *Article 1*, was published based on this data, in the peer-reviewed international journal *Hydrology* (section 2.3).

The second part of this chapter (section 2.4) reports the development of a method for sampling dissolved gases using reusable passive samplers. They consist of steel tubing fitted with Swagelok® gas-tight valves. The content of these tubes are analysed at the laboratory, firstly using a field mass spectrometer (miniRUEDI) to determine the contents of major and noble gases (N_2 , O_2 , Ar, He, Kr), and then with a gas chromatograph equipped with an electron capture detector (GC-ECD) for the analysis of anthropic trace gases (SF_6 , CFCs), commonly used for the age-dating of young groundwater. The originality of this work lies in the method of collecting gases, “passively”. Gas-permeable silicone membranes are fitted at each end of the steel tub. When the tube is immersed in water, the dissolved gases in water and those initially present inside the tube exchange until they reach an equilibrium governed by Henry’s law. This type of sampling is interesting when applied to groundwater because no pumping is required: this in turn does not disturb the natural flowlines and therefore the natural stratification of dissolved gases contents in the aquifer. This greatly improves the representativity of the samples taken. Furthermore, in the case of gas tracing experiments in groundwater, it is possible to follow the evolution of the gas concentration at different points (e.g. different wells), which greatly helps with the mapping of the tracer plume. The combination of analytical methods, miniRUEDI on one hand and GC-ECD on the other, provides access to all common, noble and anthropic trace gases from one single sample, which is extremely useful for dating recent groundwater. *Article 2*, soon to be submitted to *Rapid Communications in Mass Spectrometry*, reports on the methodological developments held in the laboratory that led to this technique, including controlled equilibration experiments and comparison with “traditional” methods (e.g. miniRUEDI’s GE-MIMS module).

2.3 The potential of isotopic tracers for precise and environmentally clean stream discharge measurements (*Article 1*)

The potential of isotopic tracers for precise and environmentally clean stream discharge measurements

Published in *Hydrology* (January 2024) <https://www.mdpi.com/2612722>

Antoine Picard ¹, Florent Barbecot ¹, Gérard Bardoux ², Pierre Agrinier ², Marina Gillon ³, José A. Corcho Alvarado ⁴, Vincent Schneider ⁵, Jean-François Hélie ¹ and Frédérick de Oliveira ¹

¹ Geotop-UQAM, Hydro Sciences, Université du Québec à Montréal, CP8888 succ. Centre-Ville,

Montreal, QC H3C 3P8, Canada; barbecot.florent@uqam.ca (F.B.); helie.jean-francois@uqam.ca (J.-F.H.); fredoudo@hotmail.com (F.d.O.)

² Institut de Physique du Globe de Paris, 1 rue Jussieu, 75005 Paris, France;

bardoux@ipgp.fr (G.B.);

agrinier@ipgp.fr (P.A.)

³ UMR 1114 EMMAH, Avignon Université, 301 rue Baruch de Spinoza, 84916 Avignon, France;

marina.gillon@univ-avignon.fr

⁴ Spiez Laboratory, Federal Office for Civil Protection, Austrasse, 3700 Spiez, Switzerland;

jose.corcho@babs.admin.ch

⁵ Andra, DI/CA/QSE, Service « Qualité Sécurité et Environnement », Centre de l'Aube BP 7, 10200 Soullaines-Dhuys, France; vincent.schneider@andra.fr

Abstract: Accurate discharge measurement is mandatory for any hydrological study. While the “velocity” measurement method is adapted to laminar flows, the “dilution” method is more appropriate for turbulent streams. As most low-gradient streams worldwide are neither laminar nor turbulent, a methodological gap appears. In this study, we demonstrate that the application of the “dilution” method to a low-gradient small stream gives very satisfactory results in addition to revealing surface/subsurface processes. A variety of chemical and isotopic tracers were injected into the stream (anions, fluorescent dyes, and chloride and hydrogen isotopes). We report the first use of ³⁷Cl for stream discharge measurement and show that ³⁷Cl and ²H can be reliably used as quantitative tracers. Discharge uncertainty calculations show that deuterium is the most accurate tracer method used. We also compare

the differences in the tailing part of the restitution curves of tracers and investigate the role of transient surface and hyporheic zones in solute transport in light of a simple transport modelling approach. We conclude that isotopic tracers can be used as “environmentally friendly” tracers for discrete stream discharge measurements and that the application of multi-tracers tests in rivers opens the path to a better understanding of surface–subsurface interaction processes.

Keywords: discharge measurement; “dilution” method; multi-tracer tests; ^2H ; ^{37}Cl ; transient storage zones

2.3.1 Introduction

Surface waters discharge measurement is a fundamental aspect of any hydrological and hydrogeological study. Indeed, accurate and precise stream discharge measurement is critical for water resource monitoring; water budget computation; hydraulic infrastructure design, such as weirs, culverts and artificial channels; flood monitoring and forecasting; and groundwater inflows calculations (Cook et al., 2006; Herschy, 2008; Jensen et al., 2022; WMO, 2008). Different field approaches can be used to determine stream discharge (ONEMA, 2011; WMO, 2008). One of the most used techniques is based on the use of current meters. The discharge is deducted by integrating the flow velocity distribution over a river cross-section area. Discharge measurement uncertainties using current meters largely depends on the velocity measure uncertainties and is usually between 2% and 20%, depending on measurement conditions (Pelletier, 1988; WMO, 2008, 2010). This technique is best suited for open channels with near-laminar flow. Indeed, the representativeness of velocity measurements is very limited in turbulent streams (Tazioli, 2011) or in the presence of dead storage zones and backwaters (Hudson & Fraser, 2005). The second technique is the so-called “gauging by tracer dilution” method. This technique consists of injecting a known mass of tracer upstream and measuring its complete restitution over time downstream (ONEMA, 2011). Several key hypotheses must be verified: (i) complete dissolution and conservation of the tracer, (ii) homogeneity of tracer concentration across the river section at the measurement point downstream (ensured by transverse and vertical dispersion), and (iii) the discharge must be under a permanent regime during the entire experiment duration (Tazioli, 2011). The

use of the tracer dilution technique is especially appropriate in shallow, turbulent streams where hydrodynamic dispersion ensures a fast tracer homogenization, i.e., in contexts not suitable for traditional current meters.

The main limitation of the “dilution” technique is the presence of transient storage zones, both at the surface and in the subsurface. Indeed, it is now widely accepted that streams exchange intimately with surrounding groundwater bodies in a variety of climates (Beck et al., 2013; Engelhardt et al., 2011; Gooseff, 2010; Sophocleous, 2002; Winter et al., 1998), especially in temperate, wet climates (Beck et al., 2013). Groundwater and surface waters act as a continuum, and exchange in the hyporheic zone, i.e., the portion of sediments surrounding the stream that is permeated with stream water, is significant (Boano et al., 2014). Transport in the hyporheic zone is thus much slower than in the main stream channel, allowing biological and geochemical processes to occur (Battin et al., 2008). In addition, the transport in the hyporheic zone, as well as in surface transient storage zones, results in a tailing effect in restitution curves of artificial tracer injection, which might limit the “dilution” method (Herschy, 2008). Exchanges with the hyporheic zone are mainly controlled by streambed porosity and permeability. They are known to be mainly advective but can be controlled by diffusion in the presence of fine streambed sediments, such as clays, in calm streams (Boano et al., 2014). Hyporheic exchanges are typically modelled using the classical advection dispersion equation (ADE) to which a sink term representing the subsurface exchanges with the stream is added (Boano et al., 2014; De Smedt, 2007; Genuchten et al., 2013a, 2013b; Runkel, 1998). Then, hyporheic flow represents the portion of stream water that is transported through the hyporheic zone before returning to the stream. In hydrological modelling, model parameters are calibrated against field data of tracer tests, often thanks to fluorescent dyes and salts tracers. Most low-gradient small streams worldwide consist of a succession of small pools and riffles, with very contrasted flow velocities, important streambed macrotopography, and the presence of transient storage zones. The flow in these rivers is not exclusively laminar or exclusively turbulent, which indicates a gap in streamflow measurement methodology.

Globally, anthropogenic activities have various negative impacts on stream quality, mainly resulting in biodiversity loss and eutrophication issues (Søndergaard & Jeppesen, 2007;

Verhoeven et al., 2006). In addition, it is well known that groundwater pumping can decrease water levels in rivers (Barlow & Leake, 2012). In this context, the application of the “dilution” method through injection of salts (e.g., NaCl) can be problematic for aquatic ecosystems (Wood & Dykes, 2002) and in rivers exploited for drinking water because their use will temporarily damage the stream quality. It is thus relevant to search for more environmentally friendly tracers for stream discharge measurements. For a given river discharge, the quantity of tracer has to be minimized but will depend on the initial stream concentration and the accuracy of the measurement. Chemical elements that are naturally found in small quantities and that can be analysed with a very high accuracy can therefore be injected in sufficiently small quantities to minimize their impact on the environment. While less used, “heavy” natural stable isotopes that are naturally present in (very) small amounts can be measured with a high precision using mass spectrometry. Hence, deuterium (^2H) is an ideal tracer of the water molecule since it is naturally bound to it and is fully conservative. It has already been used in many artificial tracer injections, especially in various groundwaters studies (Leibundgut et al., 2009) but not yet for river discharge measurements. Rarely used, chloride isotopes are interesting tracers because of the high solubility of chlorine and the fact that it is conservative in aquatic systems (Clark & Fritz, 1997). Chlorine has two common stable isotopes, ^{35}Cl and ^{37}Cl , and high-accuracy mass spectrometry measurements are very promising for environmental studies. The application of these “cleaner” isotopic tracers opens new perspectives to the understanding of environmental processes.

The objectives of this study are multiple: (i) to compare both the velocity and dilution methods for discharge measurements of a small stream, (ii) to assess the potential of isotopic tracers for more environmentally friendly discharge measurements, and (iii) to document surface–subsurface processes in the light of a multi-tracer approach. To complete these objectives, a diverse array of tracers, including electrolytes (NaBr, ^{37}Cl -enriched salt) conservative anions (bromide [Br^-] and chloride [Cl^-]), stable isotopes (deuterium [^2H] and chlorine [^{37}Cl]) and fluorescent dyes (uranine, tinopal) were injected into a small stream (Ruisseau Rousse, Québec, Canada) and analysed. We compare two approaches for stream discharge determination and hypothesize that the “dilution” method can be employed with satisfactory results for low-gradient small streams. Finally, we compare the tailing effect of tinopal, ^2H ,

^{37}Cl and Br^- in restitution curves to assess the exchange processes between the stream main channel and transient storage zones. The simultaneous injection of tracers having different chemical and physical (size) properties enabled us to gain a better understanding of these interactions/processes.

2.3.2 Materials and Methods

2.3.2.1 Description of the field site

Field work occurred in Oka, Québec, Canada in August 2022 in a small stream under baseflow conditions (coordinates: $45^{\circ}30'15.8''$ N/ $74^{\circ}02'45.9''$ W—see Figure 17) on a sunny day without any precipitation. In addition, the last precipitation event occurred 8 days before the test, roughly 4 times the recession time of this small river. The basement geology of the watershed consists of intrusive plutonic rocks (charnockite, mangerite) from the Precambrian age and Mesozoic carbonatite. It is covered by quaternary glacio-marine deposits (silts to gravel sands) that shelter the alluvial aquifer sustaining the river (SIGEOM). The local climate is continental humid, characterized by long, cold, and snowy winters and hot and wet summers. The watershed is mainly cultivated, but its southern part is occupied by the Parc National d'Oka, a protected natural area. The stream, called Ruisseau Rousse, drains the watershed and flows to the Lac des Deux Montagnes before ultimately joining the St. Lawrence River.

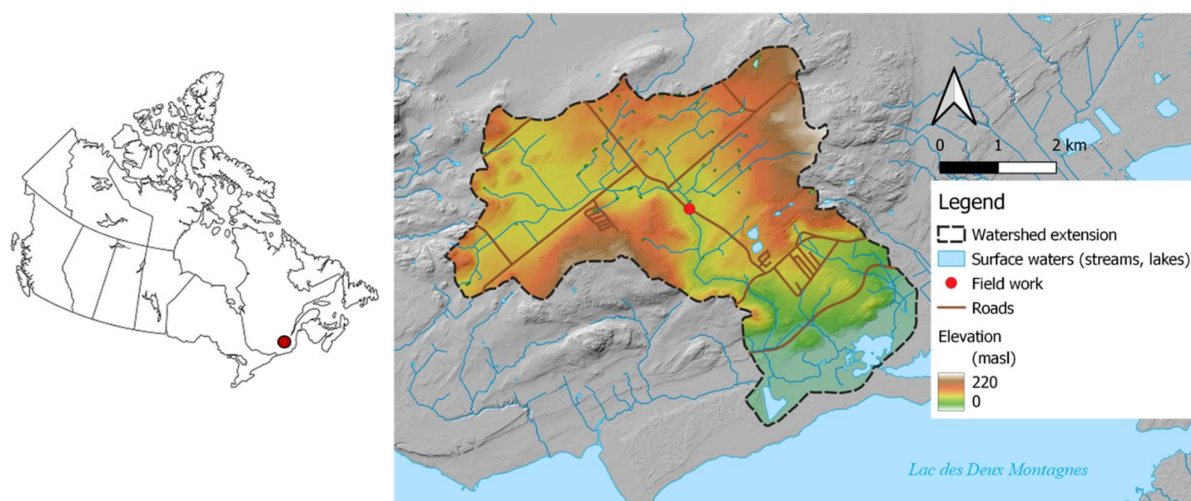


Figure 17: Map of Canada (*on the left*) and of the Ruisseau Rousse watershed (*on the right*). The red dots in both maps symbolise where the field work occurred.

The studied river transect extends 105 metres from the injection site (IS) to the restitution site (RS) (Figure 18). Similar to numerous streams in intermediate gradient plains, it is characterized by a succession of pools and small riffles with very contrasted flow velocities, river widths, and river depths. The average river width was estimated to be 2 m (2.6 m at the studied cross-section), with the maximal cross-sectional depth varying between 10 and 60 cm.



Figure 18: *On the left*: picture of the stream at the injection site (under a small culvert). We ensured tracer homogeneity by manually fanning the water under the culvert. *On the right*: picture of the restitution site with the equipment used to monitor solute concentration.

2.3.2.2 Field work

The solution used for the tracing experiment contained approximately 20 L of river water to which a variety of tracers was added: 535.13 ± 0.01 g of Cl^- with a $\delta^{37}\text{Cl}$ value of $+2.18\text{‰} \pm 0.03$ vs. SMOC (supplier: BioBasic, Markham, ON, Canada), 788.60 ± 0.01 g of Br^- (supplier: Fischer Scientific, Ottawa, ON, Canada), 403.09 ± 0.20 g of ^2H as deuterated water $^2\text{H}_2\text{O}$ (supplier: Isowater, Collingwood, ON, Canada), 2.42 ± 0.01 g of uranine, and 16.50 ± 0.01 g of tinopal (supplier: ThermoFischer, Waltham, MA, USA). The sample was placed in a sealed bucket until the salts dissolved completely, which took a few minutes. The total dissolved solids (TDS) of the mixture was 126.4 g/L. It was then injected instantaneously at IS. We ensured tracer homogeneity across the river width by manually fanning the river at IS shortly after injection (Figure 18). The injected volume has no effect regarding the total stream discharge.

Stream water velocity was measured using a SonTek FlowTracker at RS in 55 points across the river section to assess its distribution with a high spatial resolution, minutes before the

injection occurred. At RS, a total of five field multimeters (WTW) and 2 Solinst® LTC loggers were used to monitor the distribution of salt tracers (using electrical conductivity) across the section at a time step of 5 s. All of the equipment was calibrated against a 1413 $\mu\text{S}/\text{cm}$ standard in the morning of the field experiment. The mean uncertainty in electrical conductivity measurements was reported to be 1.1% of the measured value. Water fluorescence was monitored at RS in the centre of the stream (green dot in Figure 19), at a time step of 15 s using a field fluorometer (Tetraedre GGUN FL-30). Samples for anions (Cl^- , Br^-) and isotopic compositions (^2H , ^{37}Cl) were taken in the centre of stream at two points (Fluo. and WTW3) at 10 and 30 cm of depth (distance = 120 cm from the left bank, see Figure 19) in 250 mL HDPE bottles. The first discrete samples were taken every 2 min, and the time interval of sampling was progressively reduced up to 30 s when approaching to the arrival of the peak of tracer. It was then increased up to 5 min during the tailing part.

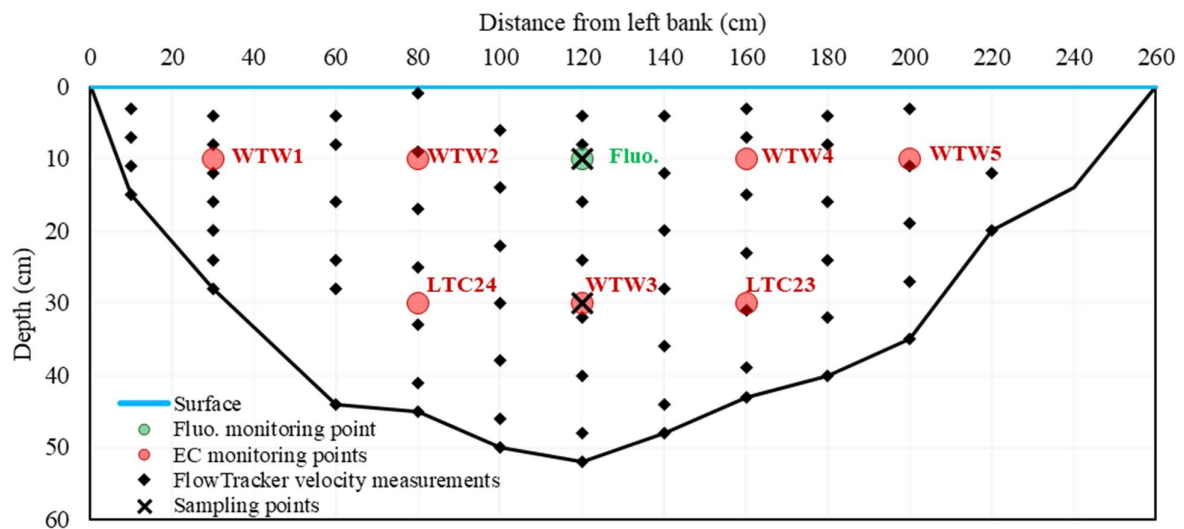


Figure 19: River working section (looking upstream) with equipment location.

2.3.2.3 Analytical methods

Since discharge computation requires concentration data, the electrical conductivity signal was converted into an added salts concentration time series. To do so, a sample of the river water was obtained prior to the injection (1L in HDPE bottle). Salts were carefully added in the same proportion as the injection mix (i.e., 40.4% of NaBr and 59.6% of ^{37}Cl -enriched salt)

and progressively dissolved, and the relationship between electrical conductivity and added dissolved salts was assessed for each field probe. The field fluorometer was calibrated at the laboratory on the day before the tracing experiment using distilled water to which uranine and tinopal were added in known quantities (7 points ranging from 0 to 160 ppb for uranine and 10 points ranging from 0 to 1300 ppb for tinopal). Anion (chloride, bromide) analyses were performed using liquid ion chromatography at the Université du Québec à Montréal, QC, Canada (Geotop-UQAM lab).

Deuterium analyses were performed at the Geotop Light Stable Isotope Geochemistry Laboratory at UQAM. Exactly 200 µL of sample water was pipetted in a 3 mL vial containing a hydrophobic platinum catalyst (Hokko beads). The vials were then closed with a septum cap, transferred to a 40 °C heated rack, and left to equilibrate for 4 h. The equilibrated samples were analysed using a dual inlet ratio mass spectrometer (Micromass Isoprime IRMS coupled to an AquaPrep system). Four in-house standards were used to normalize the results on the VSMOW-SLAP scale (standard 1: $\delta^2\text{H} = -99.45 \pm 0.56\text{‰}$ vs. VSMOW/standard 2: $\delta^2\text{H} = +118.5 \pm 4.4\text{‰}$ vs. VSMOW/standard 3: $\delta^2\text{H} = +323.5 \pm 5.1\text{‰}$ vs. VSMOW/standard 4: $\delta^2\text{H} = +740.2 \pm 3.2\text{‰}$ vs. VSMOW). Chloride isotopes analyses were performed at Institut de Physique du Globe (IPGP) in Paris, France, using the $\text{AgCl}-\text{CH}_3\text{Cl}$ method (Eggenkamp, 1994; Godon et al., 2004; Kaufman et al., 1984). The chloride isotope compositions of the samples were measured using a gas source dual inlet isotope ratio mass spectrometer (Delta V from ThermoFisher) with ionizing CH_3Cl gas. The results are reported as the $\delta^{37}\text{Cl}$ vs. SMOC (standard mean ocean chloride). The relative contents of ^2H and ^{37}Cl in stream water are expressed as δ -values, representing their deviation (in per mil) to the international standards of VSMOW (Vienna Standard Mean Ocean Water) for ^2H (Equation (1)) and SMOC (standard mean ocean chloride) for ^{37}Cl (Equation (2)):

$$\delta^2\text{H} = \left(\frac{\left(\frac{^2\text{H}}{^1\text{H}} \right)_{\text{sample}}}{\left(\frac{^2\text{H}}{^1\text{H}} \right)_{\text{VSMOW}}} - 1 \right) 10^3 \quad (1)$$

$$\delta^{37}Cl = \left(\frac{\left(\frac{^{37}Cl}{^{35}Cl} \right)_{sample}}{\left(\frac{^{37}Cl}{^{35}Cl} \right)_{SMOC}} - 1 \right) 10^3 \quad (2)$$

where $(^2H/^1H)_{VSMOW} = 1.5575 \cdot 10^{-6}$ and $(^{37}Cl/^{35}Cl)_{SMOC} = 0.324$ are the reference abundancy ratios for deuterium and chlorine-37, respectively (Clark & Fritz, 1997). Here, typical uncertainties (1σ) in the measurements of δ^2H are of the order of $\pm 1-2\%$. Concerning $\delta^{37}Cl$, the external reproducibility of the Atlantique 2 seawater chloride reference was $\pm 0.025\%$ (1σ , $n = 12$).

The raw field data for all the tracers can be found as Supplementary Material (Excel spreadsheet S1).

2.3.2.4 Data Interpretation

Traditionally, when using a current meter, the discharge is deducted by integrating the flow velocity distribution over the whole river cross-section area:

$$Q = \iint_A v(x,y) dx dy \quad (3)$$

where Q is the stream discharge [L^3T^{-1}], and v the water velocity field [LT^{-1}] that is a function of width ($x-[L]$) and depth ($y-[L]$). The variables x and y are used to define the river cross-section area, A .

Using the “dilution” method requires verification of the following hypotheses: (i) complete dissolution and conservation of the tracer, (ii) homogeneity of tracer concentration across the river section (ensured by transverse and vertical dispersion), and (iii) stream discharge under a permanent regime during the entire experiment duration (Tazioli, 2011). When such conditions are met, the discharge is computed according to the following formula (Hersch, 2008; Leibundgut et al., 2009):

$$Q = \frac{M_{tracer}}{\int_0^T C(t) dt} \quad (4)$$

where M_{tracer} is the mass of tracer that is injected [M], and $C(t)$ is the added tracer concentration at time t [ML^{-3}]. The time $t = 0$ corresponds to the time of injection, while T is the total duration of the experiment. Discharge measurements using the “dilution” method can only be overestimated if one or more of the three assumptions are not met. Usually, the denominator is calculated using a simple numerical integration scheme, such as that noted in the following:

$$\int_0^T C(t)dt = \frac{1}{2} \sum_{i=1}^{N-1} (C_{i+1} + C_i)(t_{i+1} - t_i) \quad (5)$$

where i refers to the i^{th} concentration measurement of the tracer (at time t_i), and N indicates the total number of measurements. Practically, the first sample (C_1) is taken at time 0, and the N^{th} sample (C_N) is taken at time T . Typically, when using field probes, the measurement timestep (ΔT) is constant, and Equation (5) is represented as follows:

$$\int_0^T C(t)dt = \frac{1}{2} \Delta T \sum_{i=1}^{N-1} (C_{i+1} + C_i) \quad (6)$$

In addition, the uncertainty propagation calculation was performed based on Equations (4) and (5):

$$\Delta Q = |Q| \sqrt{\left(\frac{\Delta M_{\text{tracer}}}{M_{\text{tracer}}}\right)^2 + \frac{\sum_{i=1}^{n-1} (t_{i+1} - t_i)^2 (\Delta C_{i+1}^2 + \Delta C_i^2)}{\left[\sum_{i=1}^{n-1} (t_{i+1} - t_i)(C_{i+1} + C_i)\right]^2}} \quad (7)$$

where Δ refers to the measure uncertainty (1σ) in any given measurement. This assumes that there is no uncertainty in the timing of the measurement. Of note, in the case of a constant sampling timestep ΔT (e.g., electrical conductivity monitoring), Equation (7) simplifies to the following:

$$\Delta Q = |Q| \sqrt{\left(\frac{\Delta M_{\text{tracer}}}{M_{\text{tracer}}}\right)^2 + \frac{\sum_{i=1}^{n-1} (\Delta C_{i+1}^2 + \Delta C_i^2)}{\left[\sum_{i=1}^{n-1} (C_{i+1} + C_i)\right]^2}} \quad (8)$$

Tracer experiments allow computation of stream discharge, but they also allow estimation of flow parameters, such as dispersion, velocity, and the influence of slower velocity zones. Here,

flow parameters were determined by modelling the tracers' restitution curves using a simple binary 1-D dispersion mixing model. A similar lumped parameter model approach was used to simulate the transport of an artificial tracer release in the Rhine river and is described in Leibundgut et al. (Leibundgut et al., 2009). Considering a conservative tracer, the classical 1-D lumped dispersion model can be expressed as follows (Jurgens et al., 2012):

$$C(t) = \int_{-\infty}^t C_{inj}(\tau) g(t - \tau) d\tau \quad (9)$$

Here,

$$g(\tau) = \frac{v}{x \sqrt{4\pi \frac{D}{x^2} \tau}} e^{-\frac{\left(1 - \frac{\tau v}{x}\right)^2}{4\tau \frac{D}{x^2}}} \quad (10)$$

Here, C is the tracer concentration over time [ML^{-3}], D is the longitudinal dispersion parameter [L^2T^{-1}], x the distance between the injection and measurement points [L], v the mean stream velocity [LT^{-1}], and C_{inj} is the injection function [ML^{-3}]. Here, it is a Dirac-type function with a value of C_0 at $t = 0$.

In this binary mixing model approach, the measured tracer concentration was simulated by adding a second flow component representing the slower fraction:

$$C(t) = f_1 \int_{-\infty}^t C_{inj}(\tau) g_1(t - \tau) d\tau + (1 - f_1) \int_{-\infty}^t C_{inj}(\tau) g_2(t - \tau) d\tau \quad (11)$$

The model was distributed over time and implemented in Excel (time step of 10 s). It was fitted with tracer restitution curves by minimising the normalized root mean square deviation defined as $\chi^2 = \sum \frac{(C_{meas} - C_{sim})^2}{C_{meas}}$ (where C_{meas} is the measured value, C_{sim} is the simulated value).

The parameters of the model were fitted using the restitution curves of 2H , ^{37}Cl , and Br^- .

2.3.3 Results and discussion

2.3.3.1 River section water velocity distribution

The survey performed using the FlowTracker allowed visualization of the water velocity distribution at the cross-section scale. The FlowTracker method yielded a discharge of 50.2 ± 3.6 L/s (Table 1). Zones of apparent stagnant water are identified near the banks (Figure 20), while most of the flow is in the centre of the stream at depths between 20 and 40 cm. Such discrepancies in the river velocities are expected to play a significant role in solute transport and on our tracing experiment. Their role on the interpretation of the tracer injection restitutions is discussed below.

Table 2: Discharge values measured and associated uncertainties. Note that anion (Cl^- , Br^-) uncertainties were not available.

Measuring Point	Tracer Used	Discharge (L/s)	Uncertainties (L/s—%)	f (% of Total Flow)
FlowTracker	Velocity method	50.2	3.6–7.2	Not applicable
WTW1	Electrical conductivity	56.5	1.8–3.2	8.2
WTW2	Electrical conductivity	56.9	1.3–2.3	17.4
WTW3	Electrical conductivity	55.3	1.3–2.3	34.2
WTW4	Electrical conductivity	52.6	1.8–3.4	16.5
WTW5	Electrical conductivity	53.8	1.4–2.6	3.3
LTC 23	Electrical conductivity	49.8	1.1–2.2	11.4
LTC 24	Electrical conductivity	51.5	1.2–2.2	9.1
Composite restitution	Electrical conductivity	53.3	6.5–12.2	Not applicable
WTW3	2H	51.1	0.4–0.7	Not applicable
Fluo.	Tinopal	53.0	0.5–1.0	Not applicable
Fluo.	Uranine	60.6	0.8–1.4	Not applicable
Fluo.	^{37}Cl	39.4	2.3–5.7	Not applicable

Fluo.	Cl ⁻	41.3	Unknown	Not applicable
Fluo.	Br ⁻	54.7	Unknown	Not applicable

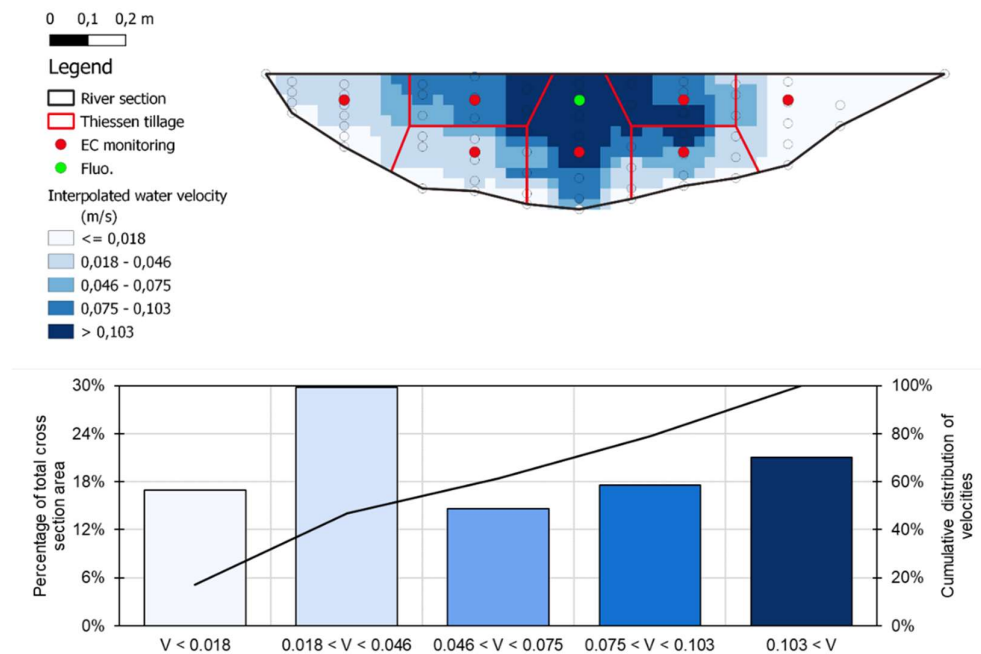


Figure 20: Distribution of interpolated river water velocity ($n = 342$). A value of zero was forced at the streambed and above the water surface for the spatial interpolation. Velocities are expressed in $m.s^{-1}$.

2.3.3.2 Using salt tracers to build a representative restitution curve for the whole section

A total of 7 restitution curves for electrical conductivity were obtained in the field. Restitution curves—expressed in mg/L of added salt tracers—are shown in Figure 21. The peak time is defined for each restitution curve as the time elapsed between the injection time and when the maximum concentration was measured. Tracer homogeneity across the river width was ensured at the injection point by laterally mixing the river water seconds after the injection. Except for WTW5, all restitution curves are very similar (Figure 21) in terms of peak time. This indicates that the transverse dispersion occurring along the reach is sufficient to ensure a good tracer homogeneity. The probe WTW5 was installed near the left bank in a zone of very low velocity with backwaters (Figure 20). Its peak height is lower than others and delayed with an increased peak width, which indicates tracer exchange between the main channel and transient storage zones (Briggs et al., 2009; Runkel & Chapra, 1993).

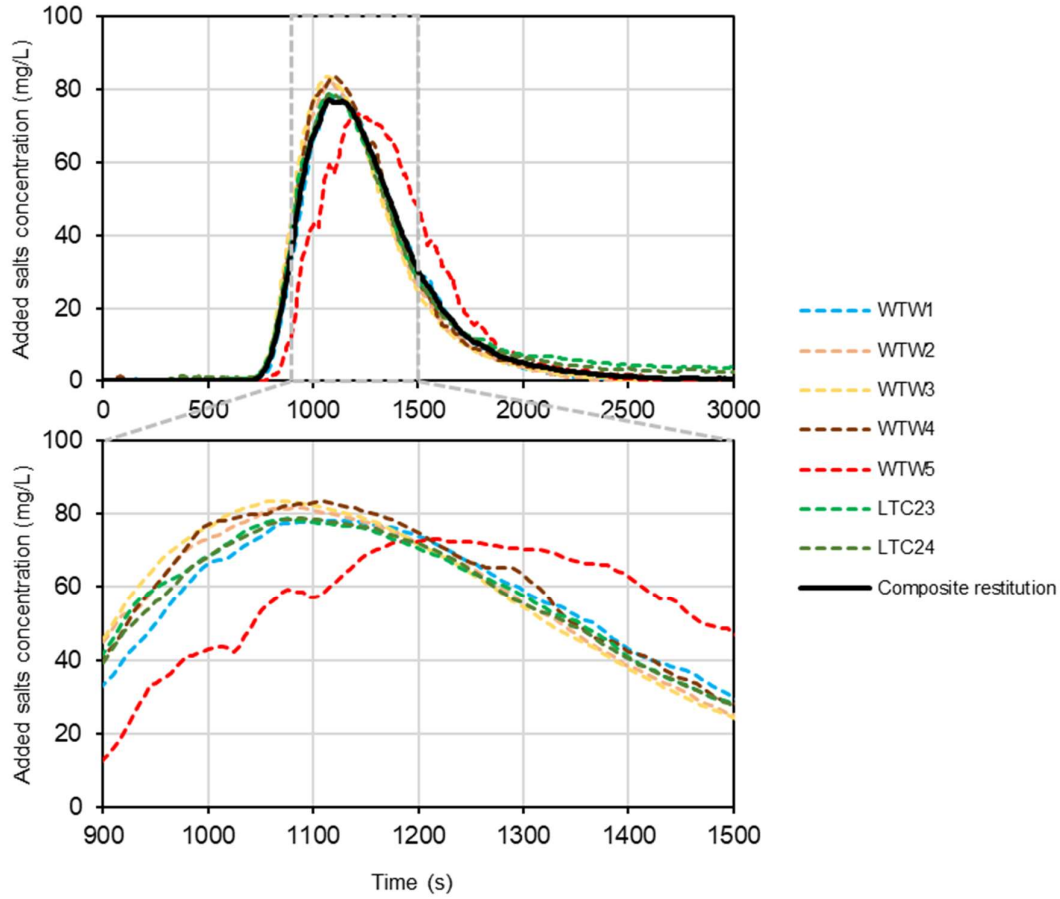


Figure 21: Upper graph: the seven salts concentration restitution functions and the composite restitution function. Lower graph: zoom-in around the peak time showing slight differences in peak heights. Background initial concentrations were removed, which explains the zero concentration at the beginning of the experiment.

Equations (4) and (5) were used to compute discharge values for each curve. In addition, the uncertainty propagation calculation was performed using the formula given in Equation (7). Discharge values are between 49.8 ± 1.1 and 56.9 ± 1.3 L/s. Most of them agree with the value obtained with the FlowTracker. However, the values obtained at measuring points WTW1, WTW2, and WTW3 are slightly above the value measured with the FlowTracker (Table 1). We suspect that there could be either a slight underestimation of the flow velocity measurements using the FlowTracker or an overestimation of the quantity of tracer. However, the latter is unlikely as it would shift all the obtained values and the quantities of tracer used were also thoroughly measured.

In all strictness, the second hypothesis of the use of Equation (4) (i.e., homogeneity of tracer concentration across the river section) is not entirely verified. We show below that Equation (4) can still be applied, with minimal effect on discharge calculations. To do so, we calculated a tracer output function averaged for the whole cross-section. This new restitution function (called “composite” in the following) includes the whole mass of tracer and is calculated as follows. Each restitution curve is supposed to be representative of the local tracer output. The river section was cut into seven sub-areas following Thiessen tillage (Figure 20), each of which were represented by one conductivity probe. The interpolated water velocity distribution presented in Figure 20 was then used to compute the discharge related to each sub-area. The latter is computed by multiplying the interpolated mean flow velocity by the surface of the sub-area. Typically, sub-areas near the banks have a lower discharge than the sub-areas located in the middle of the flow. The composite restitution function (see Figure 21) was then calculated as follows:

$$C_{\text{composite}}(t) = \sum_{i=1}^7 C_i(t) f_i \quad (12)$$

where i refers to the sub-area related to each probe (7 being the total number), C is the salt concentration [ML^{-3}] and f_i is the fraction of total discharge passing by the sub-area i (adimensional). This cross-sectional flow-averaged function is very close to restitution functions obtained from the main flow channel since the weight of the dead zones is very limited. Indeed, the discharge and uncertainty propagation calculations yielded $Q_{\text{composite}} = 53.3 \pm 6.5 \text{ L/s}$, which is very close to discharges calculated over the cross-section. This strongly suggests that the “dilution” method is adapted to such small low-gradient streams with contrasted velocities. Furthermore, the calculation proposed in this work (Equation (12)) is adapted to any stream, especially if restitution functions are much different from the banks to the middle and requires (i) a precise survey of streamflow velocities across the whole section and (ii) the monitoring of tracers at various spots across the river section. The advantage of this function is that it verifies all the hypotheses of Equation (3) since it simulates the section-integrated homogenised tracer concentration dynamics. However, its main limitation is obviously the uncertainty propagation. While individual restitutions yield discharges values

with uncertainties between 2.2% and 3.2%, the composite restitution gives uncertainties of 12.2%.

2.3.3.3 Isotopic tracers as new tracers for discrete and clean discharge measurements – Comparison with other tracers

Salt tracers are very useful for stream discharge measurements because they can easily be found, are inexpensive and are easy to monitor in the field thanks to electrical conductivity probes. However, their use can be very problematic in watersheds sheltering endangered ecosystems and species or used for surface drinking water production. In such contexts, it is worth to search for more adapted artificial tracers that can be injected in sufficiently low quantities that do not harm the environment and do not draw public attention like fluorescent dyes.

Stable isotopes tracers are now widely used in hydrology and hydrogeology as natural tracers (Clark, 2015; Clark & Fritz, 1997; Cook & Herczeg, 2000; Leibundgut et al., 2009). Their use as artificial tracers is also reported in the literature, especially in the unsaturated zone and for tracing groundwater flows over short distances (see (Leibundgut et al., 2009) and references therein). However, their potential for discrete, clean, and precise stream discharge measurements has not been addressed to date. In this work, heavy stable isotopes ^2H (deuterated water, $^2\text{H}_2\text{O}$) and ^{37}Cl (isotopically enriched salt) were used as conservative tracers for quantitative interpretation of river discharge and comparison with other tracers.

The injected mass of each isotopic tracer was determined using the known mass of injected deuterated water and salt and their isotopic contents. Indeed, the deuterated water has a ^2H abundancy of $99.90 \pm 0.05\%$, and the ^{37}Cl -enriched salt has a $\delta^{37}\text{Cl}$ value of $+ 2.18 \pm 0.03\text{‰}$ vs. SMOC, yielding totals of 403.09 ± 0.20 g of ^2H and $131.17 \text{ g} \pm 0.09$ g of ^{37}Cl . Stream discharge was computed using Equations (4) and (5), and uncertainty propagation was performed using Equation (7) (details for isotopes are also presented in Annex). Results are presented in Table 1 and the restitution curves of tracers can be found in Figure 22.

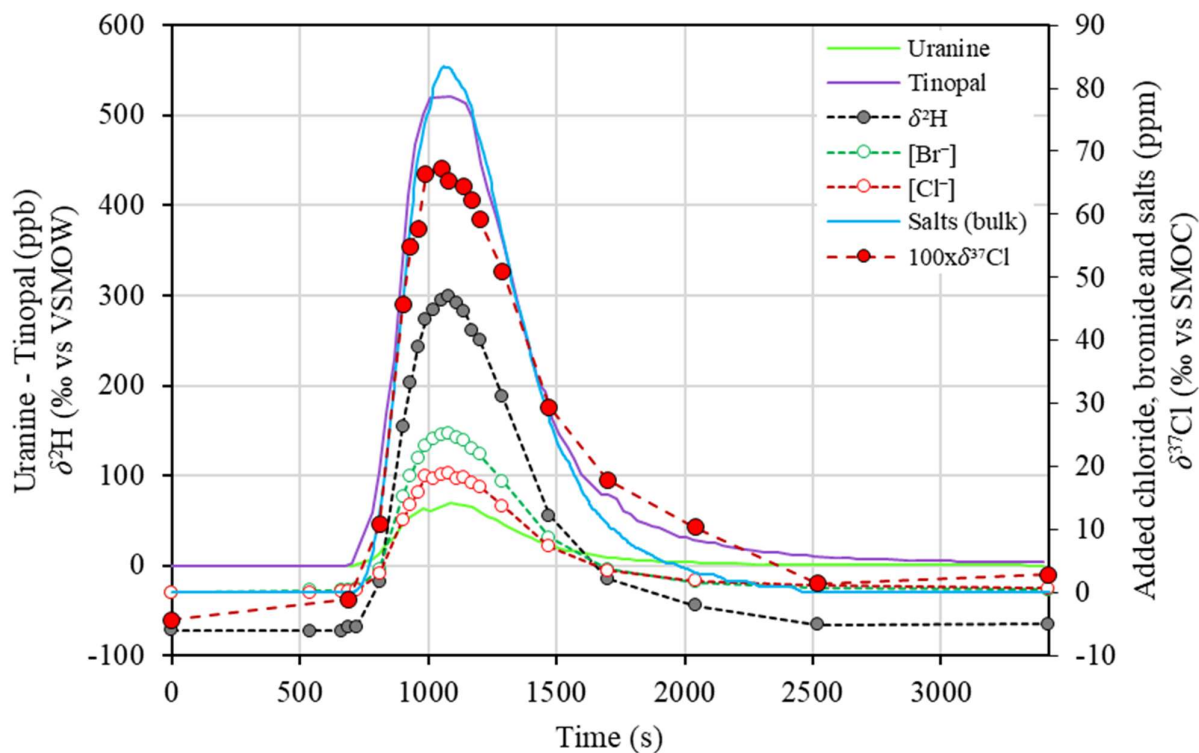


Figure 22: ^2H , ^{37}Cl , Cl^- , Br^- and fluorescent tracers (uranine, tinopal) restitutions obtained at the centre of the stream.

The highest discharge is obtained for uranine (60.6 ± 0.7 L/s). Only 2.42 g of uranine was injected, and a degradation of roughly 0.3 g could explain the shift obtained in discharge values. It is unlikely to have been considerably affected by photodegradation as the experiment time is less than 2 h, but it could be explained by an underestimation of the injected mass linked to the quality of the tracer and the fact that the calibration of the fluorometer was performed prior the field test using distilled water. Tinopal yielded a discharge value of 53.0 ± 0.5 L/s, which is in the same range as the FlowTracker measurement and electrical conductivity monitoring values. The discharge value obtained with deuterium is 51.1 ± 0.4 L/s, while ^{37}Cl data yielded a discharge of 39.4 ± 2.3 L/s. One must be aware that $\delta^{37}\text{Cl}$ measures uncertainties that are usually of the order of $\pm 0.1\text{‰}$, which is greater than the $\pm 0.03\text{‰}$ used in our calculations. These higher uncertainties would yield a total uncertainty of ± 9.0 L/s ($\pm 22.9\%$ of the discharge value). However, even though the discharge value obtained with ^{37}Cl is consistent with the discharge obtained using Cl^- , it is very different from other tracers' signals. The chloride and ^{37}Cl signals seem more concentrated relatively to other tracers' signals.

Strictly speaking, for the same mass of a tracer, the use of ^2H as an artificial tracer allows for a more precise discharge measure than the use of ^{37}Cl (Figure 23). The calculations used for Figure 23 are presented in the Appendix. However, even though deuterium analyses are widely affordable, the purchase of deuterated water is subject to governmental limitations, so one must be aware of potential difficulties in finding such a tracer in addition to the need for in-house produced enriched standards. On the other hand, while chloride is simple to find and cheap, ^{37}Cl -enriched salts are much harder to find. In addition, one must be aware that the background noise of ^2H in rivers is commonly of the order of 140 to 156 ppm (for a $\delta^2\text{H}$ ranging from -100‰ to 0‰ vs. VSMOW) and that the ^{37}Cl background noise of rivers with high chloride concentrations might be high because of the relatively high natural abundance of ^{37}Cl ($^{37}\text{R}_{\text{SMOC}} = 0.324$). In the quantities that were injected, deuterated water can be considered as the best tracer to measure stream discharge because it does not modify or alter the qualitative and ecological state of the stream while being a robust and extremely precise tracer.

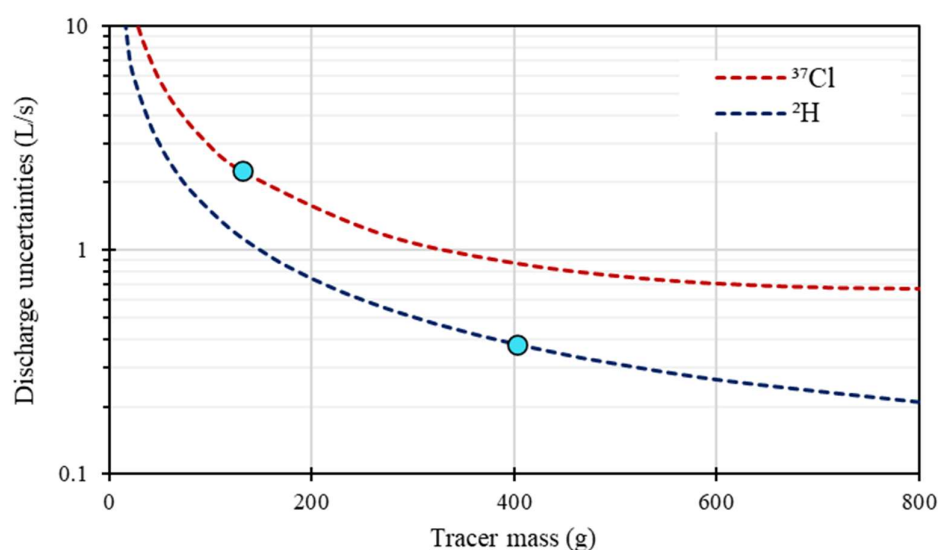


Figure 23: Discharge measure uncertainty as a function of mass of injected tracer (^2H , ^{37}Cl) for the studied river (the blue dots represent this experiment). It is important to note that the x-axis refers to the actual isotopic tracer's mass alone and not ^{37}Cl -enriched salt or deuterated water. Details on these calculations can be found in Appendix A.

2.3.3.4 Transient storage zone exchanges inferred from multi-tracer data

When a tracer is injected into the stream, advective-dispersive transport will result in solute tracer homogenization over the river width due to transverse dispersion and a classical Gaussian form of the restitution function due to longitudinal dispersion. However, the tracer will also exchange with transient storage zones, such as dead zones near the banks and/or the hyporheic zone at the bottom of the stream, and will be slowly released to the main flow channel (De Smedt, 2007; Genuchten et al., 2013b; Runkel, 1998). Transport in the hyporheic zone is known for being mainly advective (Boano et al., 2014). Since tracer residence times in the transient storage zones are typically several orders of magnitude higher than those of the tracer in the stream alone, information on hyporheic exchanges can be found on the tailing part of the breakthrough curves.

Here, we took advantage of having multiple tracer restitutions to study the interactions between the stream and the hyporheic zone in more detail. Normalized breakthrough curves (C/C_{\max}) of tinopal, ^2H , ^{37}Cl , Br^- , and Cl^- show different behaviours during the tailing part of the experiment (Figure 24). If we define persistence as the affinity of the tracer to stay in the stream for long times, bromide is the least persistent tracer, while chloride (and especially ^{37}Cl) is the most persistent. ^2H lies in between, and being part of the water molecule, is the ideal tracer of the latter. It seems that the surface solute transport is affected by one (or more) hydrological unit(s) that acts as a filter, filtering the entrance of the tracer and thus controlling the residence time of tracer within it. Such a hydrological unit could be a surface transient storage zone and/or hyporheic zone.

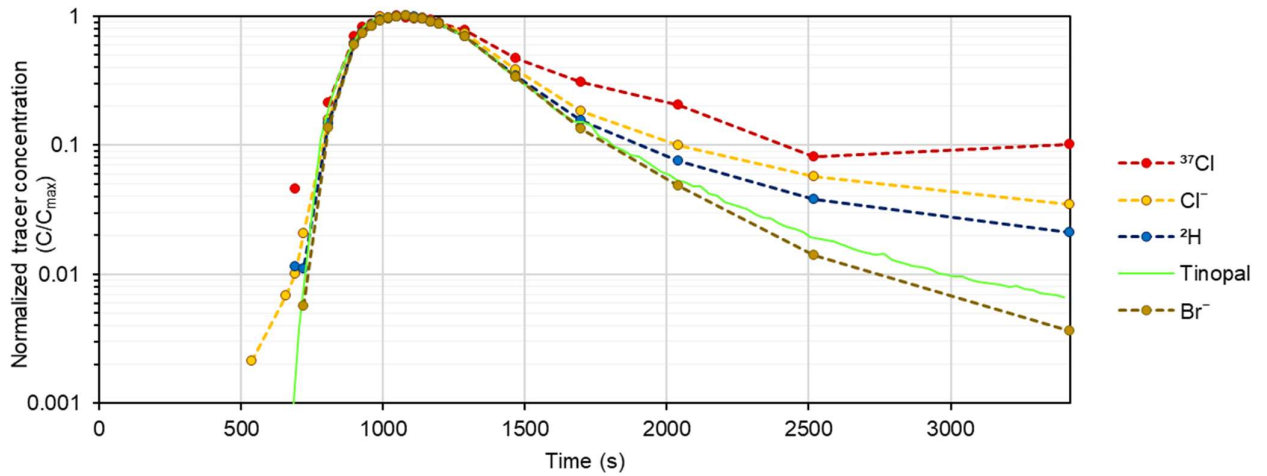


Figure 24: Normalized tracer restitution showing different tracer behaviours at times >1500 s.

Since the tracers used in this study have different chemical and physical properties, we can expect them to behave differently regarding hyporheic and surface dead zone exchanges. Exchanges between the stream and the subsurface (e.g., the hyporheic zone) are controlled by the streambed permeability and porosity (Boano et al., 2014) but might also be controlled by the effective accessible pore size of tracers. Bromide restitution shows a lower tailing effect, meaning that it is less affected by such exchanges than ^2H and ^{37}Cl . The breakthrough curves of the latter two indicates that the release of chloride is slower than that of deuterium. This makes sense, as chloride transport in a porous media might be slowed due to its size compared to ^2H . Tinopal was expected to fall below the Br^- curve since it is the largest molecule used (chemical formula: $\text{C}_{40}\text{H}_{40}\text{N}_{12}\text{O}_8\text{S}_2$). Because of its high susceptibility to be absorbed to suspended particles, such as clays and organic matter, and its low effective solubility (Licha et al., 2013; Schiperski et al., 2019), tinopal is often not considered a totally conservative tracer. This results in a prolonged tailing effect, that might explain why it is more “persistent” than bromide.

Bromide, ^{37}Cl , and ^2H restitution curves were fitted to the binary mixing model described in Equations (9)–(11) (Figure 25). The f_1 parameter that represents the fraction of the fast component as well as its velocity, v_1 , were set as the same for all tracers because this part of the flow is controlled by advective transport and should not vary from one tracer to the other. However, parameters for the slow component (dispersion and velocity) were set to vary to

model the differences in tailing seen in Figure 24 and account for the different behaviours of tracers. The set of parameters that provided the best fit is given in the Table 2. The transient zone storage fraction, f_2 ($f_2 = 1 - f_1$), is 0.42. This means that it exerts a very strong influence in the transport characteristics of the dissolved solutes. It is thought to be the fraction of the flow that is affected by both surface transient storage and transport within the hyporheic zone. Bromide and deuterium breakthrough curves are well modelled, especially at longer times. However, ^{37}Cl is affected by another phenomenon. Indeed, we saw earlier that the discharge measured using both chloride and its heavy isotope was somewhat less than that noted with other tracers. In addition, the model predicts a higher concentration than what was measured in the field. It is still unclear why chloride behaves in such a way.

Table 3: Best-fit set of parameters for the modelling of solute transport affected by diffusive transfer in the hyporheic zone.

g ₁ Parameters				g ₂ Parameters		
Tracer	f_1	D_1 (m ² /s)	v_1 (m/s)	D_2 (m ² /s)	v_2 (m/s)	χ^2 (mol/L)
^2H		0.10	0.097	0.20	0.068	9.5×10^{-4}
^{37}Cl	0.58	0.13	0.097	0.39	0.053	7.5×10^{-5}
Br^-		0.10	0.097	0.26	0.070	6.2×10^{-5}

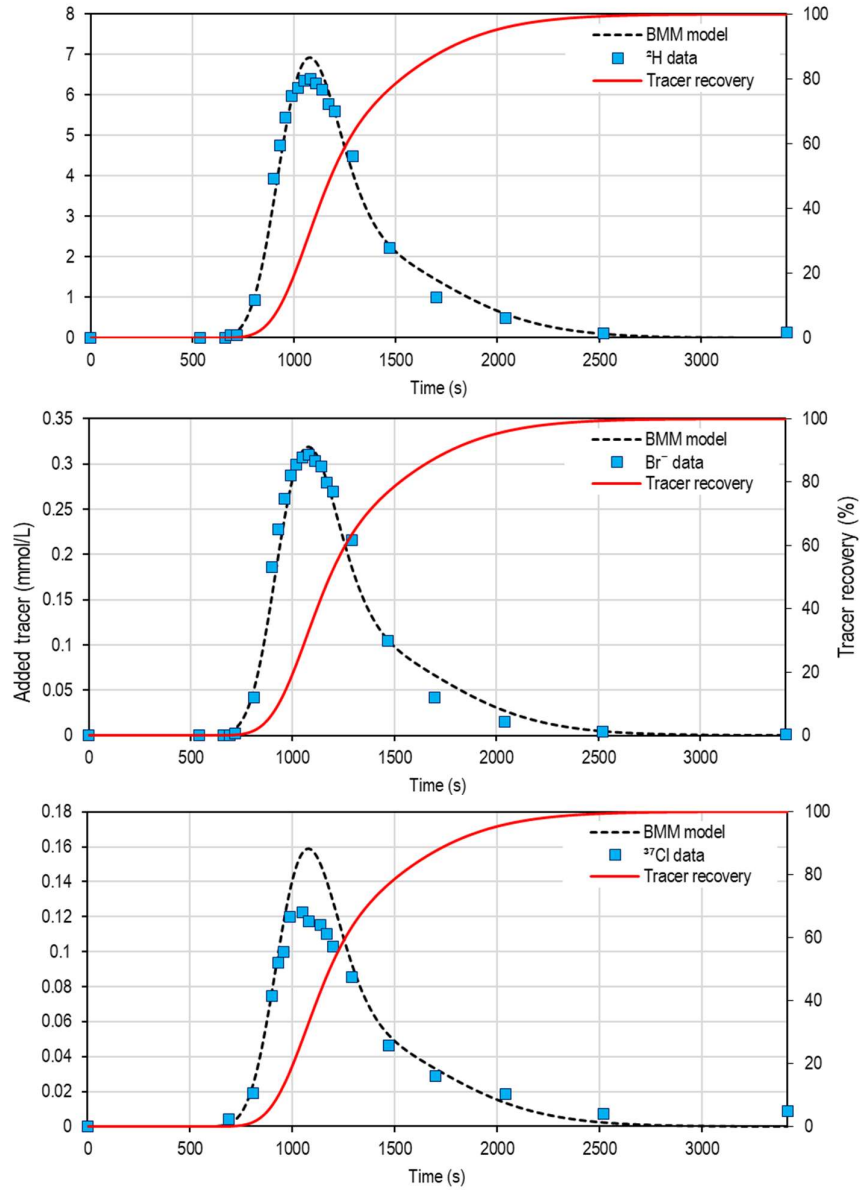


Figure 25: Tracers' concentrations modelled using a binary mixing 1D dispersion model.

2.3.4 Conclusions

Solute transport in a small low-gradient stream was studied under baseflow conditions. The stream is characterized by contrasting channel characteristics with a succession of small riffles and pools. The cross-sectional dynamics of salt tracers (monitored using the electrical conductivity signal) revealed a very good homogenization of the tracers, except in a large

dead zone near one of the banks. The computation of a composite tracer restitution, integrating the cross-sectional dynamics, showed that the “dilution” method is still applicable in such small, low-gradient, heterogeneous streams. Stable isotopes ^2H and ^{37}Cl are reliable tracers for discharge measurements in small streams. In addition, deuterium revealed to be an excellent tracer for such an experiment since it can be released in the environment in very small quantities without any environmental effect and still yielded more precise results than traditional tracers.

This multi-tracer (Br^- , Cl^- , ^2H , ^{37}Cl , uranine, tinopal and the electrical conductivity signal) approach also allows depiction of the river solute transport in detail, especially the identification of the behaviours of solutes over the longer residence times. The tailing part differences of the restitution curve of the tracers Br^- , Cl^- , ^2H , ^{37}Cl , and tinopal are attributed to differences in the tracers’ behaviours regarding transient storage zones. However, chloride shows an unexpected, prolonged tailing effect. It is unclear whether chloride was affected by another chemical process as the signal seems “diluted” relative to the other tracers. Further investigations should be performed using such a multi-tracer approach for longer experiments, including the multi-injection and monitoring of inert and reactive gases in the stream (e.g., He , N_2 , C_3H_8), to explore their potential for stream discharge measurements and transient-zone storage interactions.

2.3.5 Appendices

Appendix A

One of the objectives of this study is to compare isotopic tracers’ accuracy for discharge measurements. First, let us recall Equation (A1):

$$\Delta Q = |Q| \sqrt{\left(\frac{\Delta M_{\text{tracer}}}{M_{\text{tracer}}}\right)^2 + \frac{\sum_{i=1}^{n-1} (t_{i+1} - t_i)^2 (\Delta C_{i+1}^2 + \Delta C_i^2)}{[\sum_{i=1}^{n-1} (t_{i+1} - t_i)(C_{i+1} + C_i)]^2}} \quad (\text{A1})$$

The equation indicates that discharge uncertainty is a function of the tracer mass and the tracer concentration uncertainties (ΔM and ΔC , respectively). In the following, we show how we

computed both for ^2H and ^{37}Cl . Before going further in the calculations, we give the expression of isotopic abundancies and their uncertainty calculations:

$$\begin{cases} ab = \frac{R_{ref}(10^{-3}\delta_{value} + 1)}{1 + R_{ref}(10^{-3}\delta_{value} + 1)} \\ \Delta ab = ab \sqrt{\left(\frac{10^{-3}(\Delta\delta_{value})}{10^{-3}\delta_{value} + 1}\right)^2 + \left(\frac{R_{ref}10^{-3}(\Delta\delta_{value})}{1 + R_{ref}(10^{-3}\delta_{value} + 1)}\right)^2} \end{cases} \quad (A2)$$

where ab is the abundancy (and Δab its associated uncertainty).

Appendix A.1. ^2H Calculations:

The mass of injected deuterium is computed as follows:

$$^2M = 2 \frac{M_{sol}M_{^2H}}{M_{^{16}O} + 2M_{^1H} + 2^2ab_{sol}(M_{^2H} - M_{^1H})} ^2ab_{sol} \quad (A3)$$

where 2M is the mass of injected deuterium; M_{sol} is the mass of deuterated water that is used, i.e., 2005.4627 ± 0.0001 g; $^2ab_{sol}$ is the deuterium abundancy of the deuterated water ($99.90 \pm 0.05\%$); and $M_{^{16}O}$, $M_{^1H}$, and $M_{^2H}$ are the isotopic molar masses of ^{16}O , ^1H , and ^2H , respectively. We suppose that the only sources of uncertainties are M_{sol} and $^2ab_{sol}$, and we simplified the calculation by considering only ^{16}O for oxygen isotopes (abundance of ^{17}O being less than 0.0004). The uncertainty propagation performed for Equation (A3) gives the following:

$$\Delta^2M = 2M \sqrt{\left(\frac{\Delta^2ab_{sol}}{^2ab_{sol}}\right)^2 + \left(\frac{2(M_{^2H} - M_{^1H})\Delta^2ab_{sol}}{M_{^{16}O} + 2M_{^1H} + 2^2ab_{sol}(M_{^2H} - M_{^1H})}\right)^2} \quad (A4)$$

Then, we aim to express ^2H concentrations as a function of the $\delta^2\text{H}$ values because laboratory analyses give uncertainties for $\delta^2\text{H}$. This is shown in the following equation:

$$[^2H]_i = 2.10^6 M_{^2H} \left(\frac{^2ab_i}{M_{^{16}O} + 2M_{^1H} + 2^2ab_i(M_{^2H} - M_{^1H})} - \frac{^2ab_0}{M_{^{16}O} + 2M_{^1H} + 2^2ab_0(M_{^2H} - M_{^1H})} \right) \quad (A5)$$

where $[^2\text{H}]$ is the deuterium concentration, i represents the number of the sample, and 2ab_i and 2ab_0 are the deuterium abundancies for sample “ i ” and the initial background, respectively. Using Equations (A2) and (A5), we finally obtain the following:

$$\left\{ \begin{array}{l} \Delta[^2\text{H}]_i = \frac{[^2\text{H}]_i}{\frac{^2ab_i}{X} - \frac{^2ab_0}{Y}} \sqrt{\left(\frac{^2ab_i}{X}\right)^2 \left(\left(\frac{\Delta^2ab_i}{^2ab_i}\right)^2 + \left(\frac{\Delta X}{X}\right)^2\right) + \left(\frac{^2ab_0}{Y}\right)^2 \left(\left(\frac{\Delta^2ab_0}{^2ab_0}\right)^2 + \left(\frac{\Delta Y}{Y}\right)^2\right)} \\ X = M_{^{16}\text{O}} + 2M_{^1\text{H}} + ^2ab_i(M_{^2\text{H}} - M_{^1\text{H}}) \\ \Delta X = \Delta^2ab_i(M_{^2\text{H}} - M_{^1\text{H}}) \\ Y = M_{^{16}\text{O}} + 2M_{^1\text{H}} + ^2ab_0(M_{^2\text{H}} - M_{^1\text{H}}) \\ \Delta Y = \Delta^2ab_0(M_{^2\text{H}} - M_{^1\text{H}}) \end{array} \right. \quad (\text{A6})$$

The Equations (A4) and (A6) are then used in Equation (A1), and the discharge uncertainty can now be expressed as a function of both the mass of the tracer and the tracer output concentrations. It is easy to simulate new tracer restitutions as a function of the mass of the tracer injected: $[^2\text{H}](i, M_{\text{test}}) = [^2\text{H}](i)M_{\text{test}}/M$, where M_{test} is the mass of tracer set to vary. Note, we suppose that the ratio $\Delta M_{\text{test}}/M_{\text{test}}$ is constant for all values of M_{test} . In the particular case of deuterium, it is important to acknowledge that the $\Delta\delta^2\text{H}$ value is expressed as a function of the expected $\delta^2\text{H}$ value (see Figure 26 below).

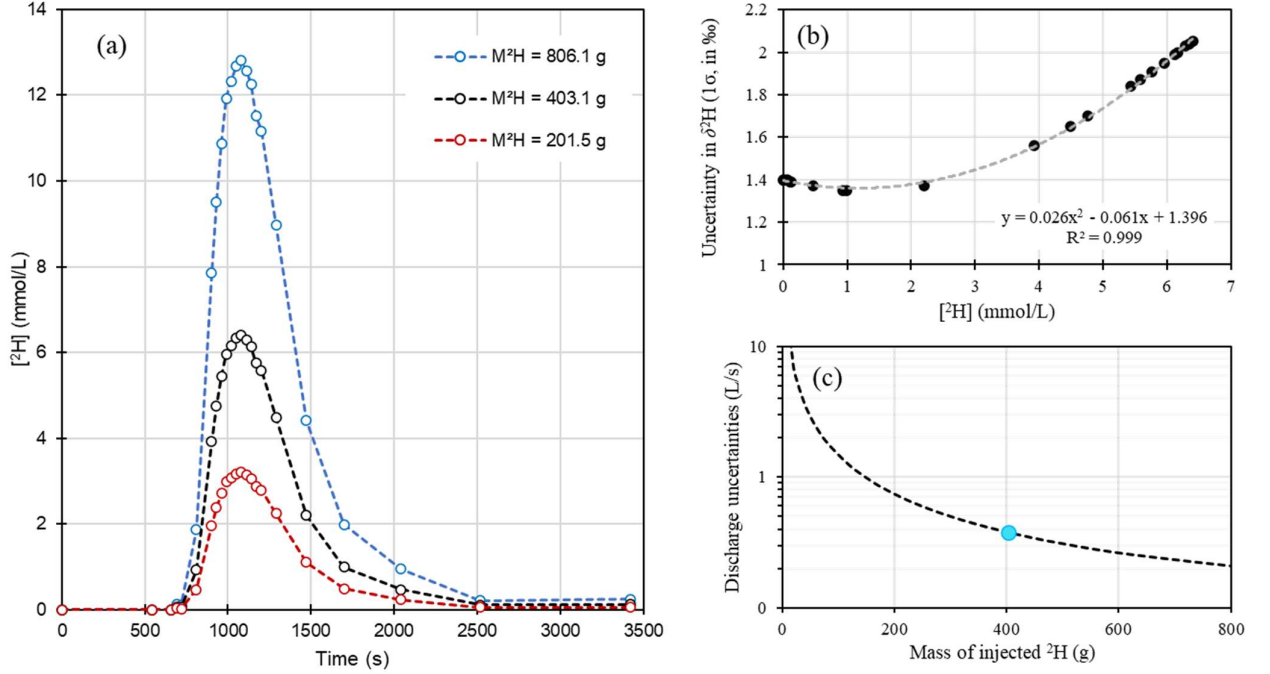


Figure 26: (a) Three examples of expected deuterium restitution curves with different tracer input masses. Note that $M^2\text{H} = 403.1 \text{ g}$ is the mass of ^2H that was injected in the stream. (b) The relationship between the measured mass of deuterium and its uncertainty (the black dots are from the field samples). (c) Graph showing the evolution of discharge uncertainties as a function of the mass of injected ^2H (the experiment described in this paper is represented by the blue dot).

Appendix A.2. ^{37}Cl Calculations:

The mass of injected ^{37}Cl (^{37}M) is computed as follows:

$$^{37}\text{M} = M_{\text{Cl}}^{37} ab_{\text{salt}} \quad (\text{A7})$$

Here, $^{37}\text{ab}_{\text{salt}}$ is the ^{37}Cl abundance of the salt that is used, and M_{Cl} the total mass of the chloride that was injected (in this study, $535.14 \pm 0.01 \text{ g}$). The $^{37}\text{ab}_{\text{salt}}$ is computed using a $\delta^{37}\text{Cl}$ value of $2.18 \pm 0.03\text{‰}$ vs. SMOC ($^{37}\text{ab}_{\text{salt}} = 0.24512 \pm 0.00003$). The calculation of $\Delta^{37}\text{M}$ is straightforward, and we obtain $\Delta^{37}\text{M} = 1.39 \text{ g}$.

Then, we use the following equation to compute the concentration of injected chloride for each sample:

$$[^{37}\text{Cl}]_i = \text{Cl}_0^- \frac{{}^{37}\text{ab}_i - {}^{37}\text{ab}_0}{1 - \frac{{}^{37}\text{ab}_i}{{}^{37}\text{ab}_{\text{salt}}}} \quad (\text{A8})$$

where Cl_0^- is the initial total chloride concentration in the stream associated with an initial isotopic abundancy ${}^{37}\text{ab}_0$ (computed knowing that $\delta^{37}\text{Cl}_0 = -0.04 \pm 0.03\text{‰}$ vs. SMOC), and the subscript “i” refers to the number of the sample. It is important to acknowledge that we could not obtain the uncertainty in chloride measurements. However, we could show that if the latter is in the range of 0.1 to 1 ppm, it has nearly no effect on the final discharge uncertainty.

Finally, we obtain the following:

$$\Delta[^{37}\text{Cl}]_i = [^{37}\text{Cl}]_i \sqrt{\left(\frac{\Delta\text{Cl}_0^-}{\text{Cl}_0^-}\right)^2 + \frac{\Delta{}^{37}\text{ab}_i^2 + \Delta{}^{37}\text{ab}_0^2}{({}^{37}\text{ab}_i - {}^{37}\text{ab}_0)^2} + \left(\frac{{}^{37}\text{ab}_i}{{}^{37}\text{ab}_{\text{salt}}}\right)^2 \left(\left(\frac{\Delta{}^{37}\text{ab}_i}{{}^{37}\text{ab}_i}\right)^2 + \left(\frac{\Delta{}^{37}\text{ab}_{\text{salt}}}{{}^{37}\text{ab}_{\text{salt}} - {}^{37}\text{ab}_i}\right)^2\right)} \quad (\text{A9})$$

Equation (A9) is then used in Equation (A1), and the discharge uncertainty can now be expressed as a function of both the mass of the tracer and the tracer output concentrations. As for deuterium, we can plot the evolution of ΔQ as a function of the mass of ${}^{37}\text{Cl}$ that is used (see Figure 23). We suppose that the $\delta^{37}\text{Cl}$ uncertainty is constant and always equal to 0.03‰, which is different from deuterium.

2.4 Simultaneous determination of major (N₂, O₂), noble (Ar, He, Kr) and anthropic trace gases (CFC-12, CFC-11, SF₆) contents from passive discrete samples (*Article 2*)

A new approach to the analysis of dissolved gases using passive samplers, with portable mass spectrometry and gas chromatography techniques.

In the process of being submitted to the journal "Rapid Communications in Mass Spectrometry" (February 2025).

Antoine Picard^{1,2}, Florent Barbecot^{1,2}, Matéo Lacheux^{1,2}, Matthias S. Brennwald³, José A. Corcho-Alvarado⁴

¹ Hydro Sciences UQAM-ETS, Département des Sciences de la Terre et de l'atmosphère, Université du Québec à Montréal, Canada.

² Geotop (Research Centre on the Dynamics of the Earth System), Montréal, Canada.

³ Nuclear Chemistry Division, Spiez Laboratory, Federal Office for Civil Protection, Austrasse, 3700 Spiez, Switzerland.

⁴ Department of Water Resources and Drinking Water, Eawag, Swiss Federal Institute of Aquatic Science and Technology, Dübendorf, Switzerland.

Abstract: The recent development of portable mass spectrometry (e.g., miniRUEDI) allowed relatively easy and cheap access to the determination of gases with unprecedented time resolution, directly in the field, from reservoirs that are constantly renewed (ex: ambient air, water bodies). However, it is not adapted to the analysis of discrete water samples of small (few cc) volumes. We address this issue with the presentation of "small" (≈ 25 cc) passive samplers for the sampling of dissolved gases in water and a simple and effective system built to connect the samplers to the miniRUEDI for gas analysis. The samplers are let to equilibrate under water for a few days, then retrieved and locked when the equilibration between the inside of the sampler and the water is attained, before being analysed by combining miniRUEDI and gas chromatography-electron capture detector (GC-ECD) techniques back in the lab. This new method enables quick and accurate determination of major (N₂, O₂), noble (here, He, Ar and Kr) and transient gas species for age dating (SF₆, CFC-12, CFC-113, etc.) from one single sample. This approach has the potential to be used to facilitate the use of

transient anthropic gas tracers for the determination of young (< 70 years) groundwater age information. In addition, the analysis of multiple gases in a single sampler as well as the easy installation of multiple samplers in groundwater and surface waters allow for cost-effective mapping of gas tracer plumes during artificial tracer release experiments.

Keywords: passive samplers, dissolved noble gases, miniRUEDI, artificial tracers.

2.4.1 Introduction

Dissolved gases, especially noble gases, are often used as both environmental and artificial tracers to study the hydro-geosphere (Brennwald et al., 2022; Burnard, 2013; Clark et al., 2005; Clark et al., 1996; Cook & Herczeg, 2000; Kipfer et al., 2002; Sanford et al., 1996; Schilling et al., 2023; Schilling et al., 2021; Stute et al., 1995). For example, groundwater dating often relies on the determination of dissolved gas contents. Sulphur hexafluoride (SF₆), chlorofluorocarbons (CFCs, more precisely: CFC-12, CFC-11 and CFC-113) and helium isotopes (especially tritiogenic ³He) are commonly used for dating “young” groundwater, *i.e.* recharged in the second half of the 20th century (Chambers et al., 2018; Cook & Herczeg, 2000; Darling et al., 2012; Gooddy et al., 2006; Kazemi et al., 2006; Meyzonnat et al., 2023; Suckow, 2014). The determination of excess air, a common feature in groundwater resulting from the entrapment of small bubbles during recharge processes, is required for the correction of dissolved gas concentration for dating purposes (*e.g.* SF₆, CFCs, ³H-³He) and can be modelled using noble gas data (Aeschbach-Hertig et al., 2008; Aeschbach-Hertig et al., 1999; Aeschbach-Hertig et al., 1998; Schlosser et al., 1989; Stute et al., 1995). The deliberate injections of inert gas tracers in streams and groundwater can be used for the study of groundwater travel times, transport mechanisms, groundwater/surface water interactions as well as streams aeration dynamics (Blanc et al., 2024; Brennwald et al., 2022; Clark et al., 2005; Sanford et al., 1996; Solomon et al., 2015).

As pointed out by Sanford et al. (1996), although gases are excellent artificial tracers for the investigation of water transport, dynamics and mixing compared to traditional tracers (salts, dyes), their use is complicated by difficulties in the sampling method leading to air contamination, and analysis procedures (*e.g.* quantitative extraction of dissolved gases from

water samples, risk of damaging the lab machines with liquid water from the samples). Classically, dissolved noble gases are sampled in copper tubes by active pumping and are then sealed using clamps. The dissolved gases in the samples are then extracted before being analysed using mass spectrometry. CFCs and SF₆ are sampled either (i) by filling glass vessels equipped with a septum cap for the application of the so-called headspace method (Busenberg & Plummer, 2010; Sliwka et al., 2004) or (ii) using stainless steel cylinders. The extraction of the dissolved gases is then necessary before analysis using, generally, gas chromatography (GC) techniques.

These two issues can be addressed by developing passive gas samplers, which originally consisted of copper tubes to which thin gas-permeable silicone membranes were attached (Gardner & Solomon, 2009; Sanford et al., 1996). These samplers are installed in water (wells, rivers, lakes) and left until equilibration with the water mass is attained (typically a few days), while gases permeate through the membranes (Musy et al., 2021; Zhang & Cloud, 2006). More recently, the development of portable field mass spectrometers, such as the miniRUEDI (Brennwald et al., 2016), has allowed a relatively easy access to the determination of (noble) gases concentrations in water. In hydrogeological investigations, high spatial resolution is often desired but is labour intensive, and thus difficult to achieve due to high costs, duplication of field equipment or the large amount of analysis. Passive samplers can overcome some of these difficulties as they can be installed in different locations in large numbers (ex: multiple wells and/or multiple depths in the same well), which is much easier and cost-effective than multiplying the installation of analysers (*e.g.* mass spectrometers) in the field.

The objectives of this paper are the following:

- (i) Construction of reusable passive samplers for dissolved gases in water, suitable for environmental sampling and artificial tracing experiments. The passive samplers presented in this study can be reused multiple times thanks to valves, and be stored before analysis for prolonged periods of time.
- (ii) Development of a cost-effective assembly for the analysis of the gas content in the passive samplers using portable mass spectrometry (miniRUEDI) and gas

chromatography (GC-ECD), allowing the determination of multiple gases in one single sample (N_2 , O_2 , Ar, CO_2 , He, Kr, CFC-12, CFC-113 and SF_6).

- (iii) Determination of the minimum time required for sampling dissolved gases using the passive samplers, and at the same time verify the absence of elemental fractionation during the equilibration process between the dissolved gases and the gas content inside the samplers.

2.4.2 Materials and methods

2.4.2.1 Passive samplers

The passive samplers used in this study are made of stainless-steel tubing (length 12 inches, outside diameter $\frac{1}{2}$ inch, wall thickness 0.05 inch), with two stainless-steel $\frac{1}{2}$ inch air-tight ball valves at each end. The internal volume of the samplers is around 26 cc. A gas-permeable silicone tube of roughly 4 inches is added at each valve via a ferrule fitting, allowing gas exchange between the inside of the sampler and the dissolved gases on the outside. A rigid PVC inner tube ensures that the silicone membrane does not collapse at high hydrostatic pressures. Holes were drilled in the inner PVC tube to let gases flow into the inner tube. The end of the silicon membranes are folded and tightly sealed using tie wraps. This simple system revealed to be impermeable as no liquid water was observed inside the samplers even after being immersed for a few days.

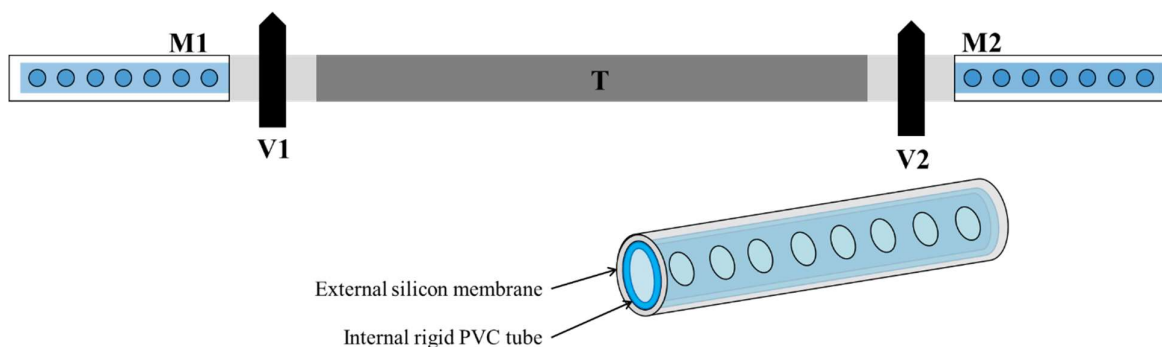


Figure 27 : Scheme of the passive samplers. "T" stands for the stainless-steel tube (length: 30 cm), V1 and V2 are the two Swagelok valves, and M1 and M2 are the two gas-permeable silicone membranes (length: 10 cm each). A cross-section of the membranes is also shown.

One of the fundamental parameters that characterize the samplers is the equilibration time, that is, the time required for a given gas partial pressure to reach equilibrium, since this time will control the time that the sampler will remain in a well. This physical process is well described elsewhere (Gardner & Solomon, 2009) and obeys Fick's first law. The equilibration time is a function of the effective diffusivity of the gases through the membrane (Gardner & Solomon, 2009; Sanford et al., 1996) and can be written as:

$$p_{i \text{ norm.}} = 1 - \exp\left(-\frac{t}{T_i}\right) \quad (1)$$

where, $p_{i \text{ norm.}}$ is the normalised partial pressure of gas i in the sample and T_i is the time constant [T⁻¹], which is a function of the gas species and the membrane properties.

2.4.2.2 Analysis of dissolved gases with the miniRUEDI.

The miniRUEDI (Brennwald et al., 2016) is a portable mass spectrometer used for environmental monitoring of (dissolved) gases (e.g. N₂, O₂, CO₂, He, Ar, Kr). For their analysis, gases are taken through a capillary from constantly renewed reservoirs, such as the atmosphere or a gas contactor, through which water is constantly renewed and equilibrated with a headspace. In its commercial version, the miniRUEDI does not allow the analysis of small, discrete finite volume samples. We addressed this gap by developing a simple system that enables the analyse of such samples with this system.

The setup is schematized on Figure 28 below. It is organized around a 4-way stainless-steel 1/8" union cross with: (i) a port for the passive sampler (stainless steel 1/2" ball valve V1), (ii) a port for a pressure sensor, (iii) a port for a primary diaphragm pump (stainless steel needle valve V4 1/8"), and (iv) a port for one of the inlet capillaries of the miniRUEDI (stainless steel ball valve V3 1/16"). Stainless steel reductions are used as adapters between the union cross and the different valves of different sizes.

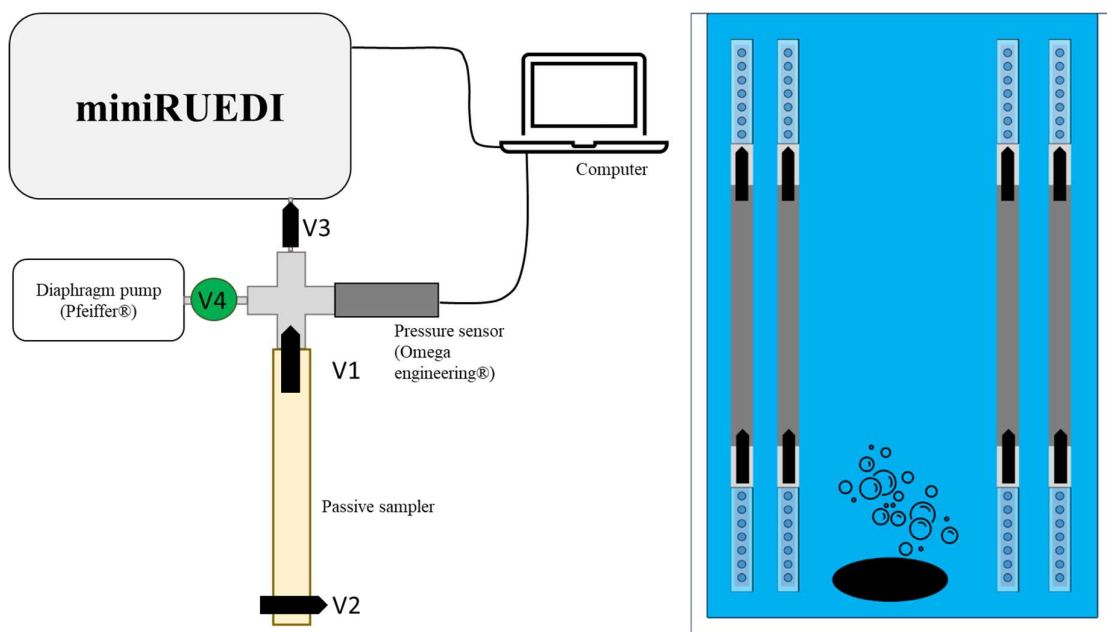


Figure 28: On the left: scheme of the setup used in analysis mode. On the right: scheme of the equilibration experiments. Passive samplers are immersed vertically in the 100 L bucket with the two ball valves open. A diffuser continuously injects air as bubble from the bottom of the bucket.

Initially, the ball valves V1 and V2 must be closed. For the analysis of a sample with the proposed setup, the following steps must be followed: (i) connect the passive sampler to the cross via one of the valves (V1 in Figure 28); (ii) activate the diaphragm pump and open the needle valve V4 and the ball valve V3 to vacuum the dead volume down to 5-7 hPa typically; (iii) close V4, then shut the diaphragm pump off and monitor the pressure using the pressure sensor to ensure there are no leaks/air contamination; and (iv) open the valve V1 (the valve plugged to the cross). Note that the use of a needle valve (V4) was motivated by the possibility of installing a turbopump between V4 and the diaphragm pump. Strictly speaking, a ball valve would also work fine if a high vacuum is not needed.

The initial total gas pressure in the sample ($P_{\text{tot,ini}}$) is calculated knowing the dead volume of the line (4-way cross + connections). In our example, the latter was calculated to 5.57 ± 0.01 mL, which is roughly 20% of the sample volume. The following protocol was adopted for the analysis of a sample using the miniRUEDI system:

- 3x blank analysis. This is done by following the steps given in the miniRUEDI software. To do so, the inlet needle valve of the miniRUEDI (see Figure 1 in Brennwald et al. (2016)) has to be manually closed. Three blanks values are necessary to further calibrate and interpret the readings of the miniRUEDI program in terms of gas partial pressures.
- 1x standard (lab atmosphere) using one of the six inlets of the miniRUEDI + 5x repeated sample analysis on the inlet connected to the apparatus described in Figure 28. The sequence (1 standard + 5 samples) is automatically repeated 5 times, for a total of 25 samples analyses. The automation is managed by the miniRUEDI software. Note that the ambient atmosphere is used as a standard here, and allows for N₂, O₂, Ar, He and Kr analysis.

The analysis time is roughly two hours and can lead to uncertainties of less than 1.0 %, even for Kr (see following sections).

First, the miniRUEDI is used to analyse the mixing ratios of the gas species in the sample by peak-height comparison relative to the standard gas. Then, the absolute partial pressures of the gas species are determined from the mixing ratios and the pressure readings in the cross. Finally, the partial pressures in the sample are determined by back-calculating the pressure drop from expanding the sample gas from the sampler into the cross. Since multiple analyses are performed on the same sample, the partial pressures in the sample are averaged to one single value to increase the accuracy.

2.4.2.3 Analysis of CFCs and SF₆ by gas chromatography

Once the analysis is completed on the miniRUEDI, the inlet ball valve V3 is closed, the pressure inside the sampler and the dead volume is recorded and the ball valve V1 is finally closed. The sampler is then connected to a GC-ECD (7890 GC system from Agilent®) analysis line which is primarily designed for the analysis of SF₆ and CFCs concentrations from water samples. The sample is then carried by research grade He to a collector. The gases pass through an activated charcoal sieve which selects out gases of interest (*e.g.* SF₆ and CFCs). The gases are then sent to the gas chromatograph and analysed. A complete analysis of SF₆ and CFCs takes up to 40 min per sample.

A standard gas mixture (National Oceanic and Atmospheric Administration, SF₆: 2.06 ± 0.03 ppt; CFC-11: 310.3 ± 1.0 ppt; CFC-12: 312.6 ± 1.1 ppt; CFC-113: 103.6 ± 0.5 ppt) is used for calibration of the GC prior to the analysis of the samples. Since the analysis result will depend on the quantity of gas still present in the tube after the miniRUEDI analyses, it is mandatory to record the total pressure in the sample after the first round of analysis with the miniRUEDI. The initial amount of SF₆ or CFCs in the sampler C_i , *i.e.* before the miniRUEDI analyses took place, is calculated as follows:

$$C_i = C_{mes} \frac{P_{mes}}{P_{ini}} \quad (5)$$

where C_i and C_{mes} are the initial (before any miniRUEDI analysis) and measured (with the GC-ECD) amounts of SF₆ or CFCs (usually in ppt), P_{mes} is the pressure recorded in the tube after the analysis with the miniRUEDI and P_{ini} is the total gas pressure initially calculated before any analysis took place and was already explicated above (both pressures are expressed in hPa). The analytical uncertainties determined from the accuracy of both standards and samples from passive samplers are less than 10 %, which is similar to reported values in the literature.

2.4.2.4 Equilibration experiments

Equilibration experiments were conducted to study the equilibration process between dissolved gas and gas in the tube, and to determine the equilibration time as well as whether elemental fractionation takes place. To do so, a controlled experiment was set up: a bucket was filled with approximately 100 L of tap water and let to equilibrate with the laboratory atmosphere for a few days. Water temperature was also monitored in the bucket as well as laboratory air temperature. A bubbling system was attached at the bottom of the bucket, allowing to constantly inject atmospheric gas as bubbles in the bucket and maintaining close to air saturated water (ASW) conditions (see Figure 28 for details).

A total of 15 passive samplers were used for the equilibration experiment. The following gases were studied: common gases, noble gases, CFC-12, CFC-113 and SF₆. The passive samplers were flushed with pure N₂ before their use. In each experiment, up to 5 passive samplers were

immersed vertically to a maximum depth of 1 m in the bucket (Figure 2b). The passive samplers were then let to equilibrate in the bucket for 0 to 14 days.

The local atmosphere (*i.e.* lab atmosphere) was also measured by filling pre-vacuumed passive samplers with air. These samplers were analysed in the same way as water-equilibrated passive samplers, using the GC-ECD (SF₆, CFC-12 and CFC-113). Since the “standard” mixture used for the miniRUEDI is the local air, it is assumed that the gases concentrations are the following: N₂ = 781 000 ppmv, O₂ = 209 500 ppmv, Ar = 9300 ppmv, He = 5.24 ppmv, ⁸⁴Kr = 0.6498 ppmv. Note that this ambient air is present in a He, Ar (and SF₆) free lab room. The concentration of the anthropic trace gases in the local atmosphere were obtained by analysing the ambient air with the GC-ECD system and are the following: SF₆ = 12.5 ± 1.3 pptv, CFC-12 = 390 ± 39 pptv, and CFC-113 = 43 ± 4.3 pptv. All these values are used as reference concentrations for the miniRUEDI and GC and as reference to determine the saturation relative to the local atmosphere for different equilibration times (see Figure 30). Other gases of interest, such as CO₂, CH₄ or Xe could also be measured using the miniRUEDI from a passive sampler as long as (i) the reference gas used contains these gases in known concentrations and (ii) the concentrations in the samples are sufficiently high to be accurately detected and measured using the miniRUEDI.

In a second part, measurements from completely equilibrated passive samplers are compared with direct measurements made using gas equilibrium membrane inlet mass spectrometry (GE-MIMS) with the miniRUEDI. A small pump (Proactive® 12V pump) was immersed in the water-filled bucket and connected to a low-flow controller (Proactive® low-flow controller) enabling a water flow of roughly 1 L/min. The pumped water is circulated through the GE-MIMS module, exchanges with the module headspace and is sent back to the bottom of the bucket.

2.4.3 Results

2.4.3.1 Air saturated water (ASW) conditions (GE-MIMS test)

Measurements of the dissolved gases in water made with the GE-MIMS are firstly used to verify the ASW (or close to ASW) conditions. To do so, the readings obtained from

measurements of the headspace in the GE-MIMS module are directly compared to the partial pressures of the gases in the atmosphere (Figure 29). This experiment was led several weeks after the bucket was filled with water and the bubbling system operational.

The results allow to demonstrate that close to ASW conditions are verified with the set up described in section *Equilibration experiments*. Interestingly, there is a slight excess in oxygen and noble gases. The higher He concentrations are thought to be due to the use of “contaminated” tubing during the experiment (some tubing have been used in the past for lab controlled tracing experiments). Except for He, the relative excess increases as the diffusivity of the gases decreases (Kr has the highest excess while N₂ excess is the lowest). This pattern suggests that at least a part of the bubbles injected by the bubbling system undergo forced dissolution, which creates excess air, as it travels from the bottom of the bucket to the surface. This excess air is then progressively lost via diffusive re-equilibration at the water/air interface and the excess air pattern is influenced by the relative diffusivity of the studied gases (Aeschbach-Hertig et al., 2008; Kipfer et al., 2002). Quantitatively, compared to the ASW, the excess air represents 0.2 ppmv for He, 200 ppmv for Ar and 0.3 ppmv for Kr.

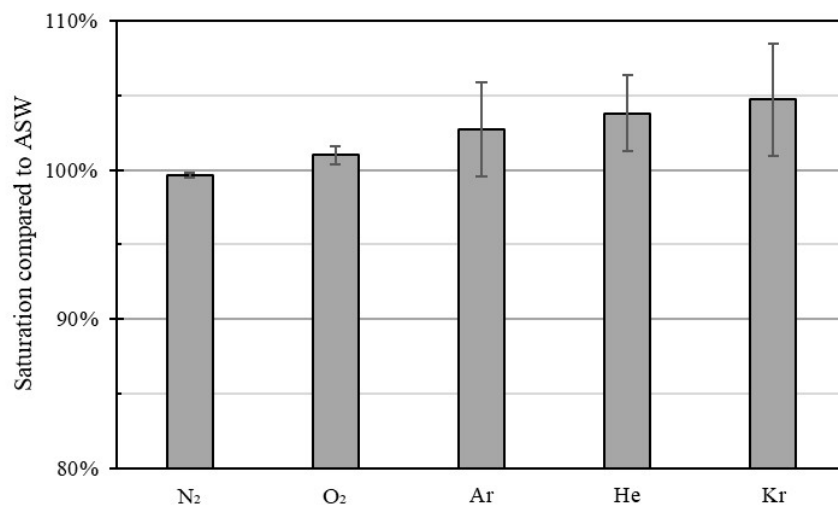


Figure 29: Results from the direct measurement of dissolved gases with the GE-MIMS module of the miniRUEDI.

2.4.3.2 Equilibration experiments

The results of the equilibration experiments are shown in Figure 30. After complete equilibration, the inside pressure of the passive samplers is expected to be 1 atm, with the partial pressures of individual gases similar to those found with the GE-MIMS test described above (Figure 29). Thus, the results of this test were taken as reference for the complete equilibration of the passive samplers.

In our experiments, as revealed by the ingrowth of major gases ($N_2 + O_2$), noble gases (He, Ar and Kr) and anthropic trace gases (SF_6 , CFC-12 and CFC-113) the equilibration is reached after 2 days (Figure 30).

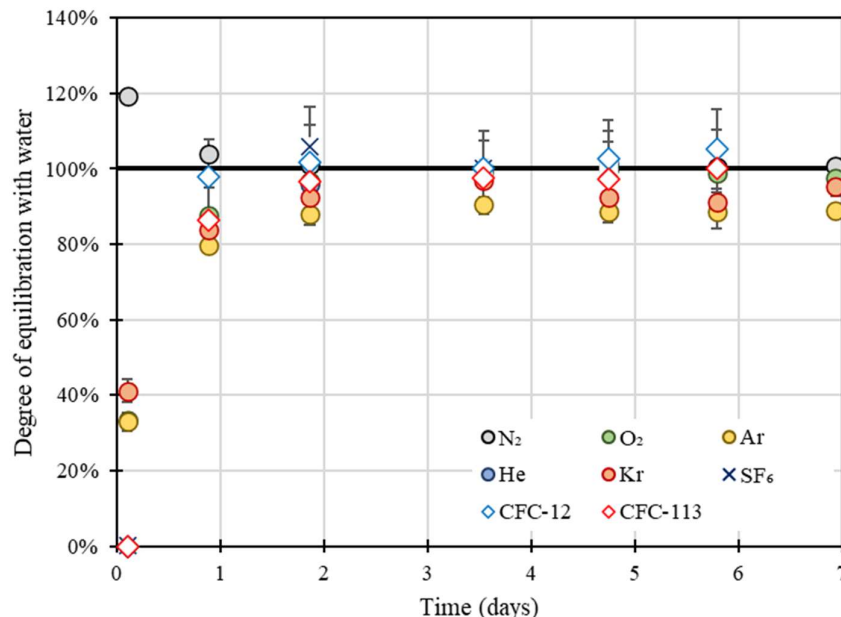


Figure 30: Results of the equilibration experiments. The dashed line represents the partial pressures expected when the gas in the passive sampler is in equilibrium with the gases in water. The “errors bars” are the standard deviations calculated from the 25 measurements for each gas for each analysis of passive sampler.

In addition, the partial pressures of all the gases in the sampler are within the range expected for the equilibration conditions found with the GE-MIMS test, except for Ar. Indeed, the latter shows a deficit of approximately 10 % with respect to the saturation value, which was not solved even by modifying the integration parameters of the miniRUEDI (*e.g.* baseline value

for integration). It seems that the current approach (passive sampler + miniRUEDI) leads to an underestimation of the dissolved Ar in the water. A passive sampler was let in the water for 14 days and yielded similar results (*i.e.* complete equilibration of all gases but lower Ar contents than what is expected). For convenience, the results for 14 days equilibration were not represented in Figure 30, otherwise details of gases with equilibration times of less than 3 days would not be clearly visible. This Ar underestimation is not linked to the equilibration of the passive samplers in water since similar results were obtained by measuring the content of a passive sampler filled with ambient air.

These results confirm that (i) the passive samplers are suitable for sampling dissolved gases, (ii) the combination of miniRUEDI and GC-ECD methods is functional with the developed system presented in Figure 28 and (iii) an equilibration time of at least 2 days is enough to ensure complete equilibration between the water and the inside of the passive samplers.

2.4.3.3 Variation of accuracy with number of analyses conducted with the miniRUEDI

One of the advantages of the approach presented is that a high measurement accuracy can be attained since it is possible to make a large number of analyses from one single passive sampler. Following the analysis protocol proposed for the miniRUEDI, where each sample is measured 25 times (approximately two hours of measurement), typical standard deviation for atmospheric gases are between 0.15 % (N₂) and 4 % (Kr) (see Figure 32). It is possible to shorten the analysis protocol down to 15 measurements while keeping very similar standard deviations results.

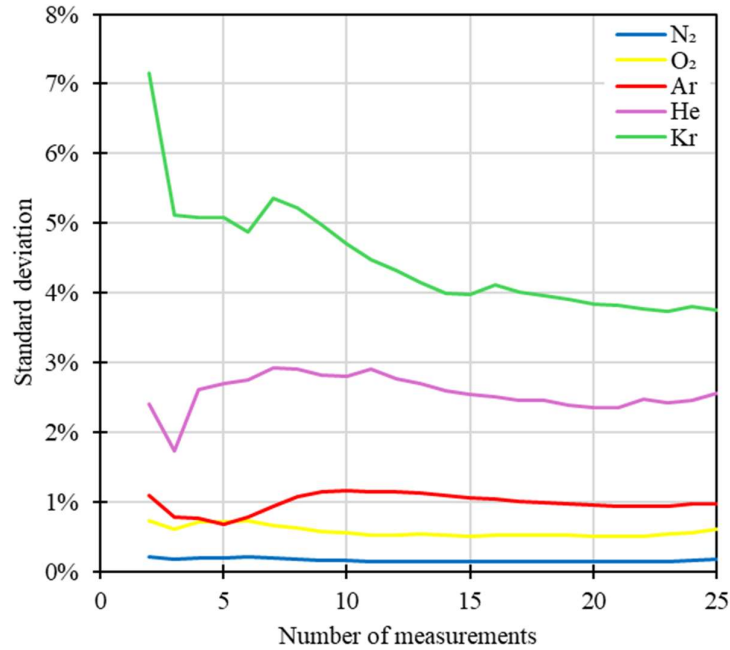


Figure 31: Variation of the accuracy (standard deviation) in gas partial pressures as a function of the number of analyses of one passive sampler conducted with the miniRUEDI.

2.4.3.4 Comparison of measurement approaches

The results of the comparison of the direct measurements with the GE-MIMS module of the miniRUEDI and those conducted using the passive samplers are presented in Figure 32. Both approaches resulted in comparable results for all the gases, except for Ar which is underestimated with the passive samplers approach. The GE-MIMS module of the miniRUEDI provided Ar partial pressures similar to those expected in water at equilibrium with the atmosphere (*i.e.* close to 9300 ppmv).

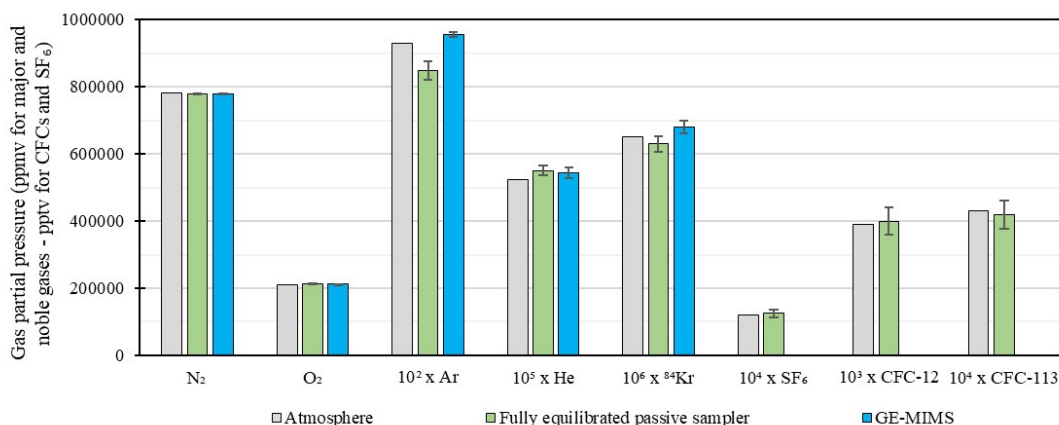


Figure 32: Comparison of the major, noble and anthropic trace gases measurements in the atmosphere and in equilibrium with the water in the bucket for the GE-MIMS and a fully equilibrated passive sampler.

2.4.4 Conclusions

We present here a robust yet simple method for reliable analyses of discrete gas samples using stainless steel passive samplers and a combination of portable field mass spectrometer (miniRUEDI) and gas chromatography (GC-ECD). First, the system built and described here enables to connect the passive samplers to the miniRUEDI by taking into account the pressure drop in the sample due to the pumping of the gas by the miniRUEDI system. It shows that the latter is not only a reliable field equipment but can also be very useful in laboratories for analysis of small volume samples (here, roughly 26 cc). This system is also adapted for further combining the miniRUEDI analysis with GC-ECD technique for the analysis of anthropic trace gases (CFCs, SF₆).

The equilibration experiments of immersed samples revealed that the samplers designed in this study are reliable for the analysis of dissolved gases, and that the typical equilibration time is of roughly 2 days for the gases studied (water at 22 °C). One of the main advantages of these passive samplers is how the sampling and analysis procedures for determining dissolved gases concentrations (here, N₂, O₂, Ar, He, Kr, CFC-12, CFC-11 and SF₆) are much facilitated compared to commonly used sampling and analysis methods.

The outcomes of this work are particularly useful for a various of gas tracers applications in the environment. For example, groundwater dating using CFCs and SF₆ can be performed from one single sample with this technique. In addition, it facilitates the use of gaseous tracers for mapping (i) natural heterogeneities (*e.g.* natural groundwater stratification (Meyzonnat et al., 2023)) and (ii) tracer plumes in deliberate tracing experiments in groundwaters (and surface waters such as lakes) as it is easy to let numerous passive samplers equilibrate in water.

2.5 Conclusion of Chapter 2

The measure of river discharge and characterisation of hyporheic exchanges can be advantageously achieved using artificial tracers injections methods. The classical use of velocimeters is adapted to channelled streams with a pseudo-laminar flow distribution. While slug injections of tracers have been preferentially used in turbulent, high gradient streams where the mixing of tracers occurs fast. Often, natural streams show a succession of these features, with calm, low energy zones following more high energy ones. In this context, it is not certain that tracer-based methods for discharge measurements give satisfactory results. Furthermore, the choice of tracers by users must be done carefully. One of the most important parameters to consider is likely to be the environmental concern, as the water quality in vulnerable catchments may suffer from the deliberate release of tracers (ex: fluorescent dyes and salts can be toxic for aquatic life at high concentrations). The work reported in *Article 1* offers new perspectives for the study of vulnerable catchments with limited impact on the qualitative state of the water resources. In this context, stable isotopes ^2H and ^{37}Cl are very effective and yield very precise stream discharge measurements, as well as estimations of the relative fractions of “fast” and “slow” components of the river flow.

Dissolved gases are excellent tracers for the characterization of a diversity of hydrological processes, both in groundwater (e.g. determination of groundwater residence time) and surface waters (e.g. quantification of groundwater inflows or air/water exchanges). The remaining issues with working with dissolved gases are (i) the difficulties for sampling, due to frequent air contamination, (ii) the access to laboratory facilities, and (iii) the cost of analysis, especially for noble gases. This limits their use during tracing experiments, for example for the characterization of groundwater/surface waters exchanges determination, while they are very meaningful. We have been able to show (*Article 2*) that the combination of passive samplers, miniRUEDI and GC-ECD offers new perspectives by filling these gaps. We have now access to a relatively cheap, easy and quick access to major, noble and anthropic trace gases from one single sample. N_2 , O_2 , ^{40}Ar , (^{36}Ar), ^4He , ^{84}Kr , CFCs and SF_6 can routinely be analysed without the use of a specialised reference gas with the miniRUEDI. It is also possible to add practically any other gas of interest (e.g. CO_2 ,

Xe) as long as a certified reference standard gas mixture is used and the partial pressures are in the analytical range of the miniRUEDI (coarsely, > 1 ppmv). Deploying passive samplers in the field is extremely easy, and this technique opens up new possibilities for mapping gas concentrations. (e.g. vertically in groundwater for assessing the natural groundwater age stratification, and laterally in the case of artificial gas tracing release).

CHAPTER 3 The true dependency of a surface water intake to groundwater inflows in a meso-scale, partially urbanised and snowmelt influenced catchment

3.1 Résumé du Chapitre 3 en français

3.1.1 Introduction du Chapitre 3

La vulnérabilité des eaux de surface face aux forçages anthropiques est contrôlée par deux principaux facteurs : la fraction d'eau souterraine (*i.e.* l'indice de débit de base) et la structure d'âge de ces apports souterrains. Le troisième chapitre vise à caractériser et quantifier les apports d'eau souterraine à la rivière Saint-Charles à Québec via l'utilisation d'une combinaison de traceurs environnementaux ($\delta^2\text{H}$ - $\delta^{18}\text{O}$, chimie des ions majeurs, éléments traces, silice dissoute). Comme décrit en détail dans la section 3.2, il s'agit d'un bassin particulier car il est utilisé pour la production d'eau potable et est partiellement urbanisé, méso-échelle (344 km²) et influencé par la fonte de neige au printemps.

Un effort important a été réalisé pour (i) suivre la dynamique spatiale et temporelle des signatures isotopiques ($\delta^2\text{H}$ - $\delta^{18}\text{O}$) des précipitations, des eaux souterraines et des eaux de surface, à l'échelle du bassin versant (voir Annexe C et section 3.2.1) et (ii) suivre la dynamique temporelle de traceurs environnementaux (chimie des ions majeurs, éléments traces, isotopes stables de la molécule d'eau, silice dissoute) à l'exutoire du bassin versant (*Article 2*, section 3.3). Dans un premier temps, les contrôles exercés par la saisonnalité et la physiographie du bassin versant sont investigués pour expliquer la variabilité temporelle et spatiale des signatures isotopiques des précipitations liquides et solides (section 3.2.1). Un gradient isotopique altitudinal, probablement le premier à être bien documenté au Québec, est clairement identifié à l'aide des données isotopiques dans les précipitations liquides. La dynamique temporelle et la quantification des apports souterrains à la prise d'eau potable est réalisée à l'aide de longues chroniques de traceurs chimiques (> 10 ans) : en particulier, les ions majeurs et les éléments traces métalliques. L'*Article 3*, dont le résumé en français est donné ci-après, rapporte la méthodologie, les résultats et

l'interprétation de ce travail (section 3.3). Par ailleurs, ce dernier est complété par l'investigation de la chronique de données de silice dissoute. Cette dernière apporte des éléments de réflexion supplémentaires sur le lien existant entre le caractère transitoire de la vulnérabilité de la ressource utilisée par l'eau potable et son temps de séjour dans le bassin versant.

3.1.2 Résumé en français de l'Article 3

L'eau de rivière est la principale source d'eau potable de nombreuses grandes villes à travers le monde. Cependant, sous climat humide et tempéré, il a été démontré que les eaux souterraines contribuent souvent de manière importante au débit des rivières. Ces apports diffus sont souvent difficiles à quantifier, en particulier dans les bassins versants hétérogènes, urbanisés et à méso-échelle. Cette quantification est pourtant cruciale lorsque l'on considère des rivières telle que la rivière Saint-Charles à Québec, qui alimente plus de 300 000 personnes en eau potable. Le bassin versant de la prise d'eau potable couvre une surface de 344 km², est influencé par la fonte des neiges et est partiellement urbanisé. Le suivi de l'hydrochimie de la rivière (ions majeurs, éléments traces) depuis 2003 a permis dans un premier temps de déterminer les échelles temporelles des variations de la qualité de la rivière. Ces données sont ensuite utilisées pour effectuer une séparation de l'hydrogramme, permettant d'estimer les apports mensuels d'eau souterraine dans la rivière entre 2012 et 2023. Un filtre mathématique est ensuite calibré à l'aide des résultats obtenus par l'approche « traceurs » pour estimer les apports souterrains quotidiens. L'interprétation des résultats montre que les eaux souterraines sont le principal contributeur à la rivière et que la minéralisation totale de la rivière est principalement contrôlée par ces apports. Contrairement à la conductivité électrique, l'alcalinité s'avère être un estimateur fiable de la fraction souterraine. Les différences des variations de l'alcalinité et de la silice dissoute donnent des indications sur la distribution du temps de résidence moyen de l'eau à l'échelle du bassin versant. En outre, une méthode simple est utilisée pour tenter d'estimer le « temps de transit moyen minimum » à l'échelle du bassin versant à partir des données de silice dissoute. Les résultats de cette étude ont de sérieuses implications pour l'étude de la vulnérabilité des prises d'eau de surface face au changement climatique et à l'urbanisation, dans des contextes climatiques similaires.

3.2 Introduction to Chapter 3

The surface waters vulnerability and resilience to anthropic forcings are controlled by two factors that are the fraction of groundwater to the total streamflow (*i.e.* the baseflow index) and the age structure of these groundwater inflows, respectively. A significant part of this PhD work consisted in characterizing the catchment temporal and spatial variability of the isotopic signal and of the geochemistry of the different hydrological compartments (surface waters, groundwater, precipitation) to quantify the groundwater fraction in the Saint-Charles River. Finding methods to provide a robust estimation of the temporal variability of these groundwater inflows to the surface waters was a challenging task since the watershed is meso-scale (344 km²), partially urbanised and influenced by snowmelt in Spring.

The description of the study site and the description of the different monitoring programs (stable isotopes, geochemistry) that took place during the PhD are presented in Appendix B and Appendix C respectively. The presentation and interpretation of the stable isotopes results are included in the following section 3.2.1. Finally, section 3.3 consists of *Article 3* which aims (i) to provide a methodology based on major ions concentration monitoring for the quantification of groundwater inflows and (ii) to explore the potential of dissolved silica as a first estimator of water residence time at the catchment scale. This work has serious implications regarding the vulnerability assessment of surface waters at the catchment scale.

3.2.1 Stable isotopes of the water molecule

In this section, we describe the results of the water stable isotopes monitoring and identify what controls the spatial and temporal variability of the isotopic signatures.

3.2.1.1 Local meteoric water line

The seasonal and monthly variability of the isotopic signal in precipitation is studied through the local meteoric water line (LMWL) and the *d-excess* and their temporal variations, as well as through the relationship between isotopic signatures and climatic data.

The local meteoric water line was drawn (Figure 33) after weighing the isotopic rainfall data, following Hughes and Crawford (2012), to avoid overestimation of the small rain events and the underestimation of the larger ones.

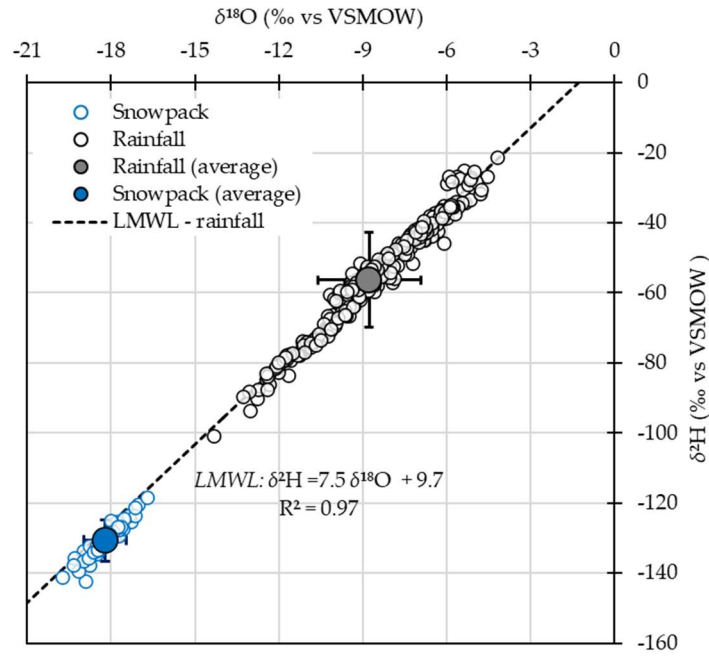


Figure 33 : Biplot of isotopic signatures in precipitation, the LMWL for rainfall is also indicated as well as average and standard deviation for rainfall and snowpack values ($n_{\text{rainfall}} = 264$; $n_{\text{snowpack}} = 52$).

The weighted average isotopic value for rainfall is $\delta^{18}\text{O} = -8.8 \pm 1.9$ ‰ vs VSMOW and $\delta^2\text{H} = -56.4 \pm 13.5$ ‰ vs VSMOW, while the average snowpack value is $\delta^{18}\text{O} = -18.2 \pm 0.7$ ‰ vs VSMOW and $\delta^2\text{H} = -130.7 \pm 5.9$ ‰ vs VSMOW. The high annual variability in rainfall isotopic values reflects the important annual variability in air temperature (Figure 34). The most depleted values are found during colder periods, while the most enriched values are usually found during summer periods.

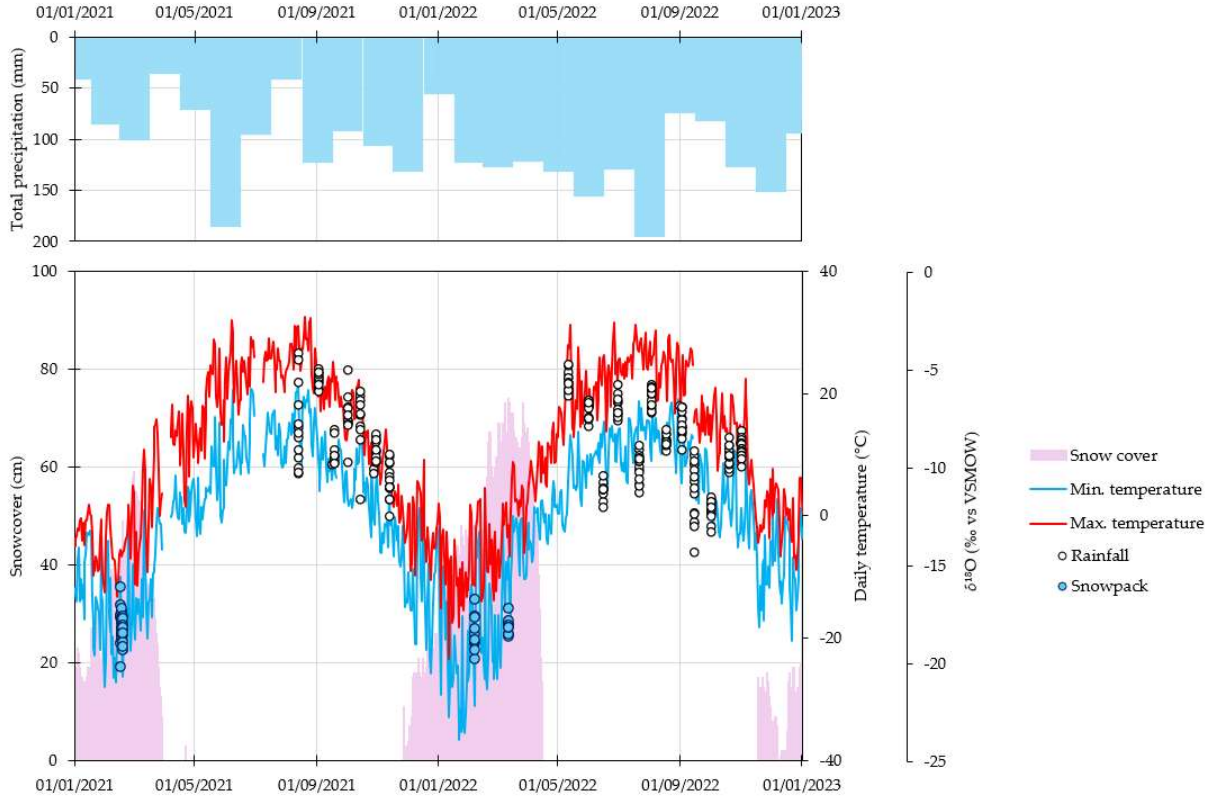


Figure 34 : Temporal patterns of (i) monthly total precipitation, (ii) snow cover, (iii) daily minimal and maximal temperatures and (iv) isotopic signatures of rainfall and snowpack for the years 2021 – 2022. The climatic data is from the Jean Lesage airport station in Québec, operated by the Government of Canada (Station ID: 71212).

The rainfall LMWL has the following equation: $\delta^2\text{H} = 7.5 (\pm 0.1) \delta^{18}\text{O} + 9.7 (\pm 0.8)$ ($R^2 = 0.97$), which is close to the global meteoric water line defined by Craig for coastal stations around the world: $\delta^2\text{H} = 8 \delta^{18}\text{O} + 10$ (Craig, 1961). Slopes of the water lines as well as *d-excess* values (intercept of the slope) can also be computed each month, thanks to the 15 stations (Figure 35). A strong positive relationship exists between *d-excess* values and the slope of these monthly LMWL. Indeed, the highest slope is 8.1 in September 2021 when rainfall occurred during wet and rather cold conditions, while the lowest *d-excess* and slope found are -6 and 5.7 respectively, in April 2022 during an unusually hot period. This is thought to be due to evaporation of droplets in the atmosphere during rainfall: its effect is more important during hot periods than during colder, wet months.

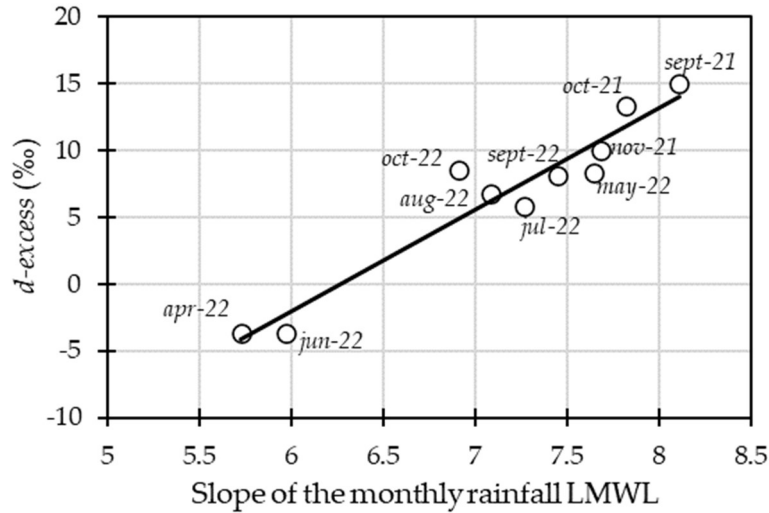


Figure 35 : Relationship between the slope of the monthly rainfall LMWL and the d-excess values.

3.2.1.2 Local altitude effect

The topography of the catchment is the dominant spatial control over the rainfall isotopic signatures, as shown in Figure 36. The altitudinal gradient was calculated by computing the average isotopic value for each station for the whole duration of the monitoring (summer and autumn 2021, and spring to autumn 2022) and plotted against the station elevation. The gradient is found to be -0.32 ‰/100 m ($R^2 = 0.94$) for $\delta^{18}\text{O}$ for this period. Given the scale of the catchment, the topography is expected to be the major control on the spatial variability of the rainfall signal. The gradient can be extremely useful to identify and protect preferential recharge areas. However, no clear relationship between snowpack elevation and isotopic signature was found.

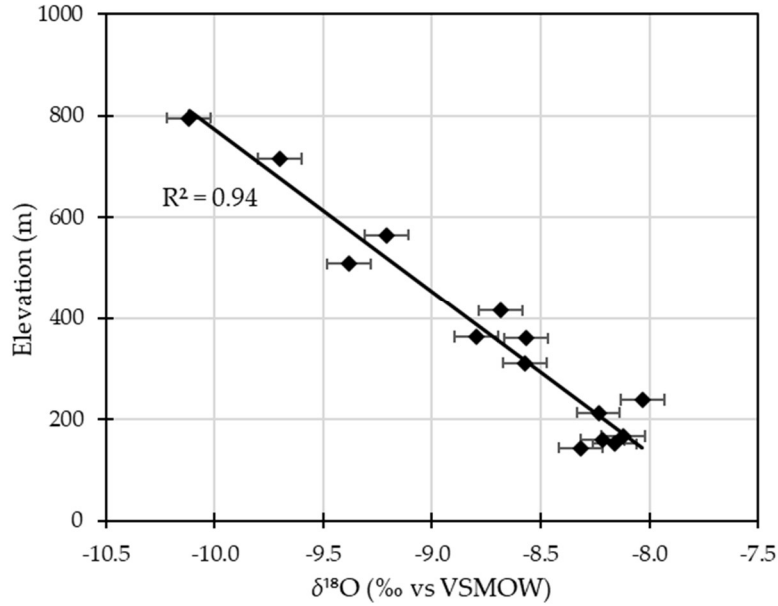


Figure 36 : Relationship between weighted average annual rainfall isotopic signatures and the elevation for the 15 stations.

3.2.1.3 Interaction between precipitation, surface water and groundwater

The isotopic values of surface waters (rivers) and groundwater are shown in Figure 37. They plot along the LMWL, between snowpack and rainfall. The average value for rivers is: $\delta^{18}\text{O} = -11.1 \pm 0.6$ ‰ vs VSMOW and $\delta^2\text{H} = -74.8 \pm 3.7$ ‰ vs VSMOW. For groundwater, the average value is extremely close to the one of streams: $\delta^{18}\text{O} = -11.5 \pm 0.5$ ‰ vs VSMOW and $\delta^2\text{H} = -77.1 \pm 3.5$ ‰ vs VSMOW. The lowest variability is found for groundwater (Figure 37 b)) and is explained by the fact that the seasonality in the isotopic signal is quickly dampened through mixing in the unsaturated and saturated zones (Barbecot et al., 2018).

Conceptually, the stream flow is composed of a fraction of recent runoff (rainfall, snowmelt) with very variable isotopic signatures, and a fraction of groundwater. However, the values and the relatively low variability of the isotopic signal of rivers further suggests that groundwater is the main contributor to surface waters.

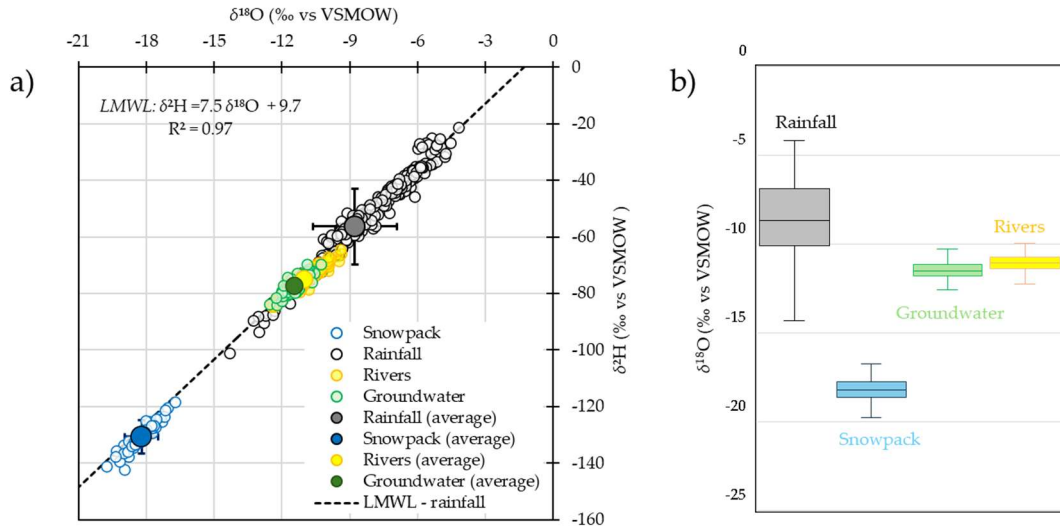


Figure 37 : (a) Biplot of isotopes in precipitation, rivers and groundwater ($n_{\text{river}} = 144$; $n_{\text{groundwater}} = 53$). The averages values are also given. (b) Box plots showing the variability of the four water masses: rainfall, snowpack, groundwater and rivers.

3.2.2 Conclusion of the introduction

The annual LMWL indicates that the contribution of continental moisture (secondary evaporation) is very limited while the examination of the monthly LMWL shows that the seasonality observed in rainfall isotopic signatures is primarily controlled by the local climatic conditions, especially by temperature which is a common feature in wet, temperate settings (Clark & Fritz, 1997). The spatial variability in rainfall isotopic signatures is controlled by the topography. A clear, and probably the first for the Province of Québec, isotopic gradient in rainfall is identified with the following value for $\delta^{18}\text{O}$: -0.32 ‰/100 m . The groundwater isotopic signatures plot on the LMWL, between snowmelt and rainfall, which indicates that recharge is a process occurring through infiltration of modern atmospheric inputs. In addition, the rivers end-member plots close to the groundwater end-member and has a similar low variability which is a first indicator of the strong interaction between groundwater and rivers in the studied catchment.

The interactions between groundwater and the Saint-Charles river are studied more in detail in the following section through *Article 3*.

3.3 The challenges of hydrograph separation and catchment mean transit time estimation in a mesoscale, urbanised, snowmelt-influenced catchment (*Article 3*)

The challenge of hydrograph separation and catchment mean transit time estimation in a mesoscale, urbanised, snowmelt-influenced catchment

Submitted to Journal of Hydrology in October 2024. Currently (February 2025) under review processes.

Preprint accessible to: https://papers.ssrn.com/sol3/papers.cfm?abstract_id=4976229

Antoine Picard¹, Florent Barbecot¹, François Proulx², José A. Corcho Alvarado³, Yohann Tremblay⁴, Laura Gâtel⁵, René Therrien⁴, Vincent Cloutier⁶, Benjamin Frot⁴, Baudelaire N'Da Angoran⁶, Christine Beaulieu⁷

¹ Geotop-UQAM, Département des sciences de la Terre et de l'atmosphère, Université du Québec à Montréal, CP8888 succ. Centre-Ville, Montréal, QC H3C 3P8, Canada

² Chaire de recherche en eau potable, Ecole supérieure d'aménagement du territoire et de développement régional, Université Laval, Pavillon F-A S, 2325, allée des Bibliothèques, Québec, QC G1V 0A6, Canada

³ Nuclear Chemistry Division, Spiez Laboratory, Federal Office for Civil Protection, Austrasse, 3700 Spiez, Switzerland

⁴ Département de géologie et de génie géologique, Université Laval, 1065, avenue de la Médecine, Québec, QC G1V 0A6, Canada

⁵ Ministère de l'Environnement, de la Lutte contre les changements climatiques, de la Faune et des Parcs 675, René-Lévesque Est, Québec (Qc) G1R 5V7, Canada

⁶ Groundwater Research Group, Research Institute on Mines and Environment, Université du Québec en Abitibi-Témiscamingue, 341 rue Principale Nord, Amos, Québec, J9T 2L8, Canada

⁷ Ville de Québec, Division de la Qualité de l'eau et du Soutien Technique, 214n avenue Saint-Sacrement, Québec, QC G1N 3X6, Canada

Abstract: Surface water extracted from rivers is the main source of drinking water of many major cities globally. In wet and temperate climates, groundwater has been shown to often contribute substantially to river discharge. Quantifying these inputs is challenging, especially in heterogeneous, urbanised, mesoscale catchments. This quantification becomes crucial when considering rivers such as the Saint-Charles River, Quebec City, Canada, as it supplies more than

300 000 people in drinking water. It is a mesoscale (344 km²), snowmelt influenced and partially urbanized catchment. The monitoring of stream hydrochemistry (major ions and trace elements) since 2003 allowed to first determine the temporal scales of variations of stream quality and to evidence the different end-members explaining the water quality. These data are used for a hydrograph separation, enabling the estimation of monthly groundwater inflows to the river between 2013 and 2023. A mathematical filter is calibrated against the tracer-based approach results to determine the daily groundwater contribution between 2013 and 2023. Results show that groundwater is the major contributor to the river and controls its total mineralization. Unlike electrical conductivity, alkalinity is a reliable estimator of the groundwater fraction. The differences between stream alkalinity and dissolved silica dynamics give insights about the distribution of the catchment water mean residence time at the and a simple method is used to determine the catchment “minimum mean transit time” using dissolved silica. The results of this study have serious implications for surface water intakes vulnerability assessment to global climate change and urbanisation, in similar climatic contexts.

Keywords: environmental tracers, hydrograph separation, groundwater/surface waters interactions, drinking water, water resources management.

3.3.1 Introduction

Surface water accounts for more than 50 % of global water consumption (Barnett et al., 2005). However, surface water is closely connected to groundwater in a large range of climates (Winter et al., 1998; Xie et al., 2024). In wet and temperate climates, groundwater provides baseflow to rivers, sustaining them during periods without any rain (Beck et al., 2013). Surface water intakes for drinking water in these climates are thus expected to significantly rely on groundwater.

Surface water and groundwater interactions have been extensively studied globally at several temporal and spatial scale scales via numerous approaches (Brunner et al., 2017; Kalbus et al., 2006). The fraction of groundwater in streams and rivers originates from past precipitation events that can have occurred days, years, decades or even centuries ago. Temporal surveys of

streamflow also revealed that pre-event water is often the dominant source to streamflow generation (Klaus & McDonnell, 2013; Ladouche et al., 2000; Uhlenbrook et al., 2002). These latter studies use passive environmental tracers (ex: ^2H - ^{18}O , chloride, electrical conductivity) as tools to identify the different end-members controlling the stream water isotopic composition and/or quality. The groundwater component, which is associated with the longer residence time within the catchment, is typically the most mineralized one, while the runoff component – considered as the fast component of the hydrograph – is the most diluted. These point tracer-based hydrograph separation results can be used as calibration data for continuous mathematical hydrograph separation models (Eckhardt, 2005, 2008; Saraiva Okello et al., 2018).

Within a catchment, the residence time of water in each of the different compartments varies from a few hours (runoff), days-months(-years) (rivers, lakes) to years-decades(-centuries) (groundwater), with overlaps between these domains (Figure 38). The total time spent by water in the catchment is closely linked to its quality and its vulnerability. Indeed, it exerts an important control over the occurrence and completion of biogeochemical reactions, contamination resilience, and informs us about how catchments retain and release solutes (McGuire & McDonnell, 2006; Purtschert, 2008; Solomon et al., 2015).

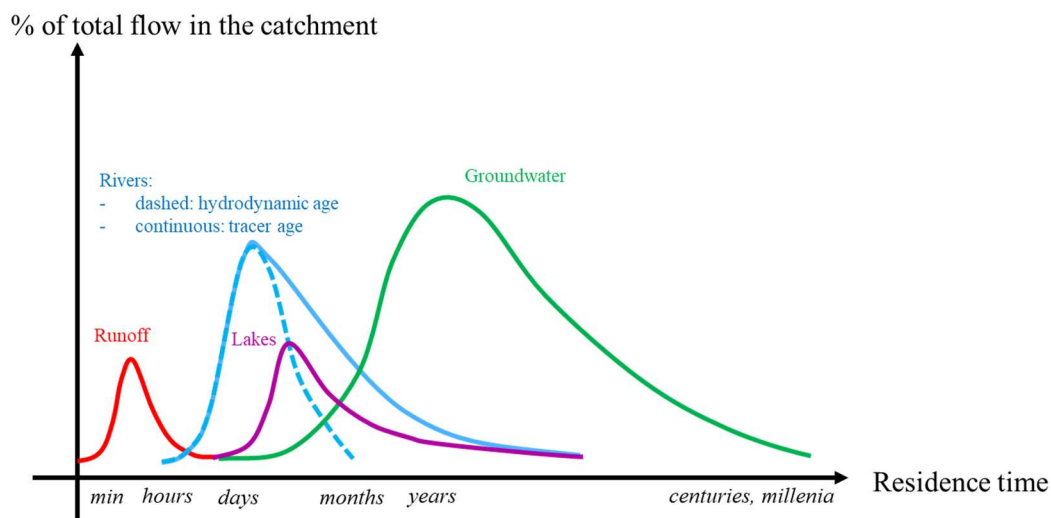


Figure 38: Conceptual scheme of the time spent by water within the different hydrogeological compartments of a watershed.

However, residence times revealed to be difficult to estimate or quantify and extremely difficult to predict (Hrachowitz et al., 2010; McDonnell et al., 2010; Tetzlaff et al., 2009). Rivers collect water from all the compartments of the catchment, naturally incorporating various water residence times. Catchment scale water residence times have been determined using environmental tracers in streams (Solomon et al., 2015). Baseflow has been dated using either the ^3H - ^3He dating technique (Stolp et al., 2010), ^3H alone (Morgenstern et al., 2010) or with anthropogenic greenhouse gases (SF_6 , CFC-11) (Jensen et al., 2022; Solomon et al., 2015). The conversion and dampening of stable isotopes (^2H - ^{18}O) and quality parameters (ex: chloride, silica, sodium) from precipitation to streams can also inform on time-variable catchment transit time distributions (TTD), improving the understanding of surface water/groundwater interactions (Benettin & Bertuzzo, 2018; Benettin et al., 2022; Harman, 2015; Jasechko et al., 2016; Kirchner et al., 2000; Rinaldo et al., 2015). Dissolved elements are generally more difficult to use, as their variations may be controlled by different processes depending on the catchment characteristics. However, dissolved silica, produced by the slow dissolution of silicate minerals by groundwater, has proved to be a reliable indicator of water residence time in streams in some studies of small ($< 20 \text{ km}^2$) catchments. For example, a very good correlation between ^3H activities and dissolved silica was reported in the Toenepi catchment, New Zealand (Morgenstern et al., 2010). In addition, the relationship between groundwater ^3H - ^3He ages and dissolved silica was used to assess the mean transit time of creek water in the Panola Mountain research watershed in Georgia, USA (Peters et al., 2013). It is however unclear whether dissolved silica could work as a reliable age-dating tracer of streamflow in a meso-scale, partially urbanised catchment.

The objectives of this work are to (i) use a multi-tracer approach for baseflow separation in a snowmelt influenced meso-scale catchment (344 km^2), (ii) identify the link between the stream water quality temporal evolution and the groundwater contribution and (iii) discuss the processes of baseflow generation using both stream dissolved silica and alkalinity while exploring the potential of dissolved silica to infer stream water age information.

3.3.2 Presentation of the study area

3.3.2.1 Study area

The Saint-Charles River surface water intake is located on the outskirts of Quebec City, Canada. The intake watershed covers an area of 344 km² and continuously supplies drinking water to over 300 000 people. Most of the watershed (67 %) is forested, especially in the northern half, while urbanisation accounts for 18 %. The valleys, and especially the southern part, are the most urbanized parts of the watershed.

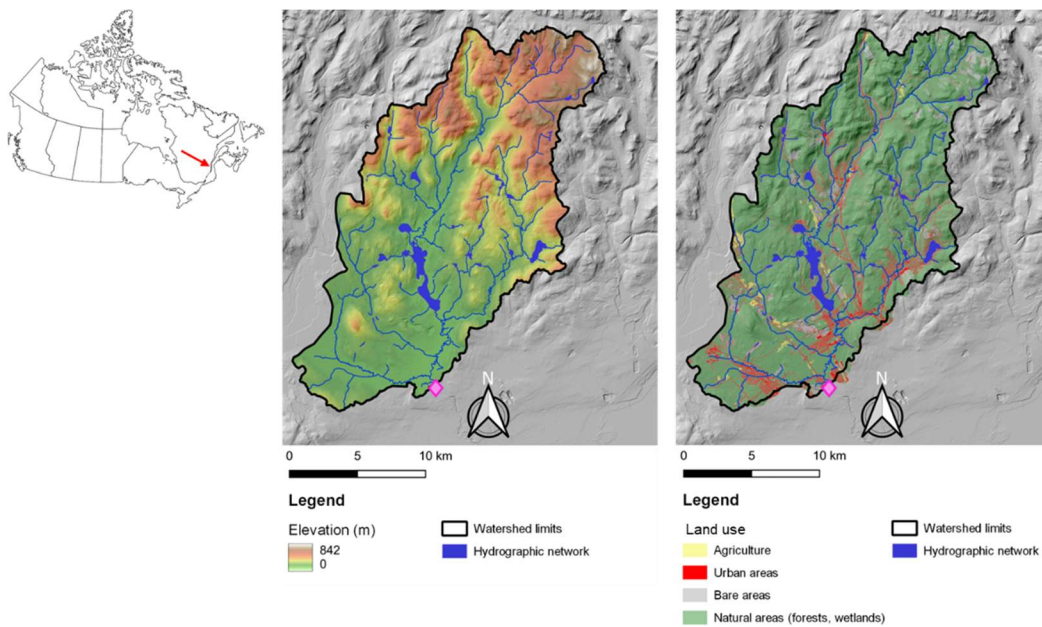


Figure 39: From left to right: map of Canada with red arrow indicating the study site location in the Province of Québec, watershed physiography, topography, hydrography and land use. The surface water intake of the Saint-Charles River is located at the outlet of the watershed (pink diamond).

3.3.2.2 Climate

The local climate is cold, humid continental and is characterized by cold winters and temperate summers. Temperature and precipitation are monitored close to the catchment, at the Jean-Lesage airport station (OMM station 71708). Climate normals (1981 – 2010) indicate that the lowest average monthly temperatures occur in January (-12.8°C), while the highest mean monthly

temperatures are in July (+ 19.3 °C) (Figure 40). The mean air temperature is usually below 0°C from November to March, which allows precipitation to fall as snow. Precipitation occurs throughout the year, with an annual total amount of around 1 200 mm (900 mm of rainfall and 300 mm of snowfall in water equivalent) on the southern part of the catchment, and almost 1 600 mm in the northern mountainous areas. The wettest months are July, August and September (~ 110 mm each) while the driest months are February, March and April (~ 80 mm each).

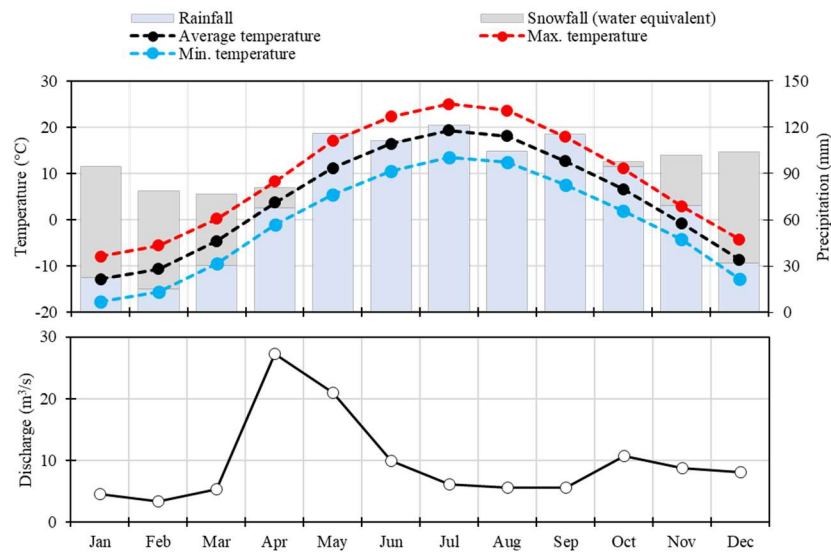


Figure 40: Climate normals (1981-2010) from Jean Lesage airport station (OMM station 71708) and mean average monthly discharge at the outlet of the catchment between 2012 to 2023 (MELCCFP station 050904 corrected from abstracted water at the pumping station).

3.3.2.3 Catchment physiography, geology and hydrology

The catchment of the Saint-Charles River water intake is characterized by an altitudinal gradient varying from about 140 m.a.s.l. to 850 m.a.s.l., with steep slopes, particularly in the northern half (Figure 39). The bedrock consists of rocks typical of the Grenville Province (e.g., migmatite, gneiss and to a lower extent, granite), with groundwater mainly flowing in fractures. The bedrock is mostly covered by unconsolidated, permeable glacial till (silts, sands) from the Wisconsinian glacial event (80 000 to 10 000 B.P.). The valleys in the catchment are filled by Quaternary fluvioglacial, marine, pro-deltaic and alluvial sediments (Talbot Poulin et al., 2013). The

fluvioglacial sediments consist of very permeable coarse materials (sands, gravels). They can be as thick as 35 m in the southwest part of the watershed and represent the most important granular aquifers with mostly young groundwaters ($^3\text{H}/^3\text{He}$ groundwater ages up to 40 years) (Murphy et al., 2010).

The hydrological cycle is characterized by rapid snowmelt in the spring, creating peaks in streamflow and water table elevations, and by two low-flow periods, in summer and particularly in winter (Figure 40). Storm events also frequently occur during the summer low-flow period.

3.3.3 Materials and methods

3.3.3.1 Chemical and isotopic analyses

The stream water is sampled, typically weekly, at the water intake for chemical analyses (see pink diamond in Figure 39). Physico-chemical parameters (electrical conductivity, pH, temperature), major ions (HCO_3^- , Cl^- , SO_4^{2-} , Ca^{2+} , Mg^{2+} , K^+ and Na^+) and trace metals were analysed at the Québec City Water quality division laboratories following *Standards Methods for the Examination of Water and Wastewater* (APHA, 2012). The methods references are given in Table 4. Only the analyses having an ionic balance (IB) less than 15 % were kept (223 samples from July 2012 to August 2023).

Table 4: Methods of measure of water quality parameters.

Parameter	Standard method (APHA, 2012)
Alkalinity	2320 B
Cations and metals	3120 B (2012 – 2015) 3125 B (2015 – 2023)
Cl^-	4500- Cl^- -G
Mg^{2+}	3120 B (2012 – 2015) 3125 B (2015 – 2023)
K^+	3120 B (2012 – 2015) 3125 B (2015 – 2023)
Na^+	3120 B (2012 – 2015)

	3125 B (2015 – 2023)
SO ₄ ²⁻	4500-SO ₄ ²⁻ -G
pH	4500-H ⁺
Electrical conductivity	2510 B

Water stable isotopes were sampled weekly at the water intake from January 2022 to October 2022, and every two weeks in the rain, from May 2022 to November 2022. An evaporation free rain collector designed as in Carton et al. (2024) was installed following recommendations from the International Atomic Energy Agency (IAEA, 2013). Groundwater was sampled seasonally in 2020 and 2021, after purging the sampled boreholes (both monitoring wells and residential wells, usually open to bedrock) three times and making sure that the physico-chemical parameters were stable. The snowpack was collected at various locations and at different altitudes across the watershed in February 2022. Trenches were dug to sample the whole snowpack thickness. The snow collected was weighted to determine the equivalent liquid water height. All samples were collected in 30 mL HDPE bottles that were regularly tightened and stored in the dark, at room temperature. The analyses were performed at the Geotop Light Stable Isotopes Geochemistry laboratory at Université du Québec à Montréal (Montréal, Canada). The samples were analysed with a Picarro L2130-i CRDS. Each sample was injected and measured 10 times in Express mode, while the first 7 analyses were removed to limit memory effects. Three internal standard waters were used to normalize the results on the Vienna Standard Mean Ocean Water (VSMOW) scale while a 4th standard water was used as an unknown to assess the exactness of the normalization. All the results are given in *delta* (δ) units, expressed in ‰ vs VSMOW. Typical uncertainties (1σ) are of ± 0.1 ‰ for $\delta^{18}\text{O}$ and ± 1 ‰ for $\delta^2\text{H}$.

Dissolved silica (Si) was analysed on HNO₃ acidified samples (pH = 2) at the Department of Earth and Planetary Sciences of McGill University (Montréal, Canada), using inductively coupled plasma optical emission spectroscopy (ICP-OES, Thermo Scientific iCAP 6000). In-house made standards ranging from 0.1 to 20 ppm were prepared by careful dilution of a certified dissolved silica reference (10 000 µg/L Si from SCP Science). Typical uncertainties in the measured concentration range are of 5 %.

3.3.3.2 Baseflow separations

Daily discharge data (MELCCFP gauging station n°050904) from July 2012 to August 2023 was used for hydrograph separations. Although the station is located 9 km downstream of the water intake, there are no major tributaries between the intake and the station, and the catchment of the station is only 6 % larger than that of the water intake. It is therefore assumed that streamflow measured at the station is representative of that at the water intake. The total daily discharge at the water intake was estimated by adding the withdrawn volume of water to volume measured at the gauging station (see Figure 40 for monthly average discharge values). Then, hydrograph separation was performed using discrete geochemical data (HCO_3^- , Cl^- , Ca^{2+} , Mg^{2+} , K^+ and Na^+) and the resulting baseflow was then used to calibrate a continuous mathematical baseflow filter (Eckhardt, 2005, 2008). The combination of these data enables to determine the daily baseflow contribution to the Saint-Charles River from July 2012 to August 2023.

3.3.3.2.1 1st baseflow separation: tracer-based hydrograph separation

- *Choice of the three end-members from PCA results*

The principal components analysis (PCA) of major ions in surface water revealed that the river flow is controlled by three “chemical” end-members (the groundwater one, and two runoff end-members):

- the first end-member (bottom corner of the triangle in Figure 41) is found during low-flow conditions and shows high total mineralization. It is attributed to the groundwater end-member
- the second end-member (top right corner of the triangle in Figure 41) is found usually during low-flows, at the end of winter, and shows elevated chloride and sodium contents. It is attributed to the runoff of urban snowmelt
- the third end-member (left corner of the triangle in Figure 41) is found during high flows with very diluted solute concentrations and is attributed to the “clean” runoff end-member, *i.e.* a runoff end-member whose quality is not affected by anthropic activities.

The PCA results were judged very satisfactory as the two first dimensions explain 71.9 % and 19.6 % of the total variance respectively.

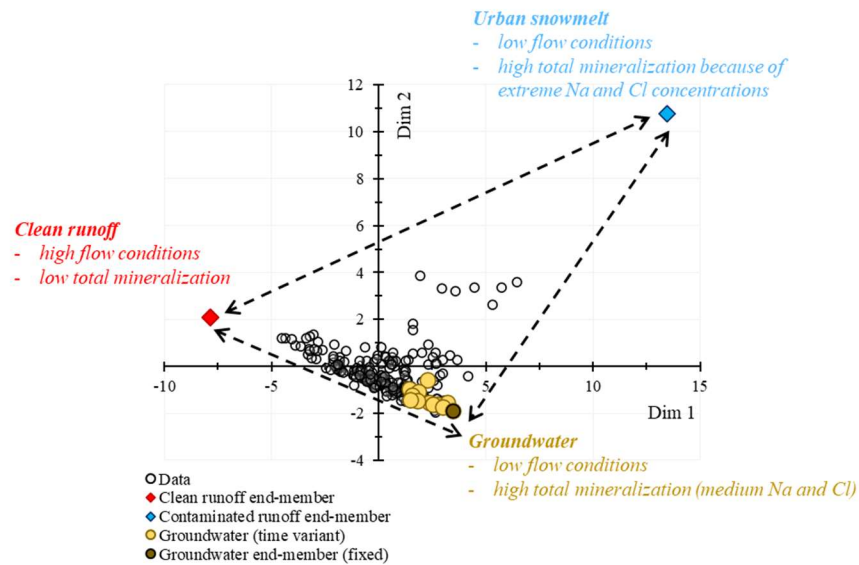


Figure 41: Three end-members put into evidence by PCA in the plane defined by the axes of dimension 1 and 2. The white dots represent the data from July 2012 to August 2023 (223 samples with $|IB| \leq 15\%$).

The runoff end-members are influenced by “clean” runoff and urban snowmelt runoff. The use of de-icing salts on roads is responsible for the quick release of snowmelt with high salinity, usually at the end of winter, characterized by high concentrations of chloride and sodium. For example, river chloride concentrations were 96 ppm on March 3rd, 2014 while chloride concentrations can be as low as 10 ppm during high flows. The contaminated runoff end-member was fixed by taking the sample with the highest chloride and sodium concentrations (blue diamond in Figure 41). “Clean” runoff end-member concentrations were determined by using the rainfall chemistry data from the nearby Lac Duchesnay (Houle et al., 1997).

The tracer-based hydrograph separation was performed using two different approaches:

- First, we considered a fixed groundwater end-member (see dark brown dot in Figure 41) for the whole period (2013-2023)

- Second, we considered the multi-annual variability of the groundwater end-member and used a different end-member for each year between 2013 and 2023 (see pale yellow dots in Figure 4). This allowed to consider the variability of the groundwater end-member and is motivated by the gradual, temporal increase in magnesium, calcium and alkalinity baselines river water concentrations during low-flow conditions. To do so, the sample thought to be the most representative of baseflow conditions was selected for each year and used as the current year end-member for groundwater.

Both approaches cannot lead to an overestimation of the contribution of groundwater since the samples chosen for the groundwater end-member are representative of late low-flow conditions with the highest solutes concentrations. However, the first choice does not consider the groundwater quality variations and selecting the highest measured concentrations during low-flow periods would result in a slight under-estimation of baseflow in the first years of the monitoring period.

- *Computation of the end-members contribution using chemical mass-balance*

At any given time, the total stream discharge is a function of the contribution of the groundwater and the fast runoff components (urban snowmelt and clean runoff). This function can be described by the following chemical mass-balance equations:

$$\begin{cases} 1 = f_{GW} + f_{US} + f_R \\ D_{1,sample} = D_{1,GW}f_{GW} + D_{1,US}f_{US} + D_{1,R}f_R \\ D_{2,sample} = D_{2,GW}f_{GW} + D_{2,S}f_{US} + D_{2,R}f_R \end{cases} \quad (1)$$

where f denotes the total discharge fraction and the subscripts GW , US and R refer to “groundwater”, “urban snowmelt” and “rainfall runoff” respectively. D_1 and D_2 represent the coordinates of the sample and end-members on Figure 41 dim 1 – dim 2 plot (Doctor et al., 2006). This system was solved to determine the groundwater, urban snowmelt and clean runoff contributions for each of the 223 available water samples. The obtained fractions of each end-members were transformed to discharge using the daily river discharge data.

3.3.3.2.2 2nd baseflow separation: mathematical model

Mathematical filters can be used to fill the gaps existing in tracer-based hydrograph separations (Duncan, 2019; Saraiva Okello et al., 2018; Zhang et al., 2013). Here, the 2-parameters Eckhardt's mathematical filter was used to obtain a continuous groundwater fraction estimation (Eckhardt, 2005, 2008). This filter was shown to give reliable results in low gradient and mesoscale watersheds and its parameters can be calibrated using environmental tracer data (Eckhardt, 2005; Gonzales et al., 2009; Saraiva Okello et al., 2018). The equation of the filter is the following:

$$Q_{bf,k} = \frac{(1 - BFI_{max})\theta Q_{bf,k-1} + (1 - \theta)BFI_{max}Q_{T,k}}{1 - \theta BFI_{max}} \quad (2)$$

where $Q_{bf,k}$ and $Q_{T,k}$ are the baseflow contribution and the total flow, respectively, on day k . Note that the Eq. (2) is subject to the following condition: $Q_{bf,k} \leq Q_{T,k}$. The recession constant (θ) can be obtained via recession analysis and was, here, determined following the methodology of Rimmer and Hartmann (2014). However, it is not possible to measure or compute the BFI_{max} (maximum long-term ratio between baseflow fraction and total discharge that can be modeled) even though it is a very sensitive parameter (Eckhardt, 2005). As proposed by Eckhardt, the tracer-based hydrograph separation results were used to calibrate its value. This was done by maximizing the Kling-Gupta efficiency (KGE) (Gupta et al., 2009; Knoben et al., 2019):

$$KGE = 1 - \sqrt{(r - 1)^2 + \left(\frac{\sigma_{sim}}{\sigma_{obs}} - 1\right)^2 + \left(\frac{\mu_{sim}}{\mu_{obs}} - 1\right)^2} \quad (3)$$

where r , σ and μ are respectively the linear correlation coefficient between estimations based on tracers and simulations, the standard deviation and the mean. The subscripts "sim" and "obs" refer to simulation and observation respectively. Baseflow and runoff components results are presented in the **Results** section. It is important to acknowledge that the "baseflow" computed using the mathematical filter approach is representative of groundwater that is feeding the river since the filter is calibrated against the "observed" groundwater inflows results from the tracer-based hydrograph separation.

3.3.3.3 Sensitivity analyses

The robustness of both hydrograph separations was explored using sensitivity analyses. To do so, the end-members were set to vary which allowed to compute new f_{gw} , BFI_{max} and KGE values for each simulation. The groundwater end-member was set to vary each year as described above. The two fast runoff end-members were set to vary individually. The concentrations of the urban snowmelt runoff end-member were let to vary in the range 100 - 120 %, while the range used for the clean runoff concentrations was 100 - 150 %, where 100 % represents the initial end-members concentrations used in the tracer-based hydrograph separation (3-2-1). The two runoff end-members concentrations were only allowed to increase because (i) the initial contaminated snowmelt end-member is the sample for which the maximum chloride and sodium content has been measured and, (ii) increasing the initial rainfall solutes concentration allows to take into account the interaction of rainfall with soil during runoff.

3.3.3.4 Estimation of a minimum hydro-chemical mean residence time using stream dissolved silica concentration

The gradual increase in stream Si concentration during low-flow periods without any liquid (rain or snowmelt) inputs is related to a first-order kinetic law. As already described by different authors (Benettin et al., 2015; Maher, 2011), this is a simple methodology for determining the “minimum mean residence time” (τ_m in the following) using only stream dissolved Si concentration. It is considered that the solution concentration of a water parcel changes with time until it reaches equilibrium concentration with the soil immobile water concentration according to Eq. 4:

$$c_{Si}(t) = c_{eq}(1 - \exp(-kt)) \quad (4)$$

This equation implies that silica has only geogenic sources and is not derived from atmospheric inputs (*i.e.* we suppose that Si is absent in precipitation). Here, k is a kinetic constant [T^{-1}] used at the whole catchment scale and spatially integrates the catchment heterogeneities (ex: pH, temperature), while c_{Si} is the measured Si concentration over time and c_{eq} is the equilibrium concentration.

The value of k was found using the following approach. There is one clear discharge peak on January 4th, 2023 followed by more than 3 months of low conditions with no inputs of snowmelt nor rain (see Figure 42). On January 4th, 2023 high-flow event, Si concentration is 3.0 ppm and it takes roughly 40 days to reach the plateau concentration of 3.9 ppm (c_{eq}). Once the plateau is reached, it is assumed that the youngest water parcel participating to streamflow is of at least 40 days. The pattern exhibited by Si concentration was fitted to Eq. 4, yielding a value of $1/k = 14.1$ days. This is very close to the value of 13 days that Benettin et al. (2015) found in their study in New Hampshire (USA).

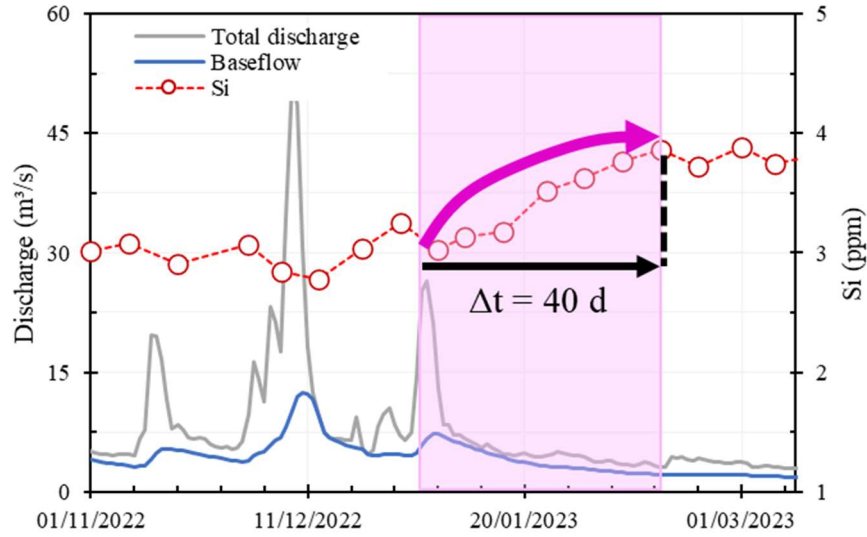


Figure 42: Evolution of discharge, baseflow and dissolved silica from November 2022 to April 2023.

The value of τ_m is determined using different TTD shapes that could describe different catchment behaviours, where the TTD is the distribution of ages of all the water parcels contributing to the river discharge. Gamma-type TTD can be used to explain streamflow generation processes (Berghuijs & Kirchner, 2017; Godsey et al., 2010; McDonnell et al., 2010) with the following expression:

$$g_{gamma}(t) = \frac{t^{\alpha-1}}{\left(\frac{\tau}{\alpha}\right)^{\alpha} \Gamma(\alpha)} e^{-\alpha \frac{t}{\tau}} \quad (5)$$

where Γ is the gamma function, α is the shape factor and τ is the mean transit time. The term α expresses the stratification of the aquifer layers contributing to the river. The classical exponential TTD expressing perfect mixing is found using $\alpha = 1$ (Eq. 6), meaning that the groundwater storage participates equally to the stream:

$$g_{exp}(t) = \frac{1}{\tau} e^{-\frac{t}{\tau}} \quad (6)$$

Previous studies (Godsey et al., 2010; Kirchner & Neal, 2013) showed that most catchments have an average α value lower than 1, meaning preferential outflow of young water but also long tailing effects. The recent developments of StorAgeSelection methods emphasized the time variability of the groundwater storage participating, implying transient TTD (Benettin et al., 2015; Benettin & Bertuzzo, 2018; Harman, 2015). The parameter α can be set to vary according to current hydrometeorological conditions, such as the wetness of the catchment (Benettin et al., 2022) (*i.e.* lower values of α during high flows and higher values during dry periods). It was not set to vary in this study, as it would need more data from other tracers. For example, the stable isotopes dataset presented here does not allow to apply such methods.

The streamflow Si concentration is then given by the following convolution integration for the general Gamma-type TTD (Benettin et al., 2015):

$$C_{Si}(t) = \int_0^\infty C_{eq}(1 - e^{-k\tau}) \frac{\tau_m^{\alpha-1}}{\left(\frac{\tau_m}{\alpha}\right)^\alpha \Gamma(\alpha)} e^{-\alpha \frac{\tau}{\tau_m}} d\tau \quad (7)$$

A value of τ_m was determined for each data point by three methods: (i) first by using the simple relation given in Eq. (4) – this approach is similar to a piston flow model (“tracer age approach” in the following), (ii) by integrating Eq. (7) using $\alpha = 1$ – thus, simulating a catchment-scale exponential behaviour (“exponential approach” in the following), and (iii) by integrating Eq. (7) using $\alpha = 0.5$ – thus simulating catchments functioning previously highlighted by authors (Kirchner et al., 2000) (“gamma model approach” in the following). Different thresholds were used to represent the data (see Figure 43):

- A first range is used for the youngest streamflow: less than 14 days, which is equal to $1/k$. This first class is related to the youngest waters
- The second threshold is method-dependent and considers the uncertainties of Si measured concentrations (5 %). The value of this threshold is the τ_m value at which the 95 % value of the maximum (*i.e.* plateau) Si value is obtained:
 - o 14 to 42 days for the “tracer age” approach,
 - o 14 to 180 days for the exponential model approach,
 - o 14 to 1 000 days for the gamma model approach
- All τ_m values above are put inside the same pool as the models outputs become extremely sensitive when Si measurements are close to the plateau concentration. This third class is related to the oldest waters.

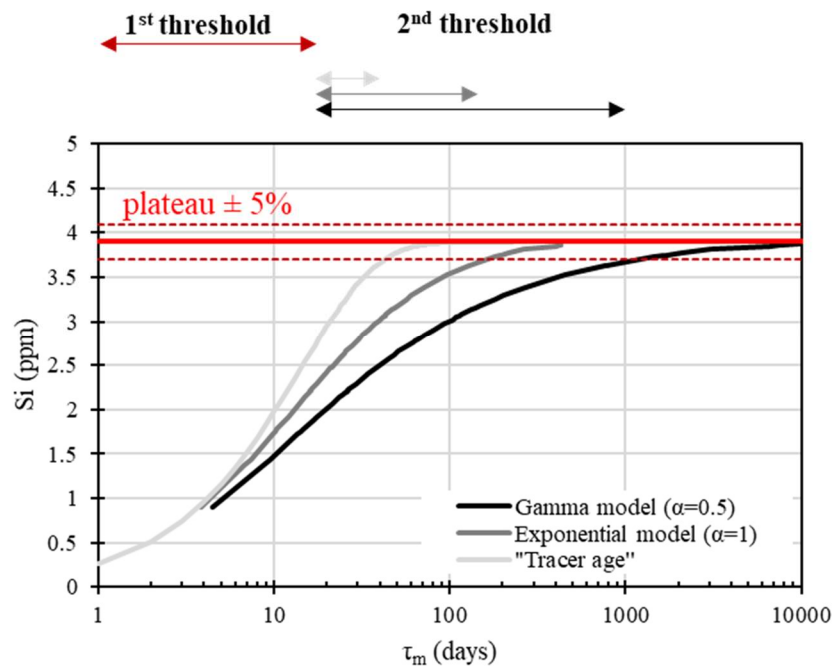


Figure 43: Relationship between the increasing stream Si concentration and the increasing “minimum mean transit time” (τ_m) for the three approaches. The range of thresholds for each model is indicated above the graph. The continuous red line represents the Si plateau concentration with $\pm 5\%$ values represented by dashed red lines.

3.3.4 Results

3.3.4.1 Stream water hydrochemistry

3.3.4.1.1 Major ions temporal variations

Monthly statistics (period 2013 – 2023) of major ions concentrations are shown in Figure 44 with box plots. The highest major ions concentrations are usually found in winter and summer, i.e. during low-flow periods when groundwater dominates the stream water total mineralization. The electrical conductivity signal follows those of chloride and sodium, with extreme values at the end of the winter because of pulses from urban, “contaminated” snowmelt. Unlike other studies (Gonzales et al., 2009; Saraiva Okello et al., 2018; Zhang et al., 2013), the electrical conductivity cannot be used solely as a reliable tracer of groundwater in such urbanised snowmelt-influenced catchments. All the chemical tracers show the same pattern between May and December. Low-flow conditions in summer result in higher concentrations, while autumn rainfall events, from October to December, induce a decrease of the major ion contents.

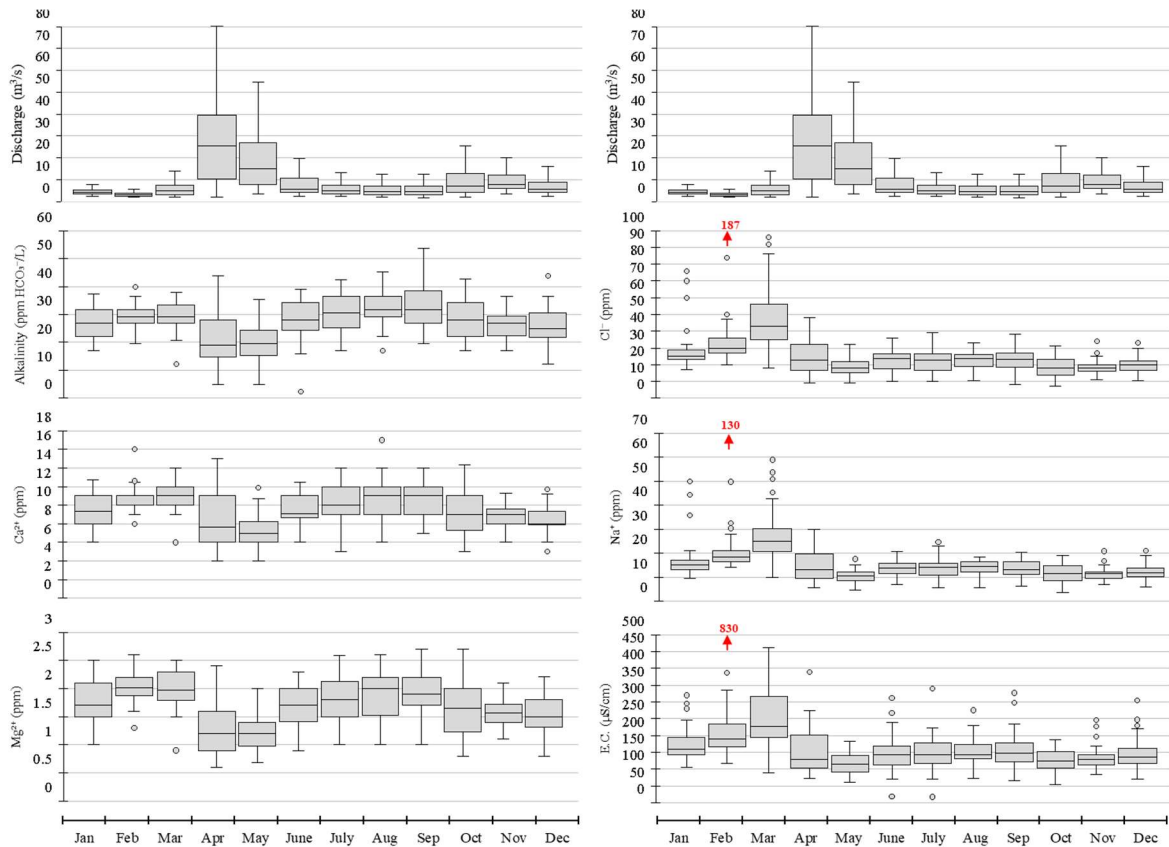


Figure 44: Box plots of total river discharge, major ions and electrical conductivity in the Saint-Charles River for each month (period 2013-2023). The numbers in red represent extreme values for chloride, sodium and electrical conductivity values.

The multi-annual evolution of electrical conductivity, alkalinity, calcium and chloride concentrations is plotted in Figure 45, for the period 2003 to 2023. The major ions Ca^{2+} and alkalinity (expressed as HCO_3^-) are mostly from geogenic origin, associated with the dissolution of carbonates minerals (Langmuir, 1997) which makes them good first indicators of the groundwater fraction in the stream. There is a clear increase in their concentrations with time. It is not a sampling artefact since samples were taken “randomly”, for very different flow conditions over the years. A multi-annual shift of the end-member controlling their concentrations may explain this behaviour. As these ions are mostly derived from water-rock interactions, this could indicate either (i) a change in the quality of groundwater sustaining the river or (ii) a shift in the groundwater fraction. These temporal variations were considered for the hydrograph separation that is presented in section 3-2 *Baseflow separations*. There are no known geogenic sources of

chloride in the catchment and its presence is essentially due to the application of de-icing road salts during the winter season. There is no clear temporal trend in chloride concentration although it is very similar to that of electrical conductivity, especially the years when high chloride concentrations are measured (ex: 2006, 2014, 2023). High chloride levels are measured during warming periods in winter when the “urban”, contaminated snowmelt reaches the watercourse (see also Figure 46). The close relationship with the extreme electrical conductivity values indicates that the total river mineralization is occasionally controlled by these inflows, when the river discharge is already very low.

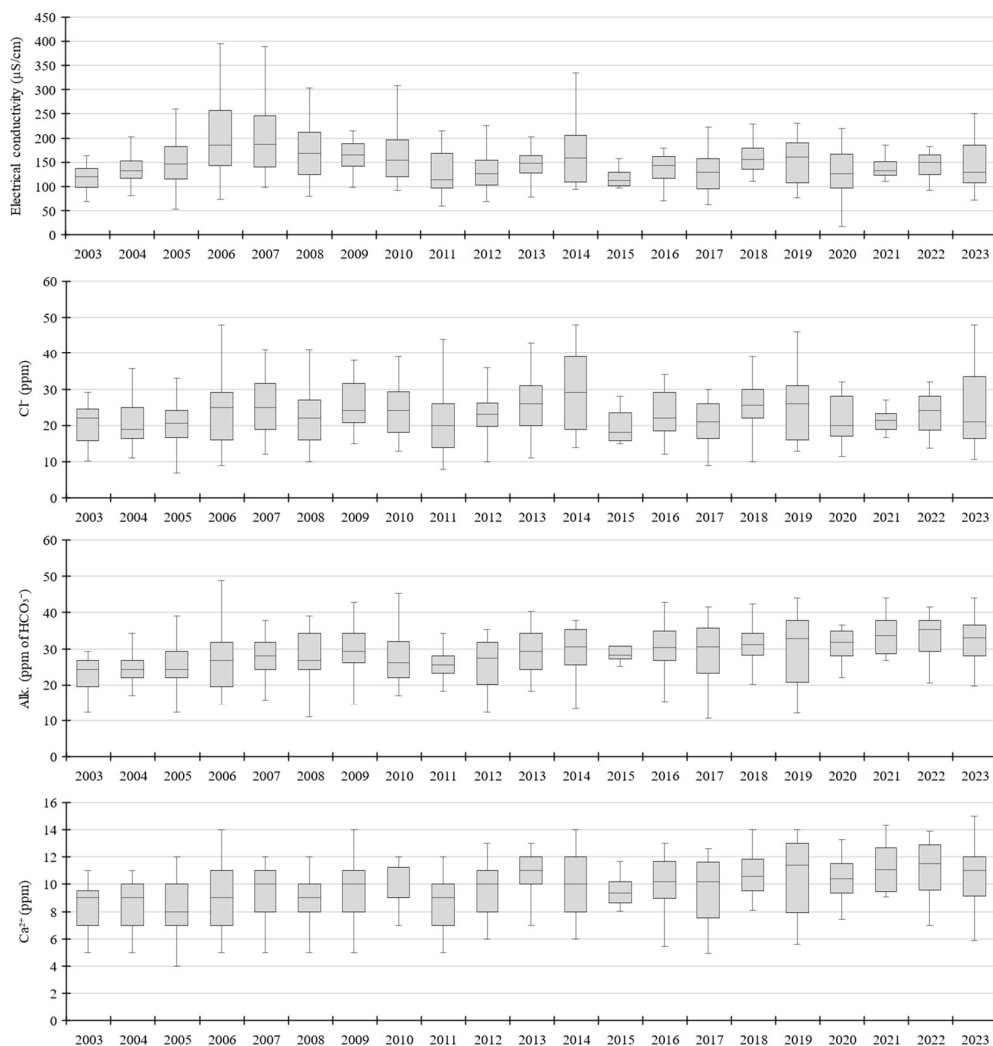


Figure 45: Multi-annual trends in electrical conductivity, alkalinity, chloride and calcium concentrations (period 2003 – 2023).

In addition, chloride is detected all year round, under all hydrological conditions. High values, up to 40 ppm, are also measured during summer and fall low-flow periods, when groundwater inflows are expected to control the water availability (Figure 46). This indicates that the groundwater sustaining the river is already largely contaminated by the application of de-icing salts over the urban areas of the catchment.

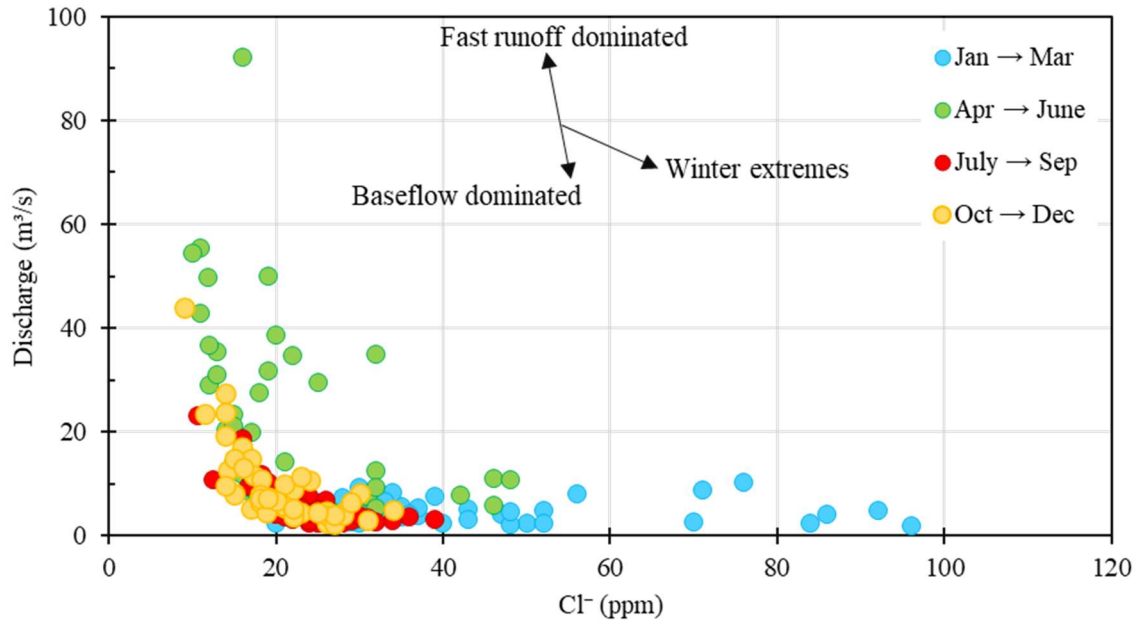


Figure 46: Seasonality in the discharge – chloride relationship, indicating different controls of the chloride concentration according to the season (see black arrows in the graph).

3.3.4.1.2 Water stable isotopes

The ranges of groundwater and snowpack isotopic signatures found across the watershed are represented in Figure 47 ($-18.7 < \delta^{18}\text{O}_{\text{snowpack}} < -17.2$; $-12.6 < \delta^{18}\text{O}_{\text{groundwater}} < -10.3$ – in ‰ vs VSMOW). Rainfall quantity and isotopic signatures were monitored at the outlet of the catchment, at the drinking water production plant ($-11.8 < \delta^{18}\text{O}_{\text{rainfall}} < -6.2$ – in ‰ vs VSMOW). Winter river isotopic signatures are very stable in winter, with values around -11.0 ‰ vs VSMOW, which is in the range of the groundwater end-member. The influence of snowmelt is visible in April with the lowest stream isotopic signatures (-12.5 ‰ vs VSMOW). Summer isotopic signatures show

the influence of recent rainfall inputs to the stream with higher values (ex: -9.4 ‰ vs VSMOW on the August 26th, 2022 after an important storm).

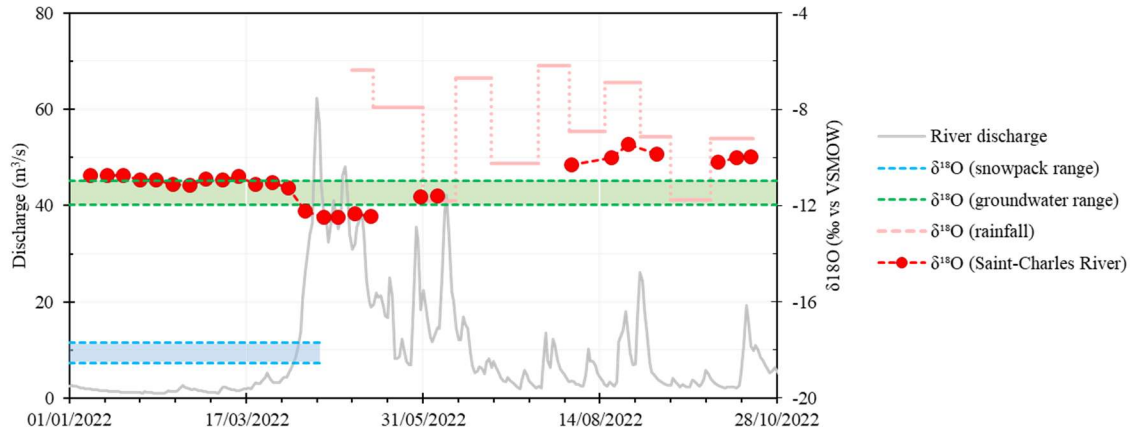


Figure 47: Discharge and stable isotopes signatures of snowpack, groundwater, rainfall and stream over time.

The low variability and the values of the isotopic signal of the river suggest that groundwater is the major contributor to the stream during the winter baseflow conditions. The stream water most depleted isotopic signatures are found during the snowmelt events (April-May 2022) because of the input of the low depleted melted snowpack. However, the shift in isotopic signatures is of less than 2 ‰ which suggests that snowmelt is not the main contributor to the stream during this period.

3.3.4.2 Baseflow separation at monthly timescale

3.3.4.2.1 Chemical hydrograph separation

The hydrograph separation was performed with an end-member mixing analysis (EMMA) approach using major ions data from July 2012 to August 2023 by solving Eq. (1). The temporal variations of the three end-members are considered to explain the temporal variations of the stream water chemistry. The results of the hydrograph separation were averaged for both approaches on a monthly basis because the timestep between two sampling days is variable and can extend from a week to a few months (ex: during the Covid-19 pandemic in 2020). The results are presented in Figure 48.

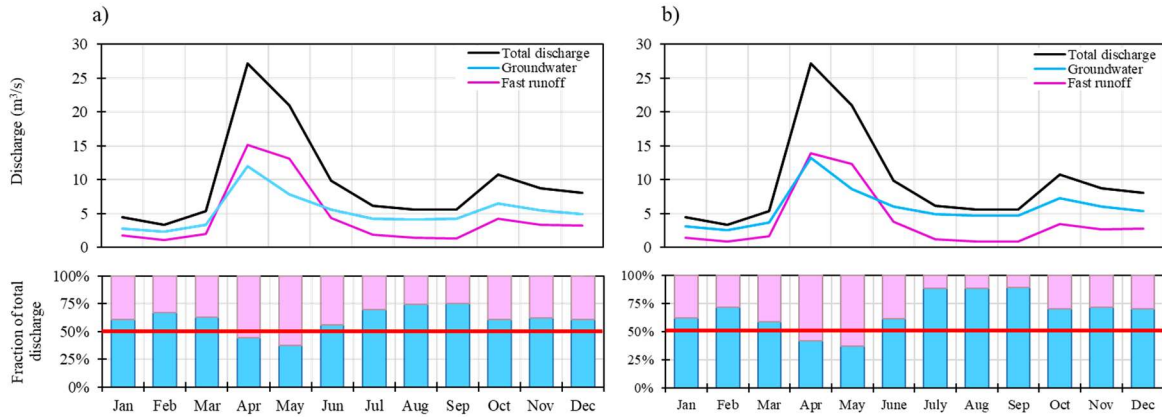


Figure 48: Average of flow components for each month of the July 2012 – August 2023 period, according to the chemical hydrograph separation: (a) fixed groundwater end-member; (b) time-variant groundwater end-member. The red bar is the 50 % bar, helping to determine which end-member controls the stream water availability.

Groundwater revealed to be the dominant contributor to the streamflow whatever the calculation approach. The fixed groundwater end-member approach yields an annual mean groundwater fraction (f_{gw}) of 0.61 while the time-variant groundwater end-member approach gives an annual mean f_{gw} of 0.68. The groundwater fraction totalizes more than 50 % of the total river flow every month, except for April and May. Indeed, these two months are influenced by the snowmelt events, resulting in the largest fractions of runoff. The increase of the groundwater fraction in summer until the start of winter is also well correlated with the global water mineralization increase during this period (Figure 44). The direct inputs via contaminated urban snowmelt are the less important contributor to the total flow and were only found from December to April. In March, they totalize 13 % of the average total discharge using both approaches. Even though their quantitative contribution is low, their impact in the stream quality is very punctual and strong. The fixed groundwater end-member approach maximizes the solutes concentrations of the groundwater end-member. This implies that it only allows to compute its minimum contribution to streamflow. This is not the case of the second approach which tries to consider the long-term variability of the groundwater end-member and is thought to give the more realistic results.

3.3.4.2.2 Mathematical filter calibrated with tracer data

Eckhardt's mathematical filter (Eckhardt, 2005) was calibrated against the tracer-based hydrograph separation. Recession analyses performed following the method described by Rimmer & Hartmann (Rimmer & Hartmann, 2014) gave a recession constant of 0.949. The BFI_{max} value giving the best fit between modelled and computed baseflow (groundwater) is 0.51 ($KGE = 0.72$) for the fixed groundwater end-member approach and 0.55 for the time-variant groundwater end-member approach ($KGE = 0.73$). These are lower baseflow index values than those found with the two tracer-based hydrograph separation approaches (0.61 and 0.68, respectively). It is explained by the fact that not all individual storm events are sampled with the tracer approach. Indeed, Figure 49 illustrates well the discrete nature of the tracer-based hydrograph separation, for which there is no sampling during or shortly after some storm events.

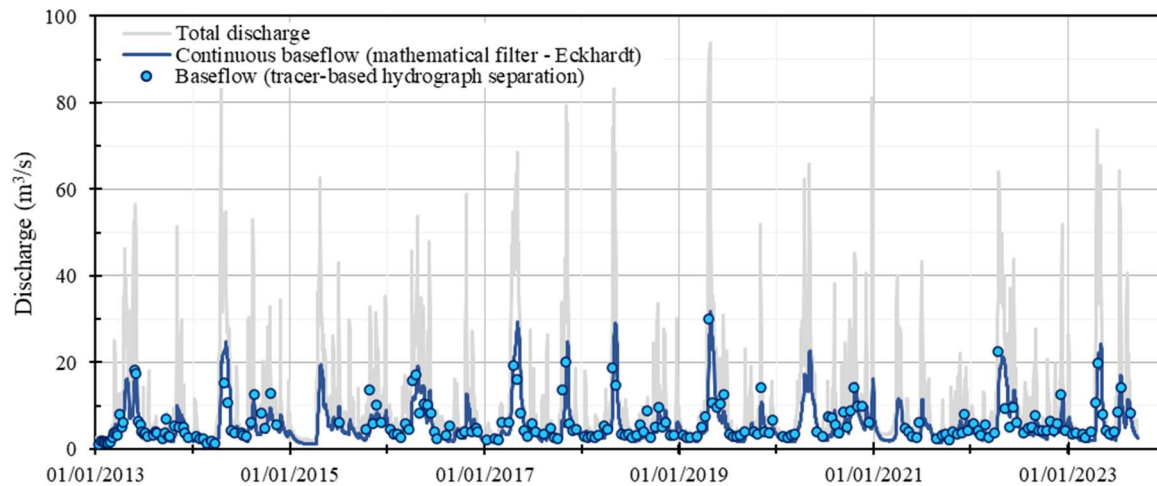


Figure 49: Continuous baseflow separation and results from the tracer-based baseflow separation from 2013 to 2023 (only the results from the time-variant groundwater end-member approach are presented).

According to the fixed and time-variant groundwater end-members approaches, groundwater contributed more than 50 % of the total daily flow for 68 % and 74 % of the time between January 2013 and August 2023, respectively. These computations consider the snowmelt period which usually lasts between April and May. Because of the hypotheses that were made, the results from the fixed groundwater end-member approach minimize the groundwater fraction. This implies

that groundwater is clearly the dominant quantitative contributor to the Saint-Charles River water intake.

3.3.4.2.3 Sensitivity analysis

The results of the sensitivity analysis are presented in Table 5. The clean and urban snowmelt runoff end-members were set to vary individually and new f_{gw} , BFI_{max} and KGE values were computed to assess the validity of the initially taken end-member and the robustness of the hydrograph separation.

The results of the sensitivity analysis reveal that changing the urban snowmelt runoff up to a factor of 1.2 does not significantly affect the computed groundwater fraction and Eckhardt's filter parameter, BFI_{max} . The same conclusions are drawn from the clean runoff that was set to vary up to 150 %. This attests the robustness of the approach and allows to have good confidence in the estimation of the groundwater fraction in both hydrograph separation methods.

Table 5: Sensitivity analysis results. "HS" stands for "hydrograph separation".

		Tracer-based HS	Eckhardt HS	
Urban snowmelt runoff (% of initial end-member)	Clean runoff (% of initial end-member)	f_{gw}	BFI_{max}	KGE
100	100	0.68	0.548	0.73
105	100	0.68	0.550	0.73
110	100	0.68	0.552	0.73
120	100	0.69	0.555	0.73
100	105	0.69	0.556	0.73
100	110	0.68	0.548	0.73
100	120	0.68	0.547	0.73
100	150	0.68	0.546	0.72

3.3.5 Discussion

3.3.5.1 Groundwater control of stream water quality

The computed groundwater fraction (f_{gw}) was plotted against quality parameters to illustrate the control exerted by groundwater on the stream water mineralization and quality (Figure 50). As expected, major ions concentrations are well correlated to the groundwater fraction, especially alkalinity ($R^2 = 0.80$), magnesium ($R^2 = 0.69$) and calcium ($R^2 = 0.65$). However, the inflow of urban snowmelt, with higher concentrations of ions, is responsible for blurring this relationship, especially for chloride and sodium. Due to the absence of geogenic sources of chloride, it is thought that most (if not all) of chloride originates from human activities. However, there is a clear increase in the chloride minimum concentrations and the increase of f_{gw} , which indicates that the quality of the groundwater sustaining the river is already altered by human activities. Therefore, recharge areas near major roads where great amounts of de-icing salts are used are critical regarding groundwater quality and should be protected.

As expected, pH is also correlated to f_{gw} with lower pH values found during high flows, due to contribution of rain, and higher values at low-flow, due to groundwater contribution. On the contrary, there is no clear trend between f_{gw} and trace metals concentrations. Aluminium and zinc

baseline concentration exhibit an inverse correlation to f_{gw} , which could be explained by leaching from roofs during periods of heavy rainfall (e.g. rain gutter, roofs) (McIntyre et al., 2019).

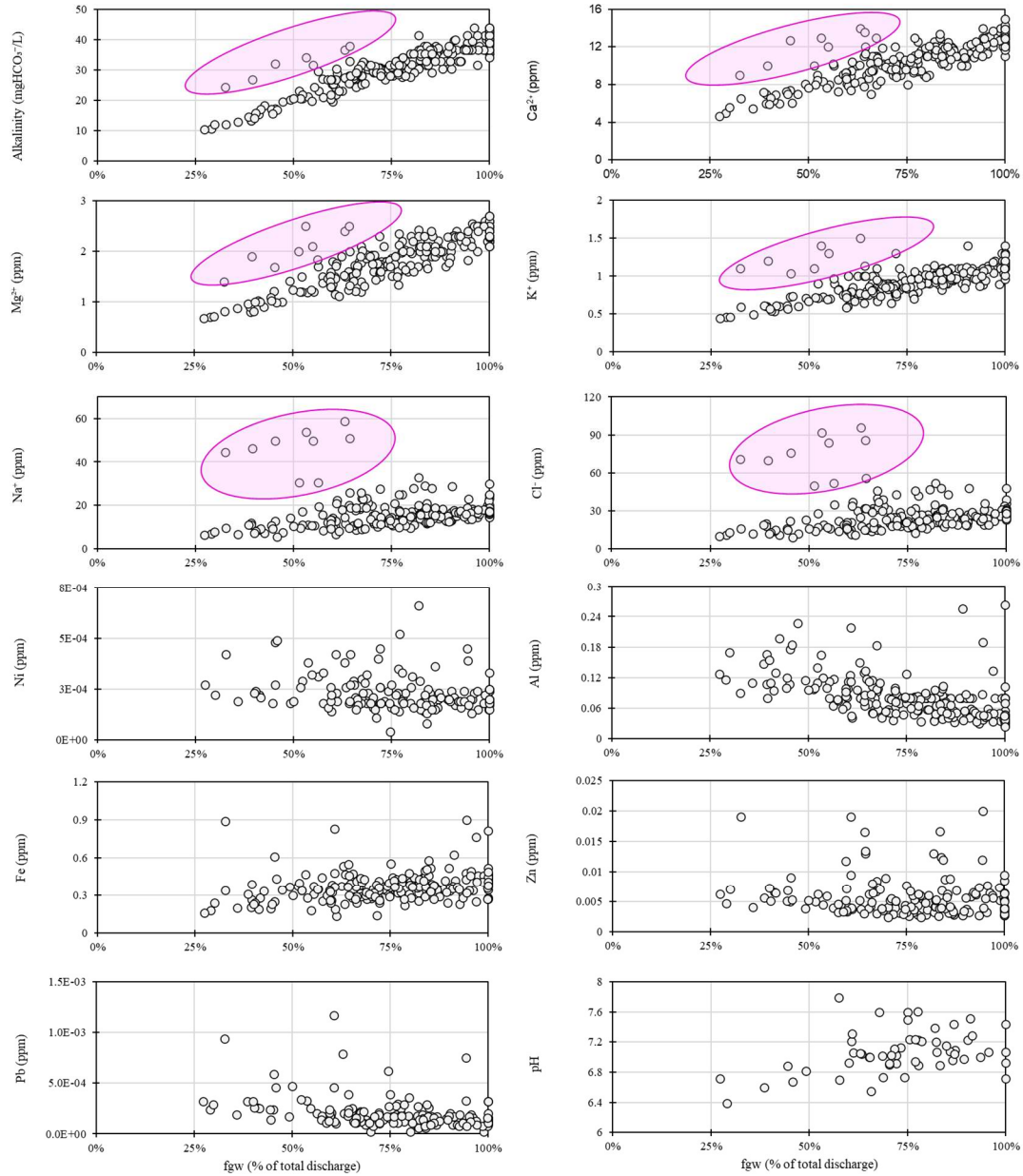


Figure 50: Relationship between the groundwater fraction (f_{gw}) and major ions concentrations (alkalinity, Ca^{2+} , Mg^{2+} , K^+ , Na^+ and Cl^-), trace metals (Ni, Al, Fe, Zn and Pb) and pH. The points influenced by urban snowmelt contribution are highlighted in the pink circles for major ions.

Clearly, groundwater is the primary control of the stream water mineralization except during punctual large releases of “urban” contaminated snowmelt pulses in winter. Unlike electrical conductivity, the alkalinity signal is not so impacted by these contaminated surface inflows. In addition, its fast response to storm events and its subsequent relationship with f_{gw} suggest that it can be used as a simple and reliable tool for the quantification of the groundwater fraction.

3.3.5.2 Alkalinity and silica signals are out-of-phase

Dissolved silica is typically absent or found in very low concentrations in both liquid and solid precipitation and is mainly obtained in groundwater by the slow dissolution of silicates minerals (Peters et al., 2013). The transit time of groundwater in the subsurface exerts a strong control on dissolved silica concentrations (Barbecot & Lefebvre, 2021). Typically, in the same hydrogeological context, the highest concentrations are associated with the oldest groundwaters. Dissolved silica has already been used as a tracer of the residence time of groundwater feeding surface waters (Benettin, Bailey, et al., 2017; Morgenstern et al., 2010; Peters et al., 2013). Dissolved silica and alkalinity are good tracers of groundwater inflows in rivers since they are essentially inherited from water rock interaction processes within the subsurface.

However, here, they do not show the same variation with time and discharge (Figure 51 a) and b)):

- Alkalinity concentrations are relatively more sensitive to storm events than dissolved silica concentrations
- The maximum concentration (plateau) is attained more quickly for alkalinity (at low-flow periods in summer, in July-August 2022) than for dissolved silica (in winter, in February 2022 and 2023)
- Surprisingly, silica concentrations are at their lowest in May, after the snowmelt period, during a baseflow dominated period as indicated by the high alkalinity concentrations.

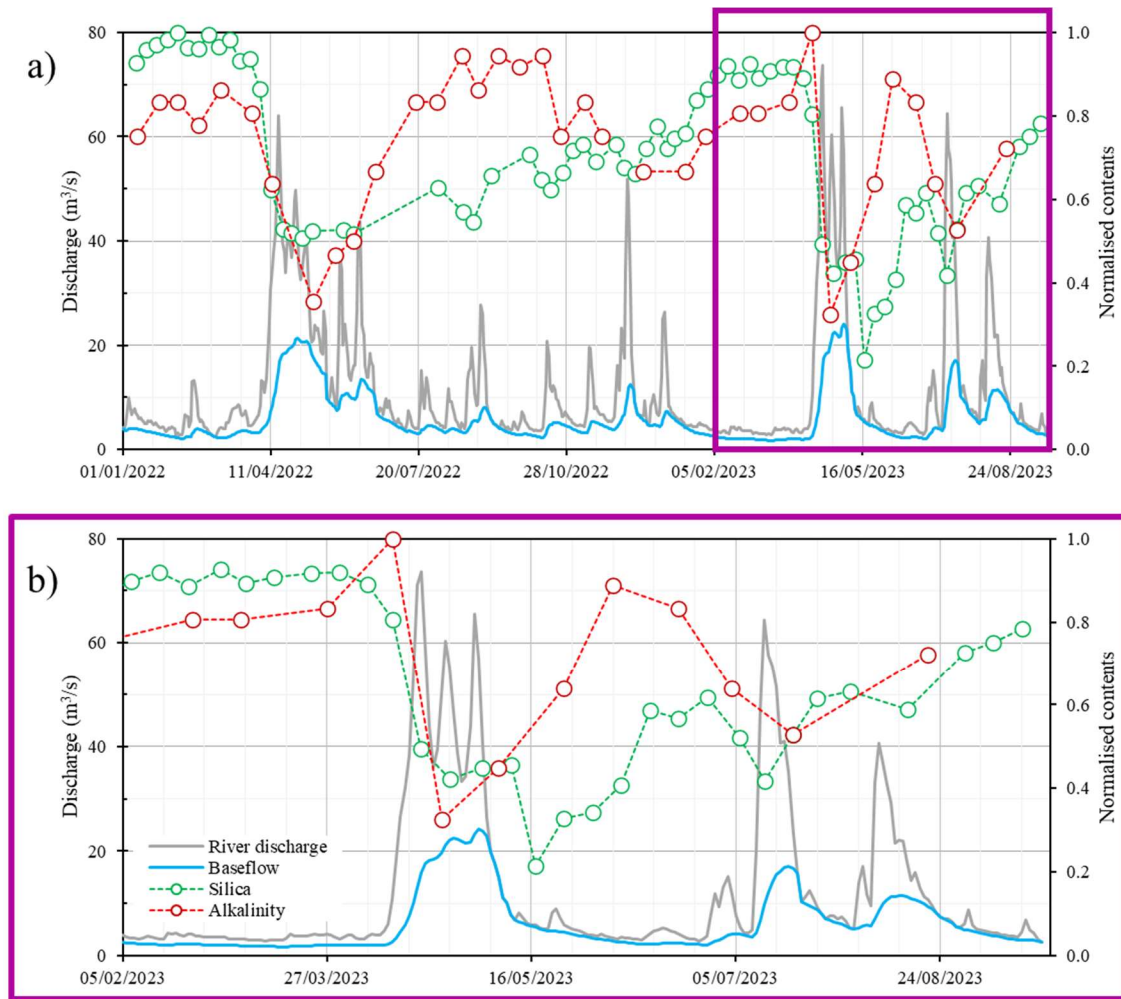


Figure 51: a) Evolution of total discharge, baseflow, normalised alkalinity and dissolved silica concentrations during the years: 2022 – 2023. b) Zoom on the period Feb. 2023 to Sept. 2023. The contents were normalised to the maximum value measured during the 2022 – 2023 period.

This confirms that alkalinity, which is mainly inherited from dissolution of rock carbonates by soil CO_2 , is a good tracer of the groundwater fraction in the river. However, it cannot reliably trace the residence time of groundwater. The variations of dissolved silica in the river are primarily controlled by the residence time of water contributing to the streamflow. The combination of alkalinity and dissolved silica is thus very useful for understanding processes leading to baseflow generation and their temporal variability. The dephasing revealed at the end of the winter period indicates that a substantial proportion of “older” water discharges to the stream during the snowmelt period compared to later in May and June. In May, groundwater contribution is high,

as indicated by the high alkalinity concentrations and low-flow conditions, but with “younger” water, as indicated by the very low silica. Slowly, during summer and autumn, the river water mean residence time increases until dissolved silica concentration reaches a plateau (ex: February 2023). This means that the maximum of the dating window of dissolved silica is attained. More age-dating tracers (ex: tritium) would be necessary to identify more precisely those associated with longer water travel times (Visser et al., 2019).

3.3.5.3 “Minimum mean residence time” estimation

The “minimum mean residence time” (τ_m) was determined using the three TTD (piston flow, exponential flow and Gamma-type flow with a shape parameter of 0.5) presented in section *Materials and Methods*. The growing concentrations of silica during winter was used to simulate a first-order kinetics pattern, that is then translated into a lumped parameter model to determine the minimum mean residence time of stream water.

The results of these simulations are given in Figure 52. First, the gradual increase in τ_m from summer to winter is clearly visible. In the absence of liquid inputs (rain and snowmelt), as in winter, the mean age increases quickly, up to a few months to a few years for both exponential and Gamma models (Figure 52 a)). The end of the snowmelt period is marked by a substantial portion of very young groundwater ($\tau_m < 10$ days) for which the three models agree well. The summer period is marked by an increase in τ_m , due to the preferential, but slow draining of the newly recharged aquifer portion in the uppermost part of the aquifer. There is a clear trend in the age-discharge relationship shown in Figure 52 b) with the highest τ_m associated with some of the lowest discharge and low τ_m associated with very high flows.

The dissolved Si concentration of the groundwater inflows were determined using the simple mass-balance below:

$$c_{Si,gw}(t) = \frac{Q_{riv}}{Q_{gw}} c_{Si,riv}(t) \quad (8)$$

Where $c_{Si, gw}$, $c_{Si, riv}$ are the groundwater and river dissolved Si concentration respectively and Q_{riv} and Q_{gw} are the river discharge and groundwater inflows respectively. This allows to draw the relationship between the estimated “minimum mean residence time” using the exponential model and the groundwater dissolved Si that is shown in Figure 52 c). Most points plot along a line in a semi-log scale. However, a few points deviate from this trend. These points are found for days when discharge is very variable, *i.e.* during or shortly after big runoff events, when the exact time at which the sampling took place is important but unknown. It is likely that this is the main reason for such discrepancies in the relationship.

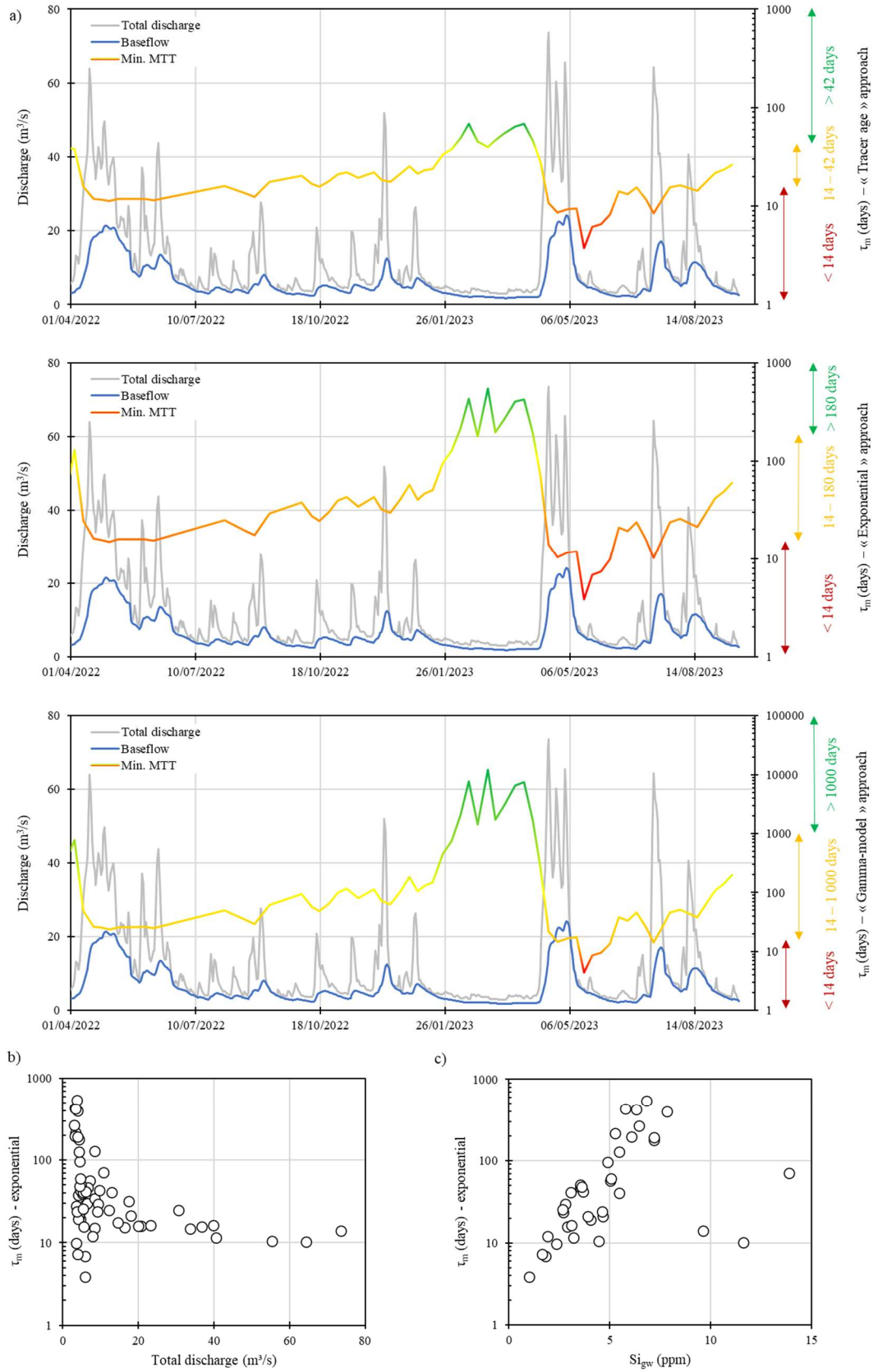


Figure 52: a) Evolution of “minimum mean transit time (i.e. τ_m)”, discharge and baseflow during 2022 and 2023 for the three approaches; b) Age-discharge relationship determined using the exponential model approach; c) Groundwater Si concentration-age relationship determined with the exponential model approach.

3.3.5.4 Implications for water resources management

Hydrograph separation is a very useful tool for water resources management. However, as pointed out by Saraiva Okello et al. (2018), its use in larger catchments can be inhibited because of spatial heterogeneity in geology, precipitation inputs and quality, land-use and urbanisation. Here, urbanisation and the use of de-icing salts, playing a very occasional but important role in stream water quality, prevents the use of straightforward binary mixing models that can be performed using a simple electrical conductivity monitoring. However, we were able to develop a robust yet simple flow components separation using EMMA with a three end-members mixing approach. The decomposition of the flow in three main sources revealed to be sufficient to accurately explain the variance of the stream water quality. This methodology allows to get a first good idea of the volumes of groundwater sustaining the river. Of course, because of the size of the catchment, the monitoring time resolution and the inherent difficulties due to the presence of large urban areas, the hydrograph separation proposed here is still broad, and it is currently not possible to go in greater detail. For example, the separation of soil water, younger and older groundwater components would be greatly beneficial to the understanding of groundwater – surface water interactions and streamflow generation processes.

Water resources managers of surface waters currently monitoring the quality of the stream could duplicate this approach to determine the dependency of the surface water resources to groundwater, thus enabling a better description of the resource vulnerability to climate change and land-use change. The latter is strongly linked to the TTD of the stream water, which is highly variable according to wet or dry periods. Figure 53 shows the Gamma-type TTD ($\alpha = 0.5$ and 1) for two selected mean transit times: 15 days (wet conditions, met during the highest flows due to snowmelt and rainfall) and 150 days (dry conditions during the winter). Contaminant transport within the catchment is strongly affected by the shape of the TTD with rapid and important

mobilization during the wettest periods and more dampened but longer mobilization during dry periods.

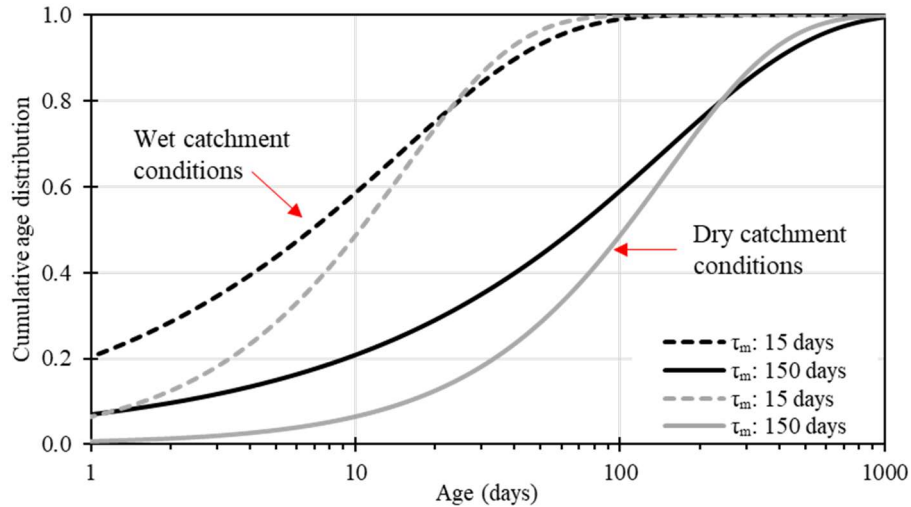


Figure 53: Cumulative age distribution representative of different catchment wetness conditions (different τ_m): $\alpha = 1$ for grey lines (exponential), and $\alpha = 0.5$ for black lines.

3.3.6 Conclusions

A multi-tracer hydrograph separation was conducted in a mesoscale, partly urbanised and snowmelt influenced catchment. The EMMA revealed that three end-members can explain the time variability of stream water chemistry: groundwater, “clean” runoff and “urban” snowmelt runoff. As the data spans from 2013 to 2023, the apparent temporal variability of the groundwater end-member was also considered. A mathematical filter was then calibrated against tracer data. All results showed that groundwater is the main contributor to streamflow, except during the snowmelt period in April and May. The relationship between the groundwater fraction and the stream hydro-geochemistry demonstrates that groundwater inflows control the stream mineralization, except during punctual releases of NaCl-contaminated snowmelt in February and March. This makes electrical conductivity unsuitable as a simple, cost-effective tracer for hydrograph separation in this catchment. However, alkalinity, that is mainly inherited from the transit of water in the unsaturated zone revealed to be a robust and reliable tracer of the groundwater fraction in the stream ($R^2 = 0.80$). Dissolved silica is thought to primarily originate

from the weathering of silicate minerals and is a good indicator of the water residence time within the catchment, which gives complementary information to alkalinity. However, they show a slightly different behaviour which could be attributed to the preferential release of newly recharged groundwater shortly after the snowmelt period. The draining of the uppermost part of the groundwater storage participating to the streamflow is represented by the relative slow increase in dissolved silica compared to alkalinity. This has serious implications in terms of vulnerability. Indeed, such behaviour suggests that surface contamination could travel fast to the stream as an important fraction of the stream water originates from relatively recent recharge. A simple method was used to determine the minimum mean transit time using three different TTD shapes. However, while it is possible to estimate the importance of the fast part of the catchment TTD, it is not possible to discuss its tailing part, sheltering the oldest water component. The complete shape of the catchment TTD would greatly benefit to water resources managers, giving information regarding the retention and release of contaminants at longer times.

3.4 Conclusion of Chapter 3

The work presented above has critical implications for the management of the water resource in the Saint-Charles river catchment as it shows that the surface waters are dominated by groundwaters, at least at the monthly and yearly scales. Not only the availability of the water is controlled by the baseflow, but also its quality as indicated by the tracers temporal dynamics.

The water stable isotopes revealed to be good tools to qualitatively identify links between the different water masses (precipitation, rivers, groundwater) although they have not been used to quantify the groundwater fraction. In addition, the strong altitudinal isotopic gradient in liquid precipitation needs to be completed with snowmelt data in the future in order to be a reliable indicator of mean groundwater recharge elevation.

The geochemistry database fed by the City of Québec was used to perform the first reported hydrograph separation in a meso-scale, partially urbanised, snowmelt influenced catchment. The decades of data revealed to be extremely useful to understand the whole catchment behaviour,

especially (i) the groundwater inflows through time, (ii) the sources of contaminants (ex: de-icing road salts or heavy metals) and (iii) calibrating a continuous mathematical baseflow separation filter. The catchment scale annual recharge rates can be estimated by assuming that the annual baseflow is a close representation of the annual recharge. The computation is done by using the following equation:

$$R_i = \frac{N_i Q_{BFA,i}}{S} \quad (Eq. 3 - 1)$$

where R_i is the annual recharge of the year i [LT^{-1}], N is the number of days in the year i , S is the catchment area [L^2] and $Q_{BFA,i}$ is the average daily baseflow for the year i [L^3T^{-1}]. The annual recharge amounts computed using this method are comprised between 370 and 570 mm (490 mm on average), which revealed to be close to what was found using a 3D-modelling of the catchment calibrated using piezometric level and discharge data by the colleagues from Université Laval (Tremblay et al., 2024). This represents roughly 35 to 40 % of the total annual precipitation. The baseflow separation data also showed that 40 % of the groundwater recharge occurs during the snowmelt period, *i.e.* from March to the beginning of May during the peak discharge. It is noteworthy that most big cities under similar climates and relying on surface waters are currently monitoring most water quality parameters (ex: major ions, electrical conductivity, trace metals, microbiology), and would greatly benefit from applying the same techniques to assess the vulnerability of their surface waters intakes. The geochemical couple alkalinity – dissolved silica shows that the contribution of groundwater have a variable mean residence time, with the lowest ages found shortly after the snowmelt period (high recharge during a short period) and the highest ages found at the end of the winter low-flow period. The coupling of these two tracers can be advantageously used in other similar geological settings, that are largely found in Eastern Canada and at least in Québec (*i.e.* crystalline basement with limited presence of carbonates).

It is possible to expect an “extreme” range of water mean residence times in the studied streams, from a few days shortly after recharge events to years or even decades during the prolonged low flow periods. The water fraction having residence times less than a few months is sensitive to

seasonality (ex: recent recharge, seasonal recharge pattern). The water having the longest transit times is less sensitive to the natural climatic seasonality and is then an excellent indicator of the catchment vulnerability and resilience. The winter is the best suited period for this kind of experiment. The TTD of winter baseflow has been determined thanks to a combination of residence time tracers (^{85}Kr , CFCs, SF_6 and ^3H) in the Nelson River, one of the main tributaries of the Saint-Charles River. This work is described through *Article 4* in the next chapter.

CHAPTER 4 Catchment water transit time distribution: the contribution of environmental and artificial tracing experiments in a partially frozen river

4.1 Résumé du Chapitre 4 en français

4.1.1 Introduction du Chapitre 4

Les chroniques de traceurs environnementaux (isotopes stables de la molécule d'eau, silice dissoute, ions majeurs et éléments traces) présentées dans le Chapitre 3 ont permis de montrer que l'état quantitatif et l'état qualitatif de la rivière Saint-Charles sont largement contrôlés par les apports d'eaux souterraines. Cela permet de répondre à la première partie de la question de recherche posée au Chapitre 1. La description de la vulnérabilité de cette ressource de surface dominée par les apports souterrains doit ensuite être complétée par la détermination des temps de résidence de ces apports (temps de résidence moyen ou distribution d'âge), puisqu'elle permet de décrire la résilience des rivières. Le Chapitre 4 apporte des éléments de réponse à cette partie de la question de recherche, *i.e.* quel est le temps de résidence moyen (ou la distribution d'âge) du débit de base des rivières du bassin versant ?

La période hivernale québécoise comporte plusieurs caractéristiques intéressantes. Elle est en général la période pendant laquelle la fraction souterraine en rivière est la plus importante (voir section 3.3), notamment à cause des températures très négatives qui empêchent à la fois le ruissellement et la recharge pendant de longues semaines. De plus, les teneurs en silice dissoute indiquent que les eaux souterraines les plus anciennes sont suspectées d'alimenter les rivières à cette période (Chapitre 3). Un ensemble de traceurs adaptés à la datation des eaux souterraines récentes (maximum quelques décennies) a été sélectionné pour dater le débit de base de la rivière Nelson, un des principaux affluents de la rivière Saint-Charles, qui est alimentée par le principal aquifère granulaire du bassin versant. Ces traceurs sont : tritium (^3H), CFCs, SF_6 et ^{85}Kr . Mis à part le tritium, ces traceurs sont sous forme gazeuse. Cela ne pose pas de contrainte majeure à leur utilisation lors de prélèvements directs d'eau souterraine dans les aquifères, via des forages. En revanche, lorsque ces traceurs sont apportés par le lit du cours d'eau, ils vont naturellement échanger avec l'atmosphère. Cela conduit à

une perte rapide de l'information apportée par les eaux souterraines et complique largement leur utilisation comme traceurs de datation des eaux de surface (Jensen et al., 2022), malgré les méthodologies robustes rapportées dans la littérature scientifique (Solomon et al., 2015; Stolp et al., 2010). Ces méthodes sont basées sur le concept de bilan de masse à l'échelle d'une section de rivière (voir section 1.2.1.4.2). Le principal avantage de cette méthode est qu'elle est très intégratrice et permet de caractériser un bassin versant au complet, puisque la rivière va naturellement recouper les lignes d'écoulement des eaux souterraines contenues dans les aquifères de dépôts meubles depuis l'amont vers l'aval du bassin. Les rigoureux hivers québécois permettent à une couche de glace de se former au-dessus des rivières, les isolant ainsi, au moins en partie, de l'atmosphère. A cette période, l'eau qui s'écoule à la surface est très froide (ex : 1°C mesuré en mars 2024) ce qui a pour principal avantage de diminuer la diffusivité des gaz. En théorie, ces caractéristiques devraient largement diminuer les échanges entre les gaz dissous et les gaz de l'atmosphère, favorisant la conservation du signal d'eau souterraine d'amont en aval. L'application d'un bilan de masse nécessite au préalable de la connaissance des vitesses d'échange air – eau en traceur, afin de déterminer la teneur des traceurs gazeux dans les eaux souterraines. Ces échanges ont été quantifiés via l'injection artificielle de gaz inertes dans la rivière Nelson (He et SF₆). Malgré le fait que la rivière Nelson n'était pas complètement recouverte de glace lors de la campagne de terrain, l'injection de deux gaz aux propriétés différentes a permis de vérifier que les échanges avec l'atmosphère étaient limités et bien inférieurs aux valeurs rapportées dans la littérature.

Le Chapitre 4 et l'*Article 4* rapportent la première utilisation de cette méthode au Canada et plus largement en « conditions froides ». Les résultats obtenus sont très encourageants et ont de sérieuses répercussions sur la manière de considérer la vulnérabilité des ressources en eaux dans les bassins versants stratégiques, comme ceux utilisés pour la production d'eau potable. Par ailleurs, cette méthodologie pourrait être affinée dans le futur (en fonction des conditions météorologiques hivernales) et appliquée dans la plupart des bassins versants de l'Est du Canada.

4.1.2 Résumé en français de l'Article 4

Les eaux souterraines représentent la principale contribution aux eaux de surface à échelle globale et constituent le débit de base qui soutient les écosystèmes de surface ainsi que les sociétés humaines tout au long de l'année. La compréhension et la prévision des effets négatifs des forçages anthropiques (urbanisation, changement climatique global), et en particulier des décalages temporels associés au transport des contaminants des zones de recharge vers les zones de décharge (typiquement, les cours d'eau), sont cruciales pour la bonne gestion des ressources en eau. La détermination de l'âge du débit de base à partir de bilans massiques de traceurs gazeux peut être compliquée en raison de la perte progressive du signal de l'eau souterraine dans le cours d'eau. Les conditions de terrain hivernales dans l'est du Canada (eau des rivières froide, rivières partiellement ou totalement couvertes de glace) peuvent être avantageuses pour l'application de ces méthodes car elles conduisent à une réduction des échanges air/eau. Une approche unique basée sur l'utilisation de plusieurs traceurs (CFCs, SF₆, ⁸⁵Kr, gaz rares et ³H) a été adoptée dans cette étude pour déterminer l'âge du débit de base dans un bassin versant de taille moyenne (rivière Nelson à Québec, 70 km²). L'injection simultanée de deux gaz inertes, He et SF₆, a permis de quantifier les échanges gazeux air/eau. Les résultats montrent que ces échanges sont limités par rapport à d'autres études, grâce aux conditions uniques de terrain. Malheureusement, les CFCs et le SF₆ ne peuvent pas être utilisés pour la datation des eaux souterraines en raison d'une contamination locale de l'aquifère. Cependant, le ³H et le ⁸⁵Kr permettent de retracer les apports d'eaux souterraines à la rivière et de déterminer le temps de transit moyen (environ 10 ans, modélisé avec les modèles Gamma et de dispersion). Cette première étude de ce type dans l'Est du Canada est très prometteuse en ce qui concerne l'utilisation de la datation du débit de base pour la description de la vulnérabilité et de la résilience des ressources en eaux à l'échelle du bassin versant aux changements à la surface.

4.2 Introduction to Chapter 4

The analysis of environmental tracers (stable isotopes of the water molecule, dissolved silica, major ions and trace metals) in Chapter 3 showed that the availability and quality of the rivers of the studied catchment are controlled by groundwater inflows. This allowed to address the first part of this thesis research question. Determining age information (TTD or MTT) of the

groundwater inflows in perennial, baseflow-dominated streams is a powerful and innovative tool to describe the surface waters vulnerability and resilience to modifications at the surface (*i.e.* urbanisation and climate change). Chapter 4 addresses the final part of the scientific question, which is: what is the MTT (and TTD) of the groundwater inflows to the rivers of the catchment?

The winter period is marked by relatively high contribution of groundwaters, as runoff is limited by freezing temperatures and snow accumulation at the surface. It is also the period where the oldest waters are expected to discharge to the stream (see *Article 3* in section 3.3). A suite of environmental tracers traditionally used for groundwater dating has been selected for winter baseflow age-dating in the Nelson river, one of the main tributaries of the Saint-Charles river that is sustained by the adjacent granular aquifer. These tracers are tritium (^3H), CFCs, SF_6 and ^{85}Kr . Except tritium, they are under gaseous form and air/water exchanges in streams would usually prevent or, at least, hinder their use for age-dating surface waters. A robust methodology inspired by previously published studies (Jensen et al., 2022; Solomon et al., 2015; Stolp et al., 2010) and based on the *reach mass balance* approach (see section 1.2.1.4.2) has been adopted to describe the whole catchment water transit times. Additionally, in winter, Québec's rivers are covered by ice which should prevent most of air/water exchanges and should help with the use of such methods in streams. The low rates of air/water exchanges were assessed by a deliberate injection of inert gas tracers in the river (SF_6 and He). The field work was carried out in February and March 2024, after a prolonged low-flow period. Unfortunately, the Nelson river was not completely covered by ice as the winter temperatures were not sufficiently cold during this winter. Nevertheless, the methodology, used and reported for the first time in Canada, is powerful because it integrates the tracers information at the catchment scale, and the results presented in this chapter and *Article 3* are promising for the study of catchment scale water resources vulnerability in Québec, and most perennial, baseflow dominated rivers under cold climates worldwide.

4.3 Deciphering river baseflow age distribution through environmental and artificial tracing experiments in a partially ice-covered river (*Article 4*)

Deciphering river baseflow age distribution through environmental and artificial tracing experiments in a partially ice-covered river (Québec, Canada)

In the process of being submitted to Journal of Hydrology (February 2025).

Antoine Picard^{1,2}, Florent Barbecot^{1,2}, José A. Corcho-Alvarado³, Roland Purtschert⁴, Douglas Kip Solomon⁵, Janie Masse-Dufresne^{1,2,6}, Benjamin Bouakline^{1,2,6}, Ahmed El-Azhari^{1,2}, Benjamin Frot⁷

¹ Hydro Sciences UQAM-ETS, Département des Sciences de la Terre et de l'atmosphère, Université du Québec à Montréal, Montréal, Canada

² Geotop (Research Centre on the Dynamics of the Earth System), Montréal, Canada

³ Nuclear Chemistry Division, Spiez Laboratory, Federal Office for Civil Protection, Austrasse, 3700 Spiez, Switzerland

⁴ Climate and Environmental Physics, University of Bern, Bern, Switzerland

⁵ Department of Geology and Geophysics, University of Utah, Utah, United States

⁶ Hydrology, climate and climate change laboratory, École de technologie supérieure, Montréal, Canada

⁷ Département de géologie et de génie géologique, Université Laval, Québec, Canada

Abstract: Groundwater is the main contributor to surface waters worldwide and provides a baseflow sustaining surface ecosystems as well as human societies all year round. Understanding and predicting the adverse effects of anthropogenic forcings (urbanisation, global climate change), and particularly the time lags associated with contaminant transport from recharge areas to discharge areas (typically, streams) is crucial for a sustainable management of the water resources. The determination of baseflow age information from gaseous tracers mass balances can be complicated due to the progressive loss of the groundwater signal in the stream. The winter season in Eastern Canada offers favourable conditions for the application of a gaseous tracers mass balance approach. The cold surface waters and partial ice cover reduce air/water exchange rates, thereby enhancing both the precision and the scale of application of tracer studies. A multi-tracer approach (CFCs, SF₆, ⁸⁵Kr, noble gases and ³H) was adopted in this study to determine baseflow age information in

a medium sized catchment (Nelson River, Québec, 70 km²). A dual inert gas injection setup allowed to continuously inject He and SF₆ into the partially ice-covered river. The deliberate injection of artificial gas tracers, under the unique field conditions, show that air/water exchanges were limited compared to other studies. Due to a local contamination of the aquifer, CFCs and SF₆ cannot be used for groundwater dating. However, ³H and ⁸⁵Kr proved to be valuable tracers of the discharging groundwater and allowed to determine a mean transit time of roughly 10 years with the exponential and the dispersion models. This first study of its kind in Eastern Canada is very promising regarding the use of baseflow age dating information for the description of catchment scale vulnerability and resilience to environmental changes.

Key-words: Baseflow dating, groundwater/surface water interaction, noble gases, water resources vulnerability.

4.3.1 Introduction

Groundwater plays a significant and active role in the global water cycle as it is the main contributor to surface waters worldwide (Xie et al., 2024). This is especially the case under temperate, cold and wet climates such as Eastern Canada where rivers are sustained all year by adjacent shallow aquifers (Beck et al., 2013). In these settings, the surface water availability and quality are controlled by the inflows of groundwater (Picard, Barbecot, Proulx, et al., 2024). Global climate change and urbanisation may then pose long-term threats to rivers if these surface changes affect shallow groundwater resources. As pointed out by Wachniew et al. (2016), water residence time estimation is particularly relevant to complement vulnerability assessments of water resources with the time lags associated with contaminant transport, from recharge areas to streams. Baseflow age information appears to be a relevant and integrative tool to describe the vulnerability and particularly the resilience of catchments to adverse anthropogenic effects (Humphrey et al., 2024; Jensen et al., 2022; Solomon et al., 2015; Stolp et al., 2010), as well as forecasting contaminant concentration in groundwater-fed streams (Jensen et al., 2024).

Various tracer-based methods for baseflow age determination are already reported in the literature, such as: diurnal variations of gases concentration (Sanford et al., 2015), reach mass balance approach (Jensen et al., 2022; Solomon et al., 2015) and the use of push-point

piezometers installed directly in the streambed (Humphrey et al., 2024). Recent developments based on the transmission and dampening of stable isotopes signal from precipitation to streams at high temporal resolution also exist but are excluded here, since they allow only to determine the younger transit times (typically less than 5 years) (Benettin, Bailey, et al., 2017; Harman, 2015; McGuire & McDonnell, 2006). The goal of the reach mass balance approach is to link spatial variations of tracer concentrations to groundwater inflows to derive groundwater age information (Cook et al., 2003; Cook et al., 2006). One major challenge of using age-dating tracers in streams is that many, especially those for young groundwaters (ex: CFCs, SF₆, ⁸⁵Kr, ³He), are gases. Their tracer signals are gradually lost due to air/water exchanges (Jensen et al., 2022). These exchanges must be quantified, usually by the deliberate injection of inert gas tracers (ex: SF₆, noble gases). Theoretically, the lower the ratio of tracer loss due to air/water exchanges to groundwater inputs, the higher the likelihood of success.

In Québec, two main factors can reduce air/water exchanges in winter, thus increasing the likelihood of success of application of such method: (i) the very low water temperatures and (ii) the presence of an ice cover that seals part of or the whole stream, preventing wind shearing effects. We report the results of the first multi-tracing experiment of this kind (CFCs, SF₆, ³H, ⁸⁵Kr) conducted in February 2024 on a medium-sized river in Québec, with a 70 km² catchment. We describe our dual inert gas injection (SF₆, He) made with a simple diffusion apparatus and supported by onsite mass spectrometry measurements (Brennwald et al., 2016). We also show that tritium (³H) can be used alone as a powerful tool for catchment scale mean transit time (MTT) determination, highlighting the potential of this method to investigate the vulnerability of groundwater dominated catchments to anthropogenic forcings.

4.3.2 Study site

The Nelson River is one of the main affluents to the Saint-Charles River. The latter is a strategic surface water resource as it is used as a drinking water source for the City of Québec. The Nelson River is perennial and drains a watershed of roughly 67 km², following the North-South axis of a small valley. Six sampling points (SW1 to SW6) along the river were used with SW6 being the most upstream (see Figure 54). The downstream part of the catchment is partially urbanised, while the northern part is dominated by forest.

The landscape is typical of the Laurentides piedmont with gentle slopes and hills up to 450 masl, and a main U-shaped valley widening on the southern part. The bedrock consists of migmatite and gneiss from the Grenville Province, whose age was determined to be close to 1 Ga (Castonguay & Nadeau, 2012). However, the Wisconsinian glaciation, deglaciation and subsequent marine incursions (80 000 to 10 000 BC) are responsible of shaping the landscape during the Quaternary. Most of the bedrock is covered by glacial till, especially on the slopes and the summit of the hills. The till is usually thin (max. 50 cm) and made of migmatite/gneiss clasts of all sizes trapped in a coarse matrix (sand to silts). Fluvioglacial stratified deposits are found in the main valley and were formed by the transport of rock fragments during the melting of the continental ice shelf. They can reach a thickness of 30 m in the studied catchment. Following the deglaciation, marine incursion (- 12 000 to - 10 000 BC) resulted in the deposition of marine sediments (from fine, deep clayey deposits to sandy and silty deltaic sediments). The youngest surface deposits are alluvial deposits, found close to the current and paleo hydrographic network. They form the actual alluvial terraces and are usually not very thick (up to 5 m).

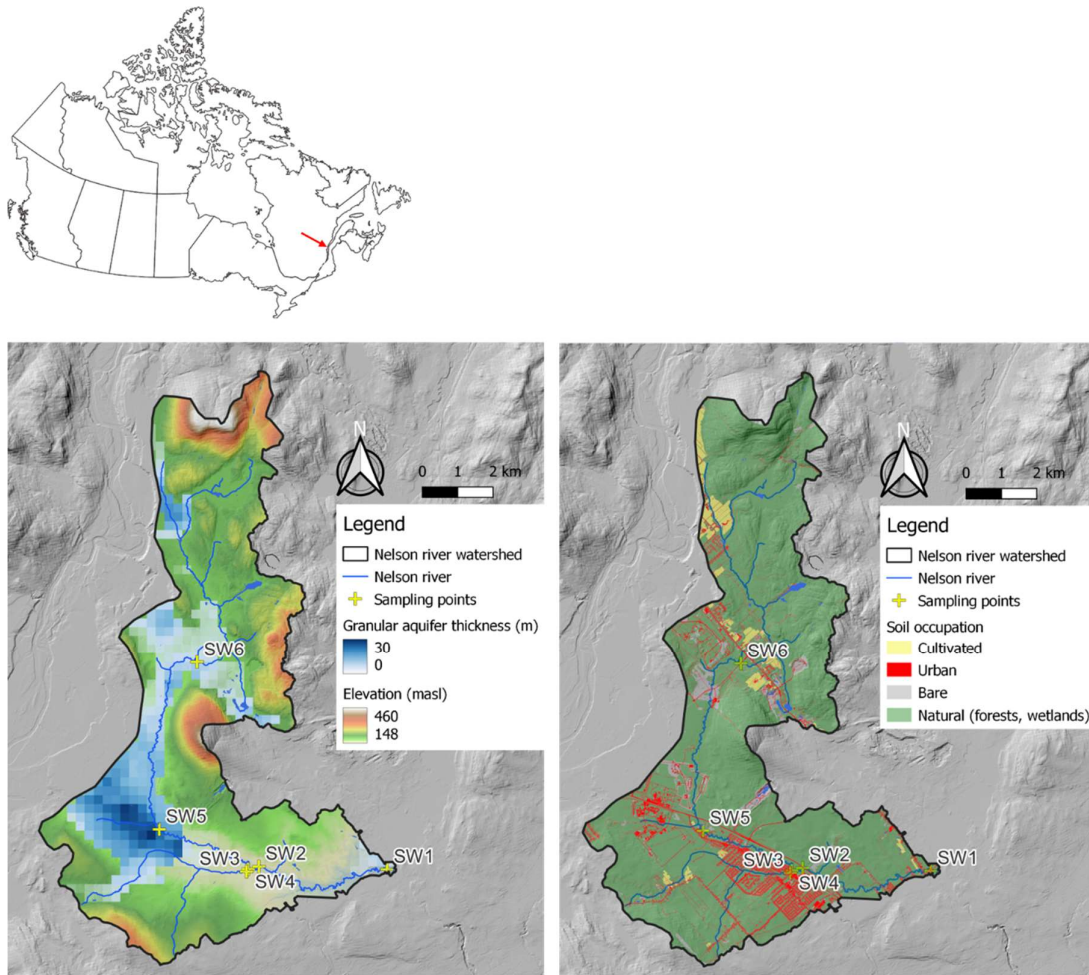


Figure 54: Above: map of Canada with the red arrow indicating the location of the study site. Below: maps of the Nelson River watershed with the 6 sampling points (SW1 to SW6): topography and granular aquifer thickness on the left, and soil occupation on the right.

A hydrological station operated by the Government of Canada is located at SW2 and monitors the discharge of the river since 2006. The hydrograph is marked by two low flow periods, one in winter (accumulation of snowpack at the surface due to freezing temperatures) and another in summer. However, due to precipitation events, high flows often interspersed the summer low flow period. The spring period is marked by the snowmelt leading to the highest recorded discharges (Figure 55). The baseflow sustains the stream all year long, and particularly in winter due to freezing conditions. The dependency of the nearby Saint-Charles River to groundwater was investigated in Picard, Barbecot, Proulx, et al. (2024). The study showed that baseflow is the main contributor to the river throughout the year (> 55 %), except in April and

May during which 40 to 50 % of the total discharge is reached. The dissolved silica dynamics in this river showed that the oldest waters are found in winter, a period during which the groundwater contribution is very high. Similar dynamics are expected in the Nelson River, one of the main tributaries of the Saint-Charles River, where groundwater inflows are suspected to mostly originate from the granular aquifer composed of fluvio-glacial deposits (Figure 54).

The local climate is marked by wet hot summers, and cold wet winters during which rivers surface often freeze completely. However, when the field work took place at the end of February 2024, the river surface was only partially frozen due to warmer than usual temperatures.

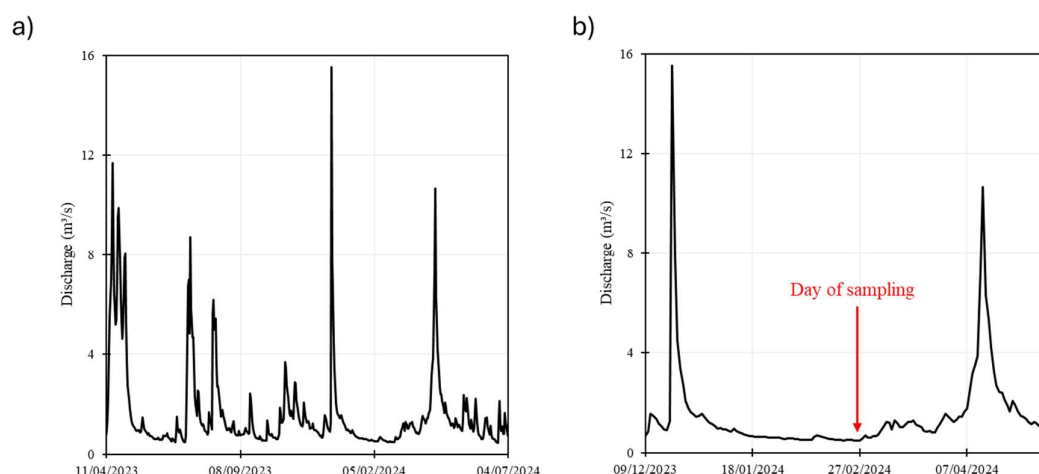


Figure 55: (a) Evolution of the Nelson River daily discharge from April 2023 to July 2024, and (b) zoom-in the 2023 – 2024 winter period, with sampling day highlighted (27/02/2024).

4.3.3 Materials and methods

The field work was carried out in two phases, during low flow conditions:

- First phase: involved field measurements of physico-chemical parameters and sampling for environmental tracers (major ions and age-dating tracers – namely ^3H , noble gases, ^{85}Kr , CFCs and SF_6).

- Second phase: involved the injection of artificial tracers, such as: (i) standard salt (NaCl) for discharge measurement, on the day following the environmental sampling, and (ii) inert gases injection (He + SF₆) for the quantification of air/water exchanges parameters.

4.3.3.1 First phase: Field measurements, sampling and analyses

Field measurements of water electrical conductivity, pH and temperature were taken in the middle of the stream using a WTW® field multimeter that was calibrated for pH and electrical conductivity on the morning of the field activities.

Wheaton® 700 mL glass bottles with septum caps were filled slowly, under the water surface, for CFCs and SF₆ analyses after ensuring that no bubble was left in the bottle or the inside of the caps. Analyses were performed at the Geotop Water Resources Geochemistry laboratory in UQAM, Montréal, using the headspace method. A headspace made of high purity He was created in the samples (typically 50 mL of headspace for 650 mL of residual water) in the laboratory and the water was let to equilibrate with the helium headspace for a few days with constant shaking (200 rpm). The laboratory temperature was monitored during the whole process at 5 minutes interval and was close to 22°C. The headspace was then extracted and analysed using GC-ECD technique. Typical uncertainties are of 5 % of the measured values based on reproducibility of standards.

⁸⁵Kr was sampled using a passive method using gas permeable membranes (Meyzonnat et al., 2023; Musy et al., 2021). A membrane contactor is placed under water and is connected to a pre-vacuumed sampling bottle with a volume of 20 L. The pressure gradient drives the gas towards the sampling bottle, taking approximately 1-3 days to obtain enough gas for an analysis. The minimum requirement for the analysis of the ⁸⁵Kr activity, conducted by low-level counting at the University of Bern (Switzerland), is 2 to 4 µL of Kr, which corresponds to at least 5 litres of gas extracted from the river water. Three similar systems were used in this study (Figure 56) and six samples were taken (5 of the river dissolved gases, and 1 of the local atmosphere). Overall, the sampling for ⁸⁵Kr in the river spanned a period of 5 days.



Figure 56: Apparatus used for in-situ sampling of ^{85}Kr (left) and river aspect during fieldwork showing the partial ice cover close to SW4 (right).

Water for ^3H analysis was sampled in 1L HDPE bottles after rinsing the bottle three times with stream water. Analyses were performed at the Deep Underground Laboratory of the University of Bern using liquid scintillation counting. The uncertainties are of ± 1.2 TU on average.

Water for noble gases analysis was sampled in copper tubes using a submersible pump and following sampling instructions given by the Noble Gas Laboratory of the University of Utah (<https://noblegaslab.utah.edu>). Duplicates were taken for each of the six points. Analyses were performed at the Noble Gas Laboratory of the University of Utah, Salt Lake City, U.S.A. The uncertainties are of the order of 1% for He and Ne, and 3% for other noble gases.

Water samples for major ions analyses were collected in 250 mL HDPE bottles. The analyses were performed at the Laboratory of the City of Québec, in Québec, using APHA methods guidelines (APHA, 2012). Only chloride analyses are discussed in this study.

The stream discharge was determined by standard salt injection and dilution technique (see for example Wood and Dykes (2002), Tazioli (2011) and Picard, Barbecot, Bardoux, et al. (2024)). Indeed, the presence of a partial ice cover is not favourable to the use of a velocimeter. Slug injections of known salt quantities were performed in 5 points, from downstream to upstream (SW1, SW2, SW3, SW5 and SW6 in this order, see Figure 54 for the localisation of the sampling and measuring points) on the same day. LTC (Level, Temperature and Electrical Conductivity) probes (Solinst®) were installed in the stream to monitor the tracer signal, downstream of each injection point and far enough to ensure enough lateral mixing. On the same day, a sample of the river water was taken prior to the injection to determine the relationship between the salt concentration and the electrical conductivity increase and interpret the tracing experiments (similarly to Picard, Barbecot, Bardoux, et al. (2024)).

4.3.3.2 Second phase: Injection of tracer gases and analyses

4.3.3.2.1 Description of the injection apparatus

A simple system was used to inject both He and SF₆ as dissolved gases directly into the stream (Figure 57), after environmental tracers sampling was completed. A research grade helium tank and a tank containing a mixture of SF₆ (100 ppm) and N₂ were installed on the riverbank. Each tank was connected to a gas permeable membrane (Zena® membranes) that was totally immersed in the middle of the stream, near the bottom. The gas pressure inside the membranes was manually controlled at the beginning of the experiment using manometers. The injection flux is primarily driven by the gas concentration gradient between each side of the membrane as the river temperature is rather stable all day. As described by Solomon et al. (2015), dissolved gases naturally present in river water, such as N₂, O₂ and Ar, diffuse from the river into the membranes, maintaining a constant total gas pressure but reducing the partial pressures of He and SF₆ on the lumen side of the membrane. This leads to a reduction of the injection rate, especially for “slow” diffusing gases, such as SF₆. To ensure constant renewal of the gas mixture on the lumen side of the membrane, the outlet of the membrane was vented to the atmosphere via a small capillary tube. Gas flow was visually assessed by allowing the capillary to bubble in the river for a few seconds during the system installation with one bubble occurring every 2-3 seconds. Unfortunately, likely due to overpressure, a part of the SF₆ membrane collapsed, causing some of the SF₆ to be injected as bubbles rather than

solely as dissolved gas. It is very likely that the injection rate of SF_6 remained constant throughout the experiment as the bubbling was minimal (one bubble every 5 s), constant in time, and because bubbles injection is not efficient compared to diffusion-controlled injections (Blanc et al., 2024). No such problem was observed for the He membrane.

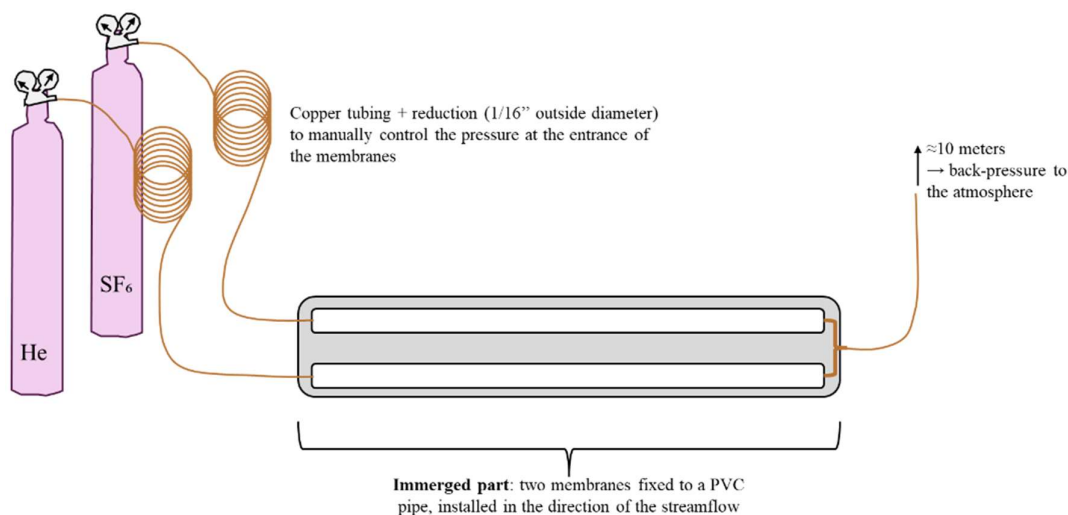


Figure 57: Scheme of the apparatus used to inject gas tracers in the stream. The immerged part was installed perpendicular to the direction of the streamflow.

4.3.3.2.2 Field measurements and sampling

The injection of He and SF_6 took place upstream from SW5 (coordinates: 46°52'36.0"N 71°27'45.3"W) after environmental samples were taken and lasted from 9:00 am to 8:00 pm on the 03/03/2024. The tracer plume was followed onsite between SW5 and SW3 by using a miniRUEDI with a GE-MIMS system (Brennwald et al., 2016) by monitoring the He concentrations over time. River water was pumped (Proactive® 12V pump) at a rate of roughly 1 L/min, thanks to a low flow controller (Proactive®), and flowed through a membrane unit (3M® membrane contactor) before being returned to the river downstream the pumping point. The air inside the membrane unit gets quickly equilibrated with the gas dissolved in the water and is continuously pumped by one of the miniRUEDI inlets. Temperature and pressure sensors are then used to transform the measured partial pressures in the headspace of the membrane to dissolved gas concentration. Typical uncertainties (1σ)

are 1-3% of the measured dissolved He value. Between 10 to 50 measurements were taken after the plateau was reached and were averaged to a single value for each measurement point.

Samples for SF₆ analysis were collected once the He plateau concentration was visually attained, using 55 mL glass vials capped with a septum. Analyses were performed using the headspace method as described above for environmental samples (here, the high-purity He headspace to water ratio was typically 12 mL to 43 mL). An additional SF₆ sample was prospectively taken 12 km downstream of the injection point on the morning of the 04/03/2024 at around 9:00 am, 24 h after the beginning of the injection and 13 h after the injection stopped. It is unknown whether the measured concentration is representative of the plateau or during the rising or tailing limb of the tracer restitution curve and this data point was not considered in the modelling of gas transfer velocity.

4.3.3.3 Modelling of dissolved tracers

4.3.3.3.1 Mass-balance approach

As most of the tracers used in this study are gases (e.g. age dating tracers), a mass balance equation for modelling the steady state advective transport of inert dissolved gases was used (Cook et al., 2003; Lefebvre et al., 2015; Solomon et al., 2015):

$$Q \frac{dc_s}{dx} = q_L(c_{gw} - c_s) + Kw(Sc_{atm} - c_s) + q_{snow}(c_{snow} - c_s) \quad (1)$$

Where Q , represents the stream discharge [L^3T^{-1}], q_L and q_{snow} denote the groundwater and “urban” snowmelt inflows per unit of length [L^2T^{-1}], respectively, c is the dissolved gas concentration in the stream (c_s), in groundwater (c_{gw}) and in “urban” snowmelt inflows (c_{snow}). S is the gas solubility and c_{atm} is the atmospheric mixing ratio [L^3L^{-3}] (Sc_{atm} is the dissolved gas equilibrium concentration), w is the stream width [L] and K is the gas transfer velocity [LT^{-1}] across the water surface (0 for non-gaseous tracers). This equation assumes that sampling and discharge measurements are conducted under steady state conditions. This assumption holds true (see Figure 55 b)) as no precipitation occurred during the field work, and air temperature remained sufficiently cold at day and night to prevent the melting of the snowpack. Evidence of “urban” snowmelt contribution is observed in the downstream part of the catchment, likely

due to the use of de-icing salts in urban areas, as revealed by elevated Cl^- and ^3H contents, as detailed in section 4-2. Elsewhere, groundwater inflows were computed as the difference between one upstream and one downstream measurement point. This assumes a linear increase in stream discharge with distance.

The discretized form of Eq. (1), accounting for tributary inflows, is expressed as follows:

$$c_{s,o} - c_{s,i} = \frac{q_L x}{Q_o} (c_{gw} - c_{s,i}) + \frac{Kw}{Q_o} (Sc_{atm} - c_{s,i}) + \frac{q_{snow} x}{Q_o} (c_{snow} - c_{s,i}) + \frac{Q_{trib}}{Q_o} (c_{trib} - c_{s,i}) \quad (2)$$

Where Q_{trib} is the tributary discharge [L^3T^{-1}], c_{trib} is the considered tracer concentration in the tributary and x is the length of spatial discretization [L], here 50 m. Q_{trib} is always equal to 0 except in cells where a tributary flows into the main river. Each river cell has an inlet (upstream) and an outlet (downstream) to which the subscripts i and o refer, respectively (see the scheme presented in Figure 58).

Eq. (2) is completed by the following Eq. (3) which represents the conservation of water fluxes along the reach, assuming no evaporation:

$$Q_o = Q_i + Q_{trib} + (q_L + q_{snow})x \quad (3)$$

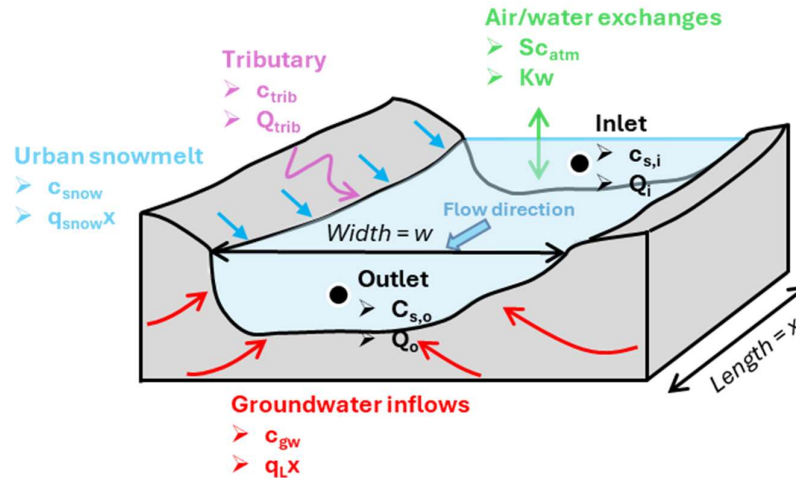


Figure 58: Scheme of a river cell with water and solutes fluxes.

Model parameters in Eq. (2) and (3), namely the gas transfer velocity, are determined by fitting to discrete (injected) stream tracer measurements. The “calibrated” model is then used to interpret the concentrations of dissolved dating tracers.

4.3.3.3.2 Determination of gas transfer velocity

The gas transfer velocities of He and SF₆ were determined by fitting the model, represented by Eq. (2) and (3), to the field measurements of He and SF₆ (section 4-1). The best-fit values were obtained by minimizing the root mean square error (RMSE) defined as $\frac{1}{N} \sqrt{\sum_{i=1}^n (c_{meas}(x_i) - c_{model}(x_i))^2}$, where n is the number of stream measurements ($N = 4$ for He and $N = 5$ for SF₆) and c_{meas} and c_{model} are the measured and modelled tracer concentration at the distance x_i from the injection site, using the Solver in Excel®.

This dual tracer injection allows to determine the n exponent in the following equation (Eq. (4)) (Jähne et al., 1987):

$$\frac{K_1}{K_2} = \left(\frac{D_1}{D_2} \right)^n \quad (4)$$

where K_1 and K_2 are the gas transfer velocities of gases 1 and 2 (here, He and SF₆) and D_1 and D_2 their aqueous diffusion coefficient [L²T⁻¹]. The exponent n ranges from 0.5 under turbulent conditions to 1 for diffusion controlled flow (Jensen et al., 2022), and is independent of the gas species. This relationship allows for the estimation of the gas transfer velocity of any other gas provided its aqueous diffusion coefficient is known.

3-3-3 Determination of concentrations of groundwater age-dating tracers

The concentration of ³H, SF₆, CFCs and ⁸⁵Kr, in groundwater inflows (prior to degassing) were determined using the Eq. (2) and (3). The uncertainties of stream discharge were estimated by error propagation similarly to Picard, Barbecot, Bardoux, et al. (2024). Typical uncertainties of measured discharge values and groundwater inflows are between 3 to 6 % and 6 to 14 % respectively. Monte-Carlo simulations were performed in Excel using the NORMINV() function (Solomon et al., 2015) to determine the standard deviation of the gas transfer velocity,

and then the standard deviation of the tracer concentrations in groundwater. To achieve this, the set of parameters was allowed to vary within their estimated uncertainties: 5% for w , 10% for D , 10% for CFCs and SF_6 measurements, 3% for onsite He concentrations (miniRUEDI), 1 % for S_{catm} and the tracer measurements.

Table 6: Discharge measurements and concentrations of groundwater age dating tracers in the stream and in the local atmosphere. Uncertainties are of 1 % for He and Ne, 3 % for heavier noble gases and 10 % for the four anthropogenic trace gases.

N° of point	Distance from upstream point (m)	Discharge (L/s)	Cl ⁻ (ppm)	³ H (TU)	⁸¹ Kr (dpm/cc _{Kr})	CFC-12 (pmol/L)	CFC-11 (pmol/L)	CFC-113 (pmol/L)	SF ₆ (fmol/L)	He (10 ⁻⁸ ccSTP/g)	Ne (10 ⁻⁷ ccSTP/g)	Ar (10 ⁻⁴ ccSTP/g)	Kr (10 ⁻⁷ ccSTP/g)	Xe (10 ⁻⁸ ccSTP/g)
SW6	0	95 ± 3	8	8.2 ± 1.2	72.5 ± 2.9	5.2	8.4	0.42	5.3	4.62	2.08	4.02	1.15	1.87
SW5	8000	174 ± 10	21	8.0 ± 1.1	64.5 ± 3.0	6.9	8.5	0.51	9.7	4.81	2.16	4.62	1.18	1.74
SW4	12750	227 ± 7	29	9.0 ± 1.2	67.4 ± 2.8	6.7	8.6	0.56	9.6	4.60	2.06	4.39	1.12	1.56
SW3	12800	107 ± 2	39	9.9 ± 1.2	73.5 ± 2.5	7.1	9.7	0.44	6.7	4.74	2.11	4.58	1.25	1.56
SW2	13250	334 ± 7	33	7.2 ± 1.1	not measured	8.1	9.8	0.60	9.2	5.32	2.18	4.57	1.09	1.48
SW1	19450	456 ± 14	107	10.7 ± 1.2	74.6 ± 3.0	14.4	9.2	0.56	11.3	5.44	2.21	4.70	1.25	1.87
Solubility equilibrium with atmosphere	N.A.	N.A.	N.A.	N.A.	78.1 ± 2.5	3.5	5.5	0.50	6.1	4.62	2.08	4.02	1.15	1.87

4.3.3.4 Groundwater inflows dating

4.3.3.4.1 Groundwater age-dating models

A lumped parameter model approach (Cook & Herczeg, 2000; Jurgens et al., 2012; Leibundgut et al., 2009) was adopted to model the expected concentration of the age-dating tracers as a function of groundwater age:

$$C_{out}(t) = \int_{-\infty}^t C_{in}(t - t') g_{\tau}(t - t') e^{-\lambda(t-t')} dt' \quad (5)$$

Where t is the sample date, λ is the decay constant in case of radioactive tracers [T^{-1}], C_{in} is the input function and C_{out} is the measured concentration of the considered tracer. The function g is the transit time distribution (TTD) and depends on the water mean transit time, which is the parameter τ [T], and other model parameters (*e.g.* dispersion parameter, shape factor). Note that the use of this equation assumes steady state conditions.

On a multi-annual basis, the recharge of the granular aquifer sustaining the stream can be considered as uniform since the only period without recharge is the winter period and lasts 2-4 months. It is then possible to approximate the age distribution of the aquifer using an exponential model (Cook & Herczeg, 2000; Jurgens et al., 2012):

$$g_{\tau}(t) = \frac{1}{\tau} e^{-\frac{t}{\tau}} \quad (6)$$

However, contrasted ages between river baseflow and the aquifer that sustain them are typically observed (Berghuijs & Kirchner, 2017), meaning that the TTD of the baseflow does not necessarily follows an exponential distribution. In fact, since the field work occurred in late February, a few weeks after the last precipitation event (Figure 55 a)), it is therefore expected that the groundwater contributions to the stream are free from “very young” (a few weeks to months) water. For these reasons, the more flexible dispersion model has been tested for the interpretation of the results hereafter (Jurgens et al., 2012):

$$g_{\tau}(t) = \frac{1}{\tau} \frac{1}{\sqrt{4\pi DP \frac{t}{\tau}}} e^{-\frac{(1-\frac{t}{\tau})^2}{4\pi DP \frac{t}{\tau}}} \quad (7)$$

where DP is the dispersion parameter, is equal to the inverse of the Peclet number and is representative of the ratio of dispersion effect (mixing) over advection.

The MTT, τ , is determined via inverse modelling of the measured tracer concentration by minimizing the RMSE between measured and output (modelled) tracer concentration.

4.3.3.4.2 Tritium (^3H)

Tritium (^3H) is a radioactive isotope of hydrogen (half-life of 12.3 years) whose activity concentration in water is usually reported in tritium units, TU (1 TU is equal to one molecule of ^3HHO in 10^{18} molecules of H_2O). ^3H has a unique atmospheric input history due to nuclear bomb testing in the 1950s and the 1960s that increased ^3H activities in precipitation and groundwater worldwide for decades. Since the ban of atmospheric nuclear bomb testing, atmospheric ^3H activities have been decreasing and now reach natural background concentrations from cosmogenic production (10 – 20 TU at higher latitudes such as in Ottawa, Canada, close to the study site).

As explained by Morgenstern et al. (2010) and Visser et al. (2019), it is important to consider the natural seasonality of the ^3H input signal in precipitation and the seasonality of infiltration to determine the correct input function for groundwater. Indeed, in New Zealand, the seasonal amplitude in ^3H activities in precipitation is of the order of 100 % while the infiltration pattern is very contrasted (Morgenstern et al., 2010).

Appendix A shows that accounting for the seasonality in ^3H activities in precipitation does not play a significant role in groundwater age-dating applications in the study site, for water more than a few months old. This is likely explained by the relatively low seasonal amplitude of ^3H in precipitation in Eastern Canada (of the order of 20 %).

4.3.3.4.3 Radiokrypton (^{85}Kr)

^{85}Kr is a radioactive isotope of the noble gas krypton with a half-life of 10.76 years. Since the 1950s, its atmospheric concentration has been rising, primarily due to the releases from nuclear fuel reprocessing plants (e.g. La Hague in France and Sellafield in the U.K.). The terrigenous production of ^{85}Kr is negligible (Cook & Solomon, 1997). It is typically reported as the ratio of ^{85}Kr to total Kr, making it rather insensitive to excess air, recharge temperature and degassing. These characteristics, in addition to its inertness, make it a very robust tracer of young (< 70 years) groundwaters (Cook & Solomon, 1997; Corcho Alvarado et al., 2007; Corcho Alvarado et al., 2005; Visser et al., 2013). To our knowledge, ^{85}Kr has not yet been used for river baseflow age dating applications. In rivers, the measured ^{85}Kr activity is the result of the competing fluxes of ^{85}Kr activities from groundwater inflows and exchanges with the atmosphere.

The works of Kersting, Schlosser, Bollhofer, et al. (2020) and Kersting et al. (2021) were used to determine the local atmospheric input function. The sample taken from atmospheric air in this study shows results consistent with the modelled local atmospheric baseline.

4.3.3.4.4 SF_6 -CFCs

Sulphur hexafluoride, SF_6 , and chlorofluorocarbons, CFCs (CCl_3F – CFC-11, CCl_2F_2 – CFC-12, $\text{C}_2\text{Cl}_3\text{F}_3$ – CFC-113), are anthropogenic trace gases widely used in groundwater dating studies, for young (< 70 years) groundwaters (Darling et al., 2012; IAEA, 2006). Since these gases are man-made, local pollutions may exist, especially near important urban centres (Höhener et al., 2003; Santella et al., 2008). This prevents any use and interpretation of these tracers for groundwater dating purposes in contaminated areas if the exact magnitude of contamination is unknown, which was unfortunately the case in the study site.

4.3.4 Results and discussion

4.3.4.1 Injection of inert gases (He and SF_6)

The injected He was detected up to 5 km downstream of the injection point while it was possible to detect the injected SF_6 up to 12 km. The concentration of injected He and SF_6 dropped by 50 %

after 2 km and 3 km respectively (Figure 59). The gas transfer velocity was found to be 1.31 ± 0.13 m/day for He and 0.51 ± 0.08 m/day for SF₆. Notably, k_{He} is roughly 2.6 times than k_{SF_6} reflecting helium's significantly higher volatility compared to SF₆.

The exponent n , defined as $n = \frac{\log\left(\frac{k_{He}}{k_{SF_6}}\right)}{\log\left(\frac{D_{He}}{D_{SF_6}}\right)}$ (Jähne et al., 1987), is estimated to be 0.91 ± 0.12 . This is

a higher value than what is found on average (Jensen et al., 2022) but is consistent with field observations. Indeed, the stream is calm with very limited high velocities turbulent zones, a low water temperature and has a protective partial ice cover.

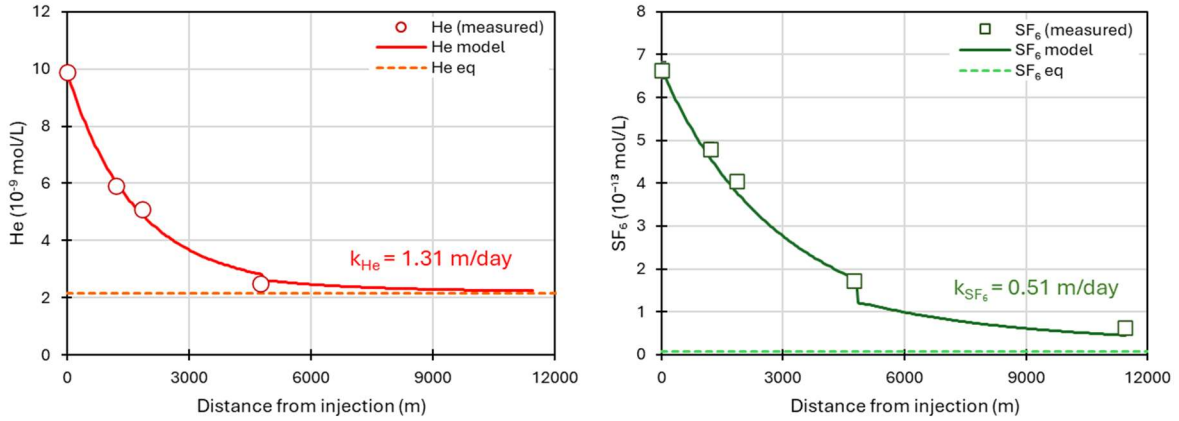


Figure 59: Tracer gas concentration plotted as a function of the distance from the injection point. The red and green points are the He and SF₆ concentrations, respectively. The dotted lines represent the equilibrium concentration relative to the atmosphere. The measurement uncertainties are smaller than the size of the points.

4.3.4.2 Estimation of the urban snowmelt contribution using chloride and ³H

The Cl⁻ concentrations increase from upstream (8 ppm in SW6) to downstream (107 ppm in SW1). However, the average Cl⁻ concentration in groundwater is estimated to be around 40 ppm according to past chemical analyses from wells located in the catchment. The increase in discharge and Cl⁻ concentration from upstream to downstream is thought to be due (i) to groundwater inflows for the upstream section (SW6 to SW2) and (ii) to the contribution of “urban” snowmelt in the downstream part (between SW2 and SW1). This is further supported by the increase in ³H

activities in the downstream section, as the snowpack consists of “modern” snow. These runoff inputs are likely to originate from urban pipes discharging melted “urban” snowpack directly in the stream due to the input of road salts over the roads close to the stream. Most of these pipes are not visible, covered by snow and ice in winter and no sample could be taken unfortunately.

The application of the mass balance approach to the age-dating tracers (section 3-3-1) requires accounting for these anthropogenic inputs. This was achieved by determining the end-member Cl^- concentration in the “urban” snowmelt contribution, estimated by a binary mixing model of Cl^- and ^3H (Figure 60). The modern ^3H winter precipitation activity was derived from Ottawa GNIP data (period: 2005 to 2020) yielding a value of 14.8 TU. Based on this, the Cl^- concentration in the “urban” snowmelt endmember was estimated at roughly 230 ppm. This value was then used for correcting the “modern” inputs in the mass balance of the age-dating tracers, whose results are presented hereafter.

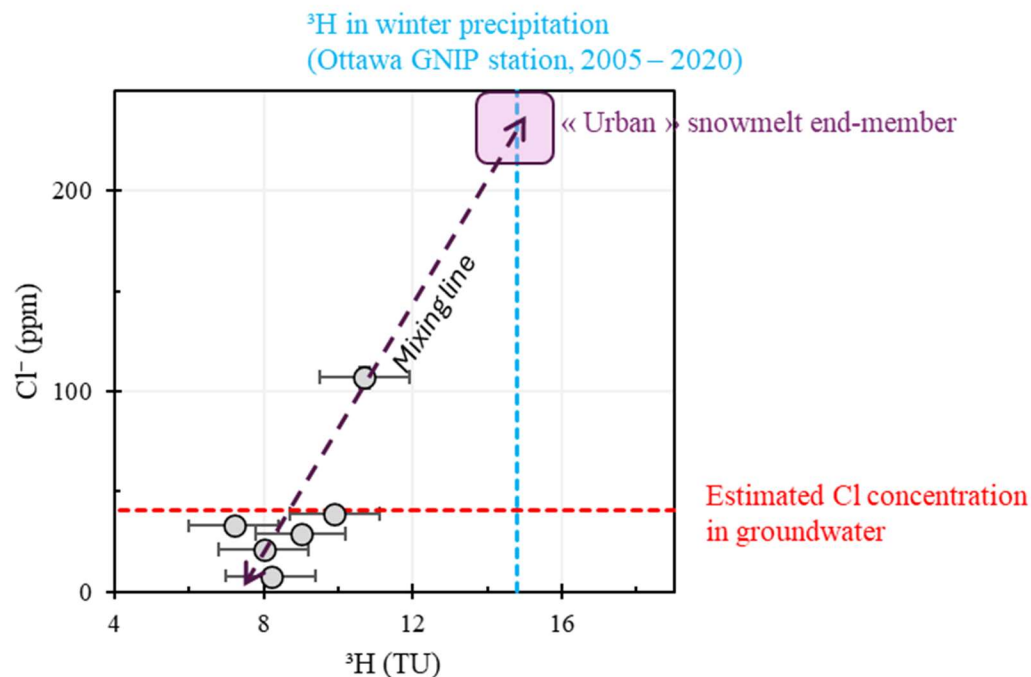


Figure 60: Biplot of chloride and ^3H contents in river water samples. The average winter ^3H activity in precipitation was obtained from the Ottawa GNIP station (2005 – 2020) (blue dashed line). The chloride concentration in groundwater (red dashed line) was estimated from measurements in wells in the catchments.

4.3.4.3 Modelling concentrations of age-dating tracers in groundwater inflows

The results of the modelling of age-dating tracers (^3H , SF_6 , CFC-12 and ^{85}Kr) are presented in Figure 61 below. According to the ^3H and Cl^- results, the river was divided into two sections, an upstream section between SW6 and SW2, where groundwater inflows are dominant ($+ 132 \pm 8$ L/s), and a downstream section between SW2 and SW1 where “urban” snowmelt contribution are dominant (92 % of the discharge difference while groundwater inflows account for 8 %).

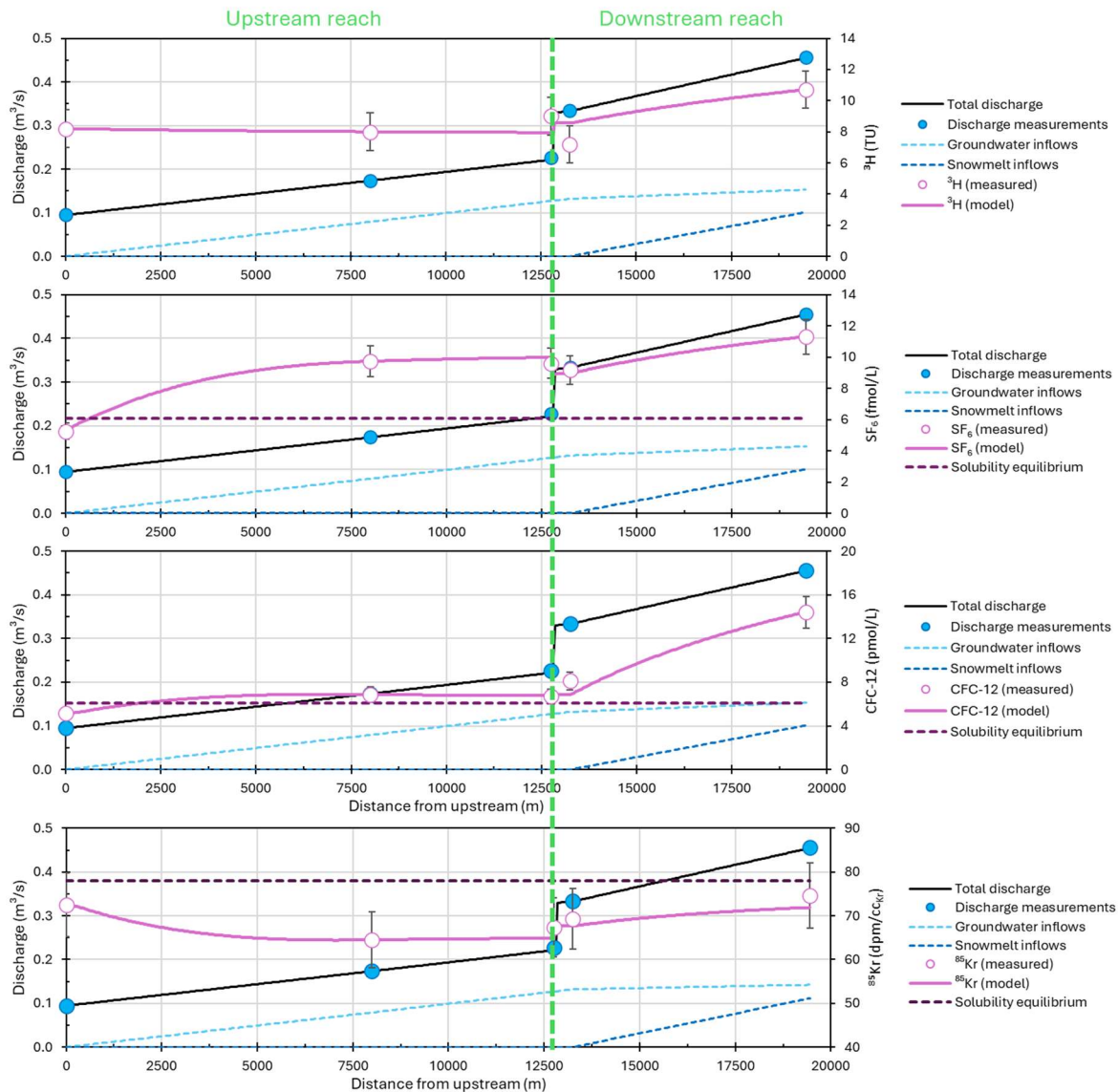


Figure 61: Spatial variation of stream discharge, groundwater inflows, urban snowmelt inflows and measured and modelled age-dating tracers (^3H , SF_6 , CFC-12 and ^{85}Kr). The solubility equilibrium for gases is also represented as dark violet dashed lines.

The discretization of Eq. (2) and Monte-Carlo simulations yielded an activity concentration of 7.8 ± 1.8 TU for ^3H in groundwater inflows. This figure is significantly below what is expected from modern precipitation (10 – 20 TU) but still reveals that a large portion of the groundwater inflows is young (on the order of the dozen of years).

As shown in Figure 61, the $^{85}\text{Kr}/\text{Kr}$ ratios measured in the stream are below that measured in the local atmosphere (78.1 ± 2.5 dpm/cc $_{\text{Kr}}$). This means that the gas in the water is likely not recent and that the ^{85}Kr groundwater signal is at least partially conserved in the stream. The ^{85}Kr activities in groundwater inflows in the downstream section were determined similarly to ^3H , assuming an activity of 78.1 dpm/cc $_{\text{Kr}}$ in the snowmelt inputs. The modelling with Eq. (1) and Monte-Carlo simulations yielded a best fit activity of 44.0 ± 5.5 dpm/cc $_{\text{Kr}}$ in groundwater inflows. This is rather consistent with the ^3H activities modelling, revealing a substantial proportion of sub-modern water in the groundwater inflows.

However, CFCs and SF_6 in water were found in large excess compared to what is expected from solubility equilibrium (see Figure 61 and Table 7 for the groundwater inflows modelling results), with an increasing trend further downstream. The elevated values are thought to be due to local anthropogenic contamination (ex: presence of high voltage electrical equipment, buried fridges, etc.) (Darling et al., 2012; Santella et al., 2008). It completely prevents the use of these tracers for groundwater dating purposes since the magnitude of the local contamination is unknown (Darling et al., 2012).

Table 7: Modelling results of groundwater dating tracers. Monte-Carlo simulations were not performed for CFCs and SF_6 results since these tracers were not used to determine baseflow age information.

Tracer	Modelled groundwater inflows contents	
	Upstream section	Downstream section

SF ₆	17.7 fmol/L	101 fmol/L
CFC-12	11.6 pmol/L	230 pmol/L

4.3.4.4 Transit times of groundwater inflows

Because of the local contamination of CFCs and SF₆, only ³H and ⁸⁵Kr were used for the interpretation of the age of the groundwater inflows. The exponential and dispersion models were used to estimate the MTT of these inflows (Figure 62).

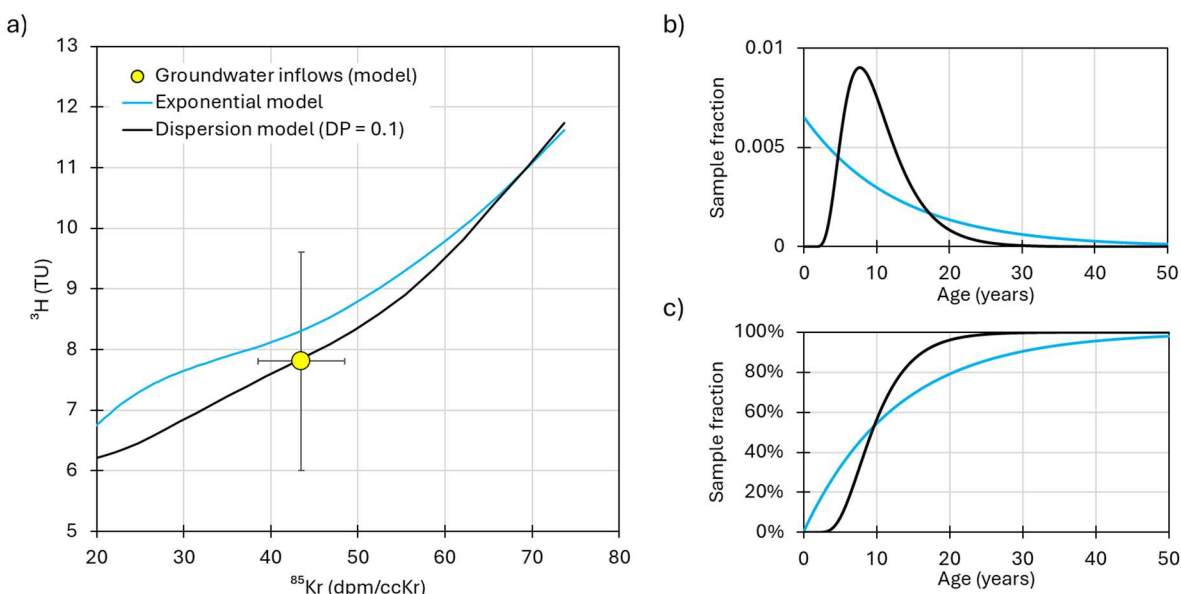


Figure 62: a) Binary plot of ³H and ⁸⁵Kr activities for two different models outputs (exponential and dispersion models) and modelled groundwater inflows, b) transit time distribution, and c) cumulative transit time distribution for the two model outputs.

The dispersion model gives the best results with DP = 0.1 and a MTT of 10.3 years. Accordingly, the exponential model falls close and is best fitted with a MTT of 12.8 years. The uncertainties in MTT were not assessed using Monte-Carlo simulations but can be estimated to be of the order of 3 years from the errors bars in Figure 62 a). The corresponding TTD suggests that the groundwater

inflows have a relatively large range of ages ranging from 3 to 30 years with the dispersion model, and 0 to 50 years with the exponential model.

The average depth of the granular aquifer sustaining the stream is of 15 m, with a porosity of 0.3 (Talbot Poulin et al., 2013). Previous works found annual recharge rates close to 450 mm for the Nelson River catchment (Talbot Poulin et al., 2013; Tremblay et al., 2024). As argued before, on a multi-annual scale, the recharge of the granular aquifer is close to be uniform (exponential model) and the MTT can be calculated as follows (Cook & Herczeg, 2000; Vogel, 1967):

$$MTT = \frac{H\theta}{R} \quad (8)$$

where H is the total thickness of the aquifer [L], R is the recharge rate [LT^{-1}] and θ is the porosity (dimensionless). A MTT of 10 years is found by using $H = 15$ m, $R = 0.45$ m/year and $\theta = 0.3$, which is of the same order of what was found using both exponential and dispersion models for the river baseflow, and the ages found in Murphy et al. (2010). This also suggests that the entire depth of the granular aquifer sustains the stream during winter, and not only just a fraction of it.

4.3.4.5 Vulnerability and resilience of rivers and implications for the management of surface water resources

The response of a river to surface contamination and quantitative and qualitative changes of groundwater can be determined by combining the river baseflow index (BFI) and the mean residence time of the river baseflow (Masse-Dufresne et al., 2021). A river with a high BFI will be less susceptible to be impacted by surface contamination and will be less vulnerable. The baseflow mean residence time can be seen as the mean flushing time of the aquifer compartment sustaining a river. It controls the resilience of the system as a higher mean flushing time is linked to a long time for returning to initial groundwater conditions, in the case of groundwater quantity and/or quality changes. These two metrics are combined in Figure 63. The latter can be separated into four zones which are defined based on river BFI and river baseflow mean residence time. Indeed, rivers vulnerability to surface contamination is high when the BFI value is less than 0.5 (*i.e.* for runoff dominated systems) (zones (3) and (4) in Figure 63). The resilience of the river to

groundwater changes is lower when the baseflow mean residence time is “low”. Here, a threshold of 5 years was chosen, as groundwater younger than 5 years remains influenced by meteorological conditions and short-term climatic variations (Arnoux, Barbecot, Gibert-Brunet, Gibson, Rosa, et al., 2017). This suggests that the rivers that are the less vulnerable to surface contamination and the more resilient to changes in groundwater quantity and/or quality are the ones in zone (2) of Figure 63, *i.e.* the rivers having the highest BFI values with the lowest baseflow mean residence times.

In the case of Eastern Canada, rivers are expected to be baseflow-dominated ($BFI > 0.5$) (Beck et al., 2013; Xie et al., 2024). The oldest groundwater ages are expected to be found in winter, after a few months of low flow conditions under freezing conditions (Picard, Barbecot, Proulx, et al., 2024). The rivers in the region are thus expected to plot in zones (1) and (2), depending on factors controlling the baseflow mean residence time such as rock formations, recharge rates and aquifer thickness. In the specific case of the Nelson River, the mean residence time of the baseflow is close to 10 years, which is linked to a relatively low resilience since it takes up to 30 years to completely flush the aquifer compartment sustaining the stream (Figure 63). The BFI value of the river was determined following Duncan’s method (Duncan, 2019) and is described in the Appendix B section. Its value is 0.77, meaning that the river vulnerability to surface contamination is relatively low.

This tool can be very useful for the integrated management of water resources as it can serve as a guide to map and classify the vulnerable and resilient catchments for drinking water production, or the planning of urban development.

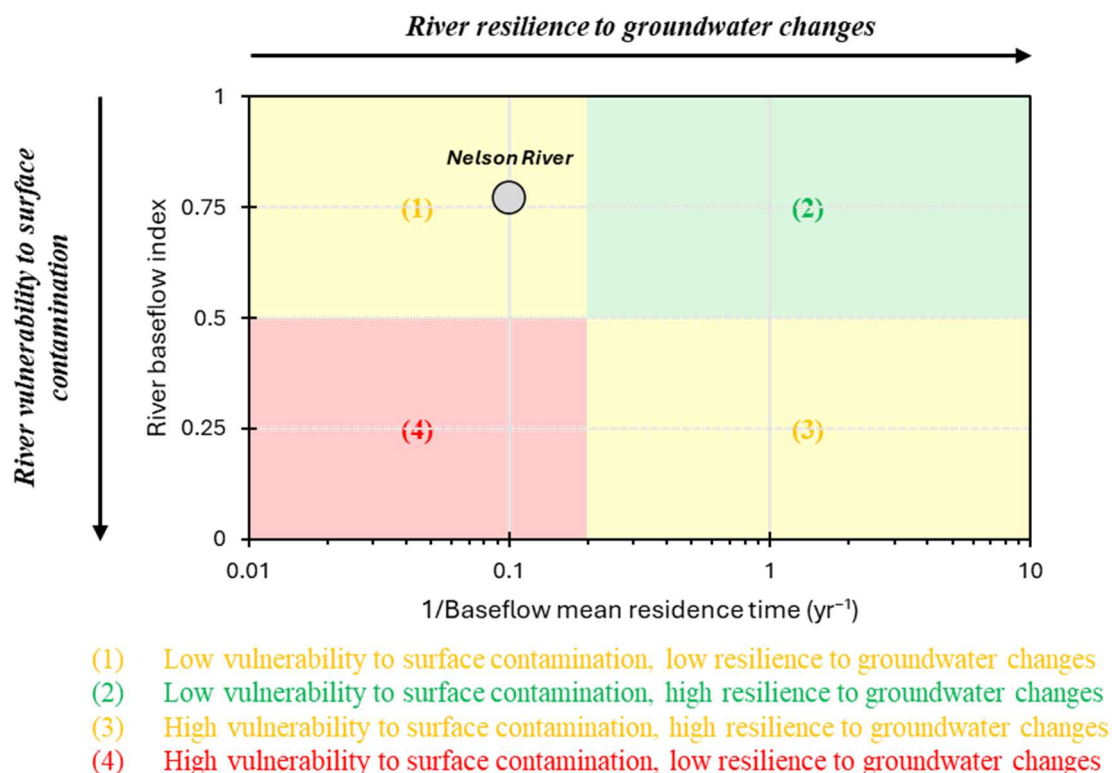


Figure 63: Grid for assessing the resilience and vulnerability of rivers as functions of baseflow mean residence time and river baseflow index respectively. The grey dot represents the long-term BFI value (0.77) with the baseflow mean residence time (10 years).

4.3.5 Conclusions

A unique combination of age-dating tracers (⁸⁵Kr, and ³H) and deliberated inert gases injection (He, SF₆) was adopted in this study to determine age information of the groundwater sustaining the Nelson river, in Québec, Eastern Canada. The specific field conditions in winter (prolonged low flow period, cold water temperature and partial ice cover over the rivers) greatly helped the application of the (gaseous) tracers mass balance to derive baseflow age information via inverse modelling. While the application of anthropic trace gases SF₆ and CFCs was not possible due to a local contamination of the aquifer, tritium and radiokrypton activities were successfully used to determine the MTT of the groundwater inflows. ³H is well suited for tracing water movement as it is an integral part of the water molecule and remains unaffected by gas exchanges with the atmosphere. While ⁸⁵Kr is more challenging to apply, it offers key advantages: it is insensitive to

local anthropogenic contamination and degassing. Gas exchange with atmospheric air can be modelled and occurs relatively slowly due to the low diffusion coefficient of krypton in water. The combination of ^3H and ^{85}Kr is particularly robust, leveraging these complementary properties for reliable groundwater dating. A dispersion model with a dispersion parameter of 0.1 and MTT of 10 years provided the best fit to the data, meaning that the groundwater inflows encompass a broad range of ages between 3 to 30 years.

The tool developed here can be used for the mapping of vulnerable catchments which has serious implications for the management of surface waters at the catchment scale, particularly in areas used for drinking water production. Indeed, the age data suggest that the studied river resilience to groundwater quality and/or quantity change is relatively low (MTT = 10 years), while its vulnerability to surface contamination is also relatively low (BFI = 0.77). It is highly beneficial to the water resources managers as it can be used to adapt contaminant mitigation measures, prioritizing the protection of the recharge areas (ex: managed aquifer recharge) and anticipate and adapt to the effects of urbanisation and global change.

Despite the challenging field conditions, the Canadian winter offers a unique opportunity to apply such methods for several reasons (i) most rivers are baseflow dominated, especially in the Eastern part of the country, (ii) the winter low flow period provides an optimal time to study the oldest fraction of the aquifer sustaining the stream since no recharge occurs for a few months and (iii) the presence of an ice cover scientifically reduces air/water exchanges and thus the loss of the groundwater signal. This method is very promising for the management of water and catchments in Eastern Canada.

4.3.6 Appendices

4.3.6.1 Appendix A: ^3H in precipitation and recharge seasonality

^3H activities in precipitation exhibit a seasonality that needs to be considered and compared to the seasonal recharge pattern (Morgenstern et al., 2010; Solomon & Gilmore, 2024; Visser et al., 2019). The tracer-based hydrograph separation of the Saint-Charles River, already described in

(Picard, Barbecot, Proulx, et al., 2024), can be used to estimate the relative contribution to groundwater recharge at a monthly timestep. The Nelson river is one of the main tributaries to the Saint-Charles river and both rivers share similar catchments characteristics (soils, climate, geology). It is assumed that the results for the whole Saint-Charles river catchment are applicable to the Nelson river sub-catchment.

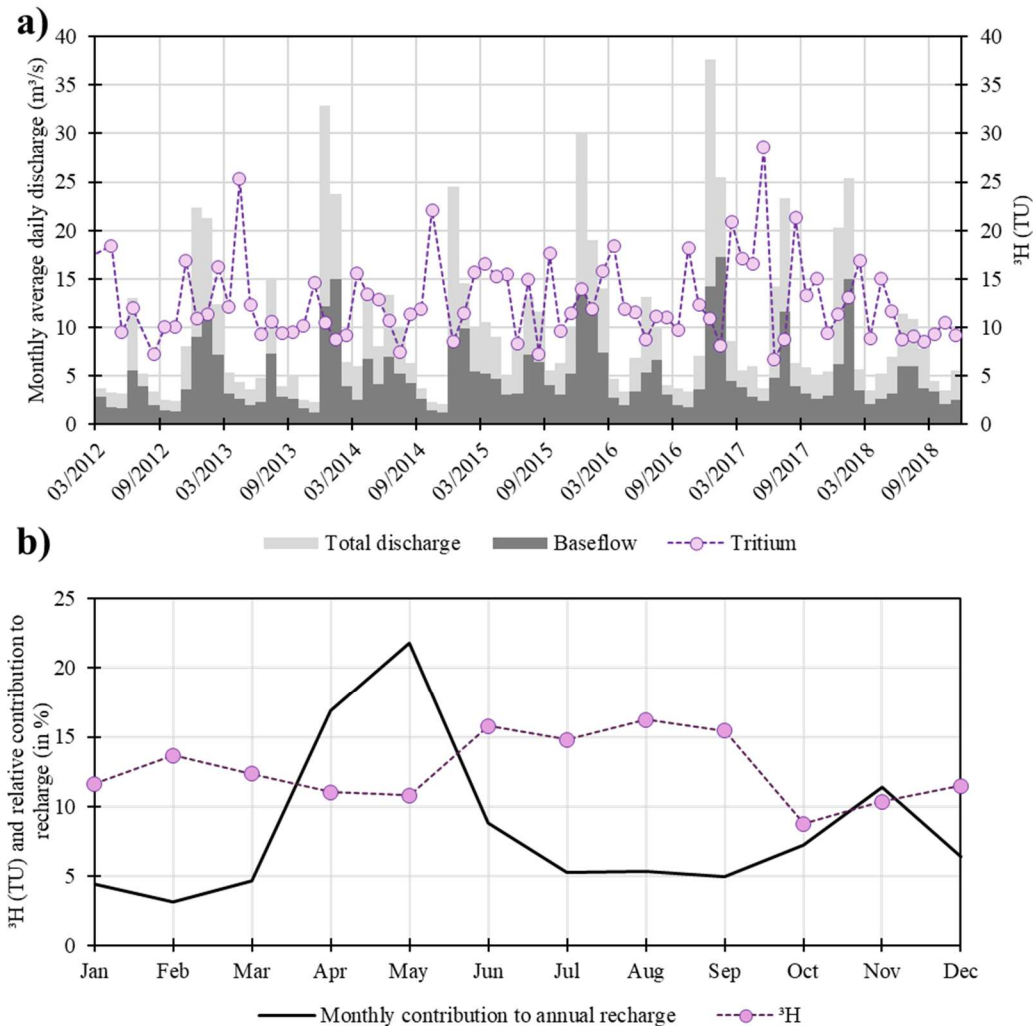


Figure 64: a) Monthly variations of total discharge, baseflow from Picard, Barbecot, Proulx, et al. (2024) and ^3H activities in precipitation (GNIP station from Ottawa) between 2012 and 2019 and b) average values for each month for recharge (estimated from baseflow values) and precipitation ^3H activities.

The annual average ^3H activity in precipitation between 2012 and 2019 is 12.7 TU. The ^3H signal exhibits a marked seasonality (Figure 64 b)) with the highest activities measured during the summer (June to September with values higher than 15 TU)) and the lowest activities measured in Autumn (October to December with values close to 10 TU). The winter period is marked by relatively high values (10 to 15 TU).

The recharge rates were estimated from baseflow data according to the following formula:

$$R_i = \frac{V_{bf,i}}{S} \quad (A1)$$

where R_i is the recharge rate for the month i , $V_{bf,i}$ is the volume of baseflow for the month i and S is the catchment area.

One of the particularities of the catchment is the presence of snowpack that builds up under freezing conditions during winter from January to April. This is why the recharge rates in January, February and March are low (less than 5 % of the total annual recharge). The melting of the snowpack during April and May is responsible for the very high recharge rates during this period, accounting for roughly 40 % of the total annual recharge.

Snowfall and snowmelt is considered to be absent or negligible from June to December. During this period, the “corrected” ^3H input can be calculated as follows (Morgenstern et al., 2010):

$${}^3H_{corr} = \frac{\sum_{i=6}^{12} {}^3H_i R_i}{\sum_{i=6}^{12} R_i} \quad (A2)$$

where ${}^3H_{corr}$ is the “corrected” ^3H input of the year j (j varies between 2013 and 2019) for the months between June to December (both included). The following formulas were adopted for April and May:

$$\begin{cases} {}^3H_{corr, Apr} = \frac{R_{Apr}}{\sum_{i=1}^{12} R_i} \frac{\sum_{i=1}^4 {}^3H_i}{4} \\ {}^3H_{corr, May} = \frac{R_{May}}{\sum_{i=1}^{12} R_i} \frac{\sum_{i=1}^5 {}^3H_i}{5} \end{cases} \quad (A3)$$

where R_{Apr} and R_{May} are the recharge amounts in April and May respectively, $\sum_{i=1}^{12} R_i$ is the total annual recharge amount and $\frac{\sum_{i=1}^4 {}^3H_i}{4}$ and $\frac{\sum_{i=1}^5 {}^3H_i}{5}$ are the average 3H activities between January and April and January and May respectively. The Eq. (A3) is a simple way to take into account the high contribution of snowmelt to recharge with the appropriate 3H activities from winter precipitation. It considers that any precipitation event between January to April (or May) contributes equally to groundwater recharge.

A comparison of the annual 3H activities in precipitation and the corrected values is shown in Figure 65. It shows that there is an excellent agreement between the raw data and the corrected values, indicating that taking into account the recharge pattern to correct the tracer input function has little to no effect. The study of (Morgenstern et al., 2010) reported the same conclusions in a small catchment in the Southern Hemisphere. Only one year (2017) plots far from the $y = x$ curve, with a much lower corrected value than what was measured. This is explained by the relatively low 3H activities during the preferential recharge periods (Spring and Autumn 2017) compared to other years. This might have an effect over groundwater dating applications for water having a very short transit times (months) but is likely to be negligible for longer transit times.

This method, yet very simple, has the advantage of being integrative of the whole catchment. This is an important advantage compared to simpler water budgets methods, that would not be adapted to the catchment physiography. For example, snowpack tends to accumulate longer in the northern (colder) parts of the catchment as well as in the north facing slopes, which delays the recharge from snowmelt.

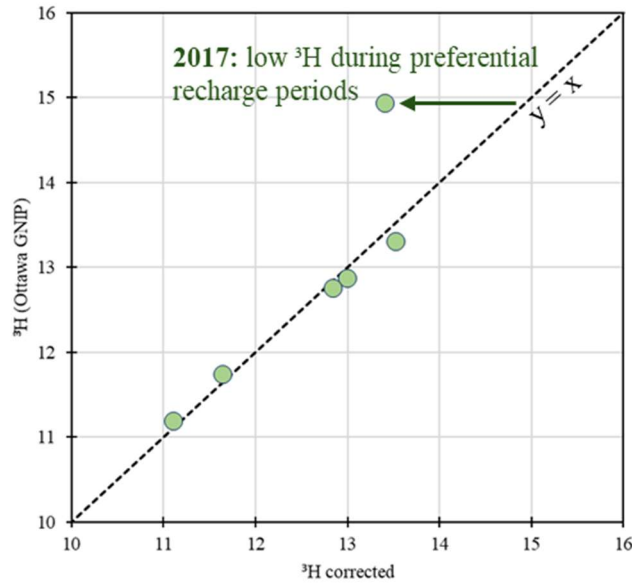


Figure 65: Comparison of the corrected (taking into account the recharge pattern) and measured annual average ^3H activities in precipitation at Ottawa.

4.3.6.2 Appendix B: Hydrograph separation of the Nelson River

The hydrograph separation method proposed by (Duncan, 2019) has been used with the Nelson River discharge data to determine the baseflow index (BFI) value of the river, between 2013 and 2024. The streamflow daily data comes from the station n°050915 operated by Québec's government (MELCCFP). The station is located at the point SW2 (Figure 66).

The application of Duncan's method (Duncan, 2019) is simple and requires only discharge data and the examination of the recession constant parameter. The latter was determined by plotting the measured discharge at the day "j+1" as a function of the discharge the previous day "j" during the recession periods (Rimmer & Hartmann, 2014). The coefficient of the regression slope gives the value of the recession parameter. In the specific case of the Nelson River, it was determined to be 0.9484, using recession periods data for the period 2013 – 2024. This value was then used in the procedure given by (Duncan, 2019), which yields a BFI value of 0.77 for the period 2013 – 2024.

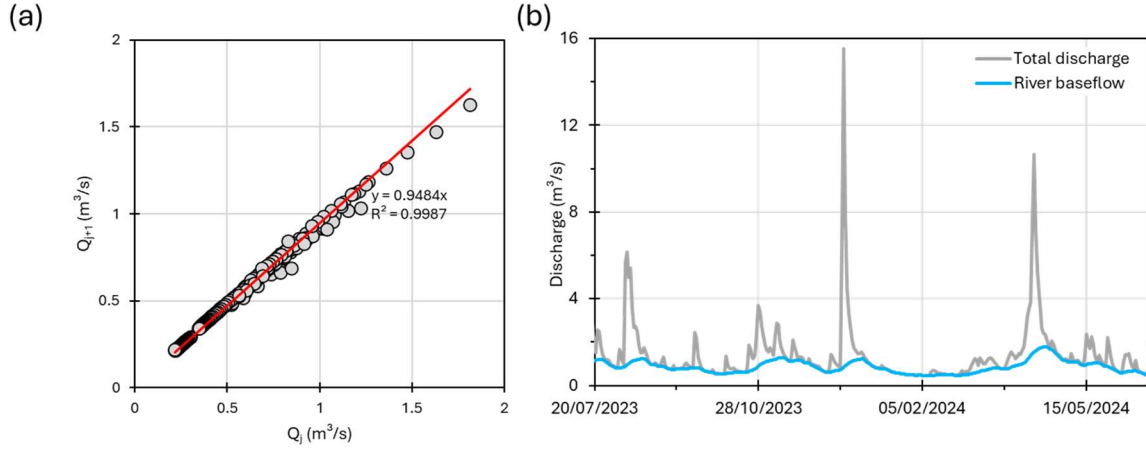


Figure 66: (a) Determination of the recession parameter of the Nelson River. (b) Baseflow separation of the Nelson River (BFI = 0.77).

4.4 Conclusion of Chapter 4

The work presented through Chapter 4 (and *Article 4*) aims to answer to the final part of the research problematic of this Ph.D. thesis, *i.e.* the determination of the baseflow transit time, in one of the baseflow-dominated rivers of the studied catchment. To decipher baseflow age information is a complicated task, because of the loss of the groundwater signal due to the inevitable air/water exchanges in rivers (Jensen et al., 2022; Solomon et al., 2015). The originality of this work lies in (i) the unique combination of age-dating tracers (CFCs, SF_6 , ^3H , ^{85}Kr) and deliberate release of inert gases ($\text{He} + \text{SF}_6$), and (ii) taking advantage of the tough Canadian winter field conditions that help to reduce air/water exchanges.

The dual release of He and SF_6 in the stream was performed by using a very efficient diffusive system. Its application was facilitated by the onsite measurements of He with the miniRUEDI. The presence of a partial ice cover helped to follow the He plume more than 5 km downstream the injection point, over the course of 12 hours. SF_6 was detected up to 12 km downstream the injection point, 24 hours after the injection started. The experiment helped to show that the air/water exchanges are limited, compared to other studies conducted in completely open rivers.

The Nelson river sub-catchment was chosen as it is the most adapted to the application of the tracer mass balance approach in the study site for various reasons:

- A thick granular aquifer (average depth 15 m, maximum depth 40 m) sustains the stream all year round. Murphy et al. (2010) investigated the age stratification of the groundwater and came up with maximum ages of 40 years old
- The average river gradient is low, which limits the presents of falls where the gaseous tracers signals can be reset. This is not the case in other mountainous streams of the catchment (ex: des Hurons River, Jaune River)
- The access to the Nelson River is easy thanks to bridges, even though the urbanisation complicated the residence time tracers interpretation (road salts application and CFCs and SF₆ contamination)

Fortunately, the combination of ³H and ⁸⁵Kr was successful and the groundwater inflows TTD was best-fitted to a dispersion model (DP = 0.1), with a MTT of 10 years. This suggests that the portion of the aquifer sustaining the river has a relatively large range of ages between 3 to 30 years. Groundwater contamination is quickly translated to the river, in under 5 years, and takes up to 30 years to be completely flushed. This further suggests that the whole thickness of the aquifer sustains the river, in winter *i.e.* under “dry” conditions.

This work, in conjunction with the work presented in Chapter 3, has serious implications for the management of the water resources, in the context of the production of drinking water from rivers. It is demonstrated through this PhD work that the rivers of the catchment are largely baseflow dominated and that the latter is very vulnerable to surface changes, at least for the Nelson River, one of the main tributaries of the Saint-Charles River. The planification of future urbanisation should be carefully done in this already impacted catchment and should minimize the risk of groundwater contamination for the preservation of the surface waters quality.

CHAPTER 5 Conclusions

5.1 Conclusions en français

L'objectif principal de ce doctorat était la mise en place de nouveaux outils permettant d'appréhender la vulnérabilité des ressources en eau de surface soumises à de multiples forçages anthropiques, en particulier dans les bassins versants vulnérables utilisés pour produire de l'eau potable. La vulnérabilité de ces rivières pérennes peut être approchée par deux paramètres, l'indice de débit de base (*i.e.* la fraction d'eaux souterraines à long-terme) et la distribution de temps de résidence dans la nappe des apports d'eau souterraine. Caractériser les interactions nappe/rivière a été au cœur du projet et a nécessité de répondre aux questions de recherche suivantes :

- (i) Comment améliorer les méthodes existantes basées sur l'utilisation de traceurs pour caractériser et quantifier les interactions entre eaux souterraines et eaux de surface ?
- (ii) Comment estimer avec précision les apports d'eau souterraine à une rivière dans le temps ?
- (iii) Comment déterminer le temps de résidence du débit de base des rivières et faire le lien avec la vulnérabilité et la résilience de la ressource en eau de surface ?

Il a été possible de répondre à ces trois questions de recherche en étudiant le bassin versant de la prise d'eau potable de la rivière Saint-Charles, dans un contexte où le travail de l'hydrogéologue-géochimiste est complexifié par l'urbanisation partielle du bassin versant, sa taille (344 km²) et le blocage partiel du cycle de l'eau au cours de l'hiver canadien. Ce chapitre de conclusions comporte deux parties : la première (5.1.1) rapporte les principales contributions scientifiques de la thèse, et la deuxième (5.1.2) les perspectives que cela ouvre pour une meilleure compréhension et gestion des ressources en eau.

5.1.1 Principales contributions

Le développement de deux méthodes est présenté dans le Chapitre 2 de ce doctorat, sous la forme de deux articles de recherche. L'*Article 1* démontre que des injections de solutions enrichies en isotopes stables (^2H et ^{37}Cl) peuvent être utilisées comme traceurs quantitatifs pour simultanément (i) mesurer le débit de petits cours d'eau avec une grande précision ($< 1\%$ de la valeur mesurée), (ii) estimer les contributions relatives des composantes « rapide » et « lente » de l'écoulement de surface, avec (iii) un impact fortement limité sur l'environnement par rapport à d'autres techniques de traçage. Cela ouvre de nouvelles perspectives pour la mesure du débit des rivières dans les bassins versants vulnérables et/ou sous toutes conditions hydrologiques. En effet, les conditions d'écoulement laminaire attendues pour l'utilisation des méthodes par mesures des vitesses sont rarement atteintes dans les faits, ce qui se traduit par de grandes incertitudes qui ne sont pas toujours bien évaluées lors de ces mesures conventionnelles.

Les gaz dissous (et en particulier les gaz rares) sont d'excellents traceurs des processus hydrogéologiques (ex : interaction nappe/rivière) et sont très utiles pour la datation des eaux. Leur utilisation est limitée du fait de difficultés techniques dans les procédures d'échantillonnage et des coûts et technicités analytiques. L'*Article 2* montre une rupture technologique originale en combinant des échantillonneurs passifs de gaz dissous, la spectrométrie de masse pour les gaz rares et de chromatographie en phase gazeuse pour les gaz anthropiques traces. Il est alors possible d'obtenir des échantillons représentatifs du milieu naturel tout en simplifiant les procédures d'analyse, en particulier pour les gaz rares. Nous avons pu montrer que le miniRUEDI peut également être utilisé comme un outil analytique fiable, sur le terrain comme en laboratoire permettant de déterminer les concentrations en gaz rares dissous à bas coût, en continu et à haute précision. Ces travaux sont également importants pour le développement d'expérience de traçage artificiel à grande échelle avec des gaz avec une résolution spatiale très fine (à la fois verticalement et latéralement), réduisant les efforts tout en accroissant la capacité d'investigation des processus in situ.

Les apports d'eaux souterraines à la rivière Saint-Charles ont été tracés et calculés de 2013 à 2023 à l'aide du suivi de la qualité de l'eau brute réalisé par la Ville de Québec. Cette décomposition de l'hydrogramme originale se base sur l'identification des pôles contrôlant la qualité de l'eau (ruissellement, eaux souterraines et fonte de neige contaminée par les sels de route) et peut servir d'outil de calibration pour une décomposition continue de l'hydrogramme à l'aide d'un modèle mathématique (ex : filtre d'Eckhardt). Ces données mettent en lumière le contrôle exercé par la part d'eaux souterraines sur la disponibilité et la qualité de l'eau de rivière. Le suivi des ions majeurs, de la silice dissoute et des isotopes stables de la molécule d'eau à l'exutoire du bassin versant de la prise d'eau de la rivière Saint-Charles indique que les eaux souterraines sont le principal contributeur en rivière, tant à l'échelle mensuelle qu'à l'échelle annuelle, entre 2013 et 2023 (*Article 3*). Le débit de base domine l'écoulement de surface pendant plus des 70 % des jours de l'année (incluant la période de fonte au printemps), bien que le bassin versant soit urbanisé. La fraction d'eau souterraine est généralement maximale en hiver où elle atteint plus de 90 % du débit total. Ce n'est que peu de temps après les événements pluvieux intenses que la composante de ruissellement semble pouvoir dépasser la composante du débit de base. Les périodes où la fraction d'eau souterraine est élevée sont marquées par une minéralisation totale plus importante, en particulier des teneurs élevées en alcalinité, calcium et magnésium. Certains métaux traces sont principalement apportés par la composante de ruissellement, par exemple le zinc, l'aluminium et le plomb. Le couple sodium + chlorures présente des teneurs élevées au début de la période de fonte du manteau neigeux, généralement au mois de mars. Cependant, leur concentration en étiage augmente d'année en année, ce qui indique que la partie de l'aquifère qui alimente la rivière Saint-Charles est déjà largement contaminée par l'application de sels de déglacage des routes. Les différences de comportements chimiques des traceurs permettent de discuter de la dynamique des écoulements dans le bassin.

L'alcalinité est un excellent indicateur de la fraction d'eau souterraine en rivière, car ce traceur est principalement hérité des fortes pressions partielles de CO_2 que l'on retrouve dans la zone non saturée. Les cinétiques de mise en solution du CO_2 sont extrêmement rapides, et la recharge même récente peut se trouver à l'équilibre en quelques heures. D'autres traceurs comme la silice dissoute

seront plus marqués par le temps de résidence des eaux de recharge dans l'aquifère. La dynamique temporelle des teneurs en silice dissoute montre que le temps de résidence de l'eau dans le bassin versant, c'est-à-dire le temps écoulé entre l'arrivée de l'eau sous forme de précipitations et son départ via la rivière, est variable et fortement influencé, d'abord par la saisonnalité, puis par les conditions météorologiques (ex : orages en été). Les temps de résidence les plus courts ont été constatés pendant les périodes de fort débit, lorsque les teneurs de silice dissoute sont les plus faibles, tandis que les temps de résidence les plus longs sont observés pendant les périodes de faible débit lorsque les teneurs de silice sont les plus élevées. Les âges les plus anciens sont attendus en hiver, en raison de la période d'étiage hivernal généralement longue (> 2 à 3 mois) pendant laquelle l'aquifère est drainé par la rivière. Pendant cette période, les eaux souterraines qui alimentent le cours d'eau ne sont pas affectées par la saisonnalité. Les très faibles teneurs en silice dissoute au printemps, après la période de fonte des neiges, indiquent que les eaux souterraines nouvellement rechargées alimentent préférentiellement le cours d'eau et sont donc rapidement évacuées du bassin versant.

La Figure 67 illustre le comportement des traceurs géochimiques utilisés en fonction du temps passé dans le bassin versant, et la manière dont ils peuvent être utilisés pour déchiffrer les informations d'âge de l'eau en rivière.

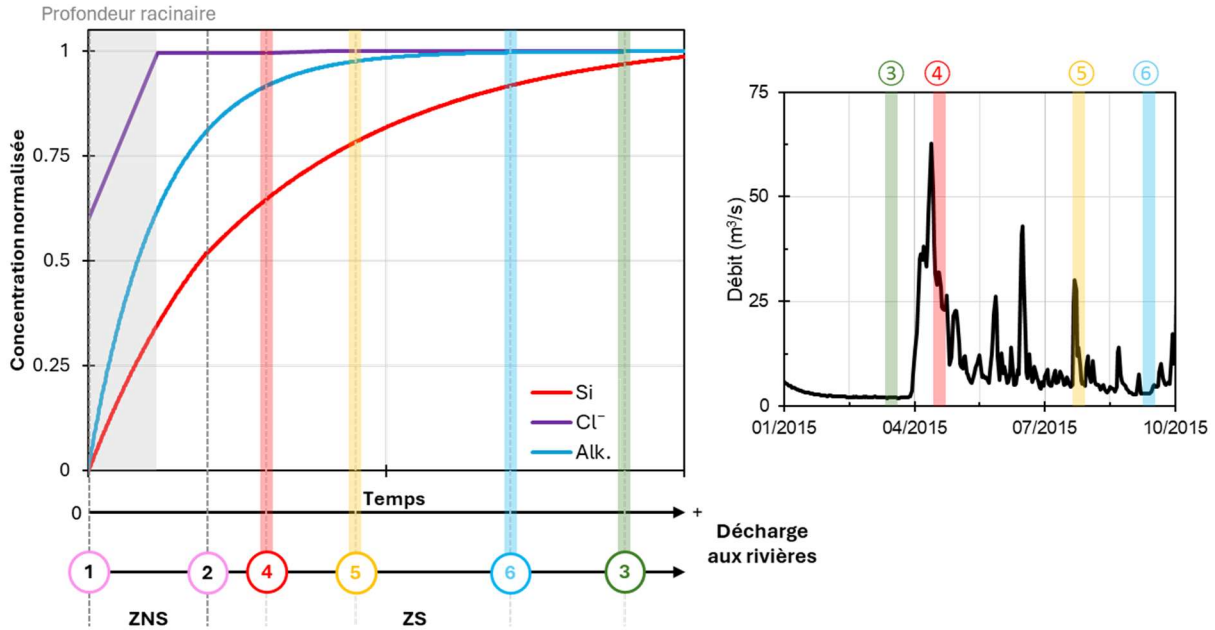


Figure 67: Modèle conceptuel de l'évolution de la signature géochimique de certains traceurs – silice dissoute, chlorures et alcalinité – en fonction du temps de résidence de l'eau, depuis les précipitations ①, passage dans la zone non saturée (ZNS), la zone saturée (ZS) jusqu'à la décharge dans les rivières du bassin-versant (③, ④, ⑤, ⑥). Le temps passé par l'eau souterraine dans l'aquifère avant d'alimenter les rivières varie en fonction des conditions météorologiques (hautes eaux/basses eaux) comme l'indique l'hydrographe à gauche et la position des points ③, ④, ⑤, ⑥ sur l'axe des abscisses.

La Figure 68 illustre quant à elle quelle partie de l'aquifère alimente préférentiellement les cours d'eau en fonction de la saison et est basée sur les informations données par le couplage alcalinité – silice dissoute.

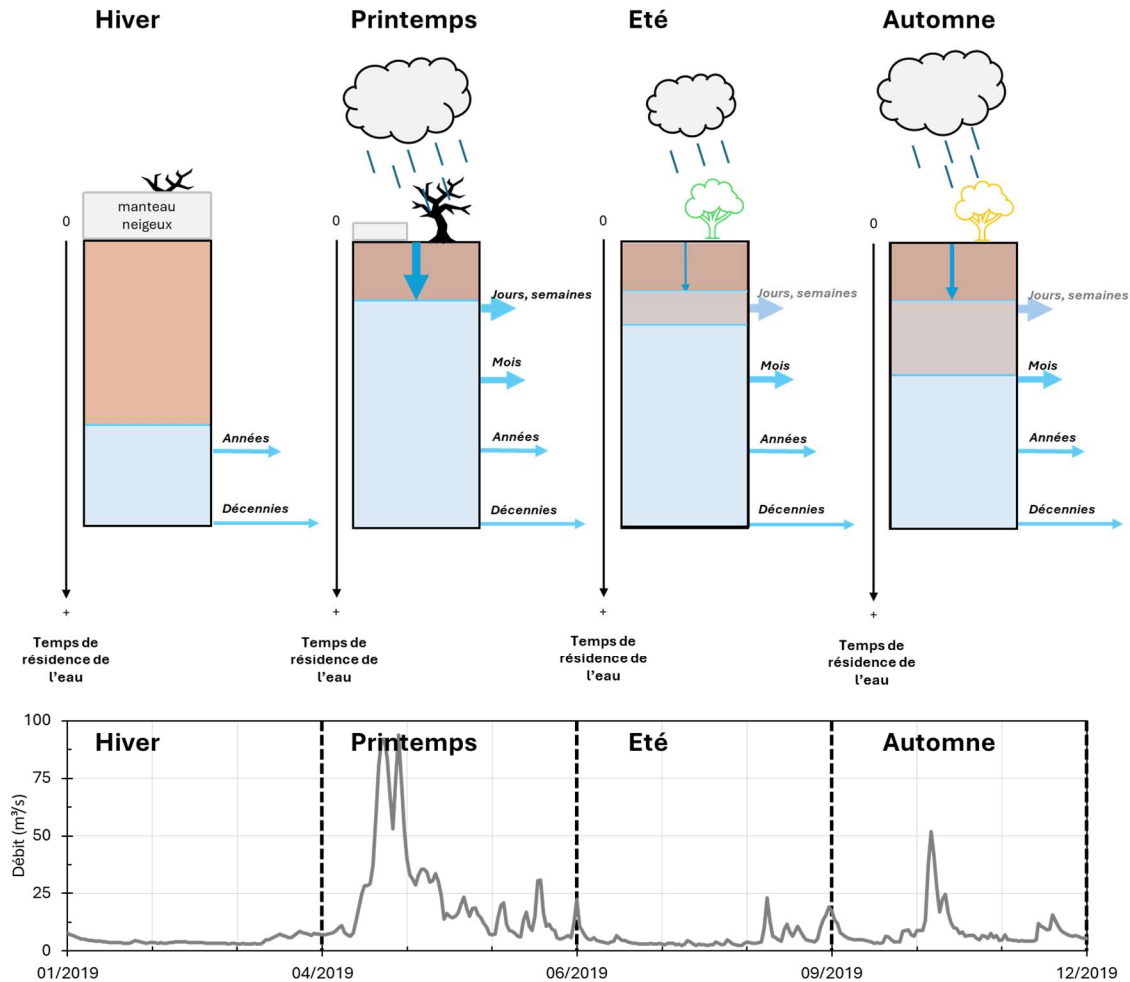


Figure 68: Alimentation des cours d'eau par différents compartiments aquifères pour les quatre saisons avec hydrogramme type (rivière Saint-Charles, année 2019). Dans ce modèle en colonne, le temps de résidence de l'eau souterraine dans l'aquifère augmente avec la profondeur. La taille des flèches représente les flux relatifs au cours d'eau. Une couleur bleu ciel pâle est utilisée pour l'eau souterraine aux temps de transit les plus courts en été et automne, associée aux épisodes de recharge ponctuels (orages, pluies). Les flux les plus faibles sont attribués au compartiment aquifère insensible à la saisonnalité naturelle dans les patterns de recharge (figure inspirée de Harman (2015)).

Le temps de séjour des apports souterrains, avant qu'ils ne soutiennent les rivières, a été investigué en détail sur le sous-bassin versant de la rivière Nelson qui est l'un des principaux affluents de la rivière Saint-Charles. Le propriété d'âge (*Article 4*) a pu être reliée à la fraction d'eau souterraine dans la rivière (*Article 3*) à l'aide d'une combinaison unique de traceurs de datation (^3H , ^{85}Kr) et le recours à des techniques de traçage artificiel (injections de gaz inertes). Les conditions hivernales de l'Est du Canada ne permettent pas d'avoir une quantification précise des

débits avec des méthodes traditionnelles, mais elles facilitent l'utilisation de méthodes géochimiques puisque la couverture de glace empêche une partie, voire la plupart, des échanges gazeux entre l'atmosphère et la rivière. Nous avons pu quantifier ces échanges par l'injection simultanée de SF₆ et d'He. Pour la première fois dans une rivière, le ³H et le ⁸⁵Kr (*Article 4*) ont été utilisés simultanément comme traceurs de datation des eaux souterraines récentes. Le temps de séjour moyen des eaux souterraines soutenant le débit de la rivière est de 10 ans (déterminé avec un modèle de dispersion). La distribution d'âge correspondante couvre des âges allant jusqu'à 30 ans. Cela signifie que toute contamination des eaux souterraines pourrait affecter la qualité du débit de base pendant des décennies. Pour les gestionnaires de la ressource, cela se traduit par une résilience du compartiment aquifère alimentant les rivières relativement faible.

En considérant les apports d'eau souterraine et notamment la vulnérabilité des rivières aux contaminations de surface et à leur résilience face aux changements de qualité et de quantité des eaux souterraines qui les soutiennent, les Chapitres 3 et 4 (*Article 3* et *Article 4*) fournissent de nouveaux outils pour la protection des ressources en eau de surface. La vulnérabilité des rivières aux contaminations de surface peut être approchée par l'indice de débit de base, puisqu'il tient compte des contributions relatives d'eau souterraine et de ruissellement en rivière. La résilience des rivières face aux changements qualitatifs et quantitatifs des eaux souterraines est, quant à elle, approchée par le temps de renouvellement des aquifères qui les soutiennent (*i.e.* le temps de résidence du débit de base). Ce dernier rend compte du temps nécessaire pour retourner à l'état initial après une perturbation (ex : contamination) des eaux souterraines. La relation entre ces deux paramètres est représentée dans la Figure 69. Un type de représentation semblable a par le passé fait l'objet de publications dans le cas de lacs dominés par les apports souterrains (Arnoux, Barbecot, Gibert-Brunet, Gibson, Rosa, et al., 2017; Masse-Dufresne et al., 2021). La Figure 69 est séparée arbitrairement en quatre secteurs de façon à discriminer théoriquement des rivières plus ou moins vulnérables aux contaminations de surface ou plus ou moins résilientes face aux forçages anthropiques. Sous ces conditions, la rivière Nelson peut être considérée comme peu vulnérable aux contaminations de surface (indice de débit de base élevé) mais en même temps peu résiliente face aux changements de qualité et quantité des eaux souterraines (temps de séjour

du débit de base relativement important). L'une des préconisations pour la Ville de Québec afin de protéger la source d'eau potable serait de mettre en place des mesures pour « déplacer » le point représentatif de la Nelson vers la zone (2) du graphique. Cela correspond à trouver des mesures, telles que de la recharge aménagée des aquifères, pour diminuer le temps de renouvellement des aquifères alimentant les rivières.

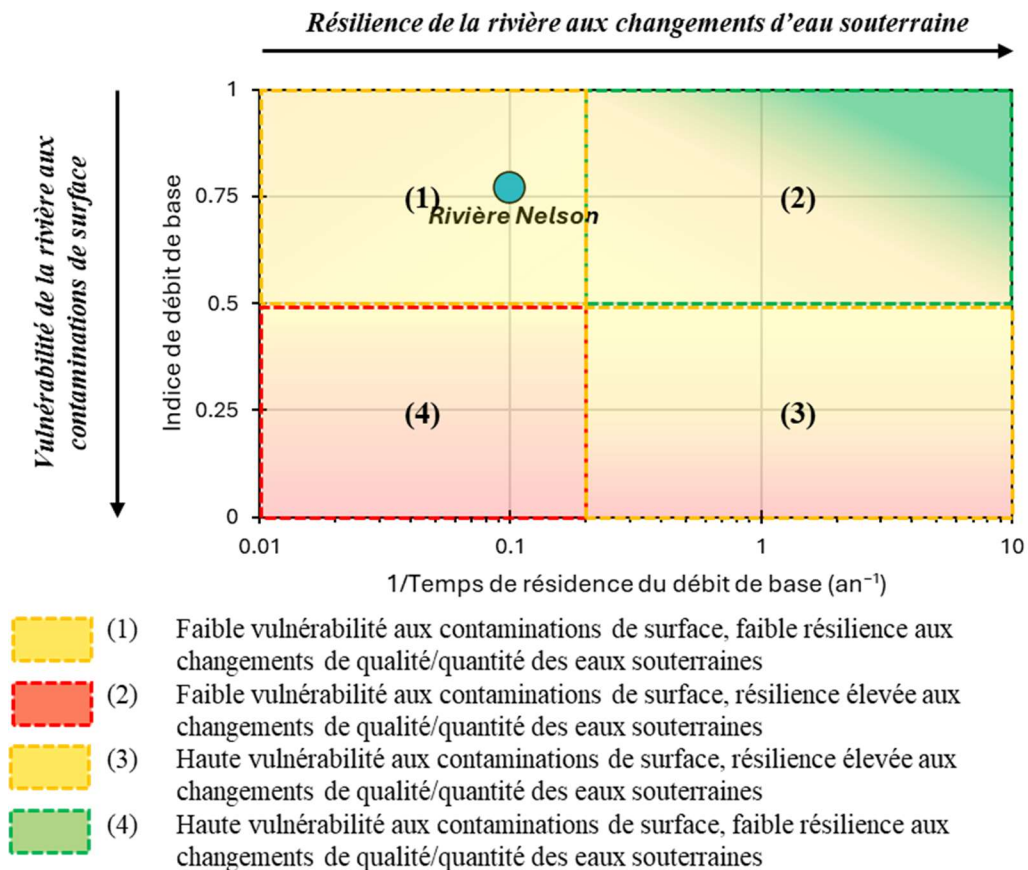


Figure 69: Diagramme de la résilience des rivières face aux changements de qualité/quantité dans les eaux souterraines (décrite par le temps de résidence du débit de base) et de la vulnérabilité des rivières face aux contaminations de surface (décrite par l'indice de débit de base).

De manière générale, ce travail de doctorat contribue à démontrer et quantifier le rôle fondamental joué par les eaux souterraines dans le cycle de l'eau, puisqu'elles contrôlent à la fois la disponibilité et la qualité des ressources en eau de surface. Pour cela nous avons réussi à développer une méthode scientifique qui s'appuie sur les quatre étapes suivantes :

- (i) Mesurer le débit de petits cours d'eau avec une grande précision (< 1% de la valeur mesurée) et un impact sur l'environnement très limité
- (ii) Quantifier les contributions relatives du ruissellement et des eaux souterraines à l'écoulement de surface
- (iii) Décrire l'origine et la dynamique des différentes réponses hydrochimiques du bassin versant
- (iv) Quantifier le temps de résidence des eaux de rivières, déterminer la résilience du bassin versant et discuter de la saisonnalité de ces paramètres.

Cela a de sérieuses implications pour la gestion des ressources en eau, en particulier dans le contexte de production d'eau potable et ouvre de nouvelles perspectives pour l'applications de méthodologies basées sur l'utilisation des traceurs environnementaux dans ce contexte. Cette recherche démontre en outre qu'il est nécessaire de considérer les relations nappe/rivière pour l'étude de la vulnérabilité des bassins versants, et des prises d'eau potable de surface.

5.1.2 Perspectives de recherche

- *Applicabilité de la méthode à d'autres bassins versants dans l'Est du Canada*

La méthode de description de la vulnérabilité et de la résilience des bassins versants s'appuie sur la séparation d'hydrogramme (calcul de la part d'eau souterraine) et de la détermination du temps de séjour du débit de base. Les gestionnaires de la ressource en eau de l'Est du Canada, en particulier au Québec, ainsi que les parties prenantes, pourraient bénéficier de la cartographie, à l'échelle régionale, des bassins versants les plus vulnérables en dupliquant la méthode à d'autres bassins versants d'intérêt. Le suivi de paramètres de la qualité aux exutoires des bassins versants (ex : au niveau de l'eau brute des prises d'eau) pourrait être utilisé avantageusement pour la séparation d'hydrogramme et la détermination de la vulnérabilité des rivières face aux contaminations de surface. Par exemple, l'alcalinité, la silice dissoute et les isotopes stables de la molécule d'eau sont d'excellents traceurs des relations nappe/rivière et pourraient être échantillonnés sur une base hebdomadaire dans les bassins versants stratégiques. Des campagnes

de terrain hivernales pourraient ensuite être envisagées, en période d'étiage, pour l'échantillonnage de traceurs de datation des eaux souterraines récentes (ex : ^3H , ^{85}Kr) afin de détailler et discuter de la résilience des rivières face aux changements d'occupation du sol et les changements climatiques.

- *Séparation d'hydrogramme à pas de temps plus resserré*

Le suivi des ions majeurs à la prise d'eau potable de la rivière Saint-Charles permet d'avoir une bonne estimation des contributions d'eau souterraine à la rivière à échelle mensuelle et annuelle, mais pas à l'échelle de l'évènement de pluie (*Article 3*). Ce travail ouvre de nouvelles perspectives pour mieux comprendre quel est le rôle joué par les eaux souterraines pendant les épisodes de crue. Notamment, la participation d'eau pré-évènement relativement anciennes (par écoulement piston), ainsi que le rôle joué par la recharge récente à l'écoulement de surface pendant et après les épisodes de pluie, sont deux processus qui ne sont toujours pas totalement compris. Pour répondre à ces questions, un suivi de traceurs géochimiques à pas de temps très resserré (ex : de 5 à 30 min) en période de crue devrait être mis en place afin de (i) quantifier avec précision les apports d'eaux souterraines en rivière, (ii) discriminer les contributions à l'écoulement en fonction de leur âge relatif et (iii) discuter de la variation temporelle des signatures géochimiques des compartiments du bassin versant participant à l'écoulement. Les traceurs pertinents pour un tel travail sont les isotopes stables de la molécule d'eau, les gaz dissous, le tritium, les radionucléides lourds, la silice dissoute et les ions majeurs.

5.2 Conclusions in English

The main target of this PhD work was to set up new tools to describe surface water resources vulnerability to anthropic forcings, especially in vulnerable catchments used to produce drinking water. The vulnerability of these perennial rivers can be approached by two parameters, which are the baseflow index of the river, and the residence time of the groundwater inflows. The characterization of groundwater – surface water interaction is at the heart of the project and led to the following main research questions:

- (i) How to improve existing tracer-based methods for characterizing and quantifying groundwater – surface water interaction?
- (ii) How to quantify the groundwater inflows to a river and their temporal variations?
- (iii) How to determine the river baseflow residence times and link it with the surface water resources vulnerability to anthropic forcings?

These questions were answered by studying the surface water uptake of the Saint-Charles River catchment. Its specific context does not facilitate the job of the hydrogeologist-geochemist since the catchment is partially urbanised, is meso-scale and is influenced by snowmelt at the end of winter. The main scientific contributions of the research as well as the perspectives for a better management of water resources are listed below.

5.2.1 Contributions of the research

Two methodological works are reported in Chapter 2 of this PhD work. *Article 1* contributes to demonstrate that stable isotopes (^2H - ^{37}Cl) can be used as quantitative tracers for simultaneously (i) measure the discharge of small streams with a high accuracy, (ii) estimate the relative contributions of the “fast” and “slow” velocity flow components, (iii) with a limited impact on the environment compared to some other tracers techniques. This opens new perspective to the measure of river discharge in vulnerable catchments and/or under any hydrological conditions.

Dissolved gases (and particularly noble gases) are excellent tracers of hydrological processes (ex: groundwater – surface water interaction) and are very useful for age-dating applications. Their

use is hindered by complex (and costly) sampling procedures and analysis. *Article 2* is an original technological breakthrough combining passive samplers for gas sampling, mass spectrometry for noble gases and gas chromatography for anthropic trace gases. It is possible to obtain samples representative of the natural environment with simplified sampling and analysis procedures, especially for noble gases. This work shows that the miniRUEDI is a reliable lab and field machine enabling relatively cheap, easy and quick access to noble gases contents determination. These works are also important for the development of large spatial scale artificial tracing experiments with gases, since it is easy to access to a fine sampling spatial resolution (both vertically and laterally), thus reducing field work efforts while increasing the capacity to investigate processes in situ.

The groundwater inflows to the Saint-Charles River have been traced and quantified from 2013 to 2023 thanks to the river water quality monitoring of the City of Québec. This original hydrograph separation is based on the identification of the poles controlling the water quality (runoff, groundwater and snowmelt contaminated with de-icing road salts) and can be used as a calibration tool for a continuous mathematical hydrograph separation. The data put into light the role played by groundwater inflows over the river availability and quality. The monitoring of major ions, dissolved silica and stable isotopes of the water molecule at the outlet of the Saint Charles River catchment indicates that groundwater is the main contributor to streamflow generation, both at the monthly and annual timescales, between 2013 and 2023 (*Article 3*). Baseflow contributes to at least 50 % of the total streamflow for more than 70 % of the days of the year. Especially in winter, the baseflow fraction reaches usually more than 90 %. In fact, it is only shortly after rain events that the runoff component seems to exceed the baseflow component. The periods with high groundwater fraction are marked with a higher total mineralization, especially higher concentrations of alkalinity, calcium and magnesium. This first tracer revealed to be an excellent indicator of the groundwater fraction in the stream, as it is mainly inherited from the transport of water through the unsaturated zone. Some trace metals are shown to be mostly brought by the runoff component, for example zinc, aluminium and lead. The couple sodium + chloride shows elevated contents during the first snowpack melting pulses, usually in March.

However, their concentration during low-flow conditions in summer increase from year to year, indicating that the part of the aquifer sustaining the Saint-Charles River is already largely contaminated with the application of de-icing road salts. The dynamics of the water fluxes within the basin can be identified thanks to the different behaviours of geochemical tracers. Alkalinity is an excellent tracer of the groundwater fraction in the stream, since it is mainly inherited from the high CO₂ partial pressures in the unsaturated zone. The CO₂ dissolution kinetics are very fast, and even the recent recharge can be at equilibrium in a few hours. Other tracers, such as dissolved silica, are markers of the recharge water residence time within the aquifer. Its dynamics revealed that the water residence time in the catchment, *i.e.* the time elapsed between the arrival of the water as precipitation and its time of leaving through the river, is transient and strongly influenced by catchment wetness conditions (seasonality and meteorological events). Indeed, shorter residence times were found in high flow periods, when dissolved silica contents are low while longer residence times are found during low-flow periods and associated with high dissolved silica contents. Due to the usually long winter low-flow period (> 2-3 months), the oldest baseflow ages are expected in winter. During this period, the groundwater that contributes to the stream is not affected by seasonality. The very low dissolved silica contents in spring, after the snowmelt period, indicates that the newly recharged groundwater preferentially sustains the stream and is quickly evacuated from the catchment.

Figure 70 illustrates the behaviour of these geochemical tracers through time spent within the catchment and how they can use to decipher information on residence time on the water contributing to the streams.

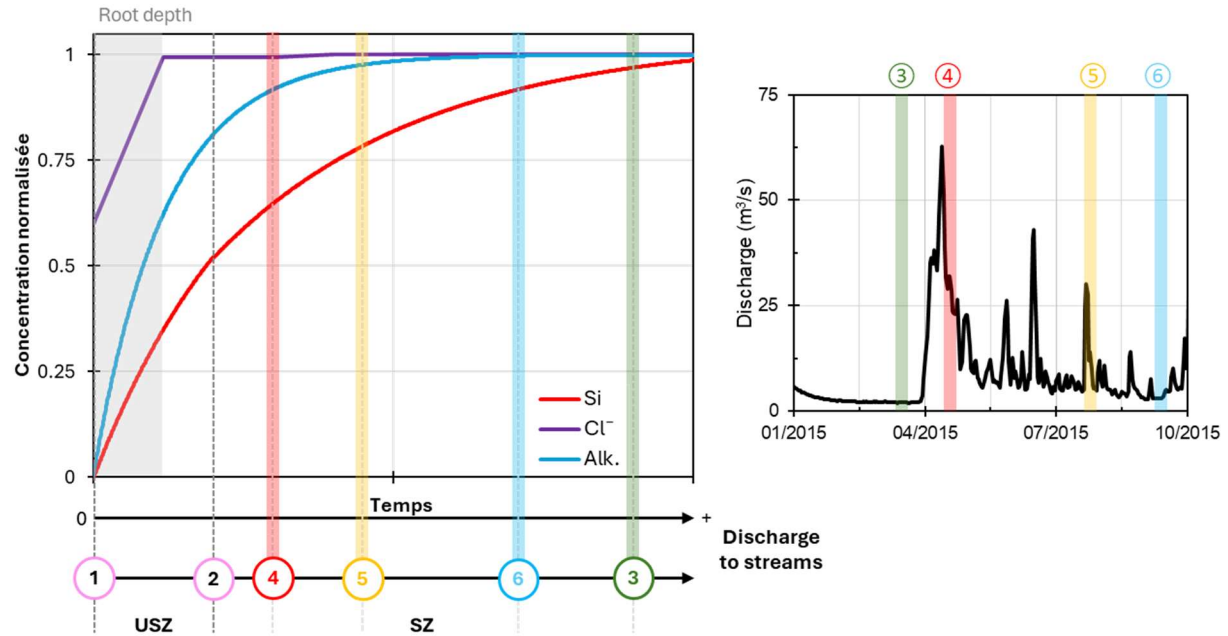


Figure 70: Conceptual model of the evolution of the geochemical signature (dissolved Si, Cl^- and alkalinity) as a function of water residence time from precipitation ①, within the unsaturated zone (USZ), the saturated zone (SZ) to the discharge in the streams of the catchment (③, ④, ⑤, ⑥). The time spent by groundwater in the aquifer before discharging to streams varies accordingly to catchment wetness conditions (high flows/low flows) as indicated by the hydrograph on the left (see the position of the numbers ③, ④, ⑤, ⑥).

Figure 71 illustrates which part of the aquifer preferentially sustains the streams, depending on the seasons. This graph is based on the information given by the couple alkalinity – dissolved silica.

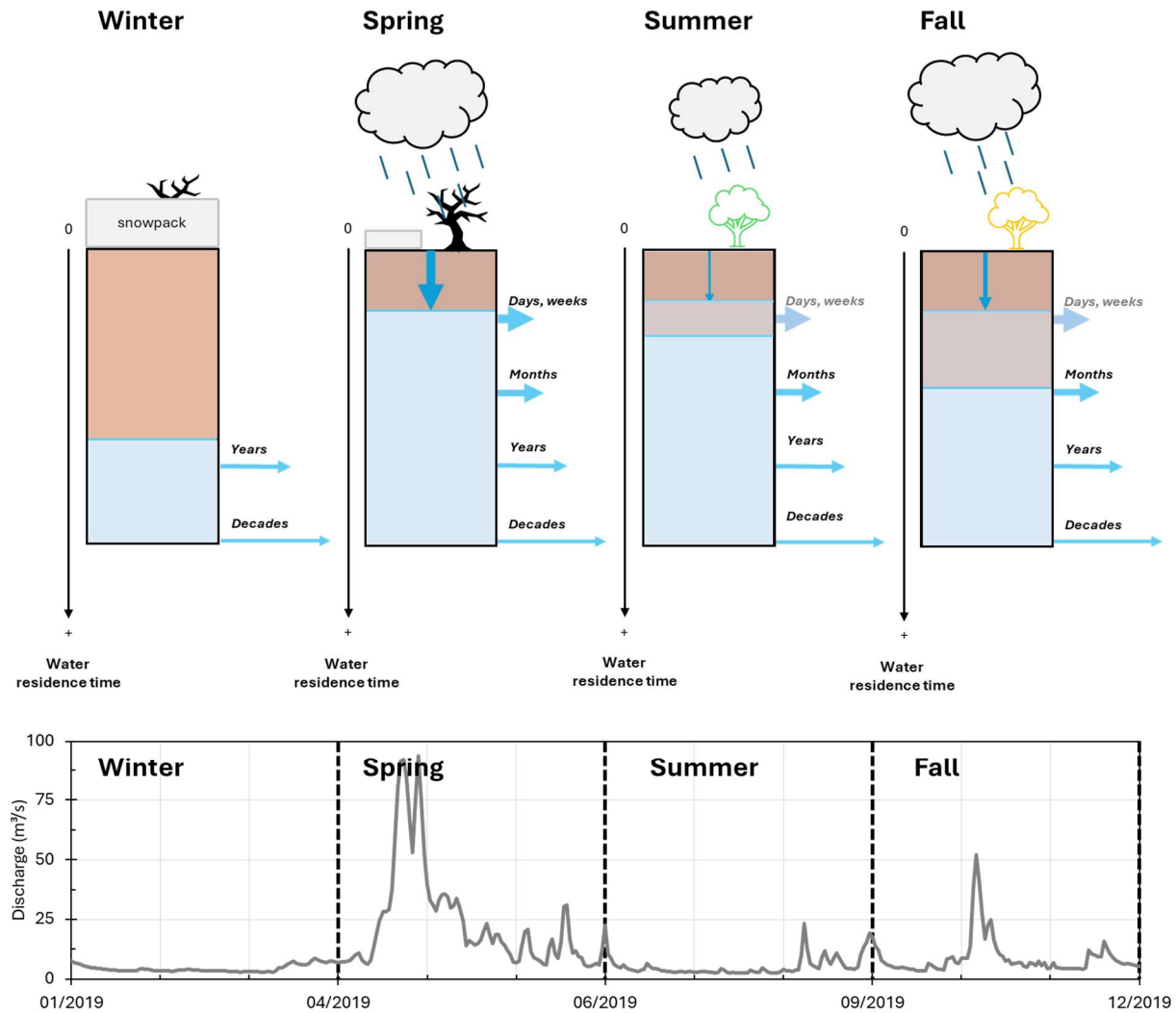


Figure 71: Differences in groundwater compartments sustaining the rivers of the catchment during the four seasons. In this “column” type model, the residence time of the groundwater increases with depth. The size of the arrows depict the relative fluxes to the stream. A light blue colour is used for groundwater in Summer and Autumn to represent the contribution of very young water to the streams during and shortly after storm events. The smallest fluxes are attributed to the aquifer compartment that is insensitive to natural seasonality in groundwater recharge patterns (inspired by Harman (2015)).

The residence time of groundwater inputs, before they feed rivers, was investigated in detail in the Nelson River sub-catchment, which is one of the main tributaries of the Saint-Charles River. The age property (*Article 4*) was linked to the groundwater fraction in the river (*Article 3*) using a unique combination of residence time tracers (^3H , ^{85}Kr) and artificial tracing experiments (inert gas injections). Winter conditions in Eastern Canada facilitate the use of such methods since the

ice cover prevents a part, if not most, of the air – water exchanges. This was assessed via a dual injection of inert gases (He and SF₆). Baseflow residence times were successfully determined using ³H and ⁸⁵Kr (*Article 4*). A mean residence times of 10 years was found for the baseflow, with a dispersion model. The corresponding age distribution covers age ranging up to 30 years. On a water management perspective, this suggests that the resilience of the aquifer portion that contributes to the stream in winter is relatively low since any contamination would affect the baseflow quality for decades.

Chapters 3 and 4 (*Article 3* and *Article 4*) provide new tools for protecting surface waters resources by considering groundwater inflows and (i) the vulnerability of rivers to surface contamination and (ii) their resilience to groundwater changes in quality and quantity. The vulnerability of rivers can be approached by the baseflow index, since it represents the relative contribution of groundwater and runoff in the streams. The resilience of rivers to groundwater changes is a function of the renewal rate of the water within the aquifer, *i.e.* its residence time. This is because the latter tells us in how much time any contamination is flushed out of the aquifer to the rivers. The relationship between these two key metrics is represented in Figure 72. A similar type of representation has been published in the past for lakes dominated by groundwater inflows (Arnoux, Barbecot, Gibert-Brunet, Gibson, Rosa, et al., 2017; Masse-Dufresne et al., 2021). This graph is separated into four parts, making it possible to distinguish rivers that are more or less vulnerable to surface contamination or more or less resilient to anthropogenic forcings. Under these conditions, the River Nelson sub-watershed can be considered as not very vulnerable to surface contamination (high baseflow index), but at the same time not very resilient to changes in groundwater quality and quantity (relatively high baseflow mean residence time). One of the recommendations for the City of Québec for protecting its drinking water source would be to “move” to the zone (2) of the graph, *i.e.* to reduce the renewal time of the aquifers feeding the rivers using managed aquifer recharge techniques.

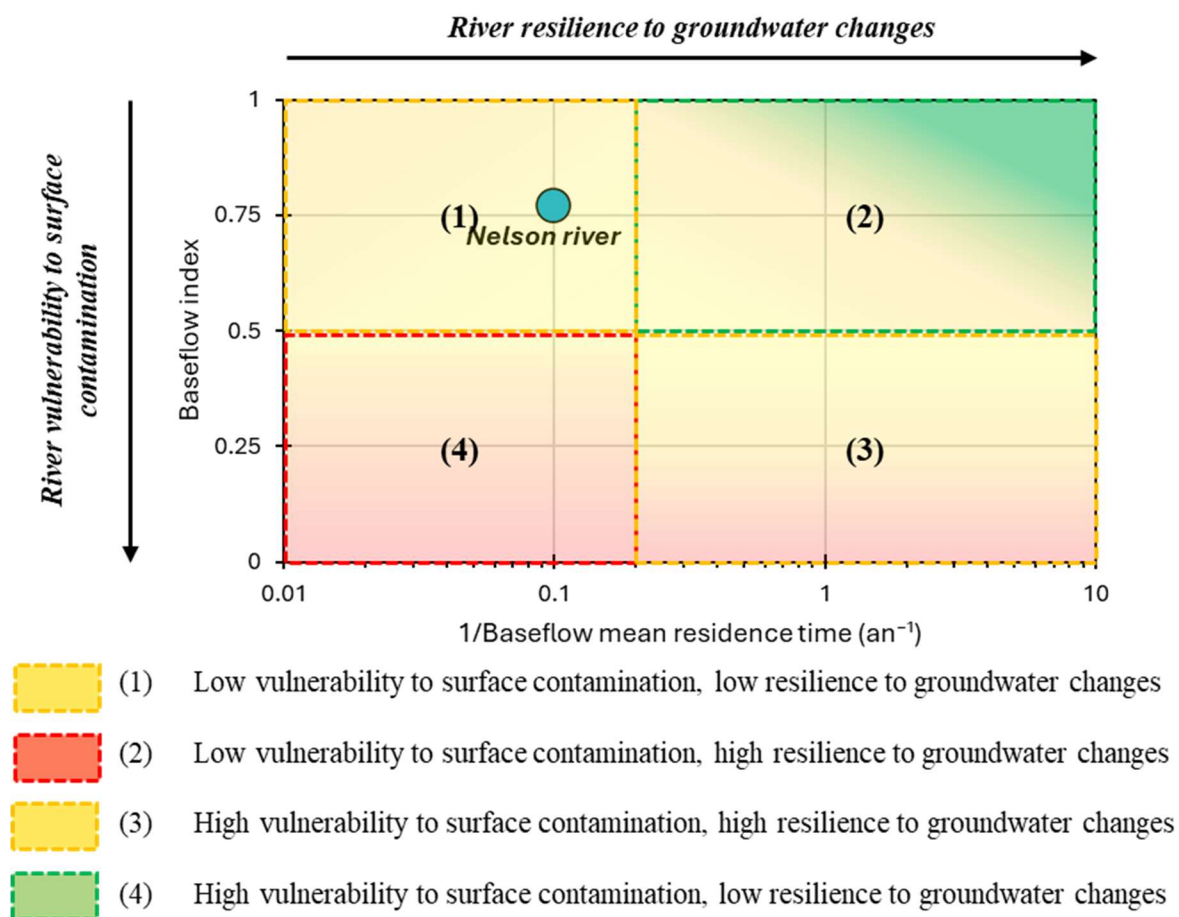


Figure 72: Plot of the resilience of rivers to groundwater changes in quality and quantity (controlled by the baseflow residence time) and the vulnerability of rivers to surface contamination (controlled by the baseflow index).

Generally speaking, this PhD work contributes to highlights the essential role played by groundwater on the water cycle, as it controls both availability and quality of the surface water. To do this, we were successful in developing a scientific method based on the following four steps:

- (i) Measure streams discharge with a high precision ($< 1\%$ of the measured value) and a limited impact on the environment
- (ii) Quantify the relative contribution of runoff and groundwater to surface waters
- (iii) Describe the origin and the dynamics of the watershed hydrochemical responses
- (iv) Quantify the residence time of streamwater, determine the watershed resilience and discuss the seasonality of these parameters.

It has serious implications for the management of water resources, especially in the context of drinking water production and opens new perspectives for tracer-based applications for water resources management. It further demonstrates that the role of groundwater – surface water interaction must be considered for the assessment of the vulnerability of surface water intakes, at least in Eastern Canada.

5.2.2 Research and application perspectives

- *Application of the method to other catchments in Eastern Canada*

The method to assess the vulnerability and resilience of catchments is based on the hydrograph separation (computation of the groundwater contribution) and the determination of the baseflow residence time. The mapping of vulnerable catchments could be highly beneficial to stakeholders and water resources managers in Eastern Canada and could be done by duplicating the method to other catchments of interest. The monitoring of major ions at the outlets of catchments could be advantageously used for hydrograph separation and the determination of the vulnerability of rivers to surface contamination. For example, alkalinity, dissolved silica and water stable isotopes revealed to be excellent tracers for understanding processes leading to streams generation and should be sampled on a weekly basis in strategic catchments for hydrograph separation. Winter field campaigns could then be carried out to sample baseflow for young groundwater tracers (especially ^3H , ^{85}Kr) and determine baseflow residence times. This would be very useful for describing the rivers resilience to global climate change and soil occupation modifications.

- *Hydrograph separation at a finer timestep*

The major ions monitoring of the Saint-Charles River has been extremely useful for proposing a first, broad hydrograph separation (*Article 3*). This allowed to estimate groundwater inflows to the river at the monthly and annual timescales, but not for shorter timescales (ex: event timescale). For now, it only suggests that groundwater plays a significant role during the rising limb of storm hydrographs. Then, this work opens new perspectives for a better understanding of the role played by groundwater inflows to streams during storm events. The contributions of “older”, pre-

event water (piston flow) and newly recharge waters during and after precipitation events are two processes that are still not completely understood. They could be addressed by monitoring a stream at a fine timestep (ex: 5 min to 30 min) for environmental tracers. This would allow us to (i) identify and quantify the mobilization of pre-event and event waters and (ii) discuss the temporal geochemical evolution of the pre-event water contributing to the stream during the storm. The relevant tracers would be major ions, dissolved gases, stable isotopes, tritium, heavy radionuclides and dissolved silica.

APPENDIX A

Development of the headspace method for simultaneous analysis of SF₆, CFC-12, CFC-11 and CFC-113 in environmental and tracing experiments samples

Theoretical equations

The theoretical equations describing the headspace method are first derived below. Then, the Eq. (A4) allows to determine the dissolved gas of interest concentration in any sample previously analysed using gas chromatography. It also allows to determine the optimum headspace volume prior analyses, depending on the studied gases and their Henry coefficient, K_H (Figure 73).

Let V_b , V_h and V_w the volumes of the bottle, of the headspace and the remaining water respectively [L³] and $n_{b,i}$, $n_{h,i}(t)$ and $n_{w,i}(t)$ the total quantity of gas i (ex: CFCs, SF₆) in the bottle and the quantities of gas i in the headspace and the water over time respectively [mol]. We have the following relationships:

$$\begin{cases} V_b = V_h + V_w \\ n_{b,i} = n_{h,i}(t) + n_{w,i}(t) \end{cases} \quad (A1)$$

Note that $n_{b,i}$ is a constant and represents the total amount of gas i in the bottle after the headspace is made. Once equilibration between the headspace and the water volume took place, Henry's law states:

$$\begin{cases} n_{w,i}^{eq} = K_{H,i} p_i^{eq} V_w \\ n_{h,i}^{eq} = p_i^{eq} \frac{V_h}{V_M} \end{cases} \quad (A2)$$

Where p_i^{eq} is the partial pressure of gas i in the headspace after equilibration (atm or cc/cc) and is usually the value found after the analysis of a sample, $K_{H,i}$ is the Henry coefficient of gas i (in mol/L/atm), and V_M is the ideal gas molar volume at standard pressure (1 bar) and temperature (0 °C) and is equal to 22.414 L/mol. The combination of Eq. (A1) and (A2) gives:

$$n_{b,i} = n_{h,i}^{eq} \left(1 + \frac{V_w}{V_h} K_{H,i} V_M \right) \quad (A3)$$

The Eq. (A3) is useful to determine the optimum gas to water ratio (V_w/V_h) for any given gas (Figure 73). It is shown to be equal to $K_{H,i}^{0.5}$ (Sliwka et al., 2004) and is therefore dependent on the gas species and the temperature at which equilibration occurs. The solubilities of SF_6 and CFCs are found in Bullister et al. (2002), Warner and Weiss (1985) and Bu and Warner (1995).

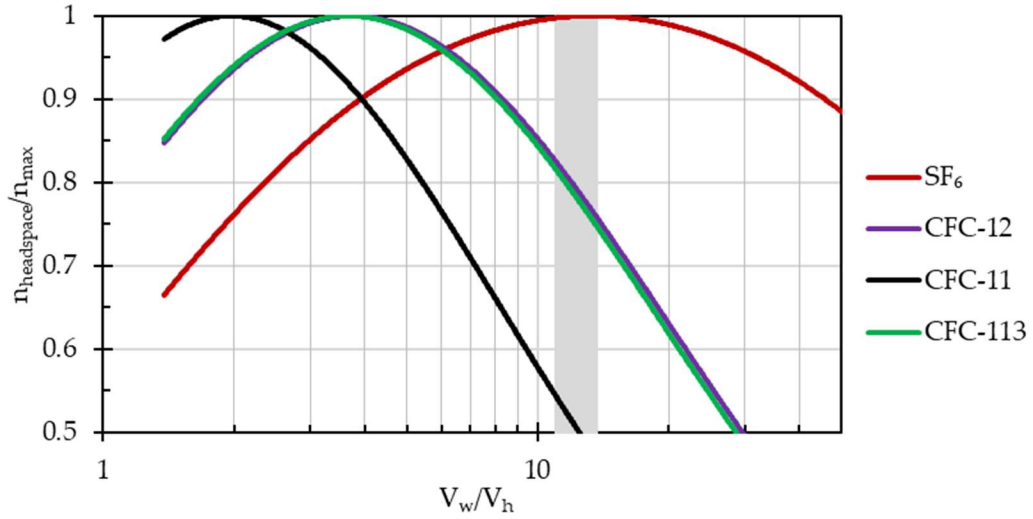


Figure 73: The ratio between the gas in the headspace and the maximum gas quantity in the headspace ($n_{\text{headspace}}/n_{\text{max}}$) as a function of V_w/V_h for CFCs and SF_6 at $T = 22^\circ\text{C}$ (average laboratory temperature). The optimum V_w/V_h is found when $n_{\text{headspace}}/n_{\text{max}}$ is equal to 1 (here, the optimum V_w/V_h ratio is ≈ 14 for SF_6 at 22°C). The grey area is the typical range of V_w/V_h values obtained with our headspace preparation protocol. Note that CFC-12 and CFC-11 curves are very close since their respective solubility coefficients are similar at temperatures close to 20°C .

The Eq. (A3) can also be written as follows:

$$c_{w,i} = p_i^{eq} \left(\frac{1}{V_M} \frac{V_h}{V_w} + K_{H,i} \right) \quad (A4)$$

The Eq. (A4) is used to determine the dissolved gas i concentration in any water sample since it links the measured concentration (p_i^{eq}) to the gas concentration in water ($c_{w,i}$). It depends on 4 parameters:

- The temperature at which the equilibration takes place. This parameter must be monitored using a temperature probe in the laboratory as it will control the value of K_H ;
- The volumes of water and headspace, which are measured using a scale;
- The moles of gas i in the headspace, that is measured during an analysis.

Analytical protocol

The three steps of the analytical protocol are described below. They are namely (i) the samples preparation, (ii) the equilibration step and (iii) the analysis using gas chromatography.

Samples consist of ≈ 700 mL Wheaton glass bottles with a septum cap. Water is typically sampled by putting the bottles in the water (ex: river water), with the bottleneck not completely put under water to avoid the presence of large bubbles. The cap are tightened carefully to avoid the presence of any bubbles. Samples are kept at room temperature after being back from the field to avoid abrupt temperature changes. Indeed, they are fragile and tend to break when they are put inside the fridge and taken out at room temperature. When high concentrations are expected (tracing experiments using SF_6), smaller volumes are sampled in 40 mL glass bottles.

The first step of the sample preparation is making the headspace. To do so, a double walled needle (Elementar) is used:

- At first, helium passes through the top hole of the needle for a few minutes to clean the line from atmospheric air
- Then, the septum is pierced with the needle. Helium is injected by the top hole while water will pass through the bottom hole of the needle
- Helium is injected as water is being replaced until the optimum ratio is reached (Figure 73). This takes usually around 8 minutes for the 700 mL bottles while it takes 1 – 2 minutes for the smaller 40 mL bottles.

Then, bottles are put in a mechanical agitator at usually 150 to 200 rpm, for at least 2 days (time necessary to reach equilibrium as shown after), and ideally 3-4 days. The laboratory temperature must be recorded continuously during the equilibrium process as it is useful for Henry's coefficient determination. A measurement interval of 15 minutes is sufficient. Long term measurement in the lab shows that there are variations of temperature in the lab during day and night, with an average temperature of 21.5 °C.

The analysis can then be performed using gas chromatography. To do so, the headspace is sampled and sent to the machine by using the same double walled needle (Elementar). Helium is let to pass through the bottom hole of the needle and the overpressure passes through the top hole of the needle to the machine (Unity then GC-ECD). The time of sampling is let to 9 minutes, which is enough to replace a few times to total volume of the headspace as determined by tests. The determination of the CFCs and SF₆ concentrations is done by integrating the chromatograph as in a regular analysis. Results are given in moles from the headspace, which can be translated to cc_{STP}/cc in water, by using the Eq. (A4) above.

Equilibration experiments

Equilibration experiments were conducted to assess (i) the time necessary for the equilibration to take place, and (ii) the validity of the analysis protocol (*i.e.* no atmospheric contamination and values in agreement with the laboratory atmosphere). The results are presented in Figure 74, where each sample was analysed for SF₆ and the three CFCs. The lab temperatures are comprised between 21.0 and 22.0 °C.

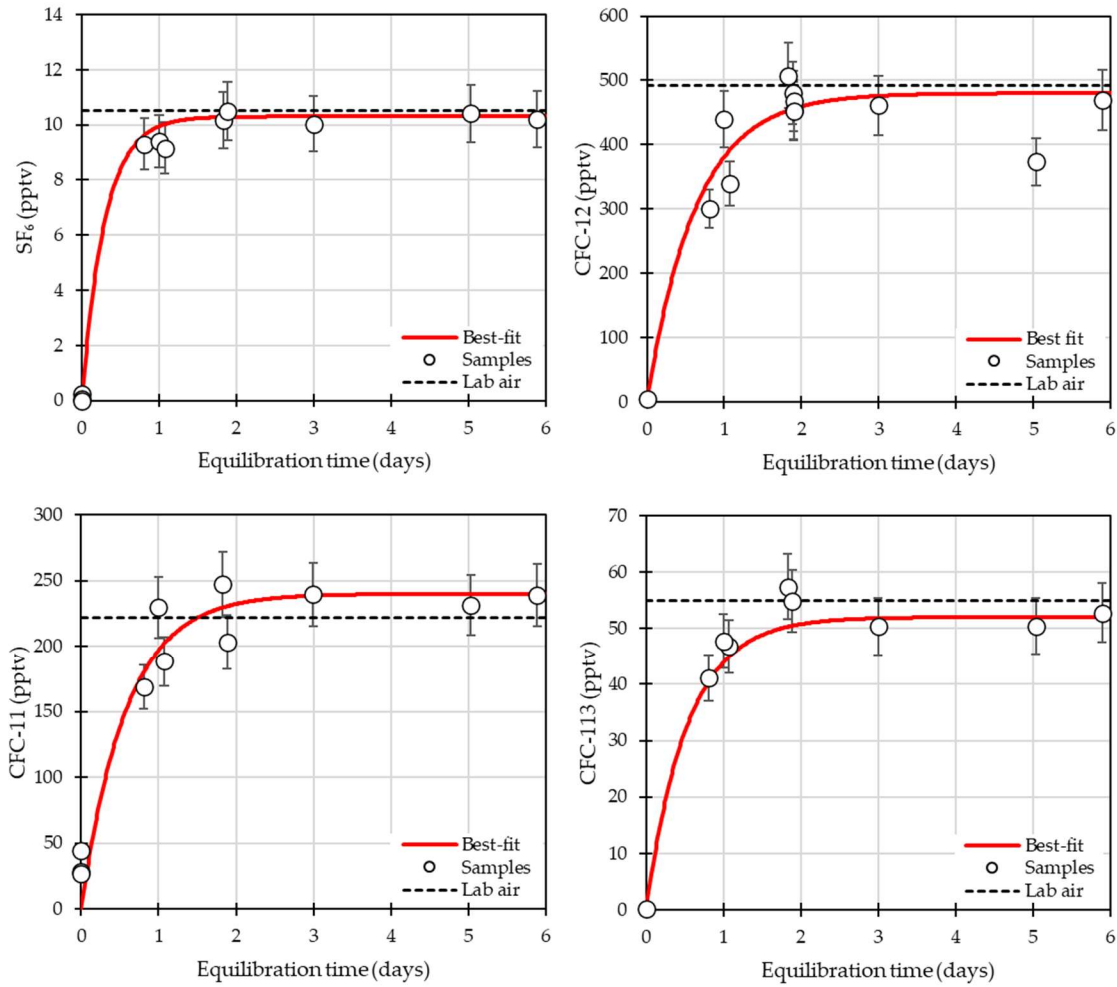


Figure 74: Results of the equilibrium experiments (March – April 2024). The analyses results have been transformed to atmospheric concentrations, assuming air saturated water. The dashed lines represent the measured concentration in the laboratory. A standard deviation of 10 % was adopted based on reproducibility results of samples and standards.

The system developed here is considered to be air-tight since no atmospheric contamination is observed (any leak from the atmosphere would result in very high gases concentration).

The best-fit curves model the ingrowth of gas inside the headspace and their expression is the following:

$$C(t) = C_{atm}(1 - \exp(-t\tau)) \quad (A5)$$

Where C_{atm} is the modern atmospheric concentration, *i.e.* the equilibrium concentration and τ is a parameter constraining the kinetics of the ingrowth, expressed in s^{-1} . The modelling of Eq. (A5) is helpful to determine the typical equilibration time of the headspace which is arbitrarily set to 95 % of C_{atm} (Table 8). The equilibration time is of roughly 2 days when the mechanical agitator is set to 200 rpm with an average lab temperature of 21.5 °C. Since the system was demonstrated to be completely gas tight, it is recommended to let the bottles shake for at least 3 days, to ensure complete equilibrium.

Table 8: Equilibration time necessary for SF_6 and CFCs. The headspace was constantly shaken under a lab temperature of 21 – 22 °C.

	SF_6	CFC-12	CFC-11	CFC-113
Parameter τ (s^{-1})	$3.9 \cdot 10^{-5}$	$1.8 \cdot 10^{-5}$	$2.0 \cdot 10^{-5}$	$2.2 \cdot 10^{-5}$
Equilibration time (days)	0.9	1.9	1.8	1.6

Conclusions

This first appendix describes the implementation of the headspace method in glass bottles for the measure of trace gases (SF_6 , CFCs) in water samples. Equilibrium experiments were conducted and allowed to determine a typical equilibration time of less than 2 days under laboratory conditions (temperature, constant shaking using a mechanical agitator). The development of the headspace method at the Hydro Sciences UQAM-ETS laboratory is considered to be very satisfactory and is an important addition to the development of further tracing experiments, especially using SF_6 (see for example section 4.3) as well as the measure of environmental samples. The last step of this work consists in determining the measure uncertainties and will be done in the near future.

APPENDIX B

Description of the Saint-Charles River catchment

The studied site is the Saint-Charles River water intake catchment. It is located in the north of the City of Québec and extends for more than 30 km to the north. The maximum width of the catchment is 15 km, with a total area of 344 km². The outlet of the catchment is the water intake of the Saint-Charles river.

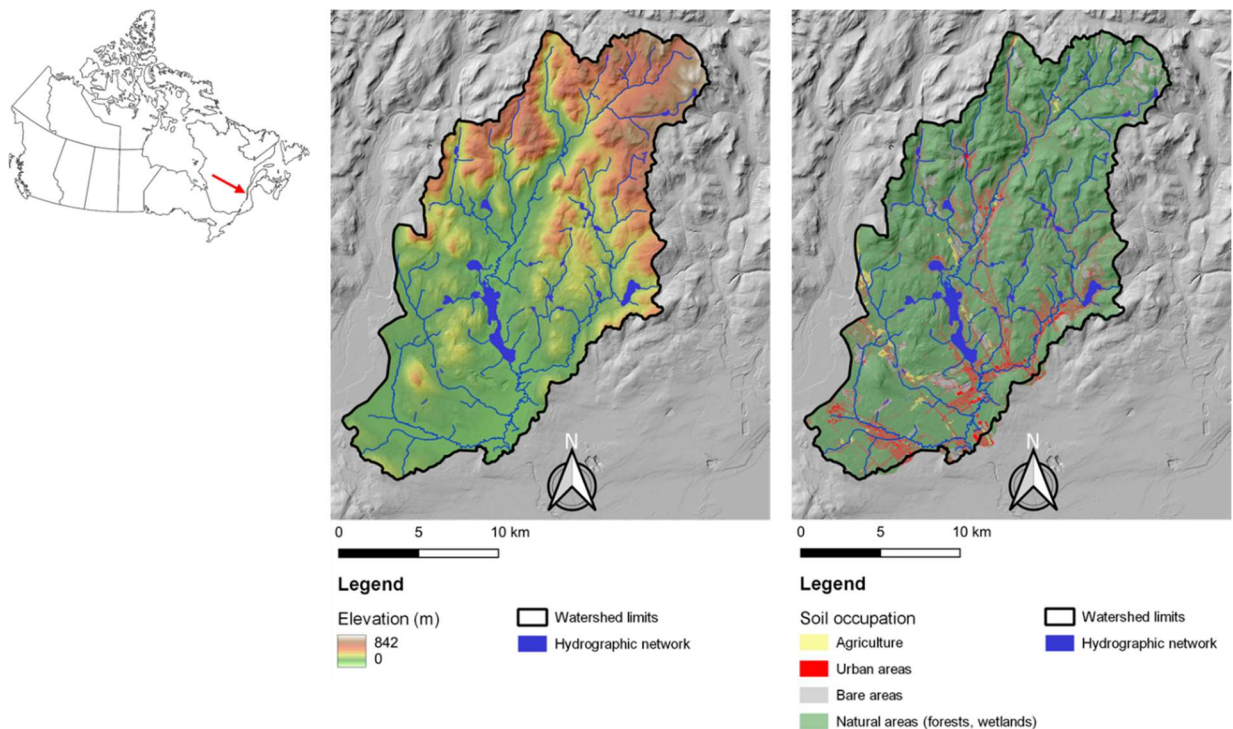


Figure 75: From left to right: map of Canada with the red arrow indicating the location of the studied watershed, topography map and land-use map of the Saint-Charles river water intake catchment.

- **Topography**

One of the main particularities of the catchment is its physiography. Indeed, a strong topographic gradient is found with altitudes ranging from 140 m in the valleys to 850 m at the highest summits. The physiography of the catchment is typical of the junction between the Saint-Lawrence

lowlands and the Laurentian shield: the northern part is the highest part and is characterized by small mountains with rather steep slopes. Narrow U-shaped valleys follow a north-south axis and get progressively wider on the south, with a transition zone (piedmont) in the middle of the catchment. The topography progressively becomes flatter close to the Saint-Lawrence lowlands.

- **Soil occupation**

The occupation of the catchment can be divided into four categories: natural areas (forests, wetlands), bare areas that have been transformed by mankind, urban areas and areas used for the agriculture. Most (67 %) of the catchment is covered by forest (lindens, maple trees, birches and firs are the dominant species). The forested areas are mainly located in the piedmont and the Laurentian shield, especially in steep and high zones. Bare areas (quarries, bare soil, forest cuts) occupy 13 % of the catchment, while urban areas represent 6 % of the total area. They are mostly found in the valleys, in the southern half of the catchment. However, the yearly growth rate of urban areas was 2.4 % on average between 2001 and 2020. Agriculture is extremely limited, with less than 1 % of the catchment area.

- **Geology and geological context**

Three main geological provinces are found in the region of Québec and form the “basement”: the Canadian shield (Grenville province), the St-Lawrence Lowlands and the Appalachian (Castonguay & Nadeau, 2012; Talbot Poulin et al., 2013). Only the rocks from the Grenville province are found in the vicinity of the catchment. The St-Lawrence Lowlands and Appalachian rock formations are found further south.

The geological history of the studied area starts around one billion years ago, when the Canadian shield collided with other continents, forming a mountain range probably of the size of the actual Himalayas. Their roots were progressively exposed due to erosion and form the actual small mountains of the catchment, called the Laurentides (Laurentian shield) in the Grenville province. These rock formations form a crystalline basement made of metamorphic rocks (migmatite, gneiss)

and cover the totality of the studied catchment (Figure 76). Then, roughly 600 million years ago, while Québec region was close to the equator, the Canadian shield mountain range collapsed due to tectonic rifting. This gave birth to the ocean Iapetus (similar to actual Atlantic Ocean). Sediments accumulated on the margin of the ocean basin and on the continental shelf between – 540 to – 445 Ma later became the sedimentary rocks found in the St-Lawrence Lowlands. These sedimentary rocks are not found in the vicinity of the catchment, but a part of it is visible in Figure 76, just south of the catchment outlet. The Iapetus ocean started to close after an inversion in tectonic forces, around 515 Ma ago. It resulted in the collision of continental masses which erupted the Appalachian mountain range between – 490 and – 260 Ma, mainly constituted of sedimentary rocks, whose remnants cannot be seen in Figure 76 (Castonguay & Nadeau, 2012)

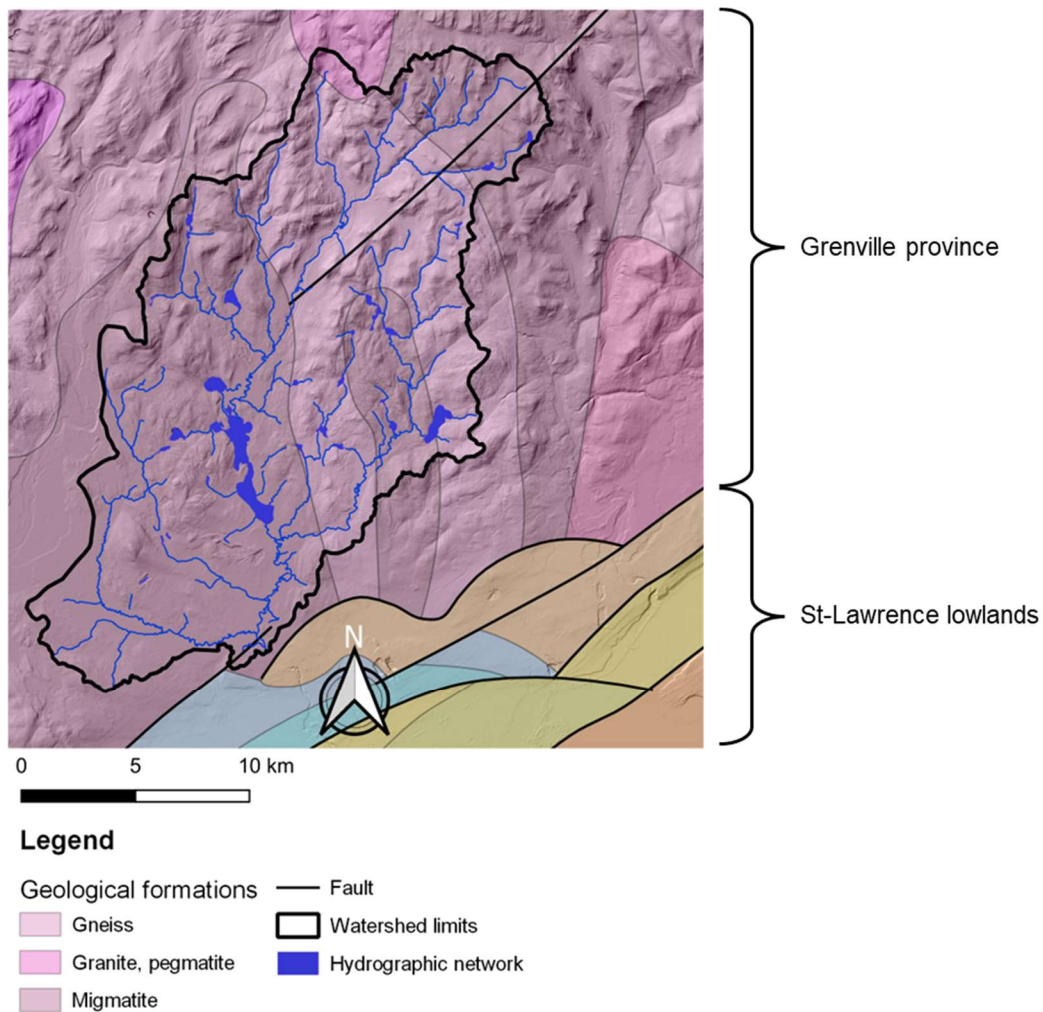


Figure 76: Geological map of the study area (data source: SIGEOM). The geological formations listed in legend are only the ones found inside the catchment.

The physiography of the catchment was then heavily modified during the Quaternary (- 2.6 Ma to present), especially because of successive glaciation events. Indeed, the Wisconsinian glaciation (- 80 000 to - 10 000 BC) is responsible of shaping the landscape and was followed by de-glaciation and marine incursions. The different surface deposits that can be found over the crystalline basement are listed in the following table (Table 9), from the oldest to the most recent. A detailed description can be found in Tremblay et al. (Tremblay et al., 2024).

Table 9: Surface deposits found across the study site (from oldest to most recent).

Type of surface deposits	Characteristics	Thickness
Glacial deposits (till)	Rock fragments from the Grenville province ripped away by glaciers form till, usually at the bottom of the latter. The till consists of clasts of all sizes in a coarse matrix (sand to silts). Till is found on hills, at higher altitudes (above 210 m, which is the maximum altitude reached by the Champlain sea).	Usually < 1 m.
Fluvioglacial deposits	These deposits are coarser and stratified and were formed by the transport of rocks fragments (from Grenville province) by the melting waters of glaciers. They form the main granular aquifer in the catchment, especially in the Nelson river valley.	Up to 40 m.
Marine deposits	The retreat of the glacier allowed the incursion of the Champlain sea in the St-Lawrence valley (from 12 000 to 10 000 BC). Marine deposits can be found in the catchment, with different grain sized, from very fine deep deposits to (pro)deltaic sediments. All these deposits are stratified.	The deltaic sediments are the thickest, up to 50 m.
Alluvial deposits	Alluvial deposits are found around the current and paleo hydrographic network and form actual alluvial terraces. Naturally, they are found in the valleys close to the rivers (des Hurons, Nelson, Jaune and Saint-Charles rivers).	Up to 3 to 5 m.

Organic sediments	Peat and organic sediments can be found in a few narrow valleys of the catchment and in the wetlands at the confluence of the des Hurons rivers with the Saint-Charles lake.	Up to 4 m.
-------------------	--	------------

- **Climate**

The local climate can be classified as continental cold and wet according to Köppen’s classification (Talbot Poulin et al., 2013; Tremblay et al., 2024). These results are based on the climate normals for the period 1981-2010 provided by governmental weather station installed close to the study site (Jean Lesage airport station located at the south of the studied catchment, and Forêt Montmorency station located 20 km north of the studied catchment).

Typically, the winters are cold with temperature below 0°C from November to March, while summers are temperate to hot (mean monthly temperature higher than 10°C from May to September) (Figure 77). Precipitation occur all the months of the year. Snowpack usually builds up from December to April, before the melting season starts. The average annual precipitation in the catchment is comprised between 1 200 mm in the south (station of Jean Lesage airport) and 1 600 mm in the North, at higher altitudes (Forêt Montmorency station). The temperatures are lower in the North (annual mean: 0.5 °C) compared to the South of the catchment (annual mean: 4.0 °C).

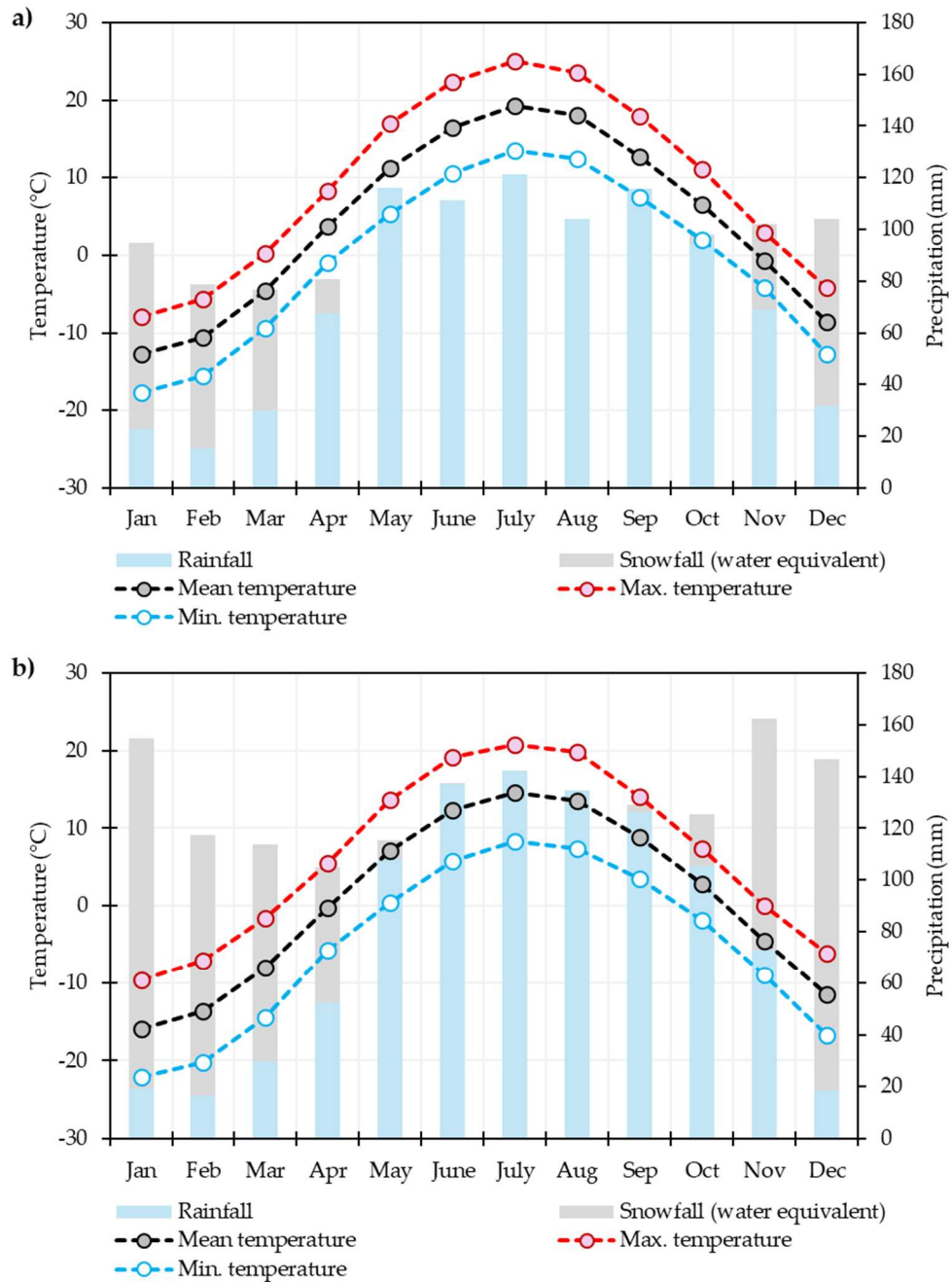


Figure 77: Average climatic data (climate normals: 1981 – 2010) for (a) Jean Lesage airport station (ID station: 71708) and (b) Forêt Montmorency station (ID station: 71212). The data was retrieved from https://climate.weather.gc.ca/climate_normals/.

- **Hydrographic network**

Three main tributaries flow to the Saint-Charles river, namely the des Hurons river, the Nelson river and the Jaune river. The des Hurons river flows into the biggest lake of the catchment: the Saint-Charles lake (350 ha). Smaller lakes (< 100 ha) are found in the northern and western parts of the catchment. Wetlands are found in the flat areas of the southern part of the catchment, but also at the confluence between the des Hurons river and the Saint-Charles lake.

The hydrographs of the three rivers are severely impacted by the seasonality of the local climate (Figure 78), with the highest discharges found in spring during the snowmelt season and the lowest found in winter during the snowpack buildup period. The autumn and summer seasons are usually wet, although the discharge in autumn is higher because of the end of the trees growing season.

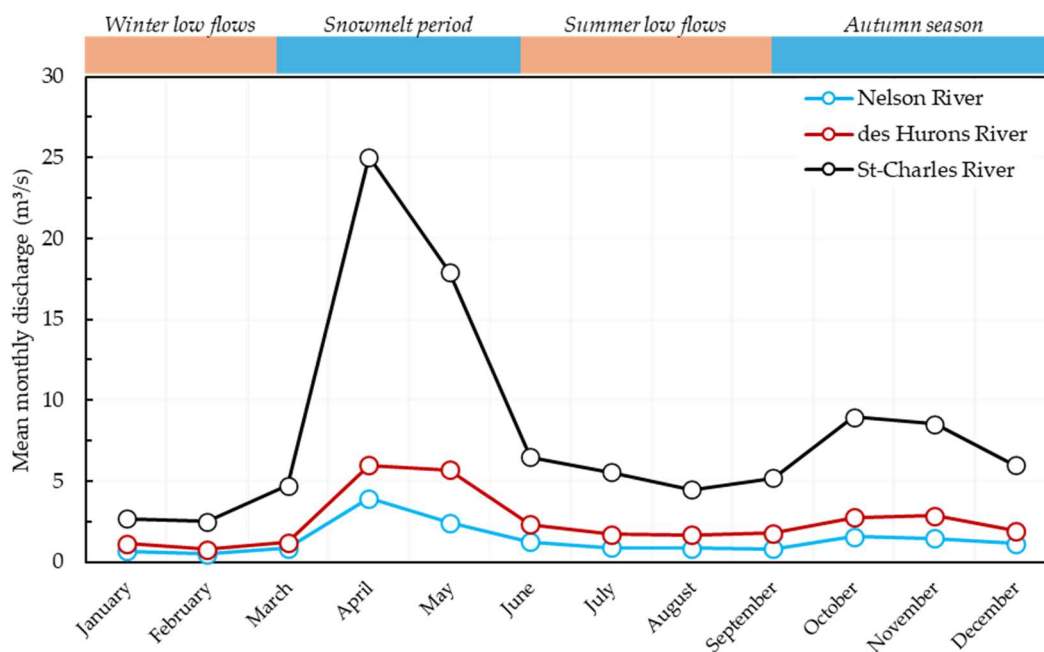


Figure 78: Hydrographs of the main rivers of the catchment (period: 2006 – 2024). The data were obtained from the governmental stations n° 050915, 050916 and 050904 and can be retrieved at the following address: <https://www.cehq.gouv.qc.ca/hydrometrie/>.

- **Water and water uses**

Water is abstracted from the Saint-Charles river at the pumping station of the City of Québec (see Figure 79). The analysis of the pumping station data revealed that the abstraction rate was, on average, 1.65 m³/s between 2012 and 2023. The water is then treated and routed to the City of Québec where it supplies more than 300 000 people. Municipalities in the vicinity of the catchment rely on groundwater, especially in the northern part (Stoneham-et-Tewkesbury, Lac-Delage and Lac-Beauport).



Figure 79: The outlet of the catchment: the water intake of Saint-Charles river. The pumping system is immersed on the bottom right part of the picture.

APPENDIX C

Monitoring of isotopes and geochemical parameters

- **Introduction to water stable isotopes**

Water stable isotopes (^2H - ^{18}O) are ideal tools for understanding the water cycle dynamics at the catchment scale (Clark, 2015; Clark & Fritz, 1997). The physical processes that take place at each step of the water cycle modify the water isotopic signal. For example, when liquid water evaporates, water molecules with the weakest intermolecular bonds, *i.e.* those comprising the lightest isotopes (^1H , ^{16}O), will be preferably incorporated to the gas phase. The heaviest molecules, *i.e.* those comprising ^2H and/or ^{18}O , will tend to stay and accumulate in the liquid phase. This isotopic selection and preferential redistribution between two exchanging phases is called “isotopic fractionation”. It is essentially thermo-dependant, and its effect decreases when temperature increases.

The isotopic signature of a water sample is commonly reported in “delta-notation” (δ), which represents the sample (s) isotopic ratio deviation to a standard (reference material) isotopic ratio and is expressed in ‰ vs VSMOW (for “Vienna Standard Mean Ocean Water”):

$$\left\{ \begin{array}{l} \delta^2\text{H}_s = \left[\frac{\left(\frac{^2\text{H}}{^1\text{H}}\right)_s}{\left(\frac{^2\text{H}}{^1\text{H}}\right)_{\text{VSMOW}}} - 1 \right] 10^3 \\ \delta^{18}\text{O}_s = \left[\frac{\left(\frac{^{18}\text{O}}{^{16}\text{O}}\right)_s}{\left(\frac{^{18}\text{O}}{^{16}\text{O}}\right)_{\text{VSMOW}}} - 1 \right] 10^3 \end{array} \right. \quad \text{Eq 3-1}$$

Within a watershed, the isotopic composition of groundwater and surface waters will be essentially a function of the season, the elevation (recharge elevation for groundwater), the mixing

between the different water masses and the climate. A marked seasonality as well as an altitudinal gradient, in precipitation (and recharge), are thus expected in the studied catchment, since the temperature signal has a strong seasonality and the elevation ranges from 50 to 850 m. The water stable isotopes were used to characterize the different hydrological compartments (rainfall, snowpack, groundwater, rivers) and trace their relationships. To do so, an important monitoring network was set up at the catchment scale during the first two years of this PhD.

- **Description of the isotope network**

Rainfall collectors were selected according to the following criteria:

- Compliance with the installation standards of the IAEA Global Network for Isotopes in Precipitation (GNIP) (IAEA, 2013). Rainfall collectors were installed on flat, open terrain. They were put at least as twice as far of obstacles as their height. The top of the collectors funnel was put at about 1.2 m above the ground
- Installation at different elevations (between 150 and 850 m) and deployment at the catchment scale to have a network as representative as possible

Rainfall was sampled every 2 weeks during July 2021 – November 2021 and April 2022 – November 2022 periods at 15 different sampling sites: 14 in the vicinity of the watershed and a fifteenth installed in the Forêt Montmorency, roughly 30 km north of the studied catchment. This was done to better characterize the isotopic signal at higher altitudes (> 700 m). A commercial Palmex® collector was used for one station (Gröning et al., 2012) while the collectors used for the 14 other sites were home built at UQAM, following Carton et al. instructions (Carton et al., 2024). The height of rainfall was also monitored by weighting the samples. Subsamples of 30 mL were stored in HDPE bottles, carefully tightened, in the dark at room temperature. Snowpack was collected in various locations at different altitudes across the watershed during the winters 2020 to 2023. Trenches were dug in order to collect the whole height of the snowpack. The snow collected was weighted to determine the equivalent liquid water height and a subsample of 30

mL was collected in HDPE bottles and stored in the same conditions as the rainfall samples. A total of 52 snowpack samples were analysed.



Figure 80 : On the left, Palmex® collector used at the lake Saint-Charles station. On the right, homemade rainfall collector installed in the catchment.

Groundwater was sampled seasonally in 2020 and 2021, after purging the sampled boreholes three times and making sure the physico-chemical parameters were stable. The 51 samples were taken in 30 mL HDPE bottles, that were carefully tightened and stored in the dark at room temperature.

Surface waters were collected in 30 mL HDPE bottles at 15 stations between November 2019 to August 2021 across the watershed. Each station was sampled 8 to 10 times for a total of 131 samples. Furthermore, a weekly sampling was conducted at the outlet of the catchment, at the water intake from January 2022 to October 2023, thanks to the support of the staff of the laboratory of the City of Québec. A total of 27 samples have been analysed for water stable isotopes.

Table 10: Number of samples analysed for water stable isotopes during the PhD.

	Number of analyses
Rainfall	264
Snowpack	52
Groundwater	53
Rivers	144
Total	513

All the samples were analysed at the Geotop laboratory in UQAM (<https://www.geotop.ca/en/laboratoires/isotopes-stables-UQAM>) with the following analytical protocol: 1 mL of water is pipetted in a 2 mL glass vessel closed with a septum. Samples are analysed using a Picarro (model L2130-i) using cavity ring down spectroscopy (CRDS). Subsamples of 1.8 μL are injected and measured 10 times using the “Express” mode. The first seven injections are rejected to limit memory effect. Three internal standards ($\delta^{18}\text{O} = +0.11 \pm 0.07 \text{ ‰}$, $-13.80 \pm 0.06 \text{ ‰}$ & $-20.37 \pm 0.03 \text{ ‰}$; $\delta^2\text{H} = +1.22 \pm 0.29 \text{ ‰}$, $-99.45 \pm 0.56 \text{ ‰}$ & $-155.92 \pm 0.33 \text{ ‰}$) are used for the normalisation of the results on the VSMOW2-SLAP2 scale. A fourth internal standard ($\delta^{18}\text{O} = -6.72 \pm 0.03 \text{ ‰}$; $\delta^2\text{H} = -50.84 \pm 0.72 \text{ ‰}$) is measured as unknown to assess the exactness of the normalisation. The results are expressed in delta units in ‰ vs VSMOW and uncertainties are less than 1‰ for $\delta^2\text{H}$ and less than 0.1 ‰ for $\delta^{18}\text{O}$.

- **Quality parameters (major ions, trace metals and dissolved silica)**

The City of Québec is already monitoring the stream water quality parameters (major ions, trace metals, microbiology) since decades at the outlet of the catchment. The time elapsed between two samplings is variable and on average around 1 week. As water stable isotopes were already sampled by the staff of the laboratories of the City, dissolved silica was prospectively added to the list of analysed parameters. Dissolved silica analyses (72 samples) took place at the Geotop ICP-OES laboratory of McGill university and uncertainties are less than 5 % of the measured values.

All these data (isotopes, dissolved silica and major ions) are used in *Article 3*, for the hydrograph separation of the Saint-Charles river (section 3.3).

BIBLIOGRAPHY

- Aeschbach-Hertig, W., El-Gamal, H., Wieser, M., & Palcsu, L. (2008). Modeling excess air and degassing in groundwater by equilibrium partitioning with a gas phase. *Water resources research*, 44, 12.
- Aeschbach-Hertig, W., & Gleeson, T. (2012). Regional strategies for the accelerating global problem of groundwater depletion. *Nature geoscience*, 5, 853-861. <https://doi.org/10.1038/NGEO1617>
- Aeschbach-Hertig, W., Peeters, F., Beyerle, U., & Kipfer, R. (1999). Interpretation of dissolved atmospheric noble gases in natural waters. *Water resources research*, 35(9), 2779-2792. <https://doi.org/10.1029/1999wr900130>
- Aeschbach-Hertig, W., Schlosser, P., Stute, M., Simpson, H. J., Ludin, A., & Clark, J. F. (1998). A $^3\text{H}/^3\text{He}$ study of groundwater flow in a fractured bedrock aquifer. *Ground Water*, 36, 10.
- Ahiablame, L., Sheshukov, A. Y., Rahmani, V., & Moriasi, D. (2017). Annual baseflow variations as influenced by climate variability and agricultural land use change in the Missouri River Basin. *Journal of Hydrology*, 551, 188-202. <https://doi.org/10.1016/j.jhydrol.2017.05.055>
- Amanambu, A. C., Obarein, O. A., Mossa, J., Li, L., Ayeni, S. S., Balogun, O., Oyebamiji, A., & Ochege, F. U. (2020). Groundwater system and climate change: Present status and future considerations. *Journal of Hydrology*, 589. <https://doi.org/10.1016/j.jhydrol.2020.125163>
- Antrop, M. (2004). Landscape change and the urbanization process in Europe. *Landscape and Urban Planning*, 67(1-4), 9-26. [https://doi.org/10.1016/s0169-2046\(03\)00026-4](https://doi.org/10.1016/s0169-2046(03)00026-4)
- APHA. (2012). *Standard Methods for the Examination of Water and Wasterwater* (22nd edition ed.). American Public Health Association, American Water Works Association, Water Environment Federation.
- Arnoux, M., Barbecot, F., Gibert-Brunet, E., Gibson, J., & Noret, A. (2017). Impacts of changes in groundwater recharge on the isotopic composition and geochemistry of seasonally ice-covered lakes: insights for sustainable management. *Hydrology and Earth System sciences*, 21(11), 5875-5889. <https://doi.org/10.5194/hess-21-5875-2017>

- Arnoux, M., Barbecot, F., Gibert-Brunet, E., Gibson, J., Rosa, E., Noret, A., & Monvoisin, G. (2017). Geochemical and isotopic mass balances of kettle lakes in southern Quebec (Canada) as tools to document variations in groundwater quantity and quality. *Environmental Earth Sciences*, 76(3). <https://doi.org/10.1007/s12665-017-6410-6>
- Barbecot, F., Guillon, S., Pili, E., Larocque, M., Gibert-Brunet, E., Hélie, J.-F., Noret, A., Plain, C., Schneider, V., Mattei, A., & Meyzonnat, G. (2018). Using Water Stable Isotopes in the Unsaturated Zone to Quantify Recharge in Two Contrasted Infiltration Regimes. *Vadose Zone Journal*, 17(1), 1-13. <https://doi.org/10.2136/vzj2017.09.0170>
- Barbecot, F., & Lefebvre, K. (2021). *Synthèse hydro-géochimique des régions couvertes par les projets d'acquisition de connaissances sur les eaux souterraines et développement d'un indice de résistance chimique des eaux souterraines du Québec*.
- Barlow, P. M., & Leake, S. A. (2012). *Streamflow Depletion by Wells - Understanding and Managing the Effects of Groundwater Pumping on Streamflow*. USGS.
- Barnett, T. P., Adam, J. C., & Lettenmaier, D. P. (2005). Potential impacts of a warming climate on water availability in snow-dominated regions. *Nature*, 438(7066), 303-309. <https://doi.org/10.1038/nature04141>
- Barron, O. V., Barr, A. D., & Donn, M. J. (2013). Effect of urbanisation on the water balance of a catchment with shallow groundwater. *Journal of Hydrology*, 485, 162-176. <https://doi.org/10.1016/j.jhydrol.2012.04.027>
- Battin, T. J., Kaplan, L. A., Findlay, S., Hopkinson, E. M., Packman, A. I., Newbold, J. D., & Sabater, F. (2008). Biophysical controls on organic carbon fluxes in fluvial networks. *Nature geoscience*, 1, 95-101.
- Baudron, P., Barbecot, F., Gillon, M., Aróstegui, J. L. G., Travi, Y., Leduc, C., Castillo, F. G., & Martinez-Vicente, D. (2016). Assessing Groundwater Residence Time in a Highly Anthropized Unconfined Aquifer Using Bomb Peak ¹⁴C and Reconstructed Irrigation Water ³H. *Radiocarbon*, 55(2), 993-1006. <https://doi.org/10.1017/s0033822200058136>
- Bazemore, D. E., Eshleman, K. N., & Hollenbeck, K. J. (1994). The role of soil water in stormflow generation in a forested headwater catchment: synthesis of natural tracer and hydrometric evidence. *Journal of Hydrology*, 162, 47-75.

- Beck, H. E., van Dijk, A. I. J. M., Miralles, D. G., de Jeu, R. A. M., Sampurno Bruijnzeel, L. A., McVicar, T. R., & Schellekens, J. (2013). Global patterns in base flow index and recession based on streamflow observations from 3394 catchments. *Water resources research*, 49(12), 7843-7863. <https://doi.org/10.1002/2013wr013918>
- Begemann, F., & Libby, W. F. (1957). Continental water balance, ground water inventory and storage times, surface ocean mixing rates and world-wide water circulation patterns from cosmic-ray and bomb tritium. *Geochimica et Cosmochimica Acta*, 12(4), 277-296. [https://doi.org/10.1016/0016-7037\(57\)90040-6](https://doi.org/10.1016/0016-7037(57)90040-6)
- Benettin, P., Bailey, S. W., Campbell, J. L., Green, M. B., Rinaldo, A., Likens, G. E., McGuire, K. J., & Botter, G. (2015). Linking water age and solute dynamics in streamflow at the Hubbard Brook Experimental Forest, NH, USA. *Water resources research*, 51(11), 9256-9272. <https://doi.org/10.1002/2015wr017552>
- Benettin, P., Bailey, S. W., Rinaldo, A., Likens, G. E., McGuire, K. J., & Botter, G. (2017). Young runoff fractions control streamwater age and solute concentration dynamics. *Hydrological processes*, 31(16), 2982-2986. <https://doi.org/10.1002/hyp.11243>
- Benettin, P., & Bertuzzo, E. (2018). tran-SAS v1.0: a numerical model to compute catchment-scale hydrologic transport using StorAge Selection functions. *Geoscientific Model Development*, 11(4), 1627-1639. <https://doi.org/10.5194/gmd-11-1627-2018>
- Benettin, P., Rodriguez, N. B., Sprenger, M., Kim, M., Klaus, J., Harman, C. J., van der Velde, Y., Hrachowitz, M., Botter, G., McGuire, K. J., Kirchner, J. W., Rinaldo, A., & McDonnell, J. J. (2022). Transit Time Estimation in Catchments: Recent Developments and Future Directions. *Water resources research*, 58(11). <https://doi.org/10.1029/2022wr033096>
- Benettin, P., Soulsby, C., Birkel, C., Tetzlaff, D., Botter, G., & Rinaldo, A. (2017). Using SAS functions and high-resolution isotope data to unravel travel time distributions in headwater catchments. *Water resources research*, 53(3), 1864-1878. <https://doi.org/10.1002/2016wr020117>
- Berghuijs, W. R., & Kirchner, J. W. (2017). The relationship between contrasting ages of groundwater and streamflow. *Geophysical Research Letters*, 44(17), 8925-8935. <https://doi.org/10.1002/2017gl074962>

- Bethke, M. C., & Johnson, T. M. (2007). Groundwater age and groundwater age dating. *The Annual Review of Earth and Planetary Sciences*, 34. <https://doi.org/10.1146/annurev.earth.36.031207.124210>
- Bhaskar, A. S., Beesley, L., Burns, M. J., Fletcher, T. D., Hamel, P., Oldham, C. E., & Roy, A. H. (2016). Will it rise or will it fall? Managing the complex effects of urbanization on base flow. *Freshwater Science*, 35(1), 293-310. <https://doi.org/10.1086/685084>
- Blanc, T., Peel, M., Brennwald, M. S., Kipfer, R., & Brunner, P. (2024). Efficient injection of gas tracers into rivers: A tool to study Surface water-Groundwater interactions. *Water Res*, 254, 121375. <https://doi.org/10.1016/j.watres.2024.121375>
- Bloomfield, J. P., Williams, R. J., Gooddy, D. C., Cape, J. N., & Guha, P. (2006). Impacts of climate change on the fate and behaviour of pesticides in surface and groundwater--A UK perspective. *Sci Total Environ*, 369(1-3), 163-177. <https://doi.org/10.1016/j.scitotenv.2006.05.019>
- Boano, F., Harvey, J. W., Marion, A., Packman, A. I., Revelli, R., Ridolfi, L., & Wörman, A. (2014). Hyporheic flow and transport processes: Mechanisms, models, and biogeochemical implications. *Reviews of Geophysics*, 52(4), 603-679. <https://doi.org/10.1002/2012rg000417>
- Böhlke, J. K., & Denver, J. M. (1995). Combined use of groundwater dating, chemical and isotopic analyses to resolve the history and fate of nitrate contamination in two agricultural watersheds, Atlantic coastal plain, Maryland. *Water resources research*, 31(9), 2319-2339.
- Boulton, A. J., Findlay, S., Marmonier, P., & Maurice Valett, E. H. (1998). The functional significance of the hyporheic zone in streams and rivers. *Annual Review of Ecology and Systematics*, 29, 59-81.
- Boulton, A. J., & Hancock, P. J. (2006). Rivers as groundwater-dependent ecosystems: a review of degrees of dependency, riverine processes and management implications. *Australian Journal of Botany*, 54(2). <https://doi.org/10.1071/bt05074>
- Brennwald, M. S., Peel, M., Blanc, T., Tomonaga, Y., Kipfer, R., Brunner, P., & Hunkeler, D. (2022). New Experimental Tools to Use Noble Gases as Artificial Tracers for Groundwater Flow. *Frontiers in Water*, 4. <https://doi.org/10.3389/frwa.2022.925294>

- Brennwald, M. S., Schmidt, M., Oser, J., & Kipfer, R. (2016). A Portable and Autonomous Mass Spectrometric System for On-Site Environmental Gas Analysis. *Environ Sci Technol*, 50(24), 13455-13463. <https://doi.org/10.1021/acs.est.6b03669>
- Brennwald, M. S., Tomonaga, Y., & Kipfer, R. (2020). Deconvolution and compensation of mass spectrometric overlap interferences with the miniRUEDI portable mass spectrometer. *MethodsX*, 7, 101038. <https://doi.org/10.1016/j.mex.2020.101038>
- Briggs, M. A., Gooseff, M. N., Arp, C. D., & Baker, M. A. (2009). A method for estimating surface transient storage parameters for streams with concurrent hyporheic storage. *Water resources research*, 45(4). <https://doi.org/10.1029/2008wr006959>
- Brujinzeel, L. A., Köhler, L., Frumau, A., & Schellekens, J. (2002). *Hydrological impacts of converting tropical montane cloud forest to pasture with initial reference to northern Costa Rica*.
- Brunner, P., Therrien, R., Renard, P., Simmons, C. T., & Franssen, H.-J. H. (2017). Advances in understanding river-groundwater interactions. *Reviews of Geophysics*, 55(3), 818-854. <https://doi.org/10.1002/2017rg000556>
- Bu, X., & Warner, M. J. (1995). Solubility of chlorofluorocarbon 113 in water and seawater. *Deep-Sea Research*, 42(7), 1151-1161.
- Bullister, J. L., Wisegarver, D. P., & Menzia, F. A. (2002). The solubility of sulfur hexafluoride in water and seawater. *Deep-Sea Research*, 49, 175-187.
- Burnard, P. (2013). *The Noble Gases as Geochemical Tracers*. <https://doi.org/10.1007/978-3-642-28836-4>
- Burri, N. M., Weatherl, R., Moeck, C., & Schirmer, M. (2019). A review of threats to groundwater quality in the anthropocene. *Science of the Total Environment*, 684, 136-154. <https://doi.org/10.1016/j.scitotenv.2019.05.236>
- Busenberg, E., & Plummer, L. N. (2000). Dating young groundwater with sulfur hexafluoride: Natural and anthropogenic sources of sulfur hexafluoride. *Water resources research*, 36(10), 3011-3030. <https://doi.org/10.1029/2000wr900151>
- Busenberg, E., & Plummer, L. N. (2010). A rapid method for the measurement of sulfur hexafluoride (SF₆), trifluoromethyl sulfur pentafluoride (SF₅CF₃), and Halon 1211

- (CF₂ClBr) in hydrologic tracer studies. *Geochemistry, Geophysics, Geosystems*, 11(11), n/a-n/a.
<https://doi.org/10.1029/2010gc003312>
- Calder, I. (2005). *Blue revolution - Integrated Land and Water Resources Management*. Routledge.
<https://doi.org/https://doi.org/10.4324/9781849770613>
- Carton, C., Barbecot, F., Helie, J. F., Horoi, V., Birks, J., Picard, A., & Mona, J. (2024). Affordable event and monthly rain samplers: Improving isotopic datasets to understand meteorological processes. *Rapid Commun Mass Spectrom*, 38(7), e9710.
<https://doi.org/10.1002/rcm.9710>
- Castonguay, S., & Nadeau, L. (2012). *Géologie simplifiée de la région de Québec, Québec*.
- Chambers, L. A., Gooddy, D. C., & Binley, A. M. (2018). Use and application of CFC-11, CFC-12, CFC-113 and SF₆ as environmental tracers of groundwater residence time: A review. *Geoscience Frontiers*, 10, 10. <https://doi.org/https://doi.org/10.1016/j.gsf.2018.02.017>
- Chapman, T. (1999). A comparison of algorithms for stream flow recession and baseflow separation. *Hydrological processes*, 13, 701-714.
- Cirpka, O. A., Fienen, M. N., Hofer, M., Hoehn, E., Tessarini, A., Kipfer, R., & Kitanidis, P. K. (2007). Analyzing bank filtration by deconvoluting time series of electric conductivity. *Ground Water*, 45, 318-328.
- Clark, I. D. (2015). *Groundwater geochemistry and isotopes*. CRC Press.
- Clark, I. D., & Fritz, P. (1997). *Environmental isotopes in hydrogeology*.
- Clark, J. F., Hudson, G. B., & Avisar, D. (2005). Gas transport below artificial recharge ponds: insights from dissolved noble gases and a dual gas (SF₆ and ³He) tracer experiment. *Environ. Sci. Technol.*, 39, 3939-3945.
- Clark, J. F., Schlosser, C., Stute, M., & Simpson, H. J. (1996). SF₆-³He tracer release experiment: a new method of determining longitudinal dispersion coefficients in large rivers. *Environ Sci Technol*, 30, 1527-1532.
- Collischonn, W., & Fan, F. M. (2013). Defining parameters for Eckhardt's digital baseflow filter. *Hydrological processes*, 27(18), 2614-2622. <https://doi.org/10.1002/hyp.9391>

- Constantz, J. (1998). Interaction between stream temperature, streamflow, and groundwater exchanges in alpine streams. *Water resources research*, 34(7), 1609-1615. <https://doi.org/10.1029/98wr00998>
- Cook, P. G. (2013). Estimating groundwater discharge to rivers from water chemistry surveys. *Hydrological processes*, 27, 3694-3707. <https://doi.org/10.1002/hyp.9493>
- Cook, P. G., Favreau, G., Dighton, J. C., & Tickell, S. (2003). Determining natural groundwater influx to a tropical river using radon, chlorofluorocarbons and ionic environmental tracers. *Journal of Hydrology*, 277, 74-88. [https://doi.org/10.1016/S0022-1694\(03\)0087-8](https://doi.org/10.1016/S0022-1694(03)0087-8)
- Cook, P. G., & Herczeg, A. L. (2000). *Environmental Tracers in Subsurface Hydrology*. Springer Science.
- Cook, P. G., Lamontagne, S., Berhane, D., & Clark, J. F. (2006). Quantifying groundwater discharge to Cockburn River, southeastern Australia, using dissolved gas tracers ^{222}Rn and SF_6 . *Water resources research*, 42, 12. <https://doi.org/doi:10.1029/2006WR004921>
- Cook, P. G., & Solomon, D. K. (1997). Recent advances in dating young groundwater: chlorofluorocarbons, $^3\text{H}/^3\text{He}$ and ^{85}Kr . *Journal of Hydrology*, 191, 245-265.
- Corcho Alvarado, J. A., Purtschert, R., Barbécot, F., Chabault, C., Rueedi, J., Schneider, V., Aeschbach-Hertig, W., Kipfer, R., & Loosli, H. H. (2007). Constraining the age distribution of highly mixed groundwater using ^{39}Ar : A multiple environmental tracer (^3H , ^3He , ^{85}Kr , ^{39}Ar and ^{14}C) study in the semiconfined Fontainebleau Sands Aquifer (France). *Water resources research*, 43. <https://doi.org/doi:10.1029/2006WR005096>
- Corcho Alvarado, J. A., Purtschert, R., Hinsby, K., Trolldborg, L., Hofer, M., Kipfer, R., Aeschbach-Hertig, W., & Arno-Synal, H. (2005). ^{36}Cl in modern groundwater dated by a multi-tracer approach ($^3\text{H}/^3\text{He}$, SF_6 , CFC-12 and ^{85}Kr): a case study in quaternary sand aquifers in the Odense Pilot River Basin, Denmark. *Applied geochemistry*, 20(3), 599-609. <https://doi.org/10.1016/j.apgeochem.2004.09.018>
- Craig, H. (1961). Isotopic Variations in Meteoric Waters. *Science*, 133(3465), 1702-1703. <https://doi.org/10.1126/science.133.3465.1702>

- Cranswick, R. H., Cook, P. G., & Lamontagne, S. (2014). Hyporheic zone exchange fluxes and residence times inferred from riverbed temperature and radon data. *Journal of Hydrology*, 519, 1870-1881. <https://doi.org/10.1016/j.jhydrol.2014.09.059>
- Darling, W. G., Gooddy, D. C., MacDonald, A. M., & Morris, B. L. (2012). The practicalities of using CFCs and SF₆ for groundwater dating and tracing. *Applied geochemistry*, 27(9), 39.
- de Graaf, I. E. M., Gleeson, T., (Rens) van Beek, L. P. H., Sutanudjaja, E. H., & Bierkens, M. F. P. (2019). Environmental flow limits to global groundwater pumping. *Nature*, 574, 90-108. <https://doi.org/10.1038/s41586-019-1594-4>
- De Smedt, F. (2007). Analytical solution and analysis of solute transport in rivers affected by diffusive transfer in the hyporheic zone. *Journal of Hydrology*, 339(1-2), 29-38. <https://doi.org/10.1016/j.jhydrol.2007.02.002>
- Doctor, D. H., Alexander, E. C., Petrič, M., Kogovšek, J., Urbanc, J., Lojen, S., & Stichler, W. (2006). Quantification of karst aquifer discharge components during storm events through end-member mixing analysis using natural chemistry and stable isotopes as tracers. *Hydrogeology Journal*, 14(7), 1171-1191. <https://doi.org/10.1007/s10040-006-0031-6>
- Dragoni, W., & Sukhija, B. S. (2008). Climate change and groundwater: a short review. *Geological Society, London, Special Publications*, 288(1), 1-12. <https://doi.org/10.1144/sp288.1>
- Duncan, H. P. (2019). Baseflow separation – A practical approach. *Journal of Hydrology*, 575, 308-313. <https://doi.org/10.1016/j.jhydrol.2019.05.040>
- Eckhardt, K. (2005). How to construct recursive digital filters for baseflow separation. *Hydrological processes*, 19, 9. <https://doi.org/10.1002/hyp.5675>
- Eckhardt, K. (2008). A comparison of baseflow indices, which were calculated with seven different baseflow separation methods. *Journal of Hydrology*, 352, 6. <https://doi.org/10.1016/j.jhydrol.2008.01.005>
- Engenkamp, H. G. M. (1994). *The Geochemistry of Stable Chlorine and Bromine Isotopes* [Utrecht University]. Utrecht.
- Ekwurzel, B., Schlosser, P., & Smethie, W. M. J. (1994). Dating of shallow groundwater: Comparison of the transient tracers ³H/³He, chlorofluorocarbons, and ⁸⁵Kr. *Water resources research*, 30(6), 1693-1708.

- Engelhardt, I., Piepenbrink, M., Trauth, N., Stadler, S., Kludt, C., Schulz, M., Schüth, C., & Ternes, T. A. (2011). Comparison of tracer methods to quantify hydrodynamic exchange within the hyporheic zone. *Journal of Hydrology*, 400(1-2), 255-266. <https://doi.org/10.1016/j.jhydrol.2011.01.033>
- Eriksson, E. (1958). The Possible Use of Tritium' for Estimating Groundwater Storage. *Tellus A: Dynamic Meteorology and Oceanography*, 10(4), 472-478. <https://doi.org/10.3402/tellusa.v10i4.9265>
- Fan, Y., Li, H., & Miguez-Macho, G. (2013). Global patterns of groundwater table depth. *Science*, 339(6122), 940-943. <https://doi.org/10.1126/science.1229881>
- Fontes, J.-C. (1976). *Isotopes du milieu et cycles des eaux naturelles : quelques aspects* Université Pierre et Marie Curie Paris VII].
- Freeze, A., & Cherry, J. (1979). *Groundwater*.
- Gardner, P., & Solomon, D. K. (2009). An advanced passive diffusion sampler for the determination of dissolved gas concentrations. *Water resources research*, 45, 12. <https://doi.org/10.1029/2008WR007399>
- Gasperi, J., Dris, R., Bonin, T., Rocher, V., & Tassin, B. (2014). Assessment of floating plastic debris in surface water along the Seine River. *Environ Pollut*, 195, 163-166. <https://doi.org/10.1016/j.envpol.2014.09.001>
- Genuchten, M. T. v., Leij, F. J., Skaggs, T. H., Toride, N., Bradford, S. A., & Pontedeiro, E. M. (2013a). Exact analytical solutions for contaminant transport in rivers 1. The equilibrium advection-dispersion equation. *Journal of Hydrology and Hydromechanics*, 61(2), 146-160. <https://doi.org/10.2478/johh-2013-0020>
- Genuchten, M. T. v., Leij, F. J., Skaggs, T. H., Toride, N., Bradford, S. A., & Pontedeiro, E. M. (2013b). Exact Analytical Solutions for Contaminant Transport in Rivers
2. Transient storage and decay chain solutions. *Journal of Hydrology and Hydromechanics*, 61(3), 250-259. <https://doi.org/10.2478/johh-2013-0032>
- Gilmore, T. E., Genereux, D. P., Solomon, D. K., & Solder, J. E. (2016). Groundwater transit time distribution and mean from streambed sampling in an agricultural coastal plain watershed,

- North Carolina, USA. *Water resources research*, 52(3), 2025-2044.
<https://doi.org/10.1002/2015wr017600>
- Giordano, M. (2009). Global Groundwater? Issues and Solutions. *Annual Review of Environment and Sciences* 34, 153-178. <https://doi.org/10.1146/annurev.envIRON.030308.100251>
- Gleeson, T., & Richter, B. (2017). How much groundwater can we pump and protect environmental flows through time? Presumptive standards for conjunctive management of aquifers and rivers. *River Research and Applications*, 34, 83-92.
- Gleick, P. H. (1989). Climate change hydrology and water resources. *Review of geophysics*, 27(3), 329-344.
- Godon, A., Jendrzewski, N., Eggenkamp, H. G. M., Banks, D. A., Ader, M., Coleman, M. L., & Pineau, F. (2004). A cross-calibration of chlorine isotopic measurements and suitability of seawater as the international reference material. *Chemical Geology*, 207(1-2), 1-12.
<https://doi.org/10.1016/j.chemgeo.2003.11.019>
- Godsey, S. E., Aas, W., Clair, T. A., de Wit, H. A., Fernandez, I. J., Kahl, J. S., Malcolm, I. A., Neal, C., Neal, M., Nelson, S. J., Norton, S. A., Palucis, M. C., Skjelkvåle, B. L., Soulsby, C., Tetzlaff, D., & Kirchner, J. W. (2010). Generality of fractal 1/f scaling in catchment tracer time series, and its implications for catchment travel time distributions. *Hydrological processes*, 24(12), 1660-1671. <https://doi.org/10.1002/hyp.7677>
- Gonzales, A. L., Nonner, J., Heijkers, J., & Uhlenbrook, S. (2009). Comparison of different base flow separation methods in a lowland catchment. *Hydrology and Earth System sciences*, 13, 2055-2068.
- Goody, D. C., Darling, W. G., Abesser, C., & Lapworth, D. J. (2006). Using chlorofluorocarbons (CFCs) and sulphur hexafluoride (SF₆) to characterise groundwater movement and residence time in a lowland Chalk catchment. *Journal of Hydrology*, 330, 44-52.
<https://doi.org/10.1016/j.jhydrol.2006.04.011>
- Gooseff, M. N. (2010). Defining Hyporheic Zones - Advancing Our Conceptual and Operational Definitions of Where Stream Water and Groundwater Meet. *Geography Compass*, 4(8), 945-955. <https://doi.org/10.1111/j.1749-8198.2010.00364.x>

- Green, T. R., Taniguchi, M., Kooi, H., Gurdak, J. J., Allen, D. M., Hiscock, K. M., Treidel, H., & Aureli, A. (2011). Beneath the surface of global change: Impacts of climate change on groundwater. *Journal of Hydrology*, 405(3-4), 532-560.
<https://doi.org/10.1016/j.jhydrol.2011.05.002>
- Gröning, M., Lutz, H. O., Roller-Lutz, Z., Kralik, M., Gourcy, L., & Pölsenstein, L. (2012). A simple rain collector preventing water re-evaporation dedicated for $\delta^{18}\text{O}$ and $\delta^2\text{H}$ analysis of cumulative precipitation samples. *Journal of Hydrology*, 448-449, 195-200.
<https://doi.org/10.1016/j.jhydrol.2012.04.041>
- Gupta, H. V., Kling, H., & Yilmaz, K. K. (2009). Decomposition of the Mean Squared Error & NSE Performnce Criteria: Implications for Improving Hydrological Modelling. *Journal of Hydrology*, 377(1-2), 80-91.
- Haase, D. (2009). Effects of urbanisation on the water balance – A long-term trajectory. *Environmental Impact Assessment Review*, 29(4), 211-219.
<https://doi.org/10.1016/j.eiar.2009.01.002>
- Hahladakis, J. N., Velis, C. A., Weber, R., Iacovidou, E., & Purnell, P. (2018). An overview of chemical additives present in plastics: Migration, release, fate and environmental impact during their use, disposal and recycling. *J Hazard Mater*, 344, 179-199.
<https://doi.org/10.1016/j.jhazmat.2017.10.014>
- Hancock, P. J., Boulton, A. J., & Humphreys, W. F. (2005). Aquifers and hyporheic zones: Towards an ecological understanding of groundwater. *Hydrogeology Journal*, 13(1), 98-111.
<https://doi.org/10.1007/s10040-004-0421-6>
- Hardison, E. C., O'Driscoll, M. A., DeLoatch, J. P., Howard, R. J., & Brinson, M. M. (2009). Urban Land Use, Channel Incision, and Water Table Decline Along Coastal Plain Streams, North Carolina. *JAWRA Journal of the American Water Resources Association*, 45(4), 1032-1046.
<https://doi.org/10.1111/j.1752-1688.2009.00345.x>
- Harman, C. J. (2015). Time-variable transit time distributions and transport: Theory and application to storage-dependent transport of chloride in a watershed. *Water resources research*, 51(1), 1-30. <https://doi.org/10.1002/2014wr015707>

- Harman, C. J., Ward, A. S., & Ball, A. (2016). How does reach-scale stream-hyporheic transport vary with discharge? Insights from rSAS analysis of sequential tracer injections in a headwater mountain stream. *Water resources research*, 52(9), 7130-7150. <https://doi.org/10.1002/2016wr018832>
- Hayashi, M., & Rosenberry, D. O. (2002). Effects of ground water exchange on the hydrology and ecology of surface water. *Ground Water*, 40(3), 309-316.
- Heaton, T. H. E., & Vogel, J. C. (1981). Excess air in groundwater. *Journal of Hydrology*, 50, 201-216.
- Herschey, R. W. (2008). *Streamflow measurement*.
- Höhener, P., Werner, D., Balsiger, C., & Pasteris, G. (2003). Worldwide Occurrence and Fate of Chlorofluorocarbons in Groundwater. *Critical Reviews in Environmental Science and Technology*, 33(1), 1-29. <https://doi.org/10.1080/10643380390814433>
- Houle, D., Paquin, R., Camiré, C., Ouimet, R., & Duschene, L. (1997). Response of the Lake Clair Watershed (Duchesnay, Quebec) to changes in precipitation chemistry (1988-1994). *Canadian Journal of Forest Research*, 27, 1813-1821.
- Hrachowitz, M., Soulsby, C., Tetzlaff, D., & Speed, M. (2010). Catchment transit times and landscape controls - does scale matter? *Hydrological processes*, 24, 117-125.
- Hubert, P., Marin, E., Meybeck, M., Olive, P., & Siwertz, E. (1969). Aspects hydrologique, géochimique et sédimentologique de la crue exceptionnelle de la Dranse du Chablais du 22 septembre 1968. *Arch. Sci. (Genève)*, 22, 581-603.
- Hudson, R., & Fraser, J. (2005). The Mass Balance (or Dry Injection) Method. *Watershed Management Bulletin*, 9(1), 6-12.
- Hughes, C. E., & Crawford, J. (2012). A new precipitation weighted method for determining the meteoric water line for hydrological applications demonstrated using Australian and global GNIP data. *Journal of Hydrology*, 464-465, 344-351. <https://doi.org/https://doi.org/10.1016/j.jhydrol.2012.07.029>
- Humphrey, C. E., Solomon, D. K., Gilmore, T. E., MacNamara, M. R., Genereux, D. P., Mittelstet, A. R., Zeyrek, C., Zlotnik, V. A., & Jensen, C. R. (2024). Spatial Variation in Transit Time Distributions of Groundwater Discharge to a Stream Overlying the Northern High Plains

- Aquifer, Nebraska, USA. *Water resources research*, 60(2).
<https://doi.org/10.1029/2022wr034410>
- IAEA. (2006). *Use of chlorofluorocarbons in hydrology : a guidebook*.
- IAEA. (2013). *Technical procedures for GNIP stations*. IAEA.
- Jähne, B., Heinz, G., & Dietrich, W. (1987). Measurement of the diffusion coefficients of sparingly soluble gases in water. *Journal of Geophysical research*, 92(C10).
<https://doi.org/10.1029/JC092iC10p10767>
- Jasechko, S. (2019). Global Isotope Hydrogeology—Review. *Reviews of Geophysics*, 57(3), 835-965.
<https://doi.org/10.1029/2018rg000627>
- Jasechko, S., Kirchner, J. W., Welker, J. M., & McDonnell, J. (2016). Substantial proportion of global streamflow less than three months old. *Nature geoscience*, 9, 126-129.
<https://doi.org/10.1038/NGEO2636>
- Jensen, C. R., Genereux, D. P., Gilmore, T. E., Solomon, D. K., Mittelstet, A. R., Humphrey, C. E., MacNamara, M. R., Zeyrek, C., & Zlotnik, V. A. (2022). Estimating groundwater mean transit time from SF₆ in stream water: field example and planning metrics for a reach mass-balance approach. *Hydrogeology Journal*. <https://doi.org/10.1007/s10040-021-02435-8>
- Jensen, C. R., Genereux, D. P., Solomon, D. K., Knappe, D. R. U., & Gilmore, T. E. (2024). Forecasting and Hindcasting PFAS Concentrations in Groundwater Discharging to Streams near a PFAS Production Facility. *Environ Sci Technol*.
<https://doi.org/10.1021/acs.est.4c06697>
- Jung, M., & Aeschbach-Hertig, W. (2018). A new software tool for the analysis of noble gas data sets from (ground)water. *Environmental Modelling & Software*, 103, 11.
- Jurgens, B. C., Böhlke, J. K., & Eberts, S. M. (2012). *TracerLPM (Version 1): An Excel Workbook for interpreting groundwater age distributions from environmental tracer data*.
- Kalbus, E., Reinstorf, F., & Schirmer, M. (2006). Measuring methods for groundwater - surface water interactions: a review. *Hydrology and Earth System sciences*, 10, 873-887.
- Kamdee, K., Corcho Alvarado, J. A., Yongprawat, M., Occarach, O., Hunyek, V., Wongsit, A., Saengkorakot, C., Chanruang, P., Polee, C., Uapoonphol, N., Mabry, J., Romeo, N., Hillegonds, D., Zappala, J. C., Mueller, P., & Matsumoto, T. (2023). Using (81)Kr and

- isotopic tracers to characterise old groundwater in the Bangkok metropolitan and vicinity areas. *Isotopes Environ Health Stud*, 1-28. <https://doi.org/10.1080/10256016.2023.2261613>
- Kaufman, R. S., Long, A., Bentley, H., & Davis, S. (1984). Natural chlorine isotope variations. *Nature*, 209, 338-340.
- Kazemi, G. A., Lehr, J. H., & Perrochet, P. (2006). *Groundwater age*.
- Kersting, A., Brander, S., & Suckow, A. (2021). Modelling (85)Kr datasets with python for applications in tracer hydrology and to investigate atmospheric circulation. *MethodsX*, 8, 101245. <https://doi.org/10.1016/j.mex.2021.101245>
- Kersting, A., Schlosser, C., Bollhofer, A., & Suckow, A. (2020). Evaluating 5 decades of atmospheric (85)Kr measurements in the southern hemisphere to derive an input function for dating water and ice with implications for interhemispheric circulation and the global (85)Kr emission inventory. *J Environ Radioact*, 225, 106451. <https://doi.org/10.1016/j.jenvrad.2020.106451>
- Kersting, A., Schlosser, C., Schmid, S., Konrad, M., Bollhofer, A., Barry, K., & Suckow, A. (2020). Krypton-85 datasets of the northern and southern hemisphere collected over the past 60 years. *Data Brief*, 33, 106522. <https://doi.org/10.1016/j.dib.2020.106522>
- Khatri, N., & Tyagi, S. (2014). Influences of natural and anthropogenic factors on surface and groundwater quality in rural and urban areas. *Frontiers in Life Science*, 8(1), 23-39. <https://doi.org/10.1080/21553769.2014.933716>
- Kim, M., Pangle, L. A., Cardoso, C., Lora, M., Volkmann, T. H. M., Wang, Y., Harman, C. J., & Troch, P. A. (2016). Transit time distributions and StorAge Selection functions in a sloping soil lysimeter with time-varying flow paths: Direct observation of internal and external transport variability. *Water resources research*, 52(9), 7105-7129. <https://doi.org/10.1002/2016wr018620>
- Kipfer, R., Aeschbach-Hertig, W., Peeters, F., & Stute, M. (2002). Noble gases in lakes and groundwaters. *Reviews in Mineralogy and Geochemistry*, 47, 615-700.
- Kirchner, J. W. (2003). A double paradox in catchment hydrology and geochemistry. *Hydrological processes*, 17, 871-874. <https://doi.org/10.1002/hyp.5108>

- Kirchner, J. W., Feng, X., & Neal, C. (2000). Fractal stream chemistry and its implications for contaminant transport in catchments. *Nature*, 403, 524-527.
- Kirchner, J. W., & Neal, C. (2013). Universal fractal scaling in stream chemistry and its implications for solute transport and water quality trend detection. *Proc Natl Acad Sci U S A*, 110(30), 12213-12218. <https://doi.org/10.1073/pnas.1304328110>
- Klaus, J., & McDonnell, J. J. (2013). Hydrograph separation using stable isotopes: Review and evaluation. *Journal of Hydrology*, 505, 47-64. <https://doi.org/10.1016/j.jhydrol.2013.09.006>
- Klöcking, B., & Haberlandt, U. (2002). Impact of land use changes on water dynamics - a case study in temperate meso and macroscale river basins. *Physics and Chemistry of the Earth*, 27, 619-629.
- Knoben, W. J. M., Freer, J. E., & Woods, R. A. (2019). Technical note: Inherent benchmark or not? Comparing Nash–Sutcliffe and Kling–Gupta efficiency scores. *Hydrology and Earth System sciences*, 23(10), 4323-4331. <https://doi.org/10.5194/hess-23-4323-2019>
- Koh, D.-C., Plummer, L. N., Busenberg, E., & Kim, Y. (2007). Evidence for terrigenic SF₆ in groundwater from basaltic aquifers, Jeju Island, Korea: Implications for groundwater dating. *Journal of Hydrology*, 339, 12.
- Konikow, L. F., & Kendy, E. (2005). Groundwater depletion: A global problem. *Hydrogeology Journal*, 13, 317-320. <https://doi.org/10.1007/s10040-004-0411-8>
- Kundzewicz, Z. W. (2008). Climate change impacts on the hydrological cycle. *Ecohydrology & Hydrobiology*, 8(2-4), 195-203. <https://doi.org/10.2478/v10104-009-0015-y>
- Kurylyk, B. L., MacQuarrie, K. T. B., & McKenzie, J. M. (2014). Climate change impacts on groundwater and soil temperatures in cold and temperate regions: Implications, mathematical theory, and emerging simulation tools. *Earth-Science Reviews*, 138, 313-334. <https://doi.org/10.1016/j.earscirev.2014.06.006>
- Ladouche, B., Probst, A., Viville, D., Idir, S., Baqué, D., Loubet, M., Probst, J.-L., & Bariac, T. (2000). Hydrograph separation using isotopic, chemical and hydrological approaches (Strengbach catchment, France). *Journal of Hydrology*, 242, 255-274.
- Lamontagne, S., Taylor, A. R., Battle-Aguilar, J., Suckow, A., Cook, P. G., Smith, S. D., Morgenstern, U., & Stewart, M. K. (2015). River infiltration to a subtropical alluvial aquifer inferred using

- multiple environmental tracers. *Water resources research*, 51, 4532-4549.
<https://doi.org/10.1002/2014WR015663>
- Langmuir, D. (1997). *Aqueous environmental geochemistry*.
- Lefebvre, K., Barbecot, F., Larocque, M., & Gillon, M. (2015). Combining isotopic tracers (^{222}Rn and $\delta^{13}\text{C}$) for improved modelling of groundwater discharge to small rivers. *Hydrological processes*, 29, 2814-2822. <https://doi.org/10.1002/hyp.10405>
- Leibundgut, C., Maloszewski, P., & Külls, C. (2009). *Tracers in Hydrology*. Wiley-Blackwell.
- Lerner, D. N. (1986). Leaking pipes recharge groundwater. *Ground Water*, 24(5), 654-662.
<https://doi.org/10.1111/j.1745-6584.1986.tb03714.x>
- Lerner, D. N. (2002). Identifying and quantifying urban recharge: a review. *Hydrogeology Journal*, 10(1), 143-152. <https://doi.org/10.1007/s10040-001-0177-1>
- Libby, W. F. (1953). The potential usefulness of natural tritium. *Proceedings of the National Academy of Science*, 39(4), 245-247.
- Licha, T., Niedbala, A., Bozau, E., & Geyer, T. (2013). An assessment of selected properties of the fluorescent tracer, Tinopal CBS-X related to conservative behavior, and suggested improvements. *Journal of Hydrology*, 484, 38-44.
<https://doi.org/10.1016/j.jhydrol.2013.01.006>
- Lyne, V., & Hollick, M. (1979). Stochastic time-variable rainfall-runoff modelling. *Proceedings of the Hydrology and Water Resources Symposium*, 89-92.
- MacDonald, A. M., Darling, W. G., Ball, D. F., & Oster, H. (2003). Identifying trends in groundwater quality using residence time indicators: an example from the Permian aquifer of Dumfries, Scotland. *Hydrogeology Journal*, 11(4), 504-517.
<https://doi.org/10.1007/s10040-003-0275-3>
- Maher, K. (2011). The role of fluid residence time and topographic scales in determining chemical fluxes from landscapes. *Earth and Planetary Science Letters*, 312(1-2), 48-58.
<https://doi.org/10.1016/j.epsl.2011.09.040>
- Maloszewski, P., Rauert, W., Stichler, W., & Herrmann, A. (1983). Application of flow models in an alpine catchment area using tritium and deuterium data. *Journal of Hydrology*, 66, 319-330.

- Mamyrin, B. A., & Tolstikhin, I. N. (1984). *Helium isotopes in nature*. Elsevier.
- Masse-Dufresne, J., Barbecot, F., Baudron, P., & Gibson, J. (2021). Quantifying floodwater impacts on a lake water budget via volume-dependent transient stable isotope mass balance. *Hydrology and Earth System sciences*, 25(6), 3731-3757. <https://doi.org/10.5194/hess-25-3731-2021>
- McDonald, R. I., Douglas, I., Revenga, C., Hale, R., Grimm, N., Gronwall, J., & Fekete, B. (2011). Global urban growth and the geography of water availability, quality, and delivery. *Ambio*, 40(5), 437-446. <https://doi.org/10.1007/s13280-011-0152-6>
- McDonnell, J. J., McGuire, K., Aggarwal, P., Beven, K. J., Biondi, D., Destouni, G., Dunn, S. M., James, A., Kirchner, J., Kraft, P., Lyon, S., Maloszewski, P., Newman, B., Pfister, L., Rinaldo, A., Rodhe, A., Sayama, T., Seibert, J., Solomon, D. K., . . . Wrede, S. (2010). How old is streamwater? Open questions in catchment transit time conceptualization, modelling and analysis. *Hydrological processes*, 24, 1745-1754.
- McGrane, S. J. (2016). Impacts of urbanisation on hydrological and water quality dynamics, and urban water management: a review. *Hydrological Sciences Journal*, 61(13), 2295-2311. <https://doi.org/10.1080/02626667.2015.1128084>
- McGuire, K. J., & McDonnell, J. J. (2006). A review and evaluation of catchment transit time modeling. *Journal of Hydrology*, 330, 543-563.
- McGuire, K. J., McDonnell, J. J., Weiler, M., Kendall, C., McGlynn, B. L., Welker, J. M., & Seibert, J. (2005). The role of topography on catchment-scale water residence time. *Water resources research*, 41. <https://doi.org/10.1029/2004WR003657>
- McIntyre, J. K., Winters, N., Rozmyn, L., Haskins, T., & Stark, J. D. (2019). Metals leaching from common residential and commercial roofing materials across four years of weathering and implications for environmental loading. *Environ Pollut*, 255(Pt 2), 113262. <https://doi.org/10.1016/j.envpol.2019.113262>
- Meixner, T., Manning, A. H., Stonestrom, D. A., Allen, D. M., Ajami, H., Blasch, K. W., Brookfield, A. E., Castro, C. L., Clark, J. F., Gochis, D. J., Flint, A. L., Neff, K. L., Niraula, R., Rodell, M., Scanlon, B. R., Singha, K., & Walvoord, M. A. (2016). Implications of projected climate

- change for groundwater recharge in the western United States. *Journal of Hydrology*, 534, 124-138. <https://doi.org/10.1016/j.jhydrol.2015.12.027>
- Menberg, K., Blum, P., Kurylyk, B. L., & Bayer, P. (2014). Observed groundwater temperature response to recent climate change. *Hydrology and Earth System sciences*, 18(11), 4453-4466. <https://doi.org/10.5194/hess-18-4453-2014>
- Meyzonnat, G., Musy, S., Corcho-Alvarado, J. A., Barbecot, F., Pinti, D. L., Purtschert, R., Lauzon, J. M., & McCormack, R. (2023). Age distribution of groundwater in fractured aquifers of the St. Lawrence Lowlands (Canada) determined by environmental tracers (3H/3He, 85Kr, SF6, CFC-12, 14C). *Hydrogeology Journal*. <https://doi.org/10.1007/s10040-023-02671-0>
- Montgomery, D. R., Dietrich, W. E., & Heffner, J. T. (2002). Piezometric response in shallow bedrock at CB1: Implications for runoff generation and landsliding. *Water resources research*, 38(12). <https://doi.org/10.1029/2002wr001429>
- Morgenstern, U., Stewart, M. K., & Stenger, R. (2010). Dating of streamwater using tritium in a post nuclear bomb pulse world: continuous variation of mean transit time with streamflow. *Hydrology and Earth System sciences*, 14, 2289-2301. <https://doi.org/10.5194/hess-14-2289-2010>
- Muller, A., Osterlund, H., Marsalek, J., & Viklander, M. (2020). The pollution conveyed by urban runoff: A review of sources. *Sci Total Environ*, 709, 136125. <https://doi.org/10.1016/j.scitotenv.2019.136125>
- Murphy, S., Ouellon, T., Ballard, J.-M., Lefebvre, R., & Clark, I. D. (2010). Tritium–helium groundwater age used to constrain a groundwater flow model of a valley-fill aquifer contaminated with trichloroethylene (Quebec, Canada). *Hydrogeology Journal*, 19(1), 195-207. <https://doi.org/10.1007/s10040-010-0662-5>
- Musy, S. (2018). *Groundwater dating with Krypton-85 in combination with borehole logging* [Master Thesis, Université de Neuchâtel, Universität Bern & UQAM].
- Musy, S., Meyzonnat, G., Barbecot, F., Hunkeler, D., Sültenfuss, J., Solomon, D. K., & Purtschert, R. (2021). In-situ sampling for krypton-85 groundwater dating. *Journal of Hydrology*, X.

- O'Driscoll, M. A., DeWalle, D. R., McGuire, K. J., & Gburek, W. J. (2005). Seasonal ^{18}O variations and groundwater recharge for three landscape types in central Pennsylvania, USA. *Journal of Hydrology*, 303(1-4), 108-124. <https://doi.org/10.1016/j.jhydrol.2004.08.020>
- Okkonen, J., & Kløve, B. (2012). Assessment of temporal and spatial variation in chemical composition of groundwater in an unconfined esker aquifer in the cold temperate climate of Northern Finland. *Cold Regions Science and Technology*, 71, 118-128. <https://doi.org/10.1016/j.coldregions.2011.10.003>
- ONEMA, C. (2011). *Guide technique pour le contrôle des débits réglementaires*.
- Paul, M. J., & Meyer, J. L. (2001). Streams in the urban Landscape. *Annual Review of Ecology and Systematics*, 32, 333-365.
- Pelletier, P. M. (1988). Uncertainties in the single determination of river discharge: a literature review. *Canadian Journal of Civil Engineering*.
- Peters, N. E., Burns, D. A., & Aulenbach, B. T. (2013). Evaluation of High-Frequency Mean Streamwater Transit-Time Estimates Using Groundwater Age and Dissolved Silica Concentrations in a Small Forested Watershed. *Aquatic Geochemistry*, 20(2-3), 183-202. <https://doi.org/10.1007/s10498-013-9207-6>
- Picard, A., Barbecot, F., Bardoux, G., Agrinier, P., Gillon, M., Corcho Alvarado, J. A., Schneider, V., Hélie, J.-F., & de Oliveira, F. (2024). The potential of isotopic tracers for precise and environmentally clean stream discharge measurements. *Hydrology*, 11(1). <https://doi.org/10.3390/hydrology11010001>
- Picard, A., Barbecot, F., Proulx, F., Corcho Alvarado, J. A., Tremblay, Y., Gatel, L., Therrien, P., Cloutier, V., Frot, B., N'Da, B., & Beaulieu, C. (2024). The challenges of hydrograph separation and catchment mean transit time estimation in a mesoscale, urbanised, snowmelt-influenced catchment. *Journal of Hydrology*.
- Popp, A. L., Pardo-Álvarez, Á., Schilling, O. S., Scheidegger, A., Musy, S., Peel, M., Brunner, P., Purtschert, R., Hunkeler, D., & Kipfer, R. (2021). A Framework for Untangling Transient Groundwater Mixing and Travel Times. *Water resources research*, 57(4). <https://doi.org/10.1029/2020wr028362>

- Priebe, E. H., Hamilton, S. M., Lemieux, A., Rowan, D. J., & Clark, I. D. (2023). Tritium across the hydrologic systems of southern Ontario, Canada: implications for groundwater age dating in the Great Lakes Basin. *Hydrogeology Journal*, 31(3), 641-659. <https://doi.org/10.1007/s10040-023-02626-5>
- Purtschert, R. (2008). *Timescale and tracers*. Blackwell Publishing.
- Purtschert, R., Love, A. J., Jiang, W., Lu, Z. T., Yang, G. M., Fulton, S., Wohling, D., Shand, P., Aeschbach, W., Broder, L., Muller, P., & Tosaki, Y. (2023). Residence times of groundwater along a flow path in the Great Artesian Basin determined by (81)Kr, (36)Cl and (4)He: Implications for palaeo hydrogeology. *Sci Total Environ*, 859(Pt 1), 159886. <https://doi.org/10.1016/j.scitotenv.2022.159886>
- Rawls, W. J., Brakensiek, D. L., & Saxton, K. E. (1982). Estimation of Soil Water Properties. *Transactions of the ASAE*.
- Riedel, T. (2019). Temperature-associated changes in groundwater quality. *Journal of Hydrology*, 572, 206-212. <https://doi.org/10.1016/j.jhydrol.2019.02.059>
- Rimmer, A., & Hartmann, A. (2014). Optimal hydrograph separation filter to evaluate transport routines of hydrological models. *Journal of Hydrology*, 514, 249-257. <https://doi.org/10.1016/j.jhydrol.2014.04.033>
- Rinaldo, A., Benettin, P., Harman, C. J., Hrachowitz, M., McGuire, K. J., van der Velde, Y., Bertuzzo, E., & Botter, G. (2015). Storage selection functions: A coherent framework for quantifying how catchments store and release water and solutes. *Water resources research*, 51(6), 4840-4847. <https://doi.org/10.1002/2015wr017273>
- Rose, S., & Peters, N. E. (2001). Effects of urbanization on streamflow in the Atlanta area (Georgia, USA): a comparative hydrological approach. *Hydrological processes*, 15(8), 1441-1457. <https://doi.org/10.1002/hyp.218>
- Runkel, R. L. (1998). *One-dimensional transport with inflow and storage (OTIS): a solute transport model for streams and rivers*.
- Runkel, R. L., & Chapra, S. C. (1993). An efficient numerical solution of the transient storage equations for solute transport in small streams. *Water resources research*, 29(1), 211-215.

- Sanford, W. E., Casile, G., & Haase, K. B. (2015). Dating baseflow in streams using dissolved gases and diurnal temperature changes. *Water resources research*, 51, 14. <https://doi.org/10.1002/2014WR016796>
- Sanford, W. E., Shropshire, R. G., & Solomon, D. K. (1996). Dissolved gas tracers in groundwater: Simplified injection, sampling, and analysis. *Water resources research*, 32 (6), 1635-1642.
- Santella, N., Ho, D. T., Schlosser, P., & Stute, M. (2008). Widespread elevated atmospheric SF₆ mixing ratios in the Northeastern United States: Implications for groundwater dating. *Journal of Hydrology*, 349(1-2), 139-146. <https://doi.org/10.1016/j.jhydrol.2007.10.031>
- Saraiva Okello, A. M. L., Uhlenbrook, S., Jewitt, G. P. W., Masih, I., Riddell, E. S., & Van der Zaag, P. (2018). Hydrograph separation using tracers and digital filters to quantify runoff components in a semi-arid mesoscale catchment. *Hydrological processes*, 32(10), 1334-1350. <https://doi.org/10.1002/hyp.11491>
- Scanlon, B. R., Faunt, C. C., Longuevergne, L., Reedy, R. C., Alley, W. M., McGuire, V. L., & McMahon, P. B. (2012). Groundwater depletion and sustainability of irrigation in the US High Plains and Central Valley. *Proc Natl Acad Sci U S A*, 109(24), 9320-9325. <https://doi.org/10.1073/pnas.1200311109>
- Schilling, O. S., Nagaosa, K., Schilling, T. U., Brennwald, M. S., Sohrin, R., Tomonaga, Y., Brunner, P., Kipfer, R., & Kato, K. (2023). Revisiting Mt Fuji's groundwater origins with helium, vanadium and environmental DNA tracers. *Nature Water*, 1(1), 60-73. <https://doi.org/10.1038/s44221-022-00001-4>
- Schilling, O. S., Parajuli, A., Tremblay Otis, C., Müller, T. U., Antolinez Quijano, W., Tremblay, Y., Brennwald, M. S., Nadeau, D. F., Jutras, S., Kipfer, R., & Therrien, R. (2021). Quantifying Groundwater Recharge Dynamics and Unsaturated Zone Processes in Snow-Dominated Catchments via On-Site Dissolved Gas Analysis. *Water resources research*, 57(2). <https://doi.org/10.1029/2020wr028479>
- Schiperski, F., Oertwich, M., Scheytt, T., & Licha, T. (2019). Solubility of TINOPAL CBS-X fluorescent dye at different EDTA concentrations and pH values: Implications regarding its applicability in field tracer tests. *Journal of Hydrology*, 578. <https://doi.org/10.1016/j.jhydrol.2019.124025>

- Schlosser, P., Stute, M., Sonntag, C., & Münnich, K. O. (1989). Tritiogenic ^3He in shallow groundwater. *Earth and Planetary Science Letters*, 94, 245-256.
- Schoonover, J. E., Lockaby, B. G., & Helms, B. S. (2006). Impacts of land cover on stream hydrology in the West Georgia Piedmont, USA. *J Environ Qual*, 35(6), 2123-2131. <https://doi.org/10.2134/jeq2006.0113>
- Sérodes, J.-B., Behmel, S., Simard, S., Laflamme, O., Grondin, A., Beaulieu, C., Proulx, F., & Rodriguez, M. J. (2021). Tracking domestic wastewater and road de-icing salt in a municipal drinking water reservoir: Acesulfame and chloride as co-tracers. *Water Research*, 203. <https://doi.org/10.1016/j.watres.2021.117493>
- SIGEOM. Gouvernement du Québec. Retrieved [accessed on the 23/10/2023 from <https://sigeom.mines.gouv.qc.ca/>
- Sliwka, I., Lasa, J., Zuber, A., Opoka, M., & Jackowicz-Korczynski, M. (2004). Headspace Extraction Method for Simultaneous Determinations of SF_6 , CCl_3F , CCl_2F_2 and $\text{CCl}_2\text{FCClF}_2$ in Water. *Chem. Anal. (Warsaw)*, 49, 535-549.
- Solder, J. E., Stolp, B. J., Heilweil, V. M., & Susong, D. D. (2016). Characterization of mean transit time at large springs in the Upper Colorado River Basin, USA: a tool for assessing groundwater discharge vulnerability. *Hydrogeology Journal*, 24(8), 2017-2033. <https://doi.org/10.1007/s10040-016-1440-9>
- Solomon, D. K., & Gilmore, T. E. (2024). Age Dating Young Groundwater from Environmental Tracer Data. <https://doi.org/https://doi.org/10.21083/LIU2727>
- Solomon, D. K., Gilmore, T. E., Solder, J. E., Kimball, B., & Genereux, D. P. (2015). Evaluating an unconfined aquifer by analysis of age-dating tracers in stream water. *Water resources research*, 51(11), 8883-8899.
- Søndergaard, M., & Jeppesen, E. (2007). Anthropogenic impacts on lake and stream ecosystems, and approaches to restoration. *Journal of Applied Ecology*, 44(6), 1089-1094. <https://doi.org/10.1111/j.1365-2664.2007.01426.x>
- Sophocleous, M. (2002). Interactions between groundwater and surface water: the state of the science. *Hydrogeology Journal*, 10, 52-67. <https://doi.org/10.1007/s10040-001-0170-8>

- Soulsby, C., Birkel, C., & Tetzlaff, D. (2014). Assessing urbanization impacts on catchment transit times. *Geophysical Research Letters*, 41(2), 442-448. <https://doi.org/10.1002/2013gl058716>
- Sprenger, M., Stumpp, C., Weiler, M., Aeschbach, W., Allen, S. T., Benettin, P., Dubbert, M., Hartmann, A., Hrachowitz, M., Kirchner, J. W., McDonnell, J. J., Orłowski, N., Penna, D., Pfahl, S., Rinderer, M., Rodriguez, N., Schmidt, M., & Werner, C. (2019). The Demographics of Water: A Review of Water Ages in the Critical Zone. *Reviews of Geophysics*, 57(3), 800-834. <https://doi.org/10.1029/2018rg000633>
- Stolp, B. J., Solomon, D. K., Suckow, A., Vitvar, T., Rank, D., Aggarwal, P. K., & Han, L. F. (2010). Age dating baseflow at springs and gaining streams using helium-3 and tritium : Fischach-Dagnitz system, southern Vienna Basin, Austria. *Water resources research*, 46, 13. <https://doi.org/10.1029/2009WR008006>
- Stute, M., Forster, M., Frischkorn, H., Serejo, A., Clark, J. F., Schlosser, P., Broecker, W. S., & Bonani, G. (1995). Cooling of tropical Brazil (5°C) during the last glacial maximum. *Science*, 269, 379-383.
- Suckow, A. (2014). The age of groundwater - definitions, models and why we do not need this term. *Applied geochemistry*, 50, 222-230. <https://doi.org/10.1016/j.apgeochem.2014.04.016>
- Talbot Poulin, M. C., Comeau, G., Tremblay, Y., Therrien, R., Nadeau, M. M., Lemieux, J. M., Molson, J., Fortier, R., Therrien, P., Lamarche, L., Donati-Daoust, F., & Bérubé, S. (2013). *Projet d'acquisition de connaissances sur les eaux souterraines du territoire de la Communauté métropolitaine de Québec, Rapport final*.
- Taylor, R. G., Scanlon, B., Döll, P., Rodell, M., van Beek, R., Wada, Y., Longuevergne, L., Leblanc, M., Famiglietti, J. S., Edmunds, M., Konikow, L., Green, T. R., Chen, J., Taniguchi, M., Bierkens, M. F. P., MacDonald, A., Fan, Y., Maxwell, R. M., Yechieli, Y., . . . Treidel, H. (2012). Ground water and climate change. *Nature Climate Change*, 3(4), 322-329. <https://doi.org/10.1038/nclimate1744>
- Tazioli, A. (2011). Experimental methods for river discharge measurements: comparison among tracers and current meter. *Hydrological Sciences Journal*, 56(7), 1314-1324. <https://doi.org/10.1080/02626667.2011.607822>

- Tetzlaff, D., Seibert, J., McGuire, K. J., Laudon, H., Burns, D. A., Dunn, S. M., & Soulsby, C. (2009). How does landscape structure influence catchment transit time across different geomorphic provinces? *Hydrological processes*, 23, 945-953.
- Tockner, K., Uehlinger, U., & Robinson, C. T. (2009). *Rivers of Europe*. London: Academic Press. .
<https://doi.org/https://doi.org/10.1016/B978-0-12-369449-2.X0001-2>
- Tremblay, Y., Gatel, L., Picard, A., N'Da, B., Frot, B., Therrien, P., Cloutier, V., Barbecot, F., Lemieux, J. M., Proulx, F., Audet, L., & Cantin, A. M. (2024). *Portrait des ressources en eaux souterraines et de leurs liens avec les eaux de surface du bassin versant de la rivière Saint-Charles, Etude réalisée dans le cadre de l'analyse de la vulnérabilité des sources d'eau potable de la Ville de Québec*.
- Uhlenbrook, S., Frey, M., Leibundgut, C., & Maloszewski, P. (2002). Hydrograph separations in a mesoscale mountainous basin at event and seasonal timescales. *Water resources research*, 38(6), 31-31-31-14. <https://doi.org/10.1029/2001wr000938>
- UNESCO. (2022). *Rapport mondial des Nations Unies sur la mise en valeur des ressources en eau 2022. Eaux souterraines - Rendre visible l'invisible*.
- Verhoeven, J. T., Arheimer, B., Yin, C., & Hefting, M. M. (2006). Regional and global concerns over wetlands and water quality. *Trends Ecol Evol*, 21(2), 96-103.
<https://doi.org/10.1016/j.tree.2005.11.015>
- Visser, A., Broers, H. P., Purtschert, R., Sültenfuß, J., & de Jonge, M. (2013). Groundwater age distributions at a public drinking water supply well field derived from multiple age tracers (^{85}Kr , $^3\text{H}/^3\text{He}$ and ^{39}Ar). *Water resources research*, 49, 7778-7796.
- Visser, A., Broers, H. P., van der Grift, B., & Bierkens, M. F. (2007). Demonstrating trend reversal of groundwater quality in relation to time of recharge determined by $^3\text{H}/^3\text{He}$. *Environ Pollut*, 148(3), 797-807. <https://doi.org/10.1016/j.envpol.2007.01.027>
- Visser, A., Thaw, M., Deinhart, A., Bibby, R., Safeeq, M., Conklin, M., Esser, B., & Van der Velde, Y. (2019). Cosmogenic Isotopes Unravel the Hydrochronology and Water Storage Dynamics of the Southern Sierra Critical Zone. *Water resources research*, 55(2), 1429-1450.
<https://doi.org/10.1029/2018wr023665>
- Vogel, J. C. (1967). *Investigation of groundwater flow with radiocarbon*

- Wachniew, P. (2015). Environmental tracers as a tool in groundwater vulnerability assessment. *Acque Sotterranee - Italian Journal of Groundwater*. <https://doi.org/10.7343/as-108-15-0135>
- Wachniew, P., Zurek, A. J., Stumpp, C., Gemitzi, A., Gargini, A., Filippini, M., Rozanski, K., Meeks, J., Kvaerner, J., & Witczak, S. (2016). Toward operational methods for the assessment of intrinsic groundwater vulnerability: A review. *Critical Reviews in Environmental Science and Technology*, 46(9), 827-884. <https://doi.org/10.1080/10643389.2016.1160816>
- Wang, S., Hrachowitz, M., Schoups, G., & Stumpp, C. (2023). Stable water isotopes and tritium tracers tell the same tale: no evidence for underestimation of catchment transit times inferred by stable isotopes in StorAge Selection (SAS)-function models. *Hydrology and Earth System sciences*, 27(16), 3083-3114. <https://doi.org/10.5194/hess-27-3083-2023>
- Wanninkhof, R., Mulholland, P. J., & Elwood, J. W. (1990). Gas exchange rates for a first order stream determined with deliberate and natural tracers. *Water resources research*, 26, 1621-1630.
- Warner, M. J., & Weiss, R. F. (1985). Solubilities of chlorofluorocarbons 11 and 12 in water and seawater. *Deep-Sea Research*, 32, 1485-1497.
- Winter, T. C., Harvey, J. W., Franke, O. L., & Alley, W. M. (1998). *Ground water and surface water, a single resource*. USGS Circular 1139.
- WMO. (2008). *Guide to Hydrological Practice Volume I - From Measurement to Hydrological Information*.
- WMO. (2010). *Manual on stream gauging Volume I - Fieldwork*.
- Wood, P. J., & Dykes, A. P. (2002). The use of salt dilution gauging techniques: ecological considerations and insights. *Water Research*, 36, 3054-3062.
- Xie, J., Liu, X., Jasechko, S., Berghuijs, W. R., Wang, K., Liu, C., Reichstein, M., Jung, M., & Koirala, S. (2024). Majority of global river flow sustained by groundwater. *Nature geoscience*. <https://doi.org/10.1038/s41561-024-01483-5>
- Zhang, H., & Cloud, A. (2006). The permeability characteristics of silicone rubber. *Global Advances in Materials and Processes*.
- Zhang, R., Li, Q., Chow, T. L., Li, S., & Danielescu, S. (2013). Baseflow separation in a small watershed in New Brunswick, Canada, using a recursive digital filter calibrated with the

conductivity mass balance method. *Hydrological processes*, 27(18), 2659-2665.
<https://doi.org/10.1002/hyp.9417>